The role of the low-molecular-weight proteins of the CP43 pre-assembly complex of Photosystem II

Harvinder Singh

A thesis submitted for the degree of
Doctor of Philosophy

University of Otago, Dunedin, New Zealand

2017

Created 8/11/2017

Abstract

The biogenesis of Photosystem II (PS II) involves the stepwise assembly of the reaction centre subcomplex together with the subsequent addition of the two chlorophyll-binding core antenna proteins, CP43 and CP47. In this study, the function of four low-molecular-weight proteins (Psb27, Psb30, PsbK and PsbZ) belonging to the CP43 pre-assembly complex was investigated in the cyanobacterium *Synechocystis* sp. PCC 6803. The PsbK, PsbZ and Psb30 polypeptides are retained in the holoenzyme, but while Psb27 appears to participate in both the biogenesis and repair pathways, it is not a constituent of the mature complex. The role of conserved amino acid residues of the Psb27 protein potentially involved in protein-protein interactions with other PS II subunits was studied by introducing amino acid substitutions in *Synechocystis* sp. PCC 6803. These amino acid substitutions did not impede the biogenesis and repair pathways of photosystem and PS II electron transport kinetics in these mutants resembled those observed for wild type. However, chlorophyll fluorescence induction measurements indicated mutations in Psb27 altered the state transitions regulating energy transfer to the Photosystem I (PS I) and PS II and the D14A, D58E, D58K, and K63D strains exhibited changes in PBS coupling and energy transfer to PS II. Additionally, Psb27 mutations were found to alter the PS I level. Whole genome sequencing of a particular Psb27 mutant line (R54E*) revealed a C to A substitution in the *psbA2* gene corresponding to a His252 to Gln substitution in the D1 reaction centre protein. Confirmation that D1:His252 was required for normal electron transfer between the primary (Q_A) and secondary (Q_B) electron acceptors was obtained by introducing point mutations into a *psbA*-deletion mutant of *Synechocystis* sp. PCC 6803. Additionally, the D1-Ser264 was also targeted, since D1-Ser264 has also been suggested to be involved in the configuration of the Q_B site and is in close proximity to His252. The D1-His252 mutants as well as D1-Ser264 mutants, displayed low PS II oxygen-evolving activity and impaired electron transfer between Q_A and Q_B supporting calculations suggesting His252 and Ser264 participate in the protonation of the Q_B^- semiquinone during the turnover of the two-electron gate. Additionally, the PsbK, PsbZ and Psb30 subunits were not absolutely required for PS II activity; however, it was found that these subunits contributed to the ability of PS II to withstand photodamage following exposure to high light. Also, the Psb27 protein appears necessary for efficient repair or photoactivation of PS II and its absence along with LMW proteins (Psb30, PsbK and PsbZ) results in an increased susceptibility to photoinhibition.

Acknowledgements

Firstly, I would like to express my special appreciation and gratitude to my supervisor Prof. Julian Eaton-Rye for his immense knowledge, endless patience, motivation and support during my PhD study. I could not have imagined having a better mentor and advisor for my PhD research study. Besides my advisor, I would like to thank the committee members of my PhD studies: Dr. Liz Ledgerwood, and Dr. Chris Brown, for their encouragement and insightful comments, which helped me to widen my research from various perspectives.

My sincere thanks also go to Jackie Daniel for her invaluable help and for keeping everything running in the lab. I would like to thank the administration as well as the IT department at the Biochemistry Department, University of Otago, Dunedin for all their support over the course of my PhD study.

I thank my past and present fellow lab mates (Lab 308) for the useful discussions, and the sleepless nights we were working together during my PhD study, and for all the fun we have had in the last 4-5 years. Also, I would like to thank my friend Rinky Parakra in particular for helping me and supporting me throughout the thesis writing journey. I am also thankful to Dr. Elizabeth Permina for guiding me during whole genome sequencing.

Last but not the least, special thanks to my family. Words cannot express how grateful I am to my father (Sh. Ujagar Singh), mother (Smt. Baljeet Kaur), sister (Amar Jeet Kaur) and brother (Sandeep Singh) for all of the sacrifices that they have made for me. Your prayer for me was what sustained me this far. I would also like to thank all of my friends who supported me in writing, and me to strive towards my goal.

List of Abbreviations

Abbreviations used within this thesis are defined below with the exception of abbreviations and symbols defined by the Nomenclature Committee of IUBMB and IUPAC-IUBMB Joint Commission on biochemical nomenclature.

Amp	Amplitude
AP	Allophycocyanin
APS	Ammonium persulfate
Bis-Tris	2-[Bis(2-hydroxyehtyl)amino]-2-(hydroxymethyl)propane-1,3-diol
BMF	Blue measuring flash
BN	Blue-native
bp	Basepair
BSA	Bovine serum albumin
cDNA	Complementary DNA
cfu	Colony forming units
Chl	Chlorophyll
CTAB	Cetyltrimethylammonium bromide
cyt	Cytochrome
DCBQ	2,6-dichlorobenzo-1,4-quinone
DCMU	3-(3,4-dichlorophenyl)-1,1-dimethylurea
DDM	β-D-dodecylmaltoside
DMBQ	2,5-dimethyl-1,4 benzoquinone
ECL	Enhanced chemiluminescence
EDTA	Ethylenediaminetetraacetic acid
EPR	Electron paramagnetic resonance
ETC	Electron transport chain
FAD	Flavin adenine dinucleotide
Fd	Ferredoxin
FDP	Flavodiiron protein
FMN	Flavin mononucleotide
F_m	Maximal chl *a* fluorescence

FNR	Ferredoxin:$NAPD^+$ oxideoreductase
FQR	Ferredoxin:quinone oxidoreductase
F_o	Initial chl *a* fluorescence
F_t	Chl *a* fluorescence at time t
F_v	Variable chl *a* fluorescence
GTO1	Glucose tolerant Otago 1
GTO2	Glucose tolerant Otago 2
h	Hour
HEPES	4-(2-hydroxyethyl)-1-piperazineethanesulfonic acid
HL	High light
Hz	Hertz
Kb	Kilobase pair
kDa	Kilodalton
L	Litre
LB	Lysogeny broth
LED	Light emitting diode
LF	Left flank
LHC	Light-harvesting complex
LL	Low light
LMW	Low molecular weight
M	Molar
m	Milli
µ	Micro
min	Minute
MQ	MilliQ (Type 1 water)
NADPH	Nicotinamide adenine dinucleotide phosphate
NMR	Nuclear magnetic resonance
NPQ	Non-photochemical quenching
OCP	Orange carotenoid protein
OD	Optical density
OEC	Oxygen evolving centre
ORF	Open reading frame

P_{680}	Photosystem II reaction centre
P_{700}	Photosystem I reaction centre
PAGE	Polyacrylamide gel electrophoresis
PBS	Phycobilisome
PC	Phycocyanin
PCC	Pasteur culture collection
PCR	Polymerase chain reaction
pD1	Precursor of D1 protein
PDB	Protein data bank
PE	Phycoerythrin
Pheo	Pheophytin
PMSF	Phenylmethylsulfonylfluoride
PQ	Plastoquinone
PQH_2	Plastoquinol
PS I	Photosystem I
PS II	Photosystem II
psi	Pound per square inch
PVDF	Polyvinyllidene difluoride
Q_A	Primary quinone electron acceptor of PS II
Q_B	Secondary quinone electron acceptor of PS II
RC47	CP43-less PS II reaction centre sub-complex
RF	Right flank
ROS	Reactive oxygen species
rpm	Revolutions per minute
SDS	Sodium dodecyl sulfate
SCP	Small chl-binding protein
s	Second
$T_{1/2}$	Half-time
TBE	Tris-borate-EDTA
TE	Tris-EDTA
TEMED	Tetramethylethylenediamine
Tris	Tris(hydroxymethyl)aminomethane
Tween-20	Polyoxyethylene sorbitan monolaurate

TyrZ	Redox active tyrosine-161 residue of D1 protein
U	Unit of enzyme activity
UV	Ultraviolet light
V	Volts
v/v	volume per volume
w/v	weight per volume

Table of Contents

List of Figures

List of Tables

Chapter One

Introduction

1.1 Photosynthesis

Photosynthesis is one of the most important biological processes of life on earth. There are two kinds of photosynthesis: oxygenic photosynthesis and anoxygenic photosynthesis. Oxygenic photosynthesis is used by plants, algae, and cyanobacteria, whereas, anoxygenic photosynthesis is utilised by purple bacteria and green sulfur bacteria. Oxygenic photosynthesis plays a vital role in sustaining aerobic life on earth by converting light energy into biologically useful chemical energy. Oxygenic photosynthesis consists of two kinds of reactions – light-dependent reactions and light independent/dark (carbon fixation) reactions. The light reactions and carbon assimilation reactions take place within the chloroplast in photosynthetic eukaryotes but occur in the cytosol of prokaryotes.

The light reactions take place through a series of pigment-protein complexes embedded in the thylakoid membranes of photosynthetic organisms. The major protein complexes include photosystem II (PS II), the cytochrome b_6f complex, photosystem I (PS I) and the ATP synthase (Nelson and Ben-Shem 2004; Nelson and Yocum 2006). The products produced in the light-dependent reactions are adenosine triphosphate (ATP) and nicotinamide adenine dinucleotide phosphate (NADPH) which are later used in the dark reactions to fix atmospheric carbon dioxide into complex carbohydrates. Oxygen is also liberated as a by-product in the light-dependent reactions by the formation of an O-O bond as part of the mechanism responsible for the splitting of water molecules (Shen 2015).

1.2 Light-dependent reactions of photosynthesis

The PS II and PS I protein complexes are linked by the cytochrome b_6f complex and other mobile electron carriers (Whitmarsh and Govindjee 1999). The reactions are illustrated in Figure 1.1.

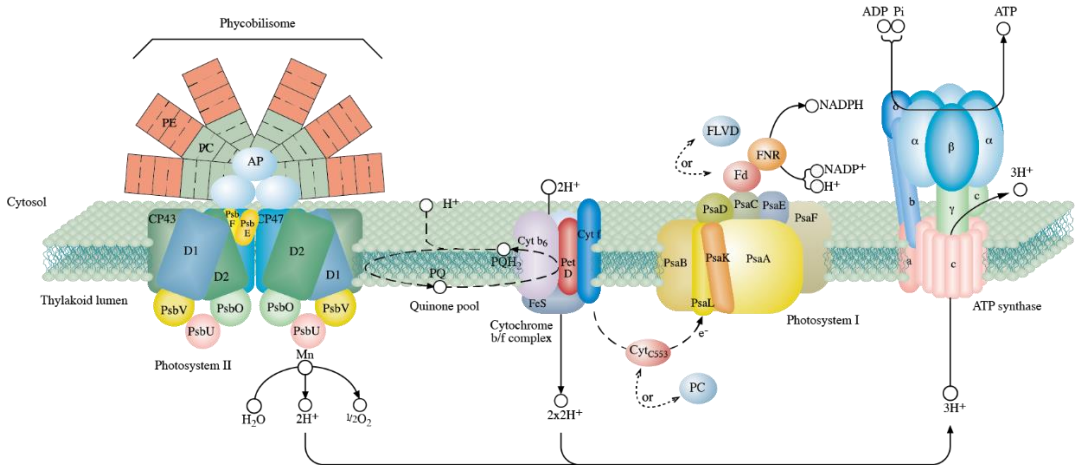

Figure 1.1 Schematic representation of the cyanobacterial photosynthetic electron transport chain. The light is captured by the reaction centre chlorophylls of PS II, PS I and primary charge separation takes place. The electrons from the excited reaction centre of PS II are transferred to Q_A and Q_B to form PQH_2. PQH_2 diffuses to the cytochrome b_6f complex where it is oxidised. The electron is transferred to PS I. Upon excitation the reaction centre of PS I transfers an electron via Fd to the flavoprotein FNR and this, in turn, leads to the conversion of cofactor $NADP^+$ to NADPH. The phycobilisomes contain PE, PC and AP pigment-proteins. PS II consists of D1 and D2 core heterodimer proteins which bind redox cofactors; cytochrome b_{559} (formed by PsbE and PsbF) is in the PS II core; CP43 and CP47 are the proximal chlorophyll-binding pigment-protein complexes, PsbO, PsbV and PsbU are the extrinsic proteins associated with the PS II complex; Mn is the Manganese cluster; PQ/PQH_2 pool is plastoquinone or plastoquinol pool, FeS is Rieske iron-sulfur cluster; Fd is ferredoxin protein; FNR is ferredoxin-$NADP^+$ reductase; cytochrome c_{553} is replaced by PC in plant chloroplasts, some algae, and cyanobacteria. PsaA and PsaB are the chlorophyll binding pigment-protein complexes of PS I that also contain the PS I reaction centre; Flvd is flavodoxin: a mobile electron carrier that accepts electrons from PS I and can substitute for ferredoxin in low-iron conditions; α to γ are the subunits of the CF_1 complex of ATP synthase; a to c are subunits of the CF_o complex of ATP synthase. Flows of electron and protons are indicated by black arrows. The figure was prepared by J. Eaton-Rye (unpublished).

Solar energy is initially harvested by distal light-harvesting antenna pigment-protein complexes. These light-harvesting complexes direct the light energy into the reaction centres via proximal antenna complexes for carrying out photochemical reactions (Grossman *et al.* 1995). The distal antenna complexes in photosynthetic eukaryotes are membrane-embedded and known as light-harvesting complexes (LHCs) containing chlorophyll *a* and *b* pigments in the cases of plants and green algae. However, red algae have two types of light-harvesting antennas: the phycobilisomes (PBS) which are directly connected to the reaction centres of PS II, and a LHC I complex connected to

the reaction centres of PS I. In cyanobacteria, the antenna complex is membrane-extrinsic and known as the PBS. Phycobilisomes possess a phycobiliprotein core made up of allophycocyanin from which rods emanate that are made up of stacked disks of additional biliproteins. In PS II, the reaction centre pigments that are excited are collectively known as P_{680}, as this depicts their absorbance maximum. Electrons from the excited P_{680} (P_{680}^{*}) are transferred to the primary plastoquinone electron acceptor (Q_A) and then to the secondary plastoquinone electron acceptor (Q_B) to form plastoquinol (PQH_2). Plastoquinol then diffuses to the cytochrome b_6f complex through the thylakoid membrane. After reaching the cytochrome b_6f complex, PQH_2 is oxidised. The cytochrome b_6f complex then transfers an electron to plastocyanin (PC). The oxidised PS II (P_{680}^{+}) reaction centre is again reduced by the oxidation of water. Plastocyanin then transfers an electron to the P_{700}^{+} reaction centre pigments of PS I. Upon P_{700} excitation, P_{700}^{*} transfers electrons via a series of iron-sulfur electron carriers to ferredoxin (Fd) and ferredoxin-NADP reductase (FNR), in turn, transfers the electrons to $NADP^{+}$ to give NADPH. During these chemical reactions, protons are translocated across the thylakoid membrane and lead to the formation of electrochemical proton gradient that drives the synthesis of ATP by ATP synthase.

1.3 Photosystem II (PS II)

The first microorganisms containing PS II evolved around ~3 billion years ago, and thus were responsible for initiating the conversion of earth`s anaerobic atmosphere to our present-day oxygen-rich atmosphere (De Marais 2000; Kasting and Siefert 2002; Hohmann-Marriott and Blankenship 2011). The PS II, multi-subunit membrane protein complex, is highly conserved across all the oxygenic photosynthetic organisms and exists in both monomeric as well as dimeric form; although dimerisation is not a critical step for PS II activity (Nowaczyk *et al.* 2006). The conservation between cyanobacterial and plant PS II has led to the cyanobacterium *Synechocystis* sp. PCC 6803 (hereafter *Synechocystis* 6803) being used to study the mechanism of PS II biogenesis, function, and repair as it can grow on glucose in the absence of PS II activity (Williams 1988). However, thermophilic cyanobacterial species have been used for structural studies (Shen 2015).

1.3.1 Structure of PS II

The crystal structure of the PS II complex has been determined by X-ray crystallography with increasing refinements since 2001 (Shen 2015). The first PS II structure was from the cyanobacterium *Thermosynechococcus elongatus* at a resolution of 3.8 Å (Zouni *et al.* 2001) with the same group increasing the resolution to 3.0 Å in 2005 (Loll *et al.* 2005); however, an important breakthrough was achieved by Barber and co-workers in 2004 also with *Thermosynechococcus elongatus* with a 3.5 Å-resolution structure that provided the first evidence for the inclusion of a Calcium ion in the oxygen-evolving complex (OEC) of PS II therefore defining the OEC as a Mn_4CaO_5 complex (Ferreira *et al.* 2004). The next major breakthrough was the 1.9 Å-resolution structure from *Thermosynechococcus vulcanus* (Umena *et al.* 2011) (PDB: 3WU2). However, the PDB: 3WU2 structure was suggested to be compromised by radiation damage to the Mn_4CaO_5 cluster but this was addressed by using femtosecond X-ray pulses provided by a free-electron laser (Suga *et al.* 2015a) (PDB: 4UB8) and the 1.94 Å-resolution 4UB8 structure is currently the most widely used for structure-based studies.

The monomer of the cyanobacterial PS II complex consists of ~20 protein subunits and other cofactors such as chlorophyll, β-carotenes, pheophytins, plastoquinones, haem irons and various other ions that are associated with the oxygen-evolving complex (Umena *et al.* 2011). The proximal antenna surrounding the PS II reaction centre proteins is provided by the chlorophyll-binding proteins CP43 and CP47 (the gene products of *psbC* and *psbB* respectively). The PS II reaction centre core consists of the D1 and D2 (the gene products of *psbA* and *psbD*, respectively) polypeptides (Fig. 1.2).

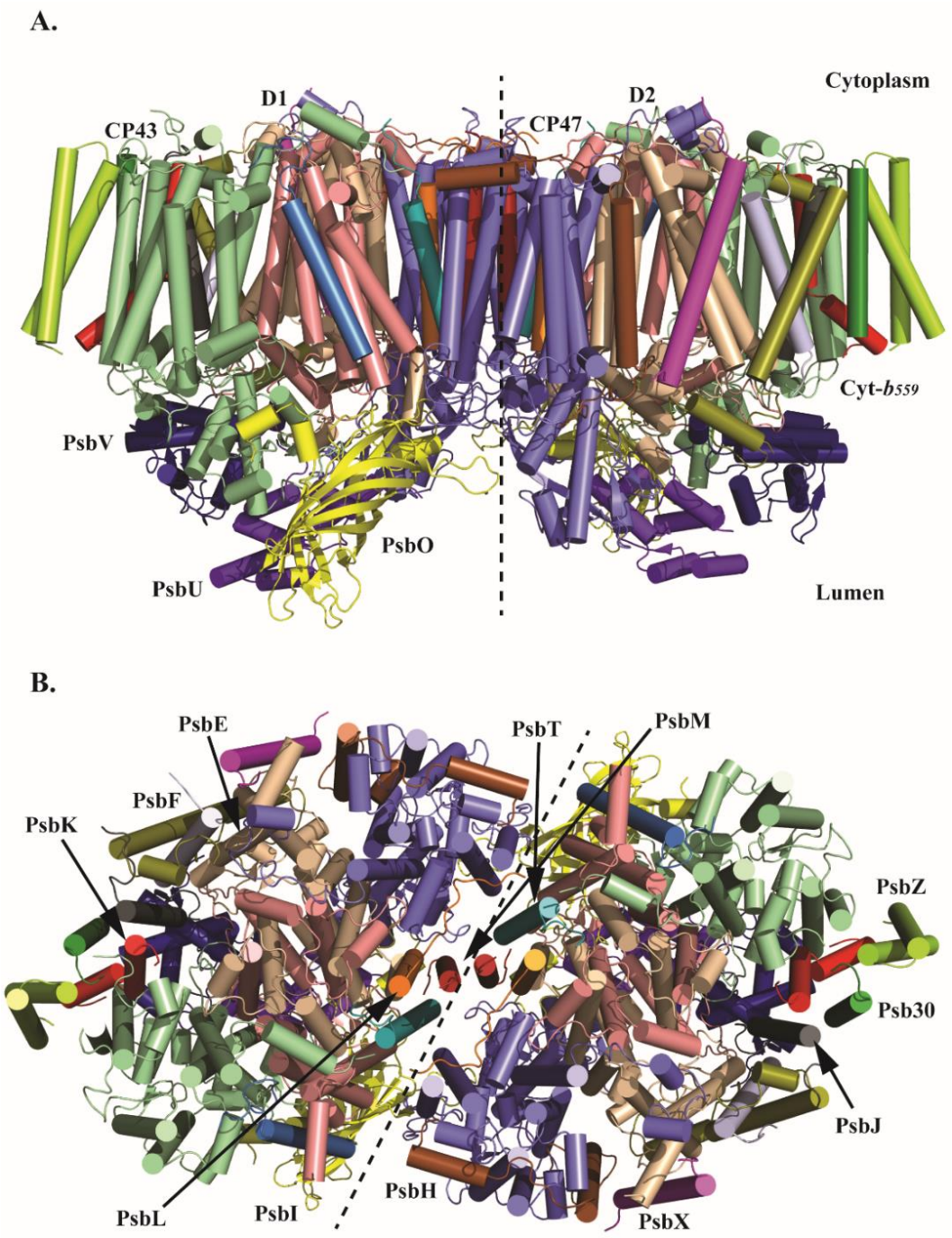

Figure 1.2 X-ray crystal structure of PS II complex from *Thermosynechococcus vulcanus*.(A) Dimeric PS II viewed along the thylakoid membrane plane. Monomer 1 (left side) and Monomer 2 (right side). The cylindrical structures show the alpha-helical nature of the protein subunits with the proximal antenna proteins CP43 (cyan green) and CP47 (denim) and the reaction centre proteins D1 (cyan pink) and D2 (cream) indicated. Also shown are the membrane extrinsic proteins PsbO (yellow), PsbU (purple) and PsbV (blue) and the α and β subunits of cytochrome b_{559} (olive green and light grey), respectively. Various low-molecular-weight (LMW) proteins are also shown. **(B) Top View of PS II dimer.** Figure was created from PDB: 3ARC (Umena *et al.* 2011).

The different protein subunits associated with the PS II complex can be broadly classified into three types: Membrane-embedded core proteins (intrinsic proteins), proteins present in the lumenal side of thylakoid membrane (extrinsic proteins) and the proteins that associate with the PS II during biogenesis and repair, but are not part of the mature active complex (auxiliary proteins).

1.3.1.1 Intrinsic proteins of PS II

The core structure of PS II monomers primarily consists of four membrane-spanning proteins. These include the reaction centre D1 and D2 polypeptides that bind chlorophyll, pheophytin and the plastoquinone cofactors involved in the photochemical charge separation across the PS II membrane (Tang *et al.* 1990; Hankamer *et al.* 2001; Zouni *et al.* 2001; Kamiya and Shen 2003; Ferreira *et al.* 2004; Loll *et al.* 2005; Wydrzynski and Satoh 2005; Rappaport and Diner 2008; Guskov *et al.* 2009; Umena *et al.* 2011). Both D1 and D2 proteins consist of five transmembrane helices and together form a heterodimer, but only the D1 protein contributes ligands to the manganese, and calcium associated with the oxygen-evolving complex.

On either side of D1 and D2 protein are the chlorophyll *a*-binding subunits CP43 and CP47. Both CP43 and CP47 are made up of six transmembrane helices (Barber 2006). CP43 binds ~13 molecules of chlorophyll *a* whereas CP47 binds ~16 molecules of chlorophyll *a*. These chlorophyll-binding proteins are interior transducers of excitation energy from the light-harvesting pigment proteins (the PBS in cyanobacteria and red algae) (Vasil'ev *et al.* 2001) and direct the light energy to the reaction centre (P_{680}) of PS II. The four chlorophylls of P_{680} are bound to the D1 and D2 proteins (Diner and Rappaport 2002; Raszewski *et al.* 2008; Renger and Renger 2008). Once the P_{680} pigments absorb the light, one of the chlorophylls donates an electron to the pheophytin (Cardona *et al.* 2012). The oxidised P_{680}^{+} is re-reduced by a nearby redox-reactive tyrosine (Tyr161) residue, denoted as (Y_z) (Kruse *et al.* 2005; Kern and Renger 2007), which in turn oxidises a manganese cluster (Mn_4CaO_5) (Barry and Babcock 1987; Debus *et al.* 1988a; Debus *et al.* 1988b; Wydrzynski and Satoh 2005; Styring *et al.* 2012). The manganese cluster acts as a catalytic centre for water hydrolysis. Electron paramagnetic resonance (EPR) spectroscopy experiments have set the number of manganese atoms in the manganese cluster at four (Dismukes and Siderer 1981; de Paula *et al.* 1986; Peloquin and Britt 2001). It was also shown that the manganese

cluster consists of a calcium atom too in addition to the four manganese atoms through EPR (Kim *et al.* 2004), extended X-ray absorption fine structure (EXAFS) (Cinco *et al.* 2002) and X-ray diffraction (Ferreira *et al.* 2004) experiments. The other components that have also been suggested as part of the manganese cluster apart from the core structure of four manganese atoms and one calcium atom includes chloride ions (Homann 2002; Pizarro *et al.* 2004). Once four electrons have been abstracted from the Mn_4CaO_5 cluster, two water molecules are split into four protons and one oxygen molecule.

The manganese cluster can exist in 5 oxidation states (S_0 to S_4) (Kok *et al.* 1970). S_0 is the most reduced state, S_1 is dark stable, and S_4 is unstable and reacts with water producing free oxygen. PS II includes 13 LMW transmembrane subunits: PsbE (α-cytochrome b_{559}), PsbF (β-cytochrome b_{559}), PsbH, PsbI, PsbJ, PsbK, PsbL, PsbM, PsbT, PsbX, Psb30 (Ycf12), PsbY, and PsbZ (Ycf9) (Ferreira *et al.* 2004; Wydrzynski and Satoh 2005; Muh *et al.* 2008; Guskov *et al.* 2009; Umena *et al.* 2011). All these subunits have molecular masses of less than 10 kDa and are single-helix membrane spanning proteins except for PsbZ, which has two transmembrane helices. Cytochrome b_{559} helps in the stabilisation, protection as well as assembly of PS II (Stewart and Brudvig 1998; Pospisil 2011). In *Synechocystis* 6803, the deletion of *psbE* (Pakrasi *et al.* 1991) or *psbF* (Pakrasi *et al.* 1990) lead to the loss of PS II activity.

Disruption of *psbH* leads to impaired Q_A to Q_B electron transfer (Mayes *et al.* 1993), and cyanobacterial cells lacking PsbH are susceptible to photodamage (Komenda and Barber 1995). The *psbH* disruption mutant in *Synechocystis* 6803 (Mayes *et al.* 1993) does grow photoautotrophically but has a slower growth rate. Deletion of PsbH has inhibitory effects on bicarbonate binding to the PS II non-heme iron (Komenda *et al.* 2002). Binding of Psb28 proteins to PS II is dependent on the presence of PsbH (Dobakova *et al.* 2009; Bialek *et al.* 2013); PsbH is also essential for the binding to PS II of HliB (also termed ScpD), a member of the family of high-light-inducible proteins (Hlips) (He *et al.* 2001) or small chlorophyll-*a*/*b* proteins (Scps) (Funk and Vermaas 1999).

The highly conserved PsbI protein is required for the stable binding of CP43 with the PS II core complex (Dobakova *et al.* 2007). PsbI is associated with the D1/D2 heterodimer (Ikeuchi and Inoue 1988; Webber *et al.* 1989). Disruption of the *psbI* gene

in *Synechocystis* 6803 and *Thermosynechococcus elongatus* is known to affect PS II activity. The *psbI* deletion strains grow photoautotrophically, but the oxygen-evolving activity of PS II is lowered as compared to the wild type (Ikeuchi *et al.* 1995b; Katoh and Ikeuchi 2001). The disruption of *psbI* in *Synechocystis* 6803 also leads to higher susceptibility to photodamage than the wild type (Katoh and Ikeuchi 2001).

The *psbJ* gene is present with *psbE*, *psbF*, and *psbL* in the form of an operon (*psbEFJL*) in most photosynthetic organisms and the PsbJ protein is highly conserved among cyanobacteria and higher plants. The ΔPsbJ strain of *Synechocystis* 6803 can grow photoautotrophically, with a slower growth rate than wild type (Lind *et al.* 1993). PsbJ also plays a role in the assembly and maintenance of the PS II complexes in *Synechocystis* 6803 (Lind *et al.* 1993; Regel *et al.* 2001).

The PsbL, PsbM, and PsbT proteins are present at the interface of each PS II monomer. PsbL is also the part of the *psbEFJL* gene cluster in *Synechocystis* 6803 and higher plants. The disruption of PsbT leads to the impaired Q_A to Q_B electron transfer (Iwai *et al.* 2004; Bentley *et al.* 2008b). The ΔPsbT mutant in *Synechocystis* 6803 displayed slower photoautotrophic growth, lower levels of PS II complexes and low oxygen evolution activity compared to the wild type (Bentley *et al.* 2008b). Deletion of PsbL, PsbM, and PsbT affects the accumulation of PS II dimers in the cyanobacteria (Bentley *et al.* 2008b; Henmi *et al.* 2008).

PsbK, PsbZ, and Psb30 have been shown to be associated with the CP43 pre-assembly complex during biogenesis (Boehm *et al.* 2011) and may be related to stabilising carotenoid binding to the CP43 (Sugiura *et al.* 2010) (Fig. 5.20).

The PsbX protein was first detected in oxygen-evolving PS II reaction centre complex of higher plants (Ikeuchi *et al.* 1989) followed by detection in various other plants and cyanobacteria (Shi *et al.* 1999; Funk 2000). The PsbX protein has been found to cross-link to cytochrome b_{559} (Shi *et al.* 1999). The removal of PsbX protein does not affect the growth rate, water oxidation ability or electron transport (Funk 2000). On the contrary, the deletion of *psbX* in the *Thermosynechococcus elongatus* was predicted to be involved be in quinone turnover at the Q_B site (Katoh and Ikeuchi 2001).

The PsbY protein is present in all photosynthetic plants, various cyanobacteria and in some algal chloroplasts (Gau *et al.* 1998). PsbY is an LMW subunit with a single

transmembrane helix located in the peripheral region close to PsbE and PsbF (the α and β subunits of cytochrome b_{559}). The loss of PsbY protein in cyanobacteria did not influence manganese binding and had no dramatic effect on PS II activity (Meetam *et al.* 1999). The cyanobacterial ΔPsbY mutants were prone to lower growth rates, higher sensitivity to photoinhibition and altered fluorescence pattern at 77 K as compared to wild type under calcium deficiency and high light (Neufeld *et al.* 2004). The PsbY protein is predicted to play a role in regulating the redox potential of cytochrome b_{559} (von Sydow *et al.* 2016).

1.3.1.2 Extrinsic proteins of PS II

The cyanobacterial PS II complexes contain the extrinsic proteins PsbO, PsbU (12 kDa protein), and PsbV (cytochrome c_{550}) (Shen *et al.* 1992; Shen and Inoue 1993; Seidler 1996), whereas PsbU and PsbV have been replaced by PsbP and PsbQ in green plant PS II (Ifuku *et al.* 2011; Bricker *et al.* 2012). The extrinsic proteins play a role in the regulation of oxygen-evolving reactions of PS II via stabilisation of the Mn_4CaO_5 cluster and Cl^- ions (Roose *et al.* 2007b; Enami *et al.* 2008; Bricker *et al.* 2012).

Recent studies using Fourier transform infrared spectroscopy (FTIR) technique showed that PsbO, PsbV in cyanobacteria (Nagao *et al.* 2015) and red algae (Uno *et al.* 2013), and PsbP in higher plants (Tomita *et al.* 2009) are important for determining the protein conformation of the oxygen-evolving complex, respectively. In cyanobacteria, the PsbO and PsbV can bind to the intrinsic proteins of PS II independently, whereas PsbU requires the presence of both PsbO and PsbV for its binding to PS II (Philbrick *et al.* 1991). The PsbO, PsbU, and PsbV proteins are suggested to affect the thermostability of PS II in *Synechocystis* 6803 (Kimura *et al.* 2002). The deletion of PsbO did not alter the photoautotrophic growth potentially suggesting that PsbO is not essential for oxygen-evolution activity in cyanobacteria as compared to its plant counterpart (Burnap *et al.* 1992). PsbO is proposed to interact with CP43, CP47, D1, D2, and PsbU subunits; PsbU with CP47, PsbO, and PsbV, and PsbV with CP43, D1, D2, and PsbU (Bricker *et al.* 2012). The deletion of the *psbO* gene affects the dimerisation process of PS II *in vivo* (Wegener *et al.* 2008).

The PsbU protein plays a role in the stabilisation of both energy transfer and electron transport in the /PS II assembly in *Synechocystis* 6803 (Veerman *et al.* 2005). The

deletion of PsbU increases the susceptibility of PS II complex to photodamage, resulting in rapid degradation of D1 protein (Inoue-Kashino *et al.* 2005; Balint *et al.* 2006). The presence of PsbU also protects PS II from dark inactivation (Veerman *et al.* 2005). The PsbV deletion strains in *Synechocystis* 6803 displayed slower photoautotrophic growth, lower oxygen-evolution activity and defects in PS II function in comparison to wild type (Shen *et al.* 1995). The crystal structure of isolated PsbV was solved to higher resolutions from three species of cyanobacteria (Frazao *et al.* 2001; Sawaya *et al.* 2001; Kerfeld *et al.* 2003). Loss of PsbV results in a decrease in oxygen-evolution rates (Kimura *et al.* 2002). PsbV can also bind independently but is stabilised by the presence of PsbO and PsbU (Shen and Inoue 1993). On the contrary, the PsbU protein cannot rebind at all in the absence of either PsbO or PsbV (Shen and Inoue 1993) but can bind with the addition of PsbV (Shen *et al.* 1997; Eaton-Rye *et al.* 2003). Thus, it is suggested that PsbO binds first, followed by PsbV and that PsbU binds third.

1.3.1.3 Auxiliary proteins of PS II

Cyanobacteria have CyanoP and CyanoQ, which are the homologues of PsbP and PsbQ, which exists in higher plants and green algae (Kashino *et al.* 2002b; Thornton *et al.* 2004b). Both CyanoP and CyanoQ were identified in isolated PS II preparations from *Synechocystis* 6803 (Kashino *et al.* 2002b; Thornton *et al.* 2004a). Moreover, both CyanoP and CyanoQ are modified by lipidation, a feature absent in plant PsbP and PsbQ (Thornton *et al.* 2004a; Fagerlund and Eaton-Rye 2011a). The CyanoP protein was found to be associated with PS II complexes sub-stoichiometrically (Enami *et al.* 2000) and it has been suggested that CyanoP occupies the same position as PsbQ in the major complex (Cormann *et al.* 2014); in contrast, the CyanoQ protein is associated with PS II stoichiometrically (Enami *et al.* 2000). The deletion of CyanoP led to the changes in the PBS coupling and energy transfer to PS II (Jackson and Eaton-Rye 2015). The deletion of CyanoP in cyanobacteria led to subtle effects in photoautotrophic growth and PS II function under $CaCl_2$-limiting conditions (Aoi *et al.* 2014) .

CyanoQ is reported to bind PS II tightly and to optimise the oxygen evolution (Roose *et al.* 2007a), and a recent study using chemical cross-linking suggests that cyanoQ is closely associated with PsbO and CP47 proteins in *Synechocystis* 6803 (Liu *et al.*

2014). Previously, it was thought that there was a single CyanoQ associated per PS II monomer (Thornton *et al.* 2004a; Roose *et al.* 2007b; Liu *et al.* 2014). However, recently, further characterisation of histidine-tagged CyanoQ PS II has identified an additional CyanoQ-containing PS II complex containing multiple copies of CyanoQ per PS II monomer (Liu *et al.* 2015). CyanoQ contributes to PS II dimer stability (Liu *et al.* 2014). The CyanoQ deletion mutant in *Synechocystis* 6803 shows a slight reduction in growth rate compared to the wild-type strain (Thornton *et al.* 2004b; Summerfield *et al.* 2005).

Ycf48 protein is transiently associated with PS II during its biogenesis and repair pathways. The removal of Ycf48 in *Synechocystis* 6803 led to decrease in the efficiency of PS II assembly and repair (Komenda *et al.* 2008). The Ycf48 has been shown to be associated with both an early assembly complex containing precursor D1 (pD1) and a D1/D2 assembly intermediate (RC II) complex which combines with the CP47 pre-assembly complex later to form RC47 precomplex (Komenda *et al.* 2008; Boehm *et al.* 2012b; Komenda *et al.* 2012b), which is in agreement with the earlier studies in *Arabidopsis thaliana* (Plucken *et al.* 2002). In the ΔYcf48 mutant, PS II electron transfer and oxygen evolution were perturbed (Jackson *et al.* 2014).

Psb27 is a lipoprotein and is found in the thylakoid lumen. It is also suggested to interact with an intermediate PS II complex which might play a role in the assembly of the Mn_4CaO_5 cluster (Nowaczyk *et al.* 2010; Komenda *et al.* 2012a; Mabbitt *et al.* 2014). Psb27 is also predicted to stabilise CP43 precomplex consisting of the LMW proteins Psb30, PsbK, and PsbZ (Komenda *et al.* 2012b).

The two homologues of the Psb28 present in cyanobacterium *Synechocystis* 6803 are Psb28-1 (*sll1398*) and Psb28-2 (*slr1739*) (Boehm *et al.* 2012b). The Psb28-1 (also known as Psb13 or Ycf79) was first identified as a component of a His-tagged PS II preparation isolated from *Synechocystis* 6803 (Kashino *et al.* 2002b). Psb28-1 is predicted to be a hydrophilic protein peripherally attached to the membrane (Dobakova *et al.* 2009). In *Synechocystis* 6803, the Psb28-1 exists as a dimer (Bialek *et al.* 2013) and was present in the RC47 complex (Dobakova *et al.* 2009; Boehm *et al.* 2012b; Sakata *et al.* 2013) in the vicinity of the PsbH subunit (Dobakova *et al.* 2009). The structure of Psb28-2 is monomeric in nature and is thought to be similar to Psb28-1 (Bialek *et al.* 2013; Mabbitt *et al.* 2014). Psb28-2 has also been detected in RC47

complexes (Boehm *et al.* 2012b). The deletion of Psb28 did little to alter the assembly of PS II complex which is in agreement with Sakata and co-workers (Sakata *et al.* 2013). The expression profiles of the *psb28-1* and *psb28-2* genes were found to be quite different in various environmental conditions in the transcriptomic study potentially suggesting a distinct functional role for each protein (Hernandez-Prieto *et al.* 2016).

Psb29 is a peripheral protein subunit and is found on the cytoplasmic side of the thylakoid membrane (Keren *et al.* 2005). The Psb29 protein is highly conserved among cyanobacteria and flowering plants (Keren *et al.* 2005). The Psb29 deletion mutants exhibit slower growth and lower PS II activity, especially under high-light conditions (Keren *et al.* 2005).

Table 1.1 Summary of different types of PS II proteins present in the mature PS II complex in *Synechocystis* 6803.

Protein	Gene	No. of amino acids	Size kDa	Structure	Function	Location
D1	*psbA2 slr1311*	344	38.0	five transmembrane α helices	reaction centre protein, helps in the repair mechanism of PS II, it binds with some of the cofactors involved in PS II-mediated electron transport chain, reaction centre protein	membrane
CP47	*psbB slr0906*	500	56.0	six transmembrane α helices arranged in a circular manner	antenna protein for reaction centre complex	membrane
CP43	*psbC sll0851*	470	50.0	six transmembrane α helices arranged in a circular manner	light harvesting system, important for water-splitting activity	membrane
D2	*psbD slr0927*	350	39.5	five transmembrane α helices, homologous to D1 protein	reaction centre protein undergoes repair mechanism under extreme conditions	membrane
α cytochrome b_{559}	*psbE ssr3451*	82	9.3	single transmembrane helix	helps in the assembly of PS II, reaction centre protein	membrane
β cytochrome b_{559}	*psbF smr0006*	38	4.4	single transmembrane helix	reaction centre protein helps in the assembly of PS II	membrane
PsbH	*psbH ssl2598*	63	7.0	single transmembrane helix	low molecular weight protein, plays a structural role during PS II assembly, helps in the PS II electron transfer between the plastoquinone primary acceptor (Q_A) and secondary acceptor (Q_B)	membrane
PsbI	*psbI sml0001*	36	4.2	single transmembrane helix	low molecular weight protein, early stages of PS II assembly	membrane
PsbJ	*psbJ smr0008*	37	4.4	single transmembrane helix	low molecular weight protein, located in highly conserved operon *psbEFJL*	membrane

PsbK	*psbK sml0005*	37	4.3	single transmembrane helix	low molecular weight protein, stability of PS II dimer	membrane
PsbL	*psbL smr0007*	37	4.4	single transmembrane helix	low molecular weight protein, PS II core assembly, required for normal functioning of Q_A site	membrane
PsbM	*psbM sml0003*	34	3.7	single transmembrane helix	low molecular weight protein, PS II core assembly	membrane
PsbO	*psbO sll0427*	240-257	26.5	elongated shape with two main domains	extrinsic protein, manganese stabilising protein	lumen
PsbU	*psbU sll1194*	131	10.5	α helix protein	extrinsic protein, stability of PS II	lumen
PsbV (cytochrome c_{550})	*psbV sll0258*	160	15.0	haem containing protein	extrinsic protein, provides Ca^{2+}/Cl^- at the catalytic site	lumen
PsbX	*psbX sml0002*	38-42	4.1	single transmembrane helix	helps in electron transfer between Q_A and Q_B	lumen
Psb30/Ycf12	*ycf12 sll0047*	32-46	3.3-5.0	single transmembrane helix	PS II stability	lumen
PsbY	*psbY sml0007*	36-41	4.2	single transmembrane helix	low molecular weight protein, regulating the redox potential of cytochrome b_{559}	lumen

Table 1.2 Summary of different types of PS II proteins that bind transiently to PS II during biogenesis and repair, but are absent in final PS II dimer in *Synechocystis* 6803.

Protein	Gene	No. of amino acids	Size kDa	Structure	Function	Location
Psb27	*slr1645*	134	12.2	four transmembrane helix	low molecular weight protein, prevents the binding of extrinsic proteins	assembly protein
Psb28	*sll1398*	112	12.5	single domain with a mixed a/b topology	low molecular weight protein, CP47 biosynthesis, PS II biogenesis	assembly protein
Psb29	*sll1414*	240	27.1	a helical bundle and an extended C terminal helix	stability of FtsH proteases involved in repair of photodamaged D1 protein	membrane
Ycf48	*slr2034*	342	-	beta sheets	PS II stability and repair	assembly factor

1.3.2 Oxygen-evolving activity of PS II

The oxygen-evolving complex of PS II consists of a manganese cluster that plays an important role in the oxidation of water via a 5-step cycle known as the S-state model (Kok *et al.* 1970) (Fig. 1.3 A and B). Each S-state (S_0 to S_4) denotes a stage of sequential oxidation of the oxygen-evolving PS II complex. The manganese atoms within the cluster (Mn_4CaO_5) form ligands with the D1 and CP43 proteins on the lumenal side of PS II (Loll *et al.* 2005). The splitting of water to molecular oxygen requires the extraction of four electrons from two molecules of water and is carried out by the oxygen-evolving complex. Following light-induced primary charge separation, the reaction centre chlorophyll P_{680}^+ is re-reduced by the extraction of electrons from the oxygen-evolving complex, which is in turn re-reduced by the removal of four electrons from water, resulting in the production of molecular oxygen. The oxygen-evolving manganese complex undergoes five different oxidation states from S_0 to S_4 and in turn oxidises two molecules of water producing oxygen and four protons (Kok *et al.* 1970) as can been seen in Fig. 1.3 B. In dark-adapted samples, most of the centres decay to S_1 state. A saturating actinic flash advances the system from one S-state to the next, and oxygen is produced at the S_4 state, which returns the system back to S_0 without any further light input (Kok *et al.* 1970). Oxygen-evolving complex returns to its S_1 state in the absence of light, and the S_1 state is stable at dark. At the S_1 state, manganese ions exist at the following oxidation states - Mn^{3+}, Mn^{3+}, Mn^{4+}, Mn^{4+}. The extrinsic proteins are predicted to play a protective role by creating a stable environment for the manganese cluster (Roose *et al.* 2007b).

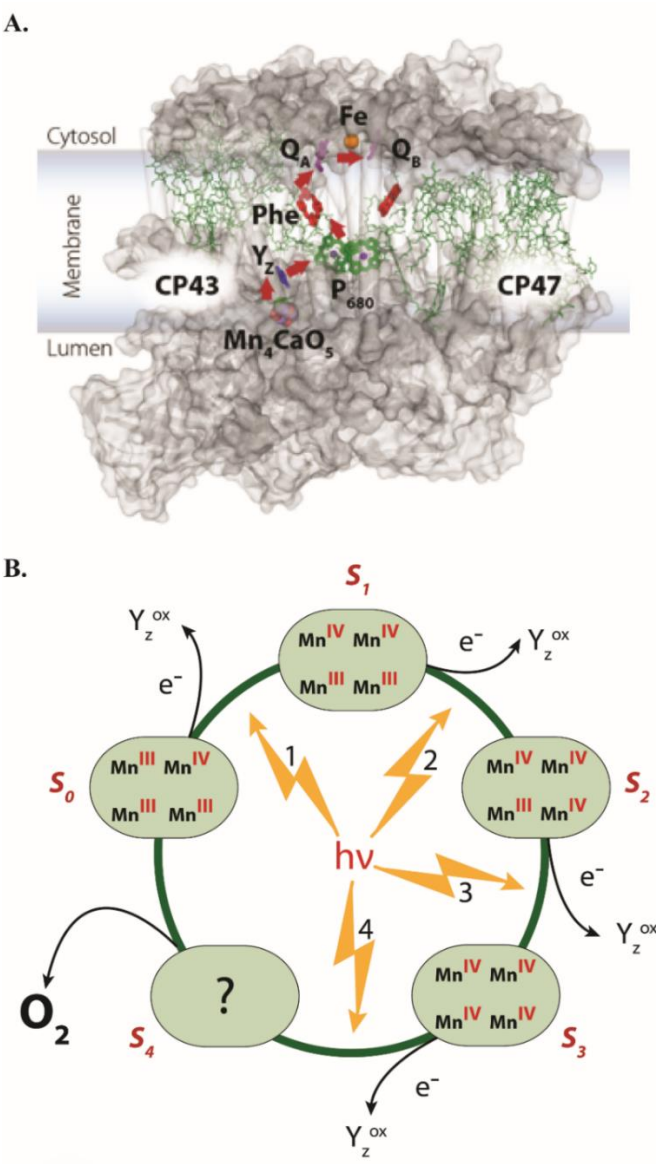

Figure 1.3 Oxygen-evolving activity of PS II.(A) Redox-active cofactors in the crystal structure of PS II core complex. View along the thylakoid membrane plane. The protein structure of a single monomer of PS II is shown in grey. Chlorophyll *a* molecule is in green, Mn_4CaO_5 is the manganese cluster, P_{680} is PS II reaction centre, Y_z is Tyrosine-161 of D1, Phe is pheophytin, Q_A is primary plastoquinone electron acceptor, Fe is a non-heme iron, Q_B is the secondary plastoquinone electron acceptor, CP43 and CP47 are the chlorophyll-binding proteins of the proximal antenna. **(B) The S state cycle of the oxygen-evolving complex.** Kok and co-workers (Kok *et al.* 1970) developed this model. The oxygen-evolving complex exists in five different oxidation states (S_0, S_1, S_2, S_3, and S_4). Flashes of light advance the system from S_0 through the increasing states of oxidation to the highest oxidation state, S_4. On exposure to flashes of light, the P_{680} reaction centre of PS II gets excited, and the excited P_{680}^* oxidises Y_z. The highest and most unstable oxidation state is S_4. S_4 state oxidises two water molecules, and one oxygen is formed and reverts to S_0 state. S_2 state is also known as the dark stable state. The figure was prepared by J. Eaton-Rye (unpublished).

1.4 Biogenesis and repair of PSII

Assembly of PS II takes place in a highly coordinated manner (Komenda *et al.* 2004). During the assembly process, several distinct assembly intermediates are formed and many proteins that are not found in the final functional PS II complex, are associated with these assembly complexes (Nixon *et al.* 2010; Komenda *et al.* 2012a). Understanding these processes can lead to the development of plants with improved growth characteristics even in the presence of stressful abiotic conditions.

The major PS II complexes formed during the assembly and repair processes are: (i) D2-cytochrome b_{559} complex which consists of D2 and cytochrome b_{559} (formed by PsbE and PsbF); (ii) the reaction centre (RC) which consists of PsbI, PsbE, PsbF and D1 in the form of either precursor D1 (pD1), intermediate D1 (iD1) or mature D1; (iii) the reaction centre 47 (RC47) complex which consists of PsbI, PsbE, PsbF, D1, D2, and CP47: this subcomplex is also known as CP43-lacking complex; (iv) the reaction centre complex 1 (RCC1) which is the monomeric form of PS II, and (v) the reaction centre complex 2 (RCC2) which is the dimeric form of PS II.

1.4.1 Biogenesis of PS II

The initial step in the biogenesis of PS II (Fig. 1.4) appears to be the formation of a complex between cytochrome b_{559} and the D2 protein resulting in the D2-cytochrome b_{559} complex (Komenda *et al.* 2004; Komenda *et al.* 2008) and then pD1 and PsbI (Dobakova *et al.* 2007) with transiently bound PratA binds with the D2-cytochrome b_{559} subcomplex to form the RC complex (Klinkert *et al.* 2004; Dobakova *et al.* 2007; Komenda *et al.* 2008; Schottkowski *et al.* 2009a; Schottkowski *et al.* 2009b). CtpA (CtpA removes the carboxyl-terminal of pD1 forming the iD1 and the mature D1) and Ycf48 protein are also bound to the RC complex. PratA (a periplasmic tetratricopeptide repeat protein involved in the biogenesis of PS II in *Synechocystis* 6803) is known to interact with CtpA (Klinkert *et al.* 2004; Komenda *et al.* 2008; Schottkowski *et al.* 2009a). Then, the CP47 protein along with PsbH subunit comes and binds to the RC complex to form an RC47 complex (Komenda *et al.* 2004; Komenda *et al.* 2008). Subsequent attachment of CP43 to the RC47 sub-complex allows the formation of the monomeric PS II core complex, RCC1. Once the RCC1 complex is formed, all assembly factors except Psb27 are released, and the biogenesis of oxygen-evolving

complex and the attachment of the lumenal bound extrinsic protein takes place (Mabbitt *et al.* 2014). Two monomeric RCC1 join with each other to form RCC2. During the biogenesis of PS II, the pD1 undergoes processing to allow the formation of the fully functional Mn_4CaO_5 cluster (Anbudurai *et al.* 1994; Nixon *et al.* 2010). The 16 amino acid residues present at the C-terminal end of pD1 in *Synechocystis* 6803 (Takahashi *et al.* 1988; Nixon *et al.* 1992) are cleaved by CtpA (Anbudurai *et al.* 1994), and eight amino acids are left as an extension (Komenda *et al.* 2007). In the beginning, pD1 is cleaved at position Ala-352, thus forming iD1 which is cleaved at position Ala-344 in the second step (Inagaki *et al.* 2001). The C-terminal extension of D1 is not required for assembly of oxygen-evolving PS II complex (Nixon *et al.* 1992; Satoh and Yamamoto 2007). However, mutants containing a modified D1 C-terminal extension are less efficient than the wild type and are more prone to photodamage (Ivleva and Merzhanov 2001; Kuvikova *et al.* 2005).

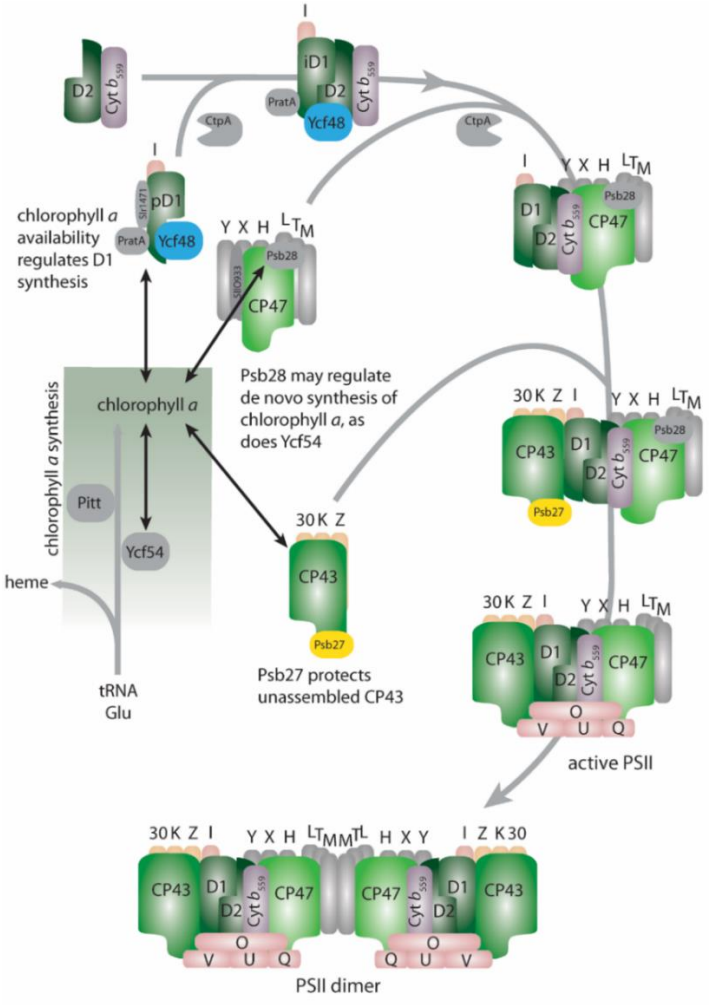

Figure 1.4 Assembly mechanism of PS II in cyanobacteria. Glutamic acid transfer RNA (Glu-tRNA) is the standard starting point for the chlorophyll *a* and heme biosynthesis pathways. Mg-protoporphyrin IX monomethyl ester cyclase activity is regulated by a Ycf54 factor. Membrane-associated Pitt factor (a tetratricopeptide repeat protein) stabilises the protochlorophyllide oxidoreductase (Schottkowski *et al.* 2009b). Mg-chelatase helps in the formation of precursor protoporphyrin ring by incorporating Mg^{2+}. Chlorophyll *a* availability regulates the D1 synthesis (Mabbitt *et al.* 2014). Biogenesis starts with the binding of the D2-cyt b_{559} complex to the D1-PsbI sub-complex along with the assembly factors PratA and Ycf48 (Komenda *et al.* 2008) to form the RC complex. A carboxyl-terminal processing protease (CtpA) (Satoh and Yamamoto 2007) removes the carboxyl-terminal of pD1 forming the iD1 and the mature D1. Then CP47 pre-complex binds to the RC complex, and the RC47 sub-complex is formed. The Psb28 protein is bound to the cytosolic surface of CP47 (Dobakova *et al.* 2009; Boehm *et al.* 2012b) and regulates chlorophyll biosynthesis. CP43 along with Psb27 (Komenda *et al.* 2012a) binds to the RC47 subcomplex to form the monomeric PS II core complex, RCC1. The Psb27 and Psb28 proteins detach from the inactive PS II complex, and the assembly of the Mn_4CaO_5 cluster starts from the formation of RCC1. The two monomeric RCC1 join with each other to form RCC2. The figure is adapted from (Mabbitt *et al.* 2014).

1.4.2 Repair mechanism of PS II

The chemistry of water oxidation by PS II inescapably leads to damage that particularly targets the D1 protein, and this inactivates the enzyme (Vass 2012). This process is known as photodamage (Aro *et al.* 1993a; Aro *et al.* 1993b; Adir *et al.* 2003) and the damage can occur even at low intensities. A PS II repair mechanism (Fig. 1.5) operates to replace the photodamaged protein, and overall rates of photosynthesis are not affected unless the rate of damage is more than the rate of PS II repair (Keren *et al.* 1995; Keren *et al.* 1997; Vass 2011; 2012). Photodamage is exacerbated under a range of adverse environmental conditions (Murata *et al.* 2007) and when the rate of repair is lower than the rate of photodamage, the plants (or algae and cyanobacteria) are said to be photoinhibited.

Under conditions where there is an unavailability of the terminal electron acceptors, excess electrons start accumulating in the photosynthetic electron transport chain, thus leading to an increase in excitation pressure from the incident radiation and the complete reduction of the plastoquinone acceptors (Q_A and Q_B) (Kyle *et al.* 1984; Vass *et al.* 1992). This over-reduction leads to a series of events such as the formation of highly reactive chlorophyll triplets (Vass *et al.* 1992; Vass and Cser 2009) and, damage of the Mn_4CaO_5 cluster (Keren *et al.* 1997; Hakala *et al.* 2005; Ohnishi *et al.* 2005; Szilard *et al.* 2005; Tyystjärvi 2008). The chlorophyll triplets formed, react with oxygen, thus producing singlet oxygen species ($^1O_2$) (Krieger-Liszkay 2005; Krieger-Liszkay *et al.* 2008; Triantaphylides *et al.* 2008; Triantaphylides and Havaux 2009; Vass 2011; Rehman *et al.* 2013). Many other assembly factors like α-tocopherol, plastoquinone and orange carotenoid-binding proteins also play an important role in photoprotection by quenching the radical oxygen species (Trebst *et al.* 2002; Kruk and Trebst 2008; Yadav *et al.* 2010; Inoue-Kashino *et al.* 2011; Sedoud *et al.* 2014).

As D1 subunit of PS II gets damaged, PS II repair cycle starts. Monomerisation of the PS II dimer takes place. CP43 detaches from the monomeric complex, and then selective replacement of the D1 protein takes place. The two steps, the CP43 attachment and PS II dimerisation, seem to be common with the biogenesis pathway of PS II (Dobakova *et al.* 2007).

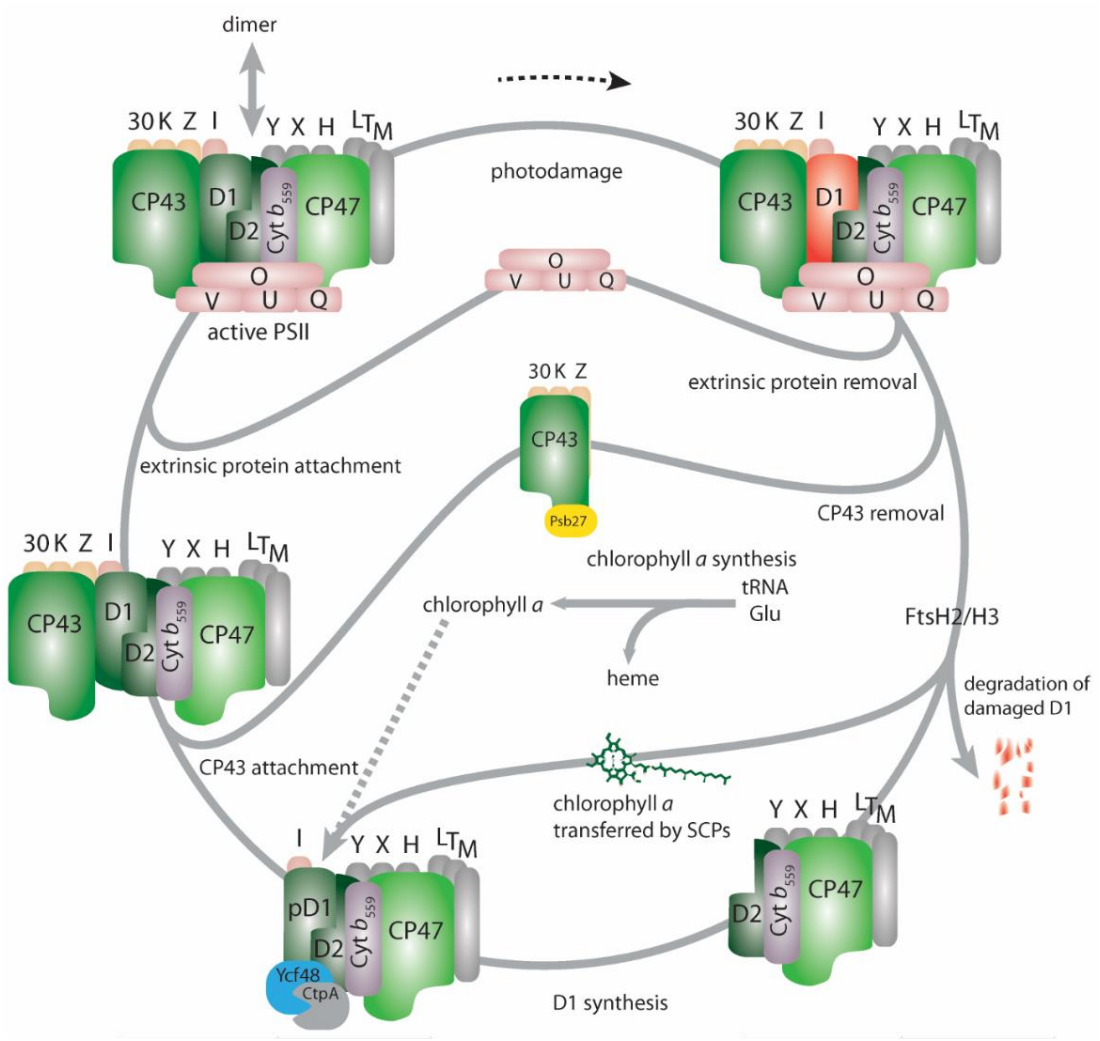

Figure 1.5 Repair mechanism of PS II in cyanobacteria. The D1 protein gets damaged in adverse environmental conditions, and then monomerisation of PS II dimer takes place. Extrinsic proteins (PsbO, PsbV, PsbU, and cyanoQ) and CP43 pre-assembly complex dissociate from the PS II monomer to replace the damaged D1 subunit with the help of FtsH2/H3 (Silva *et al.* 2003; Komenda *et al.* 2006; Boehm *et al.* 2012a). The Psb27 protein associates with CP43 (Komenda *et al.* 2012a; Komenda *et al.* 2012b) and the damaged D1 protein is replaced (Zhang *et al.* 1999; Tyystjarvi *et al.* 2001). Small chlorophyll *a*-binding proteins (SCPs) helps in the incorporation of the chlorophyll into the new D1 protein from the degraded D1 (Vavilin *et al.* 2007; Yao *et al.* 2012). The Ycf48 binds to PS II while the CtpA protease processes the carboxyl-terminal extension of pD1 (Komenda *et al.* 2008). Then again, rebinding of the CP43 protein takes place, and the Psb27 protein leaves the inactive monomeric complex allowing the binding of extrinsic proteins (PsbO, PsbU, and PsbV), dimerisation of PS II monomers, as well as the activation of manganese cluster. In the end, the fully functional PS II dimer is formed again. The figure is adapted from (Mabbitt *et al.* 2014).

1.5 CP43 preassembly complex factors

The CP43 pre-assembly complex possesses additional low-molecular-weight (LMW) proteins: membrane spanning Psb30 (3 kDa), PsbK (4 kDa), PsbZ (9 kDa) and the lumenally-located hydrophilic Psb27 (12 kDa) (Boehm *et al.* 2012b).

1.5.1 Psb27

The Psb27 protein is present in cyanobacteria, algae as well as higher plants (Peltier *et al.* 2002; Rajalahti *et al.* 2007) except *Gloeobacter violaceus* PCC 7421, which is a cyanobacterium that lacks thylakoids and may therefore have modified PS II assembly and repair processes (Nakamura *et al.* 2003). Psb27 was first identified in a PS II preparation from the *Synechocystis* 6803 (Ikeuchi *et al.* 1995a) and later named by Kashino and co-workers (Kashino *et al.* 2002b).

Psb27 was detected as an assembly factor in the non-oxygen-evolving PS II complex lacking extrinsic proteins (PsbO, PsbU, and PsbV) in *Thermosynechococcus elongatus* (Nowaczyk *et al.* 2006). Psb27 was also detected in PS II complexes from the red alga *Galdieria sulphuraria* using mass spectrometry (MS) based methods (Thangaraj *et al.* 2010) as well as from tobacco (Fey *et al.* 2008). The cyanobacterial Psb27 protein is an 11-kDa lipoprotein localised in the thylakoid lumen in photosystems that lack a functional Mn_4CaO_5 cluster and the other extrinsic proteins (Nowaczyk *et al.* 2006; Mamedov *et al.* 2007). The gene that codes for Psb27 in *Synechocystis* 6803 is *slr1645*. Psb27 contains 134 amino acids including an N-terminal signal peptide. The N-terminal region of Psb27 consists of a conserved cysteine residue (Thornton *et al.* 2004b; Nowaczyk *et al.* 2006; Fagerlund and Eaton-Rye 2011a). In cyanobacteria, N-terminal lipid modification of Psb27 helps in the tight association with the thylakoid membrane, but it is absent in Psb27 from land plants (Nowaczyk *et al.* 2006). The Psb27 protein is not present in the final PS II complex (Kashino *et al.* 2002b; Roose and Pakrasi 2004; Mamedov *et al.* 2007; Roose and Pakrasi 2008). Psb27 has been found to co-purify with various PS II protein complexes (Zouni *et al.* 2001; Umena *et al.* 2011) potentially, indicating that Psb27 binds transiently with the PS II subunits.

There are two paralogues of Psb27 in *Arabidopsis thaliana* known as Psb27-H1 (At1g03600) and Psb27-H2 (At1g05385) (also known as LPA19) and both were identified in the thylakoid lumen (Peltier *et al.* 2002; Chen *et al.* 2006; Wei *et al.* 2010)

with molecular masses of 12 kDa and 15 kDa, consisting of 174 and 199 amino acids, respectively. The lipoprotein motif is absent in these two cyanobacterial Psb27 homologues. The two mature proteins share around 23% identity (Wei *et al.* 2010; Fagerlund and Eaton-Rye 2011a). Psb27-H1 has been shown to play an important role in PS II repair (Chen *et al.* 2006) and the Psb27-H2 helps in the efficient maturation of D1 precursor (Wei *et al.* 2010).

Pakrasi and co-workers demonstrated that Psb27 binds to the lumenal surface of CP43 with 1-ethyl-3-(3-dimethylaminopropyl) carbodiimide (EDC) and 3,3'-dithiobis(sulfosuccinimidyl propionate) (DTSSP) cross-linkers (Liu *et al.* 2011a). MS based results predicted that the Psb27 binds to the loop E of CP43 via Asp-58 and Lys-63 residue. Recent studies using chemical cross-linking analysis and MS-based methods revealed a close association between Psb27 and loop E of CP43 (Liu *et al.* 2013b). Psb27 has been probed for binding to different PS II protein subunits (CP43, CP47, mD1, PsbE, and D2) using SPR spectroscopy (Cormann *et al.* 2014). The cross-link between Psb27-Lys91 and CP43-Lys381 was identified. Methods based on in-silico modelling method were also used to localise the binding site of Psb27 to the lumenal surface of PS II, and the Psb27 binding site was shown to partly overlap with the PsbO binding site (Cormann *et al.* 2009; Fagerlund and Eaton-Rye 2011a).

Psb27 is absent from the crystal structures of PS II (Umena *et al.* 2011; Suga *et al.* 2015a); however still, three different structures of cyanobacterial Psb27 has been resolved independently (Cormann *et al.* 2009; Mabbitt *et al.* 2009; Michoux *et al.* 2012). The first two Psb27 structures (PDB: 2KND, PDB: 2KMF) were obtained by NMR spectroscopy (Cormann *et al.* 2009; Mabbitt *et al.* 2009). The third Psb27 structure (PDB: 2Y6X) (Michoux *et al.* 2012) was obtained by X-ray crystallography. Psb27 protein consists of four-helices. Most of the surface part of the 3rd and 4th helices of Psb27 is highly conserved among bacteria, algae, and higher plants and might play an important role in interacting with PS II complex.

Psb27 has been proposed to help in the D1 processing and Mn_4CaO_5 cluster assembly by preventing the premature binding of extrinsic protein subunits (Roose and Pakrasi 2004; Nowaczyk *et al.* 2006; Liu *et al.* 2011a). The processing of the C-terminal extension of pD1 lead to the reduced binding affinity between CP43 and Psb27 and allows the binding of extrinsic PsbO and PsbV protein subunits (Liu *et al.* 2013b).

Psb27 protein has also been shown to play an important role in the turnover of PS II (Sirpio *et al.* 2007; Nixon *et al.* 2010).

Recently, site-directed mutagenesis of conserved amino acid residues of Psb27 was carried out in *Synechocystis* 6803, to study the effect of these mutations towards the structure and function of Psb27 towards PS II assembly and repair (Mabbitt *et al.* 2013). The studies related to the thermal stability of various Psb27 point variants was carried out using circular dichroism (CD) spectroscopy. The following mutations were introduced in Psb27 - Cys1 to Ser, Asp14 to Ala, Tyr78 to His, Glu98 to Arg, Arg94 to Glu, E103 to Arg, Arg108 to Glu, and Arg54 to Glu. The C1S, R54E, Y78H, R94E, E98R, E103R, and R108E mutants were found to be thermally stable whereas the D14A variant was less stable than the Psb27 control protein (Mabbitt *et al.* 2013).

1.5.2 Psb30/Ycf12

Psb30 was first identified in the PS II complexes of *Thermosynechococcus elongatus* (Kashino *et al.* 2007) and later in *Synechocystis* 6803 (Inoue-Kashino *et al.* 2008). Psb30 is a hydrophobic protein of 5.0 kDa with a grand average hydropathicity (GRAVY) as high as 1.30 (Kyte and Doolittle 1982). In *Synechocystis* 6803, Psb30 consists of 93 amino acid residues whereas, in *Thermosynechococcus elongatus*, Psb30 consists of only 46 amino acid residues. No homologous genes of Psb30 were found in the genomes of *Arabidopsis thaliana*. Conservation of the Psb30 gene can be seen in a wide variety of oxygenic photosynthetic organisms except for some marine cyanobacteria (Kashino *et al.* 2007) and angiosperms (Goremykin *et al.* 2003). Based on the PS II crystal structures, Psb30 is known to form a stable complex with CP43 (Boehm *et al.* 2011).

In the recent crystal structures of cyanobacterial PS II complex, Psb30 was in the periphery of cyanobacterial PS II core complex (Suga *et al.* 2015b) with its N-terminus facing towards the lumen and located near three small hydrophobic protein subunits - PsbJ, PsbK, and PsbZ in the PS II structure with resolution of 3.0 Å in *Thermosynechococcus elongatus* (Loll *et al.* 2005). Initially, Psb30 was provisionally assigned as PsbN in the PS II crystal structure by Ferreira and co-workers (Ferreira *et al.* 2004). Loll and colleagues named this helix as X1 in the PS II crystal structure proposed by them (Loll *et al.* 2005). Guskov and co-workers suggested that a water

molecule and Ca^{2+} ion might play an important role in bridging PsbK and Psb30 due to the 5.8 Å spacing (Guskov *et al.* 2009). The distance between Psb30 and cytochrome b_{559} is ~9 Å. The N-terminal region of Psb30 is thought to interact with the C-terminal region of ß-subunit of cytochrome b_{559} (PsbF) on the lumenal side of the thylakoid membrane.

The disruption of *psb30* gene displayed no significant phenotype; the mutant cells were able to grow photosynthetically and showed similar PS II oxygen-evolving activity like wild-type cells (Inoue-Kashino *et al.* 2008), whereas, the purified PS II complexes without Psb30 showed lower oxygen-evolving activity in high-light (Inoue-Kashino *et al.* 2008). It has been demonstrated that the Psb30 accumulation decreases in the PS II-deficient strains (Inoue-Kashino *et al.* 2011). In *Synechocystis* 6803, Psb30 deletion mutant exhibited ~30% lower oxygen-evolving activity than the wild type and no other significant phenotype were observed in Psb30 deletion mutant (Inoue-Kashino *et al.* 2008). The removal of Psb30 could affect Car12 molecule along with the redox potential of cytochrome b_{559}. The distance between Psb30 and β carotene 12 (Car12) is ~3.5 Å. Car12 is proposed to be a photo-oxidisable species (Tracewell and Brudvig 2008). Psb30 might not be directly involved in the water-oxidising activity of PS II complex; however, it still plays an important role in stability and efficient assembly of the PS II complex.

1.5.3 PsbK

PsbK is a small hydrophobic polypeptide with one transmembrane helix bound to PS II core complexes (Murata *et al.* 1988; Kashino *et al.* 2002a; Thornton *et al.* 2004b). The membrane-spanning segment and the N-terminal hydrophilic region of the mature PsbK protein are well conserved among the plants and cyanobacteria, whereas the pre-sequence is not conserved at all between cyanobacteria and the plants. PsbK was identified in the CP43-His complex using MS-based methods (Boehm *et al.* 2011).

PsbK is present between D2 and CP43 in the PS II structure (Ferreira *et al.* 2004). During the assembly of PS II, PsbK binds to CP43 to form a PsbK-CP43 complex which is later integrated into the CP47-reaction centre (RC) complex, to form PS II complexes (Boehm *et al.* 2011). PsbK has been shown to co-purify with CP43 sub-complexes from the partially disassembled PS II complex with the help of the

potassium thiocyanate (Ohnishi and Takahashi 2001; Sugimoto and Takahashi 2003). A tight association between CP43 and PsbK has already been documented (Sugimoto and Takahashi 2003; Schottkowski *et al.* 2009a).

Studies with *Thermosynechococcus elongatus* proposed that the PsbK subunit is required not only for the association of PsbZ and Psb30 but also plays an important role in the stabilisation of PsbZ in the thylakoid membrane (Iwai *et al.* 2010). The PsbK deletion mutant of *Synechocystis* 6803 showed a slight defect in its PS II activity (Ikeuchi *et al.* 1991); however, in *Chlamydomonas reinhardtii*, disruption of *psbK* resulted in a marked loss of the PS II complex, and the mutants were unable to grow photoautotrophically (Takahashi *et al.* 1994).

Inactivation of *psbC* (encoding CP43) leads to the additional loss of PsbK in the thylakoid membrane of *Synechocystis* 6803 (Ikeuchi *et al.* 1991), whereas, the disruption of *psbK* did not have much of an effect on CP43 accumulation in cyanobacteria. The specific interaction between CP43 and PsbK was studied and confirmed by isolation of a subcomplex consisting of CP43 and PsbK using potassium thiocyanate to separate PS II into subcore complexes followed by gel filtration chromatography (Sugimoto and Takahashi 2003; Boehm *et al.* 2012b).

Satoh and co-workers (Satoh *et al.* 1995), showed that the PS II complexes isolated from the ΔPsbK strain in cyanobacterium *Synechococcus vulcanus* had a modification at the Q_B quinone acceptor side. It was shown that PsbK plays an important role in the protection of PS II, as the ΔPsbK mutant was sensitive to the combined condition of glucose and light (50 $\mu E.m^{-2}s^{-1}$) (Kobayashi *et al.* 2005b).

1.5.4 PsbZ

The ~6.6 kDa PsbZ protein has been identified in PS II core complexes from cyanobacteria (Kashino *et al.* 2002a; Kashino *et al.* 2002b), and green algae (Swiatek *et al.* 2001) and is present in the high resolution X-ray structures of PS II from the red alga *Cyanidium caldarium* (Ago *et al.* 2016) and spinach (Wei *et al.* 2016). PsbZ is located on the outermost side of PS II and forms a shield over Psb30 and PsbK. Thus, disruption of *psbZ* exposes the Psb30 and PsbK to the surface and make them vulnerable to dissociation from the PS II complex (Takasaka *et al.* 2010).

In *Synechocystis* 6803, disruption of *psbZ* gene displayed slow growth as compared to the wild type under low-light conditions (Bishop *et al.* 2007). In thermophilic cyanobacterium, *Thermosynecococcus elongatus*, disruption of *psbZ* led to the loss of Psb30 and PsbK (Iwai *et al.* 2007). PsbZ has also been shown to play an important role in the stability of PS II light-harvesting complex II (LHC II) super-complex in green algae and higher plants (Ruf *et al.* 2000; Swiatek *et al.* 2001).

1.6 Aims of this study

The primary focus of this study is on the role of low-molecular-weight proteins (LMW) (Psb27, Psb30, PsbK, and PsbZ) belonging to the CP43 pre-assembly complex involved in the assembly and repair of PS II. The first part of this project focuses on mutating the conserved amino acid residues of the Psb27 protein that are implicated in protein-protein interactions in the studies outlined in the literature. In this thesis, the role of conserved amino acid residues of Psb27 protein was investigated to address the possibility that they might be necessary for protein-protein interactions since, the Psb27 protein is evolutionary conserved between higher plants and cyanobacteria. Additionally, previous studies have been carried on the analysis of stability of the recombinant Psb27 proteins carrying mutations at conserved amino acid residues (Mabbitt *et al.* 2013). The temperature at which the Psb27 protein became unfolded decreased by 16 ºC in the Psb27-D14A mutant protein and the Psb27-R54, Psb27-R94, Psb27-E103, and Psb27-R108 mutations also resulted in small change in the unfolding/melting temperature of Psb27 (Mabbitt *et al.* 2013). Hence, since deletion of Psb27 in cyanobacteria does not affect photoautotrophic growth (Bentley *et al.* 2008b), but does impair repair from photodamage (Nowaczyk *et al.* 2006) we designed experiments to test if misfolded Psb27 was more detrimental to PS II function than the complete absence of the polypeptide. Additionally, the amino-acid residues of Psb27 that crosslink with the chlorophyll *a*-binding core antenna protein CP43, as proposed by Pakrasi and co-workers (Liu *et al.* 2011a) – i.e., Asp58 and Lys63 were also targeted. Liu and coworkers utilised the 2KND Psb27 structure in which Glu98 is buried in the core of Psb27 (Liu *et al.* 2013a). The carboxylic acid groups near amine groups of Psb27 and CP43 peptides were cross-linked with EDC and were then identified by the use of MS. Two pairs of residues were cross-linked: Psb27-Asp58 to CP43-Lys215 and Psb27-Lys63 to CP43-Asp321 (Liu *et al.* 2011a). The distance between the two

cross-linked Psb27-Asp58 and Psb27-Lys63 residues is <20 Å whereas the distance between the two cross-linked CP43-Lys215 and CP43-Asp321 residues is >30 Å, in the respective available structures (Liu *et al.* 2011b). These residues suggested to be cross-linked are far apart from each other (and not conserved) to be close enough that they could be crosslinked. However, the disparity between the distances could only be accounted for if CP43 adopts a conformation different from those observed in PS II X-ray crystal structures upon Psb27 binding (Liu *et al.* 2011a). So, to check the model proposed by Liu and co-workers, Psb27-Asp58 and Psb27-Lys63 mutants were also constructed and characterised. Eleven variants of the Psb27 protein were introduced into the *Synechocystis* 6803 genome. The following amino acid residues were selected to perform the mutagenesis studies: Psb27-Asp14, Psb27-Arg54, Psb27-Tyr78, Psb27-Arg94, Psb27-Glu98, Psb27-Asp58, and Psb27-Lys63.

While characterising the Psb27 mutants, unexpectedly, a Psb27 mutant (named as R54E*) developed a spontaneous mutation. So, studies were performed to identify and characterise the spontaneous mutation that cropped up in the Psb27 point mutant line (R54E*) by constructing the respective mutants. The mutation discovered was the substitution of His252 to Gln in the *psbA2* copy of the D1 PS II reaction centre protein. The mutations introduced to study the identified secondary mutation in R54E* strain has been discussed in detail in chapter 4, section 4.5.

The third part of this study involved determining the role of Psb30, PsbK and PsbZ proteins in the assembly and repair of PS II as previous studies have suggested the role of Psb27 protein in the stabilisation of the unassembled CP43 in a precomplex consisting of the LMW proteins CP43, PsbK, PsbZ, and Psb30 (Komenda *et al.* 2012b). Therefore, the deletion of Psb27 protein was also performed in combination with the LMW proteins of CP43 pre-assembly complex (Psb30, PsbK, and PsbZ) to see if these proteins play any cooperative roles, as in the past no studies have been carried out on the effect of the deletion of the Psb27 protein along with the LMW proteins of CP43 preassembly complex.

.

Chapter Two

Materials and Methods

2.1 Chemicals

The chemicals, reagents, and materials used for this study were of analytical grade. They were obtained from various brands like Sigma-Aldrich, Inc., USA; ChemService, USA; Scientific Supplies Ltd., New Zealand; AJAX chemicals, Australia; BioRad, USA; Serva, Germany, DBH Chemicals Ltd., England, Scharlau Chemie, Spain.

2.2 Microbial strains

2.2.1 Escherichia coli

The *Escherichia coli* (*E. coli*) DH5α was used as the primary strain for carrying out most of the basic molecular cloning and genetic engineering work in this investigation. The DH5α strain was obtained from Invitrogen (Netherlands). The cells were maintained on LB plates (discussed in section 2.6.1.1) at 4°C for a short course of time or stored at -80°C in glycerol stocks.

2.2.2 *Synechocystis* sp. PCC 6803

The glucose-tolerant strain of Williams is referred to throughout as wild type (Williams 1988). It is a unicellular transformable cyanobacterium and has been a very popular model organism used for studying photosynthesis, respiration and other forms of metabolism, as its whole genome has been sequenced (Kaneko *et al.* 1996b).

Wild type and the mutants were derived from *Synechocystis* 6803 and grown mixotrophically in BG-11 medium (discussed in section 2.6.1.2) (Rippka *et al.* 1979) under constant illumination of 35 $\mu E.m^{-2}s^{-1}$, with constant aeration at 30°C in modified Erlenmeyer flasks. All cultures were maintained on solid BG-11 media (discussed in section 2.6.1.2) (Fagerlund and Eaton-Rye 2011b). The antibiotics used were chloramphenicol (25 $\mu g.ml^{-1}$), spectinomycin (25 $\mu g.ml^{-1}$) and kanamycin (25 $\mu g.ml^{-1}$). All the strains (discussed in section 2.9) made in this study were deposited in a laboratory culture collection in BG-11 with 15% glycerol at -80°C.

2.3 Oligonucleotide/primers

DNA constructs and oligonucleotide primers were obtained from either Sigma-Aldrich (Singapore) or Integrated DNA Technologies (Singapore) and designed using SnapGene molecular cloning software. Table 2.1 provides the information about the primers utilised in this project.

Table 2.1 List of the oligonucleotides used in this studies

Primer Name	Primer Sequences (5'- 3')
ΔPsb27	
Psb27_LF_fwd	TACCTCAGTCAAAATCGCC
Psb27_LF_rev	GTGGAGGTAATAATTGACAGCCGTGACAACTGATTTTTC
Psb27_RF_fwd	GAAAAATCAGTTGTCACGGCTGTCAATTATTACCTCCAC
Psb27_RF_rev	GGTTTCTTACGTCAGGTGGCACCTGGAATTTACCCAGGCAG
CmR_fwd	GTGCCTGGGTAAATTCCAGGTGCCACCACCTGACGTCTAAGAAACC
CmR_rev	ATGGTCGGCACTAGTTTTGG
Psb27 control	
Psb27_fwd	GCAAGAACCTAGCCAAGGC
Psb27_rev	CATGCCAGTGAGGGGAATGAG
Psb27_*Bam*HI_fwd	GCAAAAATTGCTAGTCTGGATCCTAAAAATTATCTTTGAGTCTTCC
Psb27_*Bam*HI_rev	GGAAGACTCAAAGATAATTTTTAGGATCCAGACTAGCAATTTTTGC
Psb27 mutants	
D14A_fwd	CGGCAACTATAGCCAAGCTACCCTGACGGTCATTG
D14A_rev	CAATGACCGTCAGGGTAGCTTGGCTATAGTTGCCG
R54E_fwd	AATGACTATATTTCCCGTTACGAGCGCAAAGGTGATGCCGGTGG

R54E_rev	CCACCGGCATCACCTTTGCGCTCGTAACGGGAAATATAGTCATT
Y78H_fwd	CTCAACTCCCTGGCTGGACACTACACTTCCTACG
Y78H_rev	CGTAGGAAGTGTAGTGTCCAGCCAGGGAGTTGAG
R94E_fwd	CCCATTCCCGAAAAGCTGAAAAAAGAGTTACAACTGGAATTTACCCAG
R94E_rev	CTGGGTAAATTCCAGTTGTAACTCTTTTTTCAGCTTTTCGGGAATGGG
E98R_fwd	GCTGAAAAAACGCTTACAACTGAGATTTACCCAGGCAGAAAGATCC
E98R_rev	GGATCTTTCTGCCTGGGTAAATCTCAGTTGTAAGCGTTTTTTCAGC
D58A_fwd	CGTTACCGTCGCAAAGGTGCCGCCGGTGGGCTGAAATCC
D58A_rev	GGATTTCAGCCCACCGGCGGCACCTTTGCGACGGTAACG
D58E_fwd	CGTTACCGTCGCAAAGGTGAGGCCGGTGGGCTGAAATCC
D58E_rev	GGATTTCAGCCCACCGGTCACACCTTTGCGACGGTAACG
D58K_fwd	CGTTACCGTCGCAAAGGTAAGGCCGGTGGGCTGAAATCC
D58K_rev	GGATTTCAGCCCACCGGCCTTACCTTTGCGACGGTAACG
K63A_fwd	GGTGATGCCGGTGGGCTGGCATCCTTTACCACCATGCAAACG
K63A_rev	CGTTTGCATGGTGGTAAAGGATGCCAGCCCACCGGCATCACC
K63D_fwd	GGTGATGCCGGTGGGCTGGACTCCTTTACCACCATGCAAACG
K63D_rev	CGTTTGCATGGTGGTAAAGGAGTCCAGCCCACCGGCATCACC
K63R_fwd	GGTGATGCCGGTGGGCTGAGGTCCTTTACCACCATGCAAACG
K63R_rev	CGTTTGCATGGTGGTAAAGGACCTCAGCCCACCGGCATCACC

ΔPsb30	
Psb30_US_fwd	CCTAGAAGAAATTCGGCAACTGTTGC
Psb30_DS_rev	GGCAGCCCGTTGCAAGATTAAGTC
Psb30_KanR_US_fwd	GCTTTGTTGAATAAATCGAGTGCGGCTAATAATTCC
Psb30_KanR_DS_rev	GCGCTATTCTGACCTGATCTATAGACTATGC
Psb30_KanR_fwd	GGAATTATTAGCCGCACTCGATTTATTCAACAAAGCCACG
Psb30_KanR_rev	ATAGTCTATAGATCAGGTCAGAATAGCGCTGAGGTCTGC
ΔPsbK	
PsbK_US_fwd	CCGTTCAACTGTTGTTTAACTGTC
PsbK_DS_rev	CTGGCTTTGGTCACCGATGGCCCA
PsbK_KanR_US_fwd	GTTCTGCTATGTGGCGAGCAAATAAATTGTTTCC
PsbK_KanR_DS_rev	CCGCAAGCGACAGGTTAAATAAACTGGCGATCGC
PsbK_KanR_fwd	GGAAACAATTTATTTGCTCGCGATTTATTCAACAAAGCCACG
PsbK_KanR_rev	GCGATCGCCAGTTTATTTAAAGGTCAGAATAGCGCTGAGGTCTGC
ΔPsbZ	
PsbZ_US_fwd	CCATCCTTTGGACCAAATGGCCAC
PsbZ_DS_rev	GCCATCCAAGCCATATCGGCGTTA
PsbZ_KanR_US_fwd	GCTTTGTTGAATAAATCTATGTGCCCTGAGGGAAGCACATAGC
PsbZ_KanR_DS_rev	GCGCTATTCTGACCTCTGTTGAACTTCCTGGTCGTCTAG

PsbZ_KanR_fwd	ATGTGCTTCCCTCAGGGCACATAGATTTATTCAACAAAGCCACG
PsbZ_KanR_rev	TAGACGACCAGGAAGTTCAACAGAGGTCAGAATAGCGCTGAGGTCTGC
PsbA2 mutants	
PsbA2_H252A_fwd	CTACAACATCGTTGCCGCCGCCGGCTACTTTGGTCGGTTG
PsbA2_H252A_rev	CAACCGACCAAAGTAGCCGGCGGCGGCAACGATGTTGTAG
PsbA2_H252H_fwd	CATCGTTGCCGCCCATGGCTACTTTGGTCG
PsbA2_H252H_rev	CGACCAAAGTAGCCATGGGCGGCAACGATG
PsbA2_H252Q_fwd	CATCGTTGCCGCCCAAGGCTACTTTGGTCG
PsbA2_H252Q_rev	CGACCAAAGTAGCCTTGGGCGGCAACGATG
PsbA2_H252Y_fwd	CAACATCGTTGCCGCCTACGGCTACTTTGGTCGG
PsbA2_H252Y_rev	CCGACCAAAGTAGCCGTAGGCGGCAACGATGTTG
PsbA2_S264A_fwd	GATCTTCCAATATGCTGCTTTCAACAACAGCC
PsbA2_S264A_rev	GGCTGTTGTTGAAAGCAGCATATTGGAAGATC
PsbA2_S264K_fwd	GGTTGATCTTCCAATATGCTAAGTTCAACAACAGCCGTTCCTTG
PsbA2_S264K_rev	CAAGGAACGGCTGTTGTTGAACTTAGCATATTGGAAGATCAACC
PsbA2_S264T_fwd	GATCTTCCAATATGCTACTTTCAACAACAGCCG
PsbA2_S264T_rev	CGGCTGTTGTTGAAAGTAGCATATTGGAAGATC
Plasmid primers for sequencing	
pJET_fwd	CGACTCACTATAGGGAGAGCGGC

pJET_rev	AAGAACATCGATTTTCCATGGCAG
M13_fwd	TGTAAAACGACGGCCAGT
M13_rev	CAGGAAACAGCTATGACC
Antibiotic cassette sequencing primers	
KanR_US	CGACAACGCAGACCGTTCCGTG
KanR_DS	GCCAAACTATCAGGTCAAGTCAAGC
KanR_int_fwd	CCTGCGCCGGTTGCATTCGATTCC
KanR_int_rev	CAAGTGAGAAATCACCATGAGTGAC
SpecR_US	CAAGGATCTGGATTTCGATCACGGC
SpecR_DS	GCATAATAAGCCCTACACACAAATTGG
SpecR_int_fwd	CTGCTCGCGCAGGCTGGGTGCCAAG
SpecR_int_rev	CGGATGTTGCGATTACTTCGCCAAC
CmR_US	GTGCCCTTAAACGCCTGGTGCTACG
CmR_DS	CCTCTTACGTGCCGATCAACGT

*The highlighted residues in yellow corresponds to the residues which were mutated using site-directed mutagenesis.

LF: left flanking, RF: right flanking, fwd: forward, rev: reverse, US: upstream, DS: downstream, Int: internal, CmR: chloramphenicol resistance, KanR: kanamycin resistance, SpecR: spectinomycin resistance

2.4 General techniques

For all the media and solution preparation, standard microbial sterilisation techniques were used. MilliQ water (typically 18.2 MΩcm at 25°C) was utilised for the preparation of the media and the solutions. Standard autoclaving (121°C, 15 psi, 20 min cycle) conditions were used for making sterile solutions and media. Most of the microbiological work was carried out in biosafety laminar cabinets – vertical as well horizontal types. All the enzymes, their buffers, and the DNA samples were stored at -20°C.

2.5 Molecular biology techniques

2.5.1 Genomic DNA (gDNA) isolation from *Synechocystis* 6803

The gDNA extraction protocol was adapted from the protocol of Prof. Jack Meek`s lab (Microbiology section, University of California at Davis). The liquid culture of *Synechocystis* 6803 was grown to an optical density at 730 nm (OD_{730}) to ~0.8-1.0 in 150 ml of modified Erlenmeyer flasks. One hundred millilitres of culture were harvested by centrifuging at 5000 *g* (Beckman centrifuge, swinging bucket rotor, JS 7.5). The cell pellet was washed twice with 5 M sodium chloride (NaCl) to remove the polysaccharides. The pellet was re-suspended in 1 ml of Tris-EDTA (TE) buffer and incubated at 37°C for 1 h in the presence of 1 ml of lysozyme enzyme (20 $mg.ml^{-1}$) (Sigma-Aldrich, USA). A one-hour incubation was followed by addition of 0.5 ml of 0.5 M ethylenediaminetetraacetic acid (EDTA) (pH 8.00). The cell lysate was incubated at 37°C with 1 ml of proteinase K solution (2 $mg.ml^{-1}$) (Roche, Germany) and 0.1 ml of 20% sodium dodecyl sulfate (SDS), followed by addition of the $1/6^{th}$ volume of 5 M NaCl and $1/8^{th}$ volume of cetyltrimethylammonium bromide (CTAB) solution. The cell lysate was heated to 65°C for 10 min. Centrifugation was carried out to pellet the cell debris at 10000 *g* for 10 min at room temperature (Beckman centrifuge, swinging bucket rotor, JS 7.5). The supernatant was treated with 1:1 chloroform solution for 30 min to extract the nucleic acids, followed by centrifugation at 5000 *g* for 5 min (Beckman centrifuge, swinging bucket rotor, JS 7.5). The DNA was precipitated from the supernatant with the help of 2× volume of 95% cold ethanol followed by centrifugation at 10000 *g* for 5 min (Beckman centrifuge, swinging bucket rotor, JS 7.5). The pellet was dried and dissolved in 0.5 ml of TE buffer and treated

with 2 µl of 10 mg.ml^{-1} RNase A (Roche, Germany) at 37°C for 30 min, to degrade RNA and this was followed by extraction with an equal volume of phenol:chloroform mix. The DNA was precipitated by adding the 1/10th volume of 3 M sodium acetate (pH 5.2) and 2× volume of 95% ethanol while incubated at -20°C for 1 h, followed by centrifugation at 12000 *g* for 10 min at 4°C. The DNA pellet was washed with 70% ethanol and the pellet was dried with heat block at 37°C for 10 min. In the end, the DNA pellet was dissolved in 250 µl of TE buffer.

TE buffer – 10 mM Tris-HCl pH 8.0; 1 mM EDTA

Lysozyme – 20 mg.ml^{-1} in TE

Proteinase K – 2 mg.ml^{-1} in TE

CTAB solution – 10% CTAB; 0.7 M NaCl

2.5.2 Plasmid DNA extraction from *E. coli* cells

Plasmid DNA extraction from *E. coli* was carried out using the alkaline lysis method (Birnboim and Doly 1979; Sambrook and Russell 2006). The transformed bacterial single colony was grown in 2 ml of LB overnight, and the culture was harvested by centrifugation at 12000 *g* for 1 min. The pellet was resuspended in 0.1 ml of solution 1 containing lysozyme (2 mg.ml^{-1}) followed by addition of 0.2 ml of solution 2 and 0.15 ml of solution 3. The samples were centrifuged at 12000 *g* for 5 min followed by extraction with 0.1 ml of 1:1 chloroform:phenol mix. The samples were centrifuged again at 12000 *g* for 5 min. The supernatant (~0.3 ml) was transferred to a new Eppendorf tube and washed with 0.18 ml of 100% isopropanol for 10 min at room temperature followed by centrifugation at 12000 *g* for 10 min. The cell pellet was washed with 0.8 ml of 70% ice-cold ethanol and centrifuged again at 12000 *g* for 1 min and the pellet dried on 37°C heat block for 10 min. Finally, the cell pellet was resuspended in 1 ml TE buffer and treated with 2 µl of 10 mg.ml^{-1} RNase A to remove the RNA contamination. The final samples were then stored in -20ºC or analysed further.

TE buffer – 10 mM Tris-HCl pH 8.0; 1 mM EDTA

Solution 1 – 50 mM glucose; 25 mM Tris pH 8 10 mM EDTA

Solution 2 – 0.2 M NaOH; 1% SDS

Solution 3 – 5 M potassium acetate; 3 M glacial acetic acid

2.5.3 Polymerase chain reaction (PCR)

Standard PCR – PCR reactions for amplification and cloning purposes were performed as per the manufacturer's instructions in a 50 µl volume, containing 5 µl 10× reaction buffer, 1.5 µl 50 mM magnesium chloride ($MgCl_2$), 1 µl 10 mM deoxynucleotides (dNTPs), 1 µl each primer (10 µM) (forward and reverse), 1 µl DNA template, sterile ultrapure distilled water to a total volume of 49.5 µl and 0.5 µl of high fidelity Taq polymerase (Roche, Germany). The template DNA was extracted with the gDNA extraction protocol described in section 2.5.1. The template DNA was used at a concentration of 200 ng.µl^{-1} and 300-500 ng.µl^{-1} for plasmid DNA template. All the PCR reactions were performed with an Eppendorf Master gradient thermal cycler. Typically, 30 cycles of amplification were performed using empirically determined annealing and extension parameters. The denaturation temperature was 95°C and the extension temperature 68°C.

Quick change mutagenesis PCR – Quick change mutagenesis (Kunkel 1985; Sugimoto *et al.* 1989) PCR reactions were performed as per the manufacturer's instructions in a 50 µl volume, containing 5 µl 10× reaction buffer, 1 µl 10 mM dNTP mix, 1.5 µl of each primer (10 µM), ~80 µg of plasmid DNA template, sterile ultrapure distilled water to a total volume of 49.5 µl and 0.5 µl of Pfu DNA polymerase (Agilent Technologies). The template plasmid DNA was used at a concentration of 80-100 ng. All the PCR reactions were carried out with an Eppendorf Master gradient thermal cycler. Typically, 18 cycles of amplification were performed using empirically determined annealing and extension parameters. The denaturation temperature was 95°C and the extension temperature 68°C.

Colony PCR - Colony PCR was used to verify the segregation of *Synechocystis* 6803 mutants from the whole cells. Standard PCR conditions were used, except the template DNA was replaced by addition of 1-2 µl of cells (consisting of a few colonies) diluted in 20 µl of distilled water. The initial denaturation period of the PCR reaction was extended to 5 min to ensure the proper lysis of the cells. High fidelity Taq polymerase (Roche, Germany) was used. Typically, 30-35 cycles of amplification were performed

using empirically determined annealing and extension parameters. The denaturation temperature was 95°C and the extension temperature 72°C.

2.5.4 Restriction digestion

Restriction enzymes were obtained from New England Biolabs (USA) or Roche (Germany). Restriction digestion was carried out using manufacturer's instructions in a total volume of 10 µl containing 3-5 µg of DNA. Typically, 0.5 µl or 1 unit of restriction enzyme was used per microgram of DNA, and the samples were incubated at the indicated temperature for 60-90 min.

2.5.5 Ligations

Ligations into vectors of interest (pGEM T-Easy (Promega. Madison, USA), pJET Promega. Madison, USA or pUC19 (Yanisch-Perron *et al.* 1985)) were carried out using 3-5 units of T4 DNA ligase (Promega, USA) using ligation buffer containing DNA fragment of interest and vector DNA in 1:3 ratios. Typically, ~150 ng of DNA insert was ligated into 50 ng of vector in a 10 µl reaction. The ligation reactions were performed overnight at 22°C and then were used for transforming into competent DH5α cells as described in section 2.6.2.2. Two kinds of ligations were carried out:

Sticky end ligation – For filling recessed 3` termini (e.g., *Hin*dIII, *Eco*RI digests), the DNA samples were treated with 1 mM dNTPs and 1 unit of Klenow (Roche, Germany) per µg DNA. The samples were incubated for 15 min at room temperature and the enzyme heat inactivated at 75°C for 10 min.

Blunt-end ligation – For removing protruding 3` termini (e.g., *Pst*I), the DNA sample was treated with 2 mM dNTPs and 1-2 units of T4 DNA polymerase (Roche, Germany) per µg DNA, incubated for 15 min at 12°C and then the enzyme was heat inactivated at 75°C for 10 min.

2.5.6 DNA purification

Typically, the PCR products and the restriction digested DNA fragments were purified from reaction mixtures using PureLink spin columns (Invitrogen, USA) as per the manufacturer's instructions. DNA was eluted in a final volume of 20 µl and quantified by UV-Vis spectrophotometry.

2.5.7 Agarose gel electrophoresis

DNA samples were visualised by agarose gel electrophoresis using 0.8% to 1.0% agarose gels and 0.30 $\mu g.ml^{-1}$ ethidium bromide in 1× Tris/Borate/EDTA (TBE) buffer. Typically, 10-12 µl of samples containing 1-2 µl of DNA sample and 2 µl of 6× DNA loading buffer (New England BioLabs) were loaded into the wells and run at 100 V for 50 min. One microlitre of 1 Kb plus DNA ladder (1 $\mu g.\mu l^{-1}$) (Invitrogen, USA) was loaded onto the gel to determine the sizes of the DNA samples of interest. Gels were visualised and documented with UV transilluminator (Kodak) and the Kodak imaging software.

50× TBE buffer – 0.5 M Tris; 0.5 M acetic acid; 10 M EDTA

6× DNA loading buffer – 1.5% bromophenol blue; 1.5% xylene cyanol FF; 30% glycerol

2.5.8 Spectroscopic Quantification

Protein and DNA concentrations were quantified by absorption spectroscopy using a Nanodrop ND-2000 UV-VIS spectrophotometer (Biolabs Ltd, USA) with a 1.5 µl sample.

2.5.9 Sanger-dideoxy sequencing

The sequencing of the plasmid or DNA constructs was carried out by Genetic Analysis Services (Dept. of Anatomy, University of Otago, New Zealand) by employing the chemistry BigDye Terminator Version 3.1 Ready Reaction Cycle Sequencing Kit. Sequencing samples were prepared in total volume of 5 µl with the following final concentrations: primer concentration = 3.2 $pmol.5\ \mu l^{-1}$; PCR sample concentration = 1 ng/100 bp/5 µl and plasmid concentration = 150 $ng.5\ \mu l^{-1}$ for plasmids up to 4 kb and 200 $ng.5\ \mu l^{-1}$ for larger plasmids. DNA was sequenced on an ABI 3730X1 DNA analyser, and the sequencing data was analysed using SnapGene software.

2.6 Growth and maintenance of microbial strains

2.6.1 Media used

2.6.1.1 *E. coli*

LB – 1% bactotryptone; 0.5% yeast extract; 1% NaCl and 1.5% agar (for solid media).

ΨB media – 2% bactotryptone; 0.5% yeast extract; 10 mM potassium chloride (KCl); 34 mM magnesium sulfate ($MgSO_4$); adjusted to pH 7.6 with potassium hydroxide (KOH). Sterile $MgSO_4$ added after autoclaving.

Antibiotics – Antibiotics were added to solid and liquid media as per the following final concentrations: Ampicillin (25 $\mu g.ml^{-1}$): made in water and filter sterilised, stored at 4°C; kanamycin (50 $\mu g.ml^{-1}$): made in water and filter sterilised, stored at 4 °C; spectinomycin (50 $\mu g.ml^{-1}$): made in water and filter sterilised stored at 4°C; chloramphenicol (30 $\mu g.ml^{-1}$): made in ethanol and stored at -20°C.

2.6.1.2 *Synechocystis* 6803

100× BG-11 (without iron, phosphate and carbonate) – 1.76 M sodium nitrate ($NaNO_3$); 30.4 mM magnesium sulfate heptahydrate ($MgSO_4.7H_2O$); 24.5 mM calcium chloride dihydrate ($CaCl_2.2H_2O$); 2.86 mM citric acid ($C_6H_8O_7$); 220 µM EDTA (pH 8.0); 10% trace minerals (v/v).

Trace minerals stock – 46.26 mM boric acid (H_3BO_3); 8.9 mM manganese chloride tetrahydrate ($MnCl_2.4H_2O$); 770 µM zinc sulfate heptahydrate ($ZnSO_4.7H_2O$); 320 µM copper sulfate pentahydrate ($CuSO_4.5H_2O$); 170 µM cobalt nitrate hexahydrate ($Co(NO_3)_2.6H_2O$)

BG-11 media – 1× BG-11; 6 $\mu g.ml^{-1}$ ferric ammonium citrate ($C_6H_8FeNO_7$); 20 $\mu g.ml^{-1}$ sodium carbonate (Na_2CO_3); 30.5 $\mu g.ml^{-1}$ dipotassium hydrogen orthophosphate (K_2HPO_4).

BG-11 media (pH 7.5) – 1× BG-11 media described above and then adjusted to pH 7.5 with 25 mM 4-(2-hydroxyethyl)-1-piperazineethanesulfonic acid/sodium hydroxide (HEPES/NaOH).

BG-11 solid agar plates - 1× BG-11; 6 µg.ml^{-1} $C_6H_8FeNO_7$; 20 µg.ml^{-1} Na_2CO_3; 30.5 µg.ml^{-1} K_2HPO_4; 10 mM 2-[Tris(hydroxymethyl)-methylamino]-ethanesulfonic acid-sodium hydroxide (TES-NaOH) (pH 8.2); 0.3% sodium thiosulfate ($Na_2S_2O_3$) and 1.5% agar (Fagerlund and Eaton-Rye 2011b).

The distilled water containing all the chemical ingredients were mixed with magnetic bead on magnetic stirrer.

2.6.2 E. coli

2.6.2.1 Preparation of competent cells of *E. coli*

A single colony of freshly cultured DH5α was inoculated in 10 ml of LB media, followed by incubation at 37°C on a shaker overnight. One millilitre of the above-grown culture was transferred to two sterile conical flasks containing 100 ml pre-warmed ΨB media and incubated for two h with shaking at 37°C until the OD_{600} reaches ~0.3-0.4. Then, the cells were kept on ice for 5 min followed by harvesting of cells by centrifugation at 2760 *g* at 4°C in IEC table top centrifuge. The supernatant was discarded, and the pellet was resuspended in 15 ml of transformation buffer I (TfBI). After, resuspension, cells were centrifuged at 2760 *g* for 10 min at 4°C in IEC table top centrifuge. The pellet was resuspended gently in 2 ml of chilled transformation buffer II (TfBII). The cells were then snap-frozen using dry ice and ethanol and stored in -80°C for future use.

TfBI – 30 mM potassium acetate (KAc); 100 mM potassium chloride (KCl); 10 mM calcium chloride ($CaCl_2$); 50 mM manganese chloride ($MnCl_2$); 15% glycerol; pH adjusted to 5.8 with 0.2 M acetic acid (CH_3COOH).

TfBII – 10 mM 3-(N-morpholino) propanesulfonic acid (MOPS); 75 mM $CaCl_2$; 10 mM rubidium chloride ($RbCl_2$); 15% glycerol.

2.6.2.2 Transformation of competent *E. coli* cells

E. coli transformation was performed using the heat-shock transformation method (Van Die *et al.* 1983). Transformations were carried out in 200 µl aliquots of cells with 1 µl of the plasmid. Cells were incubated on ice for 30 min after the addition of plasmid DNA. The cells were given a short heat shock treatment at 40°C for 3 min followed by

the incubation on ice for 3 min or more. Then, the cells were added to 2 ml of LB in a sterile test tube and incubated at 37°C on the shaker for 90 min at 150 rpm. The cells were concentrated by spinning them down at 12000 *g* for 30 s in a microfuge. The pellet was resuspended in 200 µl of LB and plated onto LB plates containing the appropriate antibiotics. Typically, a transformation efficiency of ~4 × 10^8 cfu.µg^{-1} was achieved, determined by transformation of 1 ng of pUC19 vector.

2.6.3 *Synechocystis* 6803

2.6.3.1 Cyanobacterial Transformation

Starter cultures were grown as described in section 2.7.1 to an OD_{730} of ~0.8-1.0. Cells were harvested by centrifugation at 2760 *g* for 8 min at 22°C and subsequently resuspended in 500 µl BG-11 to an OD_{730} of 2.5. Five hundred microliter of cells were placed in a sterile test tube along with 10-50 µg of plasmid DNA and incubated for 6 h at 30°C under standard white light (30 µE.m^{-2}s^{-1}) on a shaker (50-100 rpm). Samples were then spread over BG-11 plates containing sterile filters and glucose for overnight incubation, and then the filter containing the culture was transferred to a new selective medium with glucose and appropriate antibiotics. Plates were incubated at 30°C under standard white light (30 µE.m^{-2}s^{-1}) until colonies of transformants appeared. Transformed colonies were picked and re-streaked for successive generations until complete segregation could be verified by colony PCR (Fagerlund and Eaton-Rye 2011b).

2.7 Physiological characterisation of *Synechocystis* 6803 strains

2.7.1 Starter cultures

Synechocystis 6803 starter cultures were grown in the presence of 5 mM glucose with constant aeration to an OD_{730} of 0.8-1.0 (measured with a Jasco V-550 UV/Vis spectrophotometer; Jasco International). Cells were harvested using centrifugation at 2760 *g* for 8 min at 24°C and resuspended in BG-11 to a volume of 3-5 ml and then used for inoculating into working cultures of 150 or 300 ml volume. Cultures were acclimatised under normal growth conditions without aeration for 3-4 h after which the aeration of the cultures was begun.

2.7.2 Photoautotrophic growth

The cells were grown and harvested as discussed in section 2.7.1. The cells were then washed twice with BG-11 (pH 7.5) and resuspended in BG-11 to a volume of 3-5 ml. Cultures were then inoculated in modified Erlenmeyer flasks containing 150 ml of BG-11 to a final OD_{730} of ~0.05. The cultures were grown under the constant light of 35 $\mu E.m^{-2}s^{-1}$ at 30°C without glucose. The OD at 730 nm of the cultures was measured every 12 h for seven days. The data collection and data normalisation was performed as described in reference (Bentley *et al.* 2008a) . However, the doubling time of the strains were calculated as per the following equation from the Roth V. 2006 Doubling Time Computing, Available from: http://www.doubling-time.com/compute.php.

Doubling Time = duration ∗ log (2)/log (final concentration) − log (initial concentration).

Where "log" is the logarithm to base 10.

2.7.3 Analysis of chlorophyll *a* concentration

The concentration of chlorophyll *a* in each sample was determined by absorption at 663 nm (a concentration of 1 $mg.ml^{-1}$ chlorophyll *a* corresponds to an A_{663} of 82). It was measured with a Jasco V-550 UV/Vis spectrophotometer; Jasco International) in methanol (10 µl cells in 1 ml methanol, centrifuged at 15000 *g* for 5 min) and adjusted to 5 $\mu g.ml^{-1}$ with new BG-11 media.

2.7.4 Oxygen evolution

Cells were grown in BG-11 with 5 mM glucose to an OD_{730} ~0.8-1.0 and harvested using centrifugation (2850 *g* for 8 min). The cells were washed once with BG-11 containing 25 mM HEPES-NaOH, pH 7.5. The cells were then maintained in BG-11 at 30°C at chlorophyll *a* concentration of 5 $\mu g.ml^{-1}$ for 20 min with constant shaking at 200 rpm. Oxygen evolution of 1 ml of cells was measured using a Clarke-type electrode (Hansatech, King's Lynn, UK) maintained at 30°C by a recirculating water bath using 2,5-dimethyl-p-benzoquinone (0.2 mM DMBQ) or 2,5-dichloro-1,4-benzoquinone (0.2 mM DCBQ) with 1 mM potassium ferricyanide ($KFe(CN)_6$) or alternatively 15 mM sodium bicarbonate as the electron acceptors. Saturating illumination (red light at an intensity of 5000 $\mu E.m^{-2}s^{-1}$ of the sample was provided by the FLS1 tungsten bulb light

source (Hansatech, UK) equipped with a 580 nm long-pass filter (Melles-Griot, USA). Illumination was carried out as follows - 3 min pre-record, 1 min with the light off, 4 min light on and 1 min light off. The rate of oxygen evolution per hour per mg chlorophyll *a* was calculated based on the initial slope (30 s) for DCBQ and DMBQ artificial quinone acceptors and initial slope (90 s) for bicarbonate after the illumination; assuming that oxygen saturated water contains 0.235 µmol of oxygen per ml at 30°C (Truesdale and Downing 1954) using the formula described below. The oxygen evolution traces shown in the results chapter are average of three independent biological replicates. The data collection and data normalisation was performed as described in reference (Bentley *et al.* 2008a).

Rate (µmol O_2.mg $Chl^{-1}.h^{-1}$) = (0.235 µmol.ml^{-1})*(sample volume, ml)*(60 $min.h^{-1}$)*(slope, $mV.ml^{-1}$/(calibration voltage, mV)*(Chl *a*, $mg.ml^{-1}$)

The raw data in triplicate for the oxygen evolution rate has been shown in appendix

Slope calculation in detail

Oxygen evolution was determined in the presence of the either DCBQ or DMBQ by determining the rate of oxygen evolution between 30 s and 60 s after the actinic light was turned on. These times points correspond to the maximum slope of the measurement obtained with these electron acceptors (Burnap and Sherman 1991) (Appendix, Section L, Fig. A.2, A.3, A.4 and A.5). When bicarbonate was used as the electron acceptor the rate of oxygen evolution was determined between 60s and 90 s after the actinic light was turned on as this corresponds to the maximum slope obtained when bicarbonate is used (Burnap and Sherman 1991) and (Appendix, Section L, Fig. A.2, A.3, A.4 and A.5).

2.7.5 77 K fluorescence emission spectroscopy

Cells were grown, harvested, resuspended and incubated as per the oxygen measurement protocol discussed in section 2.7.4 at a chlorophyll *a* concentration of 5 $\mu g.ml^{-1}$. A small volume of the portion of the cells was diluted immediately before analysis by mixing 0.5 ml of cell suspension with 0.5 ml of BG-11 in an Eppendorf tube. Then, 0.5 ml of diluted cells (2.5 $\mu g.ml^{-1}$) from the Eppendorf tube were transferred to a thin glass capillary tube (4 mm internal diameter, 6 mm external diameter) and frozen in liquid nitrogen slowly. For data collection with an excitation

wavelength of 440 nm, the excitation and emission slit widths were set at 12 and 2 nm, respectively. For excitation, at 580 nm the slit widths were set at 8 nm and 2 nm. The scan speed was set to 4, which corresponds to a rate of ~100 $nm.min^{-1}$. The spectral data were averaged before curve fitting and normalisation to the PS I peak. The data were recorded between the wavelength range of 600-800 nm. The data collection, data normalisation and data analysis was performed as described in reference (Jackson and Eaton-Rye 2015).

2.7.6 Room temperature chlorophyll *a* fluorescence

2.7.6.1 Variable chlorophyll *a* induction and decay measurements

Cells were grown in BG-11 with 5 mM glucose to an OD_{730} of 0.8-1.0 and harvested using centrifugation (2850 *g* for 8 minutes). The cells were washed once with BG-11 containing 25 mM HEPES-NaOH, pH 7.5. The cells were then maintained in BG-11 at 30°C at a chlorophyll *a* concentration of 5 $\mu g.ml^{-1}$ for 20 min with constant shaking at 200 rpm. Chlorophyll *a* fluorescence measurements were performed using an FL-3500 double modulation fluorometer (PSI instruments, Czech Republic) by employing a single blue measuring flash (BMF-455 nm) actinic illumination. Cells were diluted to a final chlorophyll *a* concentration of 2.5 $\mu g.ml^{-1}$ with BG-11 up to a volume of 2 ml and dark adapted for 8 min in 3 ml transparent plastic cuvettes before measurement. Four BMF pulses, each with an interval of 200 ms apart, were used to calculate the initial fluorescence (F_o) of dark-adapted samples, followed 200 µs later by a 30 µs saturating actinic flash and then followed by a sequence of multiple measuring low-intensity flashes beginning 50 µs after the actinic flash. The samples were measured in the presence and absence of 50 µM 3-(3,4-dichlorophenyl)-1,1-dimethylurea (DCMU). The data collection, data normalisation and data analysis was performed as per the standard method used in cyanobacterial field. The data collection, data normalisation and data analysis was performed as described in reference (Jackson and Eaton-Rye 2015).

2.7.6.2 Analysis of chlorophyll *a* fluorescence decay kinetics

Analysis of the decay of chlorophyll fluorescence following one or more actinic flashes in the absence of DCMU was carried out by the fitting two exponential phases and one hyperbolic phase as per the following equation (Vass *et al.* 1999; Cser and Vass 2007).

$F_{(t)} - F_o = A_1 \exp(-t/T_1) + A_2 \exp(-t/T_2) + A_3/(1+t/T_3)$

Where F(t) is the variable fluorescence at a time point after the saturating single turnover flash, F_o is the initial fluorescence before the saturating single-turnover flash, A_1, A_2, and A_3 are the percentage amplitudes of each component of the decay and T_1, T_2 and T_3 are the time constants from which the half time for the exponential phase can be calculated as $T_{1/2} = (\ln_{(2)}/T_n)$. For hyperbolic phase, it can be calculated as $T_{1/2} = T_3$ (Vass *et al.* 1999). Using this model, the fast phase (200-400 µs) consists of electron transfer from Q_A^- to Q_B. The intermediate phase (milliseconds) reflects the binding of the plastoquinone molecule to the Q_B site and the slow phase (seconds) reflects charge recombination between Q_A^- and the donor side of PS II.

The analysis of the decay of chlorophyll fluorescence after a single actinic flash in the presence of DCMU was carried out by fitting one exponential phase and one hyperbolic phase according to the following equation (Fufezan *et al.* 2007).

$F_{(t)} - F_o = A_1 \exp(-t/T_1) + A_3/(1+t/T_3) + c$

Where A_1, A_3 are the amplitudes of each component and T_1, T_2 are the time constants, from which the half time for the exponential phase can be calculated as $T_{1/2} = (\ln_{(2)}/T_n)$ and for hyperbolic phase, it can be calculated as $T_{1/2} = T_3$, c is a constant. Curve fitting was performed with the help of SciDavis and Prism. The data collection, data normalisation and data analysis was performed as per the standard method used in cyanobacterial field.

2.7.7 Photoinhibition

2.7.7.1 Oxygen evolution

To study the susceptibility of the *Synechocystis* 6803 mutants to the high-light, cells were suspended to final chlorophyll *a* concentration of 10 µg.ml^{-1} in BG-11 and allowed to acclimatise for 20 min with constant stirring at 200 rpm before measurements. The cells were subjected to high-intensity white light of 2000 ± 100 µE.m^{-2}s^{-1} using an Ektalite slide projector (Kodak, USA) for up to 45 min and this was followed by recovery under normal white light (35 µE.m^{-2}s^{-1}) in the culture room for a further 180 min. PS II activity was measured using oxygen evolution in the presence of different electron acceptors as described in section 2.7.4. The oxygen evolution of each

sample was measured after every 15 min of incubation. The data collection, data normalisation and data analysis were performed as described in reference (Bentley *et al.* 2008a).

2.7.7.2 Measurement of decay of chlorophyll *a* fluorescence

Photoinactivation and recovery assay measurements were also performed for flash-induced chlorophyll *a* fluorescence relaxation in the presence or absence of 40 µM DCMU. The blue measuring flash light was used to measure the fluorescence yields. Four measuring flashes at a time interval of 200 µs was used to determine the initial fluorescence (F_o). The wild type and the mutant cells were prepared and suspended to a chlorophyll *a* concentration of 5 $\mu g.ml^{-1}$ as described previously in chlorophyll *a* fluorescence induction measurements section (section 2.7.6.1). The cells were subjected to high-light treatment for 45-60 min and then allowed to recover in low light for 180 min. The cells were harvested at a time interval of 15 min, and their fluorescence decay kinetics were measured. The sequential PS II turnover was also analysed by measuring fluorescence decay after a series of saturating flashes spaced 200 ms apart.

2.7.8 Isolation of thylakoid membranes

Cells were grown in BG-11 with 5 mM glucose to an OD_{700} of 0.8-1.0 and harvested using centrifugation (5000 *g* for 10 min). The cells were washed once with cell wash buffer. Then the cells were re-suspended in 2 ml of disruption buffer and transferred to multiple microcentrifuge tubes filled with 700 µl of 0.1 mm zirconia/silica beads (BioSpec Products Inc., Bartlesville, OK, USA). Cells were incubated on ice for 30 min in the dark, and cell disruption was carried out using a mini-bead beater (BioSpec Products Inc., Bartlesville, OK, USA). Typically, 5 bead beating cycles consisting of 20 s of agitation at 4800 rpm followed by 5 min rests on the ice were carried out. Beads and the cell debris were removed by centrifuging the cells twice at 2000 *g* for 2 min. The supernatant was then centrifuged at 8000 *g* for 5 min to remove the remaining cell debris. Thylakoids were harvested by centrifugation at 60000 *g* for 60 min at 4°C using a TL-100 ultracentrifuge (Beckman Coulter Inc. Indianapolis, IN, USA). Thylakoids were re-suspended in disruption buffer and then centrifuged again at 60,000 *g* for 25 min at 4°C to wash away the excess PBS proteins. In the end, thylakoids were finally resuspended in solubilisation buffer for blue native polyacrylamide gel electrophoresis

(BN-PAGE) or cell disruption buffer for sodium dodecyl sulfate polyacrylamide gel electrophoresis (SDS-PAGE). Isolated thylakoids were frozen in liquid nitrogen and stored at -80°C.

Cell-washing buffer – 50 mM HEPES-NaOH (pH 7.5); 20 mM $CaCl_2$; 10 mM $MgCl_2$; 1 mM 6-aminocaproic acid; 1 mM phenylmethylsulfonylfluoride (PMSF); 2 mM benzamidine ($C_7H_8N_2$).

Disruption buffer - 50 mM HEPES-NaOH (pH 7.5); 20 mM $CaCl_2$; 10 mM $MgCl_2$; 800 mM sorbitol ($C_6H_{14}O_6$); 1 M betaine monohydrate ($C_5H_{14}NO_3$); 1 mM 6-aminocaproic acid; 1 mM phenylmethylsulfonylfluoride (PMSF); 2 mM $C_7H_8N_2$.

Solubilisation buffer – 25 mM Bis-Tris HCl (pH 7.0); 20% glycerol; 0.20 $mg.ml^{-1}$ Pefabloc ($C_8H_{10}FNO_2S.HCl$).

2.7.9 Blue native polyacrylamide gel electrophoresis (3-12% BN-PAGE)

Isolated thylakoids were solubilised at a chlorophyll *a* concentration of 0.5 $mg.ml^{-1}$ with solubilisation buffer. The solubilised thylakoid samples were treated with 20 µl of 3% β-dodecyl maltoside (Affymetrix, USA), three times with a time interval of 2 min between each successive addition. The treated thylakoid samples were then incubated on ice for 15 min and centrifuged at 16500 *g* for 15 min to remove the insoluble fraction. Finally, solubilised thylakoid samples containing chlorophyll *a* concentration of 5 µg along with 4× BN-PAGE loading buffer and 5% serva blue G250 were loaded onto 3-12% Bis-Tris 1.0 mM NativePAGE precast gel (Life Technologies, USA) and run at 4°C.

4× BN-PAGE sample buffer – 50 mM Bis-Tris; 6 M HCl; 10% glycerol; 50 mM NaCl; 0.001% Ponceau stain.

10× BN-PAGE running buffer – 50 mM Bis-Tris; 50 mM Tricine (pH 6.8).

10× cathode buffer additive – 0.2% Serva Blue G-250 in distilled water.

1× anode buffer – 10× BN-PAGE running buffer diluted to 1×.

1× dark blue cathode buffer – 10× BN-PAGE running buffer diluted to 1× and 10× cathode buffer additive diluted to 1×.

1× light blue cathode buffer – 10× BN-PAGE running buffer diluted to 1×, 1:100 dilution of 10× cathode buffer.

2.7.10 Sodium dodecyl polyacrylamide gel electrophoresis (SDS-PAGE)

The protein expression analysis was performed using 15% SDS-PAGE acrylamide gels. Gels were prepared using 30% acrylamide: bisacrylamide 37.5:1 stock solution (Bio-Rad Laboratories, Hercules, USA) in mini gel system (Protean III). The isolated thylakoid samples along with the cell disruption buffer were mixed with loading buffer and heated for 3 min at 90°C before electrophoresis. The gel electrophoresis was performed at 100 V for the stacking portion of the gel and 180 V for the resolving part of the gel. Gels were run in duplicates and one gel used for staining with Coomassie brilliant blue R-250 and then destained, and other gel was used for immunoblotting using nitrocellulose membrane to probe the membrane with specific protein antibodies to check the protein expression.

Sample buffer – 62.5 mM Tris-HCl pH 6.8; 2% SDS; 10% glycerol; 0,05% bromophenol blue; 5% β-mercaptoethanol.

Running buffer – 20 mM Tris-HCl pH 8.3; 200 mM glycine; 0.1% SDS

12% resolving gel – 375 mM Tris-HCl pH 8.8; 4 ml of 40% acrylamide; 0.1% SDS; 0.1% ammonium persulphate (APS); 0.1% N,N,N',N'-tetramethylethylenediamine (TEMED).

15% resolving gel – 375 mM Tris-HCl pH 8.8; 5 ml of 40% acrylamide; 0.1% SDS; 0.1% APS; 0.1% TEMED.

4% stacking gel – 125 mM Tris-HCl pH 6.8; 0.1% SDS; 665 µl of 40% acrylamide; 0.1% APS; 0.1% TEMED.

Coomassie blue stain - 25% isopropanol; 10% acetic acid; 0.05% coomassie brilliant blue R250.

Destain – 5% isopropanol; 7% acetic acid; 4% glycerol.

2.7.11 Western blotting

For immunoblotting and detection, the BN-PAGE gels containing the proteins were transferred to polyvinylidene difluoride membrane (PVDF) using electroblotting at 35 V for 20 h at 4°C in electroblot buffer. To destain the membranes, methanol washing was done, and this was followed by blocking using the blot-O solution. The proteins were probed with protein-specific primary antibodies - D1, D2, CP43, and CP47 (Agrisera, Sweden). For SDS-PAGE gels, the proteins were transferred to a nitrocellulose membrane using transfer buffer containing 0.05% SDS at 100 V for 45 min and the membrane was washed with water and then blocking was done using blot-O solution, and the proteins were probed with the protein-specific primary antibodies. Secondary antibodies (Sigma, USA) conjugated to peroxidase were used for detection using enhanced chemiluminescence (ECL). Detection was done using a CCD detector system (Fuji image PS3000) by incubating the membrane in freshly prepared ECL reagent (Abcam, UK).

Electroblot buffer – 25 mM Tris; 192 mM glycine; 20% methanol.

Blot O – 4% bovine serum albumin (BSA); 0.02% sodium azide (NaN_3); tris-buffered saline (TBS) pH 7.4.

Primary antibody – D1 antibody raised in rabbit against PsbA2 (D1) peptide; CP43 antibody raised in rabbit against PsbC (CP43) peptide; CP47 antibody raised in rabbit against PsbB (CP47) peptide; a D2 antibody raised in rabbit against PsbD (D2) peptide.

TBS (pH 7.4) – 0.137 M NaCl; 2.7 mM KCl; buffered with 25 mM Tris and pH adjusted to 7.4 with 37% HCl.

Secondary antibody – Anti-rabbit IgG peroxidase antibody produced in goat by Sigma, diluted 1:15000 in 50 mM Tris-HCl (pH 7.5); 150 mM KCl; 3% BSA in distilled water.

2.8 Whole genome sequencing

Whole genome sequencing of three strains was carried out – R54E*, ΔPsbK and ΔPsbZ using Illumina HiSeq2500 V4 platform at the New Zealand Genomics Limited (NZGL). The Illumina TruSeq DNA library kit was used for carrying out the whole

genome sequencing. The gDNA of the three strains was extracted using the protocol discussed in section 2.5.1. Bio-IT computing platform was used to perform the processing and analysis of the data. The Burrows-Wheeler Aligner (BWA) (Li and Durbin 2009) and Samtools (Li *et al.* 2009) were used for reference mapping, and Picard (http://picard.sourceforge.net) and Freebayes (Garrison and Marth 2012) were used for variant calling. Picard was used for removing the PCR duplicate reads from the sequenced data. The variant calling was performed as per FreeBayes best practice settings. FreeBayes is a Bayesian genetic variant detector. In reference mapping, all the samples were mapped using the original *Synechocystis* 6803 sequence from Kaneko and co-workers (Kaneko *et al.* 1996a; Kaneko *et al.* 1996c) that is available at cyanobase and major plasmid sequences (Kaneko *et al.* 2003) as a reference templates (GenBank accession numbers: chromosome, BA000022; pSYSA, AP004311; pSYSG, AP004312; pSYSM, AP004310 and pSYSX, AP006585). BWA-mem algorithm was used, for mapping long reads with default settings. The Samtools package was used for Sam to Bam conversion and for sorting and indexing bam files. Sam is a text format for storing sequence data in series of tab-delimited ASCII columns, mostly about sequence alignment to the reference. The BAM format is the binary version of SAM data and helps in compressing the enormous amount of data.

2.9 *Synechocystis* sp. PCC 6803 strains used in this study

Strain	Description
Wild type (WT)	Glucose-tolerant *Synechocystis* sp. PCC 6803 strain (Williams 1988)
Psb27 deletion and Psb27 control strain	
ΔPsb27^{C}	*slr1645* gene deleted in wild type with chloramphenicol-resistance cassette
Psb27 control^{S}	*slr1644-slr1645-slr1646* genes complemented by wild-type strain DNA under the selection of spectinomycin-resistance cassette
Psb27 mutants (Conserved residues)	
D14A^{S}	Asp-14 of Psb27 mutated to Arg under the selection of spectinomycin-resistance cassette
R54E^{S}	Arg-54 of Psb27 mutated to Glu under the selection of spectinomycin-resistance cassette
Y78H^{S}	Tyr-78 of Psb27 mutated to His under the selection of spectinomycin-resistance cassette
R94E^{S}	Arg-94 of Psb27 mutated to Glu under the selection of spectinomycin-resistance cassette
E98R^{S}	Glu-98 of Psb27 mutated to Arg under the selection of spectinomycin-resistance cassette
Psb27 mutants (Cross-linking residues)	
D58A^{S}	Asp-58 of Psb27 mutated to Ala under the selection of spectinomycin-resistance cassette
D58E^{S}	Asp-58 of Psb27 mutated to Glu under the selection of spectinomycin-resistance cassette
D58K^{S}	Asp-58 of Psb27 mutated to Lys under the selection of spectinomycin-resistance cassette
K63A^{S}	Lys-63 of Psb27 mutated to Ala under the selection of spectinomycin-resistance cassette

K63D^{S}	Lys-63 of Psb27 mutated to Asp under the selection of spectinomycin-resistance cassette
K63R^{S}	Lys-63 of Psb27 mutated to Arg under the selection of spectinomycin-resistance cassette
PsbA deletion strains/PsbA2 mutants	
H252A^{K}	His-252 residue of PsbA2 mutated to Ala under the selection of kanamycin-resistance cassette
H252H^{K}	His-252 residue of PsbA2 mutated to His under the selection of kanamycin-resistance cassette
H252Q^{K}	His-252 residue of PsbA2 mutated to Gln under the selection of kanamycin-resistance cassette
H252Y^{K}	His-252 residue of PsbA2 mutated to Tyr under the selection of kanamycin-resistance cassette
S264A^{K}	Ser-264 residue of PsbA2 mutated to Ala under the selection of kanamycin-resistance cassette
S264K^{K}	Ser-264 residue of PsbA2 mutated to Lys under the selection of kanamycin-resistance cassette
S264T^{K}	Ser-264 residue of PsbA2 mutated to Thr under the selection of kanamycin-resistance cassette
Low-molecular-weight protein deletion strains	
ΔPsb30^{K}	*sll0047* gene deleted in wild type with kanamycin-resistance cassette
ΔPsbK^{K}	*sml0005* gene deleted in wild type with kanamycin-resistance cassette
ΔPsbZ^{K}	*sll1281* gene deleted in wild type with kanamycin-resistance cassette
ΔPsb27^{C}:ΔPsb30^{K}	*slr1645* gene deleted with chloramphenicol-resistance cassette and *sll0047* gene deleted with kanamycin-resistance cassette
ΔPsb27^{C}:ΔPsbK^{K}	*slr1645* gene deleted with chloramphenicol-resistance cassette and *sml0005* gene deleted with kanamycin-resistance cassette
ΔPsb27^{C}:ΔPsbZ^{K}	*slr1645* gene deleted with chloramphenicol-resistance cassette and *sll1281* gene deleted with kanamycin-resistance cassette

*C: chloramphenicol, K: kanamycin, S: spectinomycin

Chapter Three

Site-directed mutagenesis of the Psb27 protein in *Synechocystis* sp. PCC 6803

3.1 Introduction

The cyanobacterial Psb27 protein is an 11-kDa thylakoid lumen-localised lipoprotein. This protein was first discovered in PS II of *Synechocystis* 6803 (Ikeuchi *et al.* 1995a) and later named by Kashino and coworkers (Kashino *et al.* 2002b). The Psb27 lipoprotein plays an important role in the assembly and repair mechanism of PS II in cyanobacteria (Roose and Pakrasi 2004; Nowaczyk *et al.* 2006; Mamedov *et al.* 2007; Roose and Pakrasi 2008) and plants (Chen *et al.* 2006). The Psb27 protein is not present in the final PS II complex (Kashino *et al.* 2002b; Roose and Pakrasi 2004; Mamedov *et al.* 2007; Roose and Pakrasi 2008), but it has been found to co-purify with various other PS II protein complexes (Mabbitt *et al.* 2014) potentially indicating that Psb27 binds transiently with the PS II subunits. The Psb27 protein was also detected as an assembly factor in the non-oxygen-evolving PS II complex lacking extrinsic proteins (PsbO, PsbU, and PsbV) in *Thermosynechococcus elongatus* (Nowaczyk *et al.* 2006).

It has been suggested that Psb27 works as a gatekeeper during the assembly process of the water-oxidising complex in the PS II (Liu *et al.* 2013b; Mabbitt *et al.* 2014). The Psb27 protein is present in all oxygenic photosynthetic organisms (Peltier *et al.* 2002; Rajalahti *et al.* 2007) except *Gloeobacter violaceus* PCC 7421, a cyanobacterium that lacks thylakoids and may, therefore, have modified PS II assembly and repair processes (Nakamura *et al.* 2003).

3.2 Structure of Psb27

The cyanobacterial Psb27 protein consists of an N-terminal signal peptide which contains a conserved cysteine residue (Nowaczyk *et al.* 2006; Fagerlund and Eaton-Rye 2011a). In cyanobacteria, N-terminal lipid modification of Psb27 has been proposed to help in the tight association of the protein with the thylakoid membrane, but, as noted above, the conserved cysteine required for lipid modification in cyanobacteria is absent in Psb27 from land plants (Nowaczyk *et al.* 2006).

Psb27 is absent from the crystal structures of PS II (Umena *et al.* 2011; Suga *et al.* 2015a); however, three different structures of isolated cyanobacterial Psb27 have been resolved independently (Cormann *et al.* 2009; Mabbitt *et al.* 2009; Michoux *et al.* 2012). The first two Psb27 structures were obtained from *Synechocystis* 6803 by

nuclear magnetic resonance (NMR) spectroscopy (Cormann *et al.* 2009; Mabbitt *et al.* 2009) and the third structure by X-ray crystallography from *Thermosynechococcus elongatus* (Michoux *et al.* 2012). The PDB identification number for these structures are 2KND (Cormann *et al.* 2009), 2KMF (Mabbitt *et al.* 2009) and 2Y6X (Michoux *et al.* 2012).

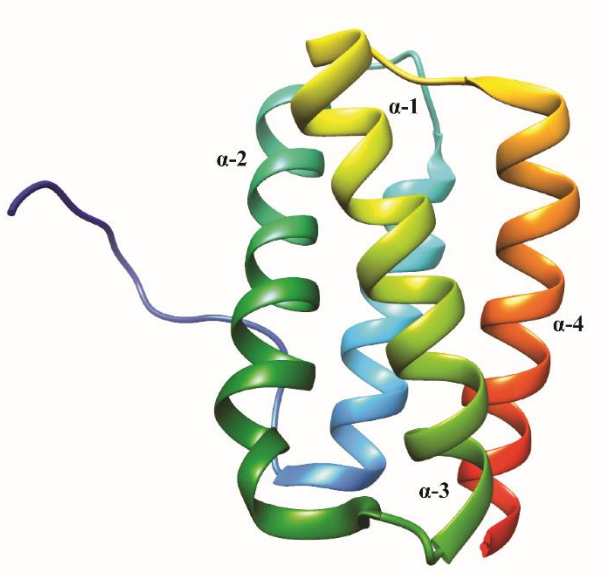

Figure 3.1 Solution structure of Psb27. The Psb27 structure consists of 4 helices. The four helices are labelled in the illustration as α-1, α-2, α-3, and α-4. The amino terminus is also shown. The structure has been created from solution structure of Psb27 (PDB: 2KMF) (Mabbitt *et al.* 2009).

However, the overall structure of 2Y6X X-ray crystallography structure of Psb27 from *Thermosynechococcus elongatus* looks more similar to the 2KMF NMR structure of Psb27 from *Synechocystis* 6803, with average distances between the two superimposed models (RMSD) reaching ~1.8 Å, whereas when 2Y6X model is superimposed on 2KND model, it reaches to a value of 4.1 Å. Additionally, the surface charges can also be correlated in a better way between the 2Y6X and 2KMF Psb27 structure model. For example, the Psb27 structures (2KMF and 2Y6X) used to study the interaction between Psb27 and CP43 place residue Psb27-Glu98 amino acid residue on the surface of Psb27 and also the Psb27-Asp14 has been shown to stabilise the amino terminal of Psb27 by forming hydrogen bonds; whereas, according to the 2KND structure model, the Psb27-Gln98 is rather embedded in the Psb27 protein surface and also disagrees with the interaction of the Psb27-Asp14 in the stabilisation of the folding of the Psb27 structure.

However, overall the Psb27 protein consists of a four-helices (1, 2, 3 and 4) which have been labelled as α1, α2, α3 and α4 in Fig. 3.1. Most of the surface part of the 3rd and 4th helices of the Psb27 protein is highly conserved as can be seen in Fig. 3.4 and might play an important role in binding to the PS II complexes.

3.3 Objective

The Psb27 protein is evolutionarily conserved between higher plants and cyanobacteria, potentially indicating the functional importance of the protein. Little is known about the functional roles of the conserved amino acid residues of the Psb27 protein in the interaction with other protein subunits of the PS II complex. Various models have been proposed to illustrate Psb27 binding to PS II (Liu *et al.* 2011a; Liu *et al.* 2013a; Cormann *et al.* 2016). In this chapter, the validity of these models will be discussed regarding the biophysical properties of the Psb27 protein and the physiology of the *Synechocystis* 6803 cells with the mutated versions of the Psb27 protein. In this study, 2KMF structure of Psb27 was used for performing the site-directed mutagenesis. The reason for choosing this Psb27 structure has been described in previous Section 3.2. The basic approach involved mutating the conserved amino acids as well as those residues involved in cross-linking between Psb27 and CP43 that are implicated in protein-protein interactions in the studies outlined in the literature. A *psb27 in vitro* mutagenesis system was also constructed so that the contribution of the individual Psb27 residues to the binding of Psb27 to PS II could be determined. Eleven variants of the Psb27 protein were introduced into the *Synechocystis* 6803 genome. The following amino acid residues were selected to perform the mutagenesis studies (Fig. 3.2 A): Asp-14, Arg-54, Tyr-78, Arg-94, Glu-98, Asp-58, and Lys-63. The amino acid substitutions were carried out by focussing on the charge reversal mutations or changing the side chains of amino acids of interest thinking that this substitution might prove detrimental for the structural and functional roles of the Psb27 protein. The substitutions have been described in detail as follows: Psb27-Asp14 is negatively charged and mutated to non-polar amino acid Ala. Psb27-Arg54 and Psb27-Arg94 is positively charged amino acid with a long side chain mutated to Glu amino acid which is negatively charged. Psb27-Tyr78 is non-polar with aromatic chain mutated to positively charged His amino acid. Psb27-Glu98 amino acid are negatively charged mutated to positively charged Arg amino acid. However, to study the effect of mutation of crosslinking amino acid

residues of Psb27-Asp58 and Psb27-Lys63, a series of different combination of mutations. Psb27-Asp58 (negatively charged amino acid) was mutated to Ala (nonpolar amino acid), Glu (negatively charged amino acid) and Lys (positively charged amino acid). Psb27-Lys63 (positively charged amino acid) was mutated to Ala (nonpolar amino acid), Glu (negatively charged amino acid) and Asp (negatively charged amino acid). A *psb27* deletion strain was also constructed, to use it as a reference for analysing the phenotypes of the site-directed Psb27 mutants and for introduction of the mutated copy of *psb27*. The mutants were constructed and analysed physiologically and biochemically to provide insights into the functional importance of the conserved amino acid residues of the Psb27 protein.

This chapter also discusses the evolutionary analysis of the Psb27 protein. Most of the residues chosen for site-directed mutagenesis were selected because they were solvent exposed or conserved or involved in cross-linking. The Psb27-Asp58 and Psb27-Glu98 residues are shown to be protected from the solvent when Psb27 is bound to the PS II complex (Liu *et al.* 2013a). The tyrosine residue located at the 78th position of the *Synechocystis* 6803 Psb27 protein is replaced with the histidine residue in most of the other cyanobacterial Psb27 protein (Mabbitt *et al.* 2009; Michoux *et al.* 2012). The Psb27-Arg54 and Psb27-Arg94 side chains are both at the surface of the protein. The Psb27-Asp14 helps in the stabilisation of the amino terminal of Psb27 by forming hydrogen bonds to the backbone of Psb27-Thr8 and Psb27-Gly9. Consistent with this, the thermal stability of recombinant *Synechocystis* 6803 Psb27 protein with an Asp14Ala mutation was greatly reduced (Mabbitt *et al.* 2013). The targeted amino acid residues have been shown in Fig. 3.2 A and are denoted using the single letter code.

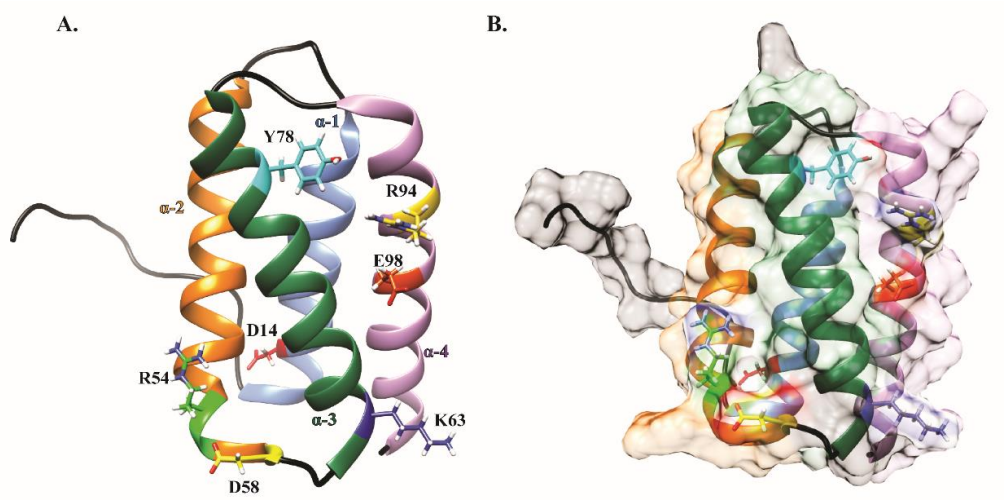

Figure 3.2 Selected amino-acid residues for Psb27 mutagenesis study.(A) Ribbon diagram of Psb27 protein. The amino acid residues shown in the ribbon diagram of Psb27 were selected for carrying out the mutagenesis studies. The amino acid residues are shown as sticks. A1, α2, α3 and α4 corresponds to α-helix 1, 2, 3 and 4. D14 from helix-1, R54 from helix-2, D58 from loop connecting helix-2 and helix-3, K63, Y78 from helix-3, R94 and E98 from helix-4. The D14A helps in the stabilisation of the amino terminal of Psb27 by forming hydrogen bonds to the backbone of Thr8 and Gly9 (not shown in Fig.). The R54, Y78, R94, and E98 were solvent exposed or surface residues. D58 and K63 were the residues proposed to cross-link with the chlorophyll *a*-binding core antenna protein: CP43 by Pakrasi and co-workers (Liu *et al.* 2011a). The structure has been created from the solution structure of Psb27 (PDB: 2KMF) (Mabbitt *et al.* 2009). **(B) Surface representation of Psb27**.

3.4 Protein sequence and analysis of *Synechocystis* 6803 Psb27 protein

The Psb27 protein sequence from *Synechocystis* 6803 was aligned with different homologues of Psb27 from algae, cyanobacteria and higher plants (Fig. 3.3 A and B). The Psb27 homologues were selected based on the percentage of similarity and the phylogenetic diversity (Fagerlund and Eaton-Rye 2011a) that they shared with the *Synechocystis* 6803 Psb27. Only the mature *Synechocystis* 6803 Psb27 protein sequence has been shown in the alignment. As discussed earlier, cysteine is the 1st amino acid residue in *Synechocystis* 6803 at the N-terminal region of Psb27. Therefore, cysteine has been assigned position one in the alignments. In Fig. 3.3 A and B, the Psb27 protein sequence has been started from a Leu residue numbered at position 7, as the first six amino-acid residues were trimmed. It can be seen in the alignment that the Tyr-11 is the first highly conserved residue between cyanobacteria and plants. Also, many other

Psb27 protein amino acid residues were conserved among the phyla (Fig. 3.4). The aromatic residues Tyr-11, Tyr-49, Tyr-53 present in the helix 1 and 2 (Fig. 3.4 A); Phe-65, Tyr-78, Tyr-79, Tyr-82 residues found in the helix 3 (Fig. 3.4 B) and Phe-99 present in the helix 4 (Fig. 3.4 C) were also conserved. Many non-aromatic residues: Val-18, Leu-22, Ile-26 (helix 1) (Fig. 3.4 A); Met-68, Leu-72, Leu-75 (helix 3) (Fig. 3.4 B) and Leu-95 (helix 4) (Fig. 3.4 C) were also conserved. Some other highly conserved amino acid residues were Ser-64, Ile-86, Val-88 present between the helix 3 and 4. As already noted, a histidine residue is usually present at the 78 position of the Psb27 protein in higher plants and other cyanobacteria, whereas in *Synechocystis* 6803, this histidine is substituted to a tyrosine residue. The Thr-15, Val-18, Leu-22, Ile-26, Ser-64, Met-68, Leu-72 and Leu-75 residues are found in the Psb27 core (Fig. 3.4 A and B). The Tyr-15, Val-18, Lys-22, Ile-26 are present in the interior of the Psb27 protein. Many polar residues: Arg-54, Thr-70, Asn-73, Ser-74, Tyr-78, Arg-94 were also conserved. The Glu-103 and Arg-108 present at the carboxyl terminal end of helix 4 were also conserved. The Pro-86 and Arg-94 residues are surfaces exposed. The residues of helix 1 and helix 2 are less conserved as compared to the residues in helix 3 and 4. In Fig. 3.3, highly conserved Psb27 residues have been colored red. Blue and white colour corresponds to less conserved Psb27 residues among the phyla shown.

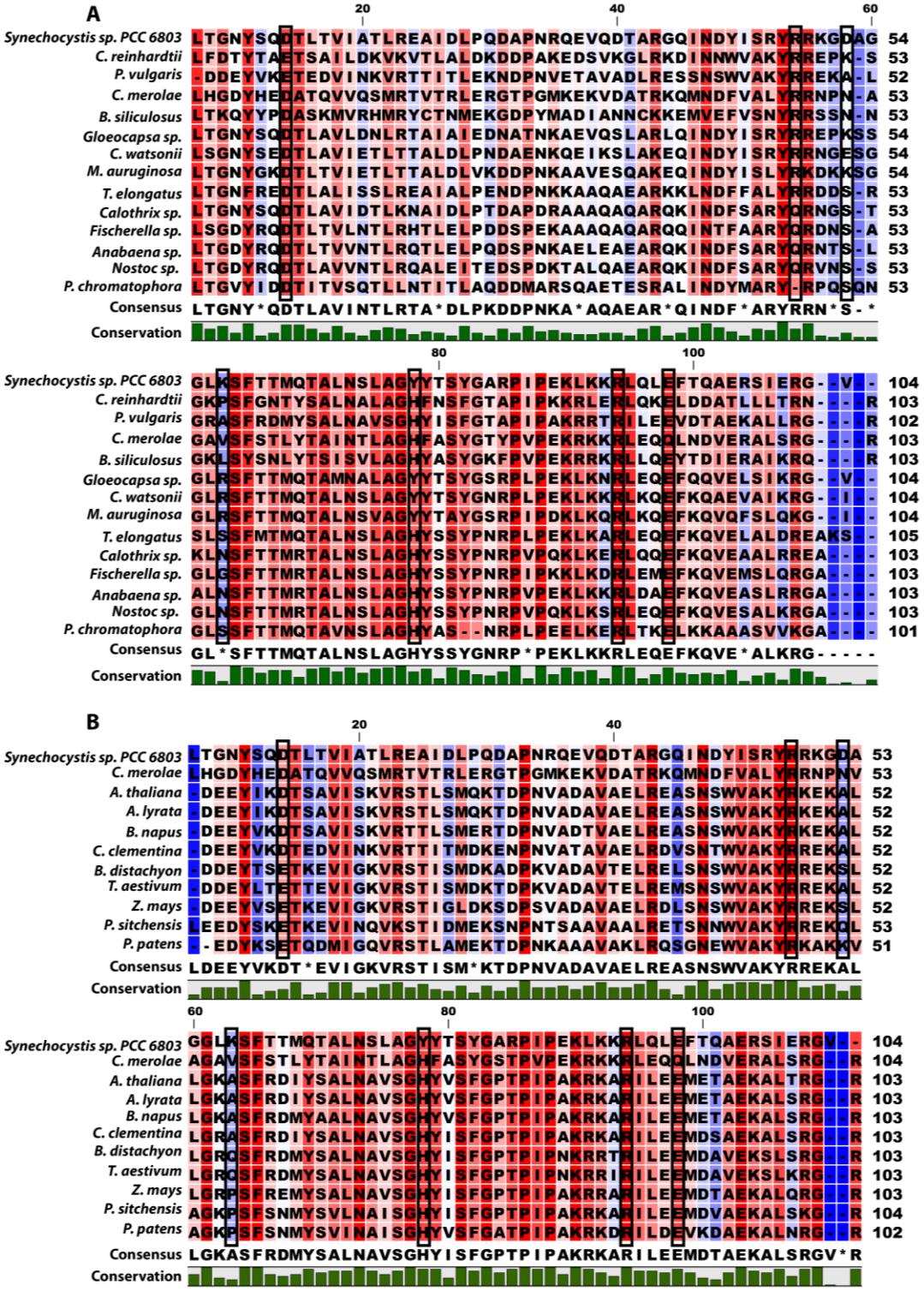

Figure 3.3 Comparison of *Synechocystis* 6803 Psb27 protein sequences. (A) Comparison of the *Synechocystis* 6803 Psb27 protein sequence with algae, and cyanobacteria. The Psb27 sequence from *Synechocystis* 6803 was aligned with algae, and other cyanobacteria to study the conservation of Psb27. Cysteine is the first amino-terminal residue for the mature *Synechocystis* 6803 Psb27 protein. The sequences have been trimmed, and the Psb27 protein sequence has been started from the 7th residue Lysine. **(B)** Comparison of the *Synechocystis* 6803 Psb27 protein sequence with Psb27

from plants. The Psb27 sequence from *Synechocystis* 6803 was also aligned with plants. Highly conserved Psb27 residues have been coloured red. Blue and white colour corresponds to less conserved Psb27 residues among the species shown. The amino acid residues targeted in this study has been highlighted with black box. The alignments were performed using Clustal Omega default parameters.

Conserved residues among Psb27 protein from all organisms are shown in the ribbon diagram in Fig. 3.4. Helix III is more conserved as compared to helix I, helix II and helix IV.

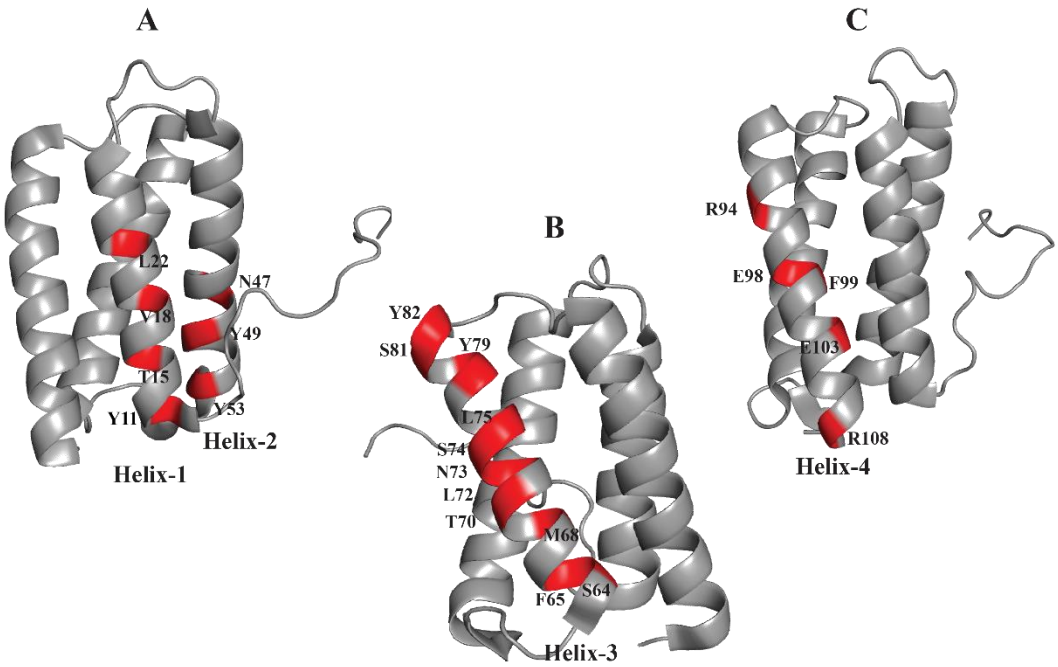

Figure 3.4 Psb27 structure with conserved amino acid residues. The Psb27 structure consists of 4 helices. Here ribbon diagram of Psb27 is shown with highly conserved amino acid residues (red colour) present on the surface of cyanobacteria, algae, and higher plants. **(A)** Conserved residues of helix-1 and helix-2. The conserved residues shown here on helix-1 are Tyr-11, Thr-15, Val-18, Leu-22, Ile-26 and on helix-2 are Tyr-49, Tyr-53. **(B)** Conserved residues of helix-3. The conserved amino acid residues on helix-III are Ser-64, Phe-65, Met-68, Thr-70, Leu-72, Asn-73, Ser-74, Leu-75, Tyr-78, Tyr-79, Ser-81 and Tyr-82. **(C)** Conserved residues of helix-4. The conserved residues shown here on helix-4 are Arg-94, Gln-98, Gln-103, and Arg-108. Helix-3 is highly conserved as compared to the other three helices. The positions of conserved amino acid residues have been shown as red coloured surfaces. The structure has been created from the solution structure of Psb27 (PDB: 2KMF) (Mabbitt *et al.* 2009).

3.5 Site-directed mutagenesis of the *Synechocystis* 6803 Psb27 protein

3.5.1 *psb27* deletion strain

To construct the ΔPsb27 deletion strain, a plasmid was generated using fusion PCR, in which most of the *psb27* gene was deleted and replaced by a chloramphenicol-resistance cassette (camR) (Fig. 3.5 A). The plasmid was named pΔPsb27-camR (Fig. 3.5 B). To construct the ΔPsb27 plasmid, upstream and downstream flanking regions of *psb27* were amplified with primers Psb27_LF_fwd, Psb27_LF_rev and Psb27_RF_fwd, Psb27_RF_rev (Chapter 2, Table 2.1). The primers Psb27_LF_rev and Psb27_RF_fwd had overhangs which were complementary to the sequence of the chloramphenicol-resistance cassette, derived from pBR325 (Bolivar 1978). The chloramphenicol-resistance cassette was amplified in a separate PCR reaction using primers CmR_fwd and CmR_rev (Chapter 2, Table 2.1). The resulting fusion PCR product was ligated into a pGEM-T expression vector (Promega. Madison, USA) (Fig. 3.5 B) and verified by restriction digestion and sequencing (Fig. 3.5 C). The final cloned PCR product was used to transform wild-type *Synechocystis* 6803 cells. The complete segregation of all strains was confirmed by PCR analysis (Fig. 3.5 D).

3.5.2 *psb27* mutagenesis system

To construct a system for the introduction of the point mutations into Psb27 protein, a ~1.9 kb DNA fragment containing *psb27* as well as its surrounding region was amplified by PCR using primers Psb27_fwd and Psb27_rev (Chapter 2, Table 2.1) (Fig. 3.6 A). The PCR product was subcloned into the pGEM-T expression vector (Promega, Madison, USA) (Fig. 3.6 B) and verified by restriction digestion and sequencing (Fig. 3.5 B and C). A *Bam*H1 restriction site was introduced 124 basepairs downstream of the *psb27* gene using primers Psb27_*Bam*H1_fwd and Psb27_*Bam*H1_rev primers (Chapter 2, Table 2.1) to clone the spectinomycin-resistance cassette (specR) (Fig. 3.6 A). The spectinomycin-resistance cassette was derived from pHP45Ω (Prentki and Krisch 1984). The plasmid was named pPsb27-specR (Fig. 3.6 B). The resulting pPsb27-specR were transformed into the ΔPsb27 strain. The complete segregation of all strains was confirmed by PCR analysis of each locus (Fig. 3.6 E, F, and G). The resulting plasmids containing the amino acid substitutions were introduced into the

ΔPsb27 deletion strain, and transformants were confirmed by Sanger di-deoxy sequencing.

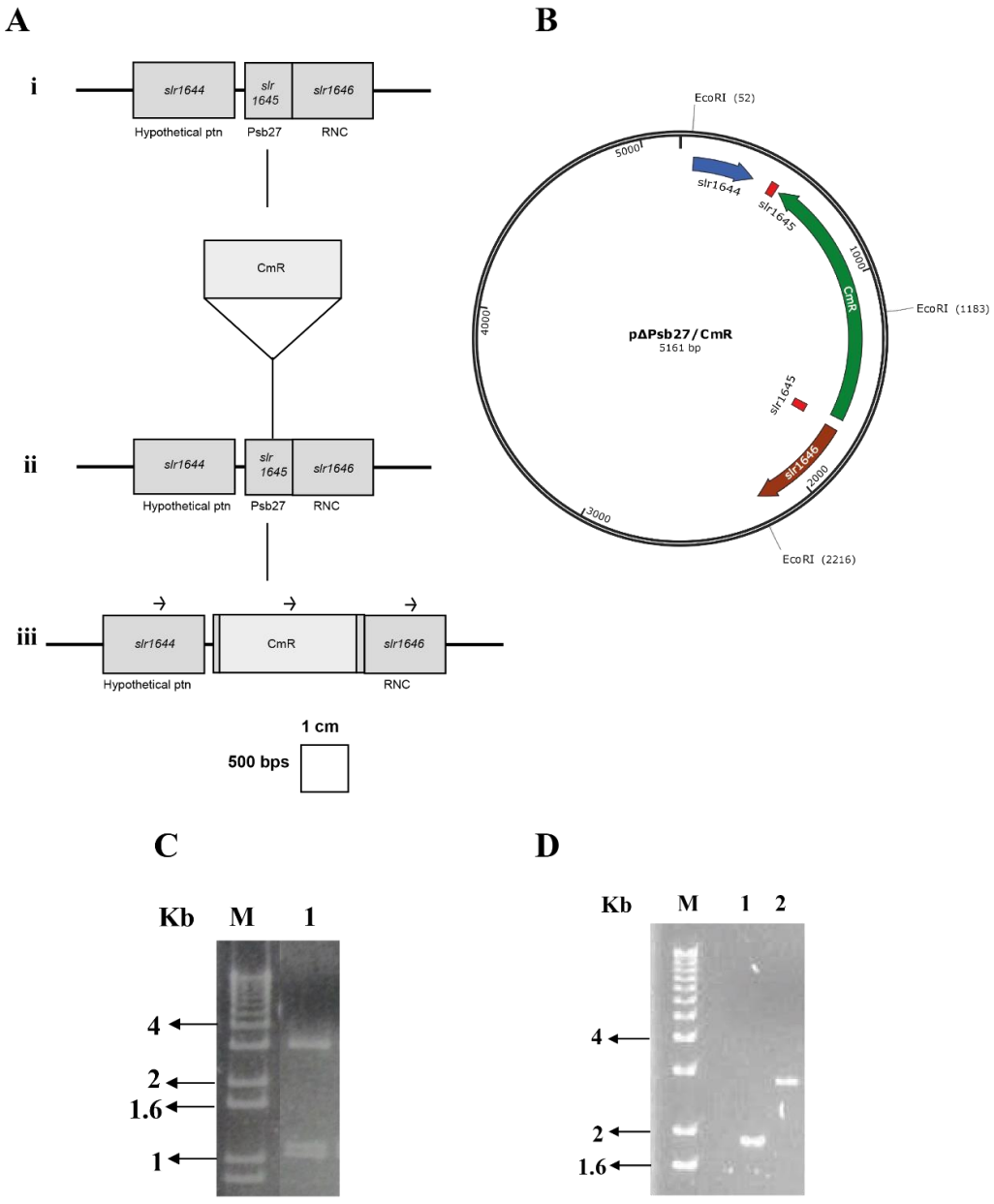

Figure 3.5 Construction of *Synechocystis* 6803 *psb27* deletion strain.(A) Insertion of a 2.0 kb chloramphenicol-resistance cassette between left flanking region and right flanking region of *psb27*. One cm corresponds to 500 bp **(B)** Plasmid map of pΔPsb27-camR. This plasmid was used for transforming wild-type *Synechocystis* 6803 to produce the ΔPsb27 strain. The mutants were grown and segregated on chloramphenicol-containing selective media. **(C)** Verification of pΔPsb27 by *Eco*RI restriction digestion. The PCR products shown on the gel are; 1, *Eco*RI digested pΔPsb27-camR. **(D)** Confirmation of the complete segregation of the ΔPsb27 strain by colony PCR. PCR products shown on the gel are; 1, wild type; 2, ΔPsb27. Lane M is the 1 Kb Plus DNA Ladder (Invitrogen, CA).

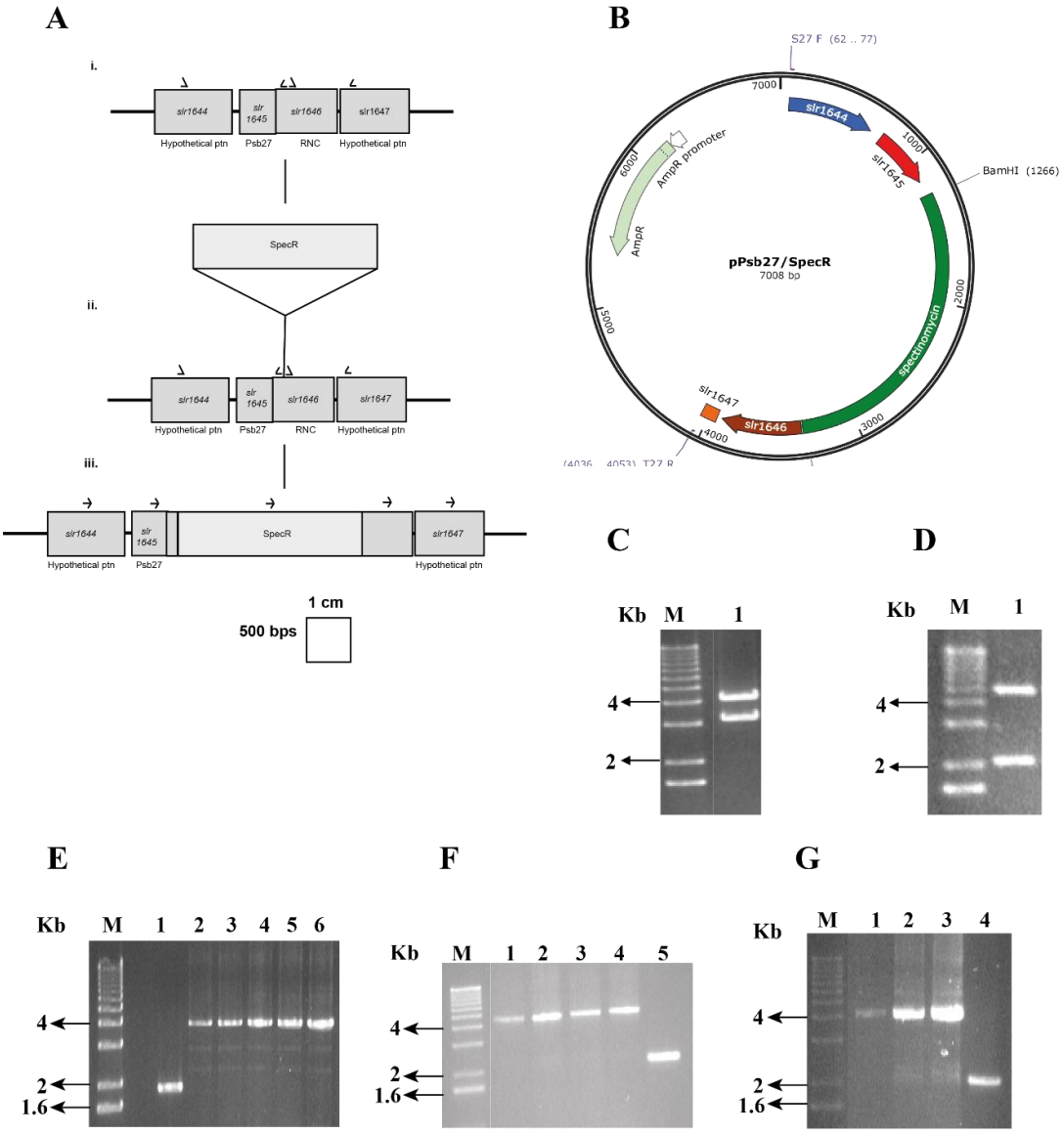

Figure 3.6 Construction of *Synechocystis* 6803 *psb27* mutants.(A) Insertion of 2.0 kb spectinomycin-resistance cassette at the unique *Bam*H1 site created using site-directed mutagenesis downstream of *psb27*. One cm corresponds to 500 bp. **(B)** The plasmid map of pPsb27-specR. This plasmid was used as a template for introducing site-directed mutagenesis and used for transforming ΔPsb27 strain to produce the strains containing the altered Psb27. The mutants were grown and segregated on spectinomycin-containing selective media. **(C)** Verification of pPsb27 by *Eco*RI restriction digestion. **(D)** Verification of pPsb27 by *Hin*dIII restriction digestion. **(E)**, **(F)**, **(G)** Confirmation of the complete segregation of Psb27 point mutants with the help of colony PCR. PCR products shown on the gel are **(E)** 1, wild type; 2, D14A; 3, R54E; 4, Y78H; 5, R94E; 6, E98R. **(F)** 1, Psb27 control; 2, D58A; 3, D58E; 4, D58K; 5, wild type. **(G)** 1, K63A; 2, K63D 2; 3, K63R; 4, wild type. Lane M is the 1 Kb Plus DNA Ladder (Invitrogen, CA).

3.6 Characterisation of *psb27* mutants

Once complete segregation of the targeted mutants was confirmed by sequencing, the phenotypic characterisation of the strains was carried out.

3.6.1 Psb27 protein expression

First, the expression of the Psb27 protein was measured in the key mutants to check the efficiency of the *psb27* mutagenesis system. Thylakoids from the ΔPsb27 strain, the control strain containing an unmodified copy of *psb27* and the strains containing the targeted mutations (R54E* and R94E) were isolated and their proteins separated using 15% sodium dodecyl sulfate polyacrylamide electrophoresis (SDS-PAGE) followed by immunoblotting with a Psb27-specific antibody (Fig. 3.7). It can be seen in Fig. 3.7, the Psb27 expression level in the wild type, *psb27* control strain and R94E mutant are similar. In the ΔPsb27 strain, the Psb27 protein was absent confirming the gene had been deleted when inserting the chloramphenicol-resistance cassette.

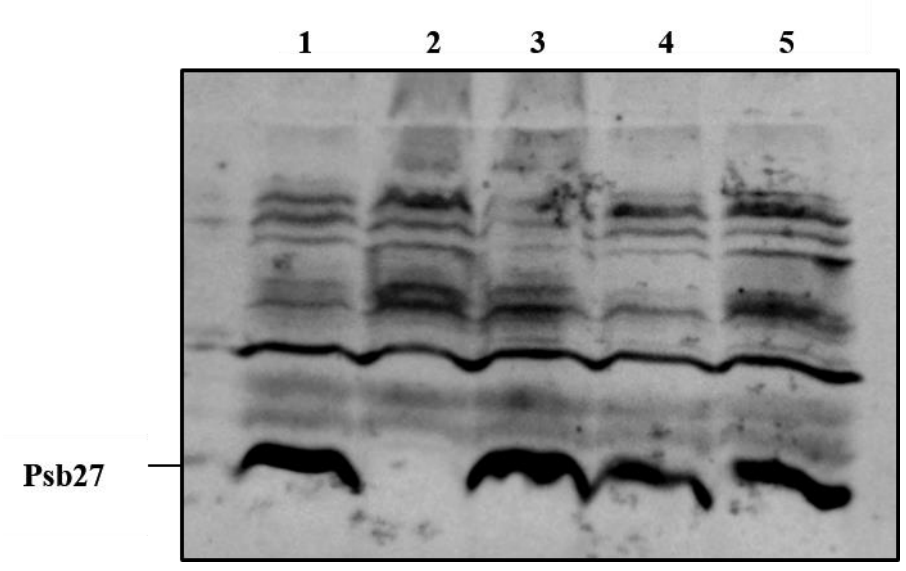

Figure 3.7 Expression of Psb27 in different strains using immunoblotting Thylakoid membranes from the various strains were analysed by denaturing 15% SDS-PAGE, and Psb27 was detected using Psb27 specific antibody. 5 µg of chlorophyll *a* were loaded onto the gel for each sample in each lane. Lanes are (1) wild type, (2) ΔPsb27, (3) Psb27 control strain, (4) R54E* and (5) R94E. The Psb27 protein expression was detected with the help of enhanced chemiluminescence (ECL) technique. The R54E* strain has been discussed in Chapter four.

3.6.2 Photoautotrophic growth

To investigate the impact of introducing the specific point mutations into the Psb27 protein, photoautotrophic growth curves were initially performed (Fig. 3.8). The optical density (OD) at 730 nm was measured every 12 h for seven days.

Fig. 3.8 shows the photoautotrophic growth characteristics of the wild type, ΔPsb27, Psb27 control strain, D14A, R54E, Y78H, R94E, E98R, D58A, D58E, D58K, K63A, K63D and K63R mutants over a period of 168 h. The doubling time of each strain is presented in Table 3.1. The doubling time of the wild type was ~13.1 ± 0.6 h, while the R54E mutant had the doubling time of ~18.4 ± 0.9 h. The other strains exhibited doubling times ranging from 15.1 ± 0.2 h to 17.2 ± 1.3 h. The *psb27* mutants were then characterised further. The doubling time of Psb27 control was 17.2 ± 1.3 h in comparison to the doubling time exhibited by the wild type. The reason might be as all the mutants were grown in the presence of the selective antibiotic (spectinomycin) except the wild type.

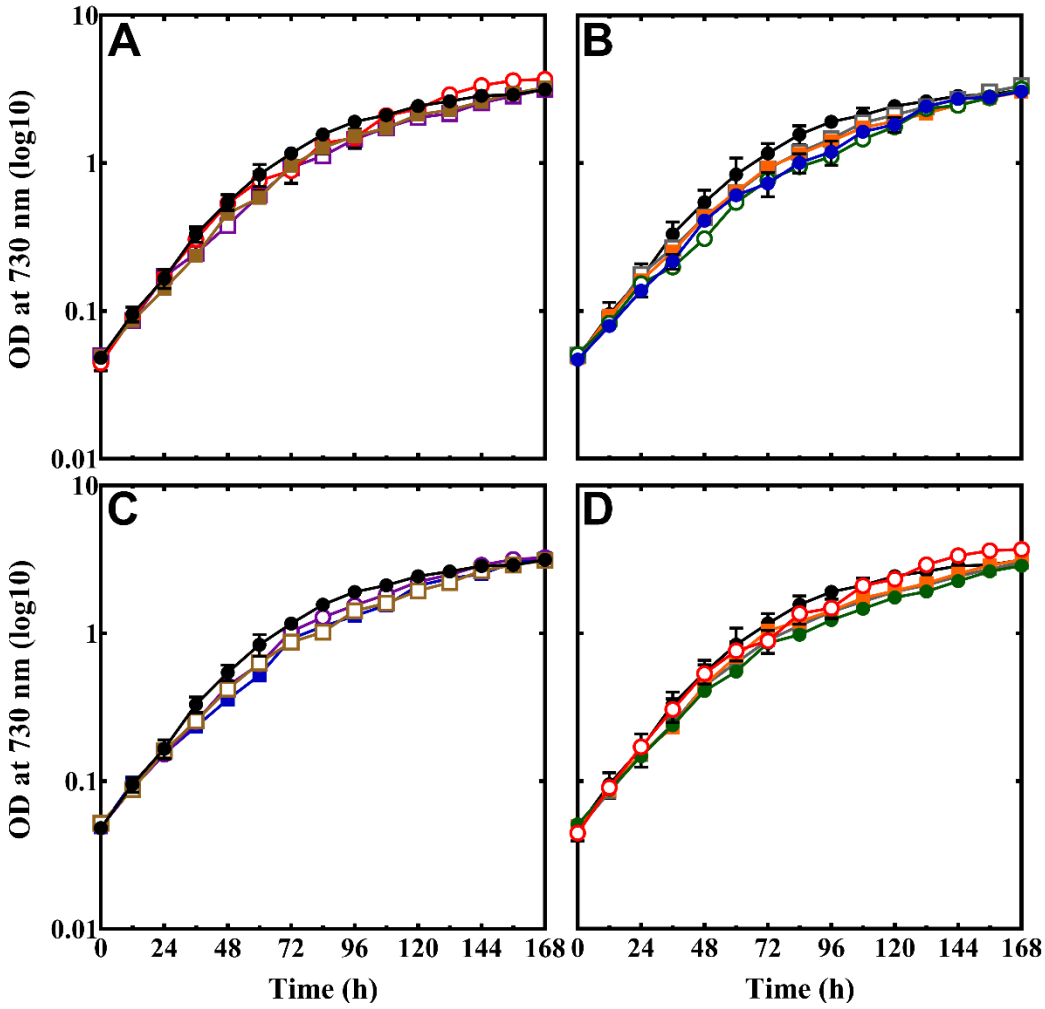

Figure 3.8 Photoautotrophic growth of *Synechocystis* 6803 and *psb27* strains.The photoautotrophic growth of *Synechocystis* 6803 and *psb27* mutants in BG-11 media as measured by optical density at 730 nm. The strains shown are **(A)** wild type (black, close circles), Psb27 control (red, open circles), D14A (brown, close squares) and E98R (purple, open squares). **(B)** wild type (black, close circles), ΔPsb27 (blue, close circles), R54E (green, open circles), R94E (orange, close squares) and Y78H (grey, open squares). **(C)** wild type (black, close circles), D58A (brown, open squares), D58E (purple, open circles), and D58K (blue, close squares) and **(D)** wild type (black, close circles), Psb27 control (red, open circles), K63A (green, close circles), K63D (orange, close squares) and K63R (grey, open squares). Data shown are the average of three independent experiments. The standard error bars have also been shown.

Table 3.1 Photoautotrophic growth of wild type and the Psb27 mutants. The doubling time of the wild type and the Psb27 strains grown photoautotrophically in the presence of the corresponding antibiotic used to select the transformants. The cells were inoculated to an initial OD_{730} of ~0.05.

Strain	Doubling time[1] (h)
WT	13.1 ± 0.6[2]
ΔPsb27	16.4 ± 0.4
Psb27 control	17.2 ± 1.3
D14A	16.0 ± 0.4
R54E	18.4 ± 0.9
Y78H	15.1 ± 0.4
R94E	15.2 ± 0.7
E98R	16.1 ± 0.6
D58A	16.2 ± 0.8
D58E	15.2 ± 0.2
D58K	16.1 ± 0.4
K63A	16.3 ± 0.8
K63D	16.2 ± 0.2
K63R	15.1 ± 0.2

[1]The data shown are the mean doubling times over the first 36 h of the growth. Data shown is average of three independent experiments.
[2]The standard error have also been shown.

3.6.3 PS II-specific oxygen evolution assay

PS-II specific oxygen evolution assays were carried out for the wild type, the Psb27 control strain, the ΔPsb27 mutant and each of the strains carrying the single amino acid substitutions to assess the impact of the introduced changes onto the capacity of the PS II to support electron transfer between water and the added electron acceptor. Two different artificial quinone acceptors were used: 2,6-dichloro-1,4-benzoquinone (DCBQ) and 2,5-dimethyl-1,4-benzoquinone (DMBQ) along with potassium ferricyanide ($K_3Fe(CN)_6$). Potassium ferricyanide helps in maintaining the oxidised form of the quinone acceptors. Sodium bicarbonate was also used to assess whole chain electron transport.

Fig. 3.9 and Fig 3.10 shows the oxygen evolution traces obtained using DCBQ (A), DMBQ (B) and sodium bicarbonate (C). The average oxygen evolution rates for each Psb27 strains have been presented in Table 3.2.

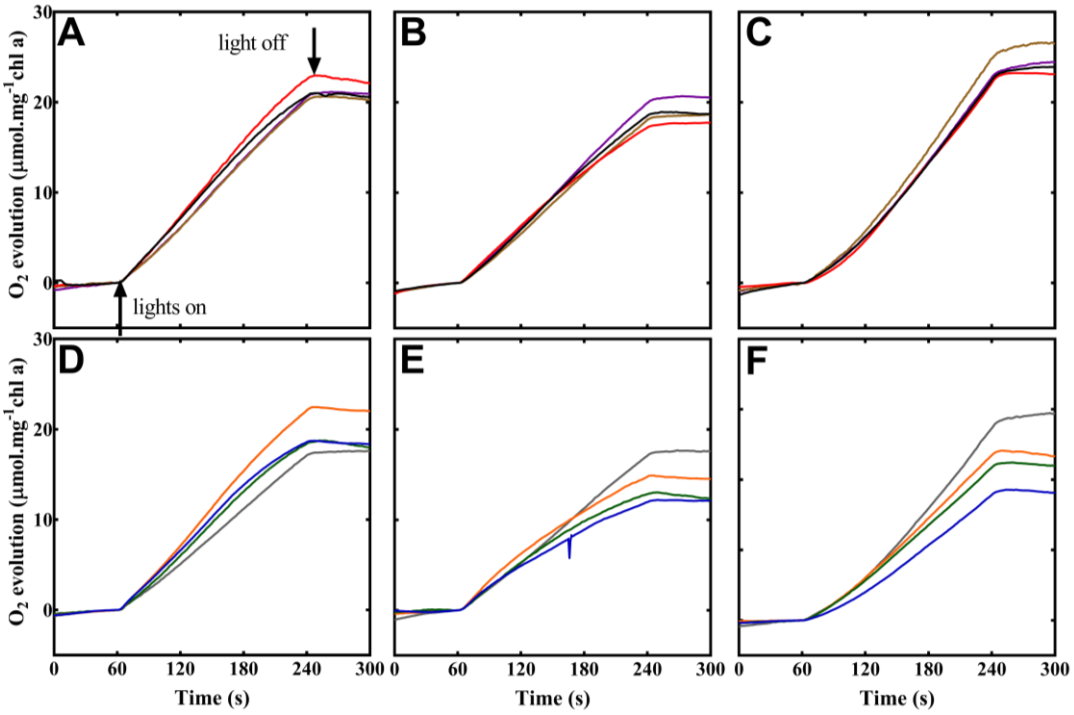

Figure 3.9 Oxygen evolution assay traces for the strains with amino acid substitutions at Asp-14, Arg-54, Tyr-78, Arg-94 and Glu-98 in Psb27. Panels **(A)** and **(D)** Oxygen evolution measured in the presence of DCBQ. Panels **(B)** and **(E)** Oxygen evolution measured in the presence of DMBQ. Panels **(C)** and **(F)** Oxygen evolution measured in the presence of sodium bicarbonate. The strains in panels **(A)**, **(B)** and **(C)** are wild type (black), Psb27 control (red), D14A (brown) and E98R (purple) and the strains in panels **(D)**, **(E)** and **(F)** are ΔPsb27 (blue), R54E (green), R94E (orange) and Y78H (grey). Data shown are the average of three independent experiments. The average oxygen evolution rates have been presented in Table 3.2.

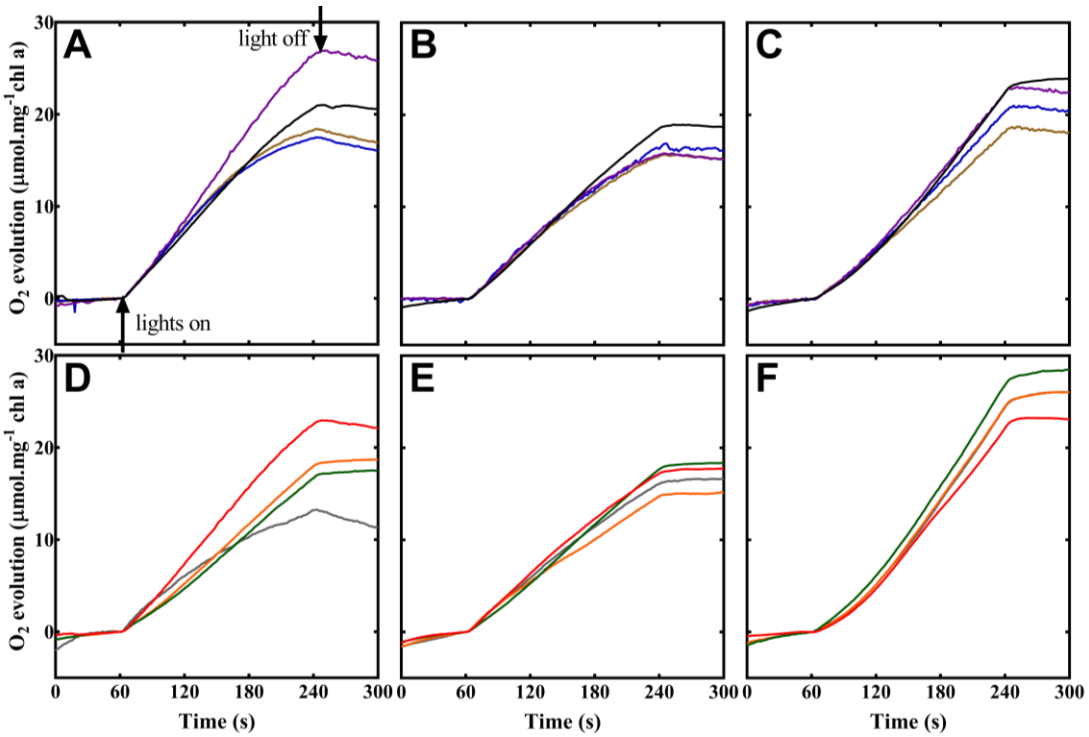

Figure 3.10 Oxygen evolution assay traces for the strains with amino acid substitutions at Asp-58 and Lys-63 in Psb27 Panels **(A)** and **(D)** Oxygen evolution measured in the presence of DCBQ. Panels **(B)** and **(E)** Oxygen evolution measured in the presence of DMBQ. Panels **(C)** and **(F)** Oxygen evolution measured in the presence of sodium bicarbonate. The strains in panels **(A)**, **(B)** and **(C)** are wild type (black), D58A (brown), D58E (purple) and D58K (blue) and the strains in panels **(D)**, **(E)** and **(F)** are Psb27 control (red), K63A (green), K63D (orange) and K63R (grey). Data shown are the average of three independent experiments. The average oxygen evolution rates have been shown in Table 3.2.

The oxygen-evolution rates of the Psb27 mutants were similar to the wild type. The wild type had an oxygen evolution rate of around 400 ± 20 µmol O_2 (mg of chl)$^{-1}$ h^{-1} with DCBQ, 330 ± 30 µmol O_2 (mg of chl)$^{-1}$ h^{-1} with DMBQ and 470 ± 40 µmol O_2 (mg of chl)$^{-1}$ h^{-1} with sodium bicarbonate. The Psb27 control strain also had oxygen evolution rates similar to the wild type. The oxygen evolution rates of K63D (300 ± 20 µmol O_2 (mg of chl)$^{-1}$ h^{-1}), Y78H (300 ± 30 µmol O_2 (mg of chl)$^{-1}$ h^{-1}) and K63A (320 ± 20 µmol O_2 (mg of chl)$^{-1}$ h^{-1}) were lower, as compared to the oxygen-evolution rates of the wild type and the Psb27 control strain in the presence of DCBQ. Out of all the Psb27 mutants, D14A had the lowest oxygen evolution rate of ~250 ± 10 µmol O_2 (mg of chl)$^{-1}$ h^{-1} in the presence of DMBQ. Overall, point mutations in Psb27 did little to alter the oxygen-evolving activity.

Table 3.2 Oxygen evolution rates of Psb27 mutants. The strains were grown in the presence of glucose and the corresponding antibiotics.

Strains	Oxygen evolution[1] (µmol O_2 (mg of chl)$^{-1}$ h^{-1})		
	DCBQ	DMBQ	Bicarbonate
WT	400 ± 20[2]	330 ± 30	470 ± 40
ΔPsb27	380 ± 20	320 ± 30	340 ± 20
Psb27 control	390 ± 20	340 ± 10	500 ± 20
D14A	330 ± 20	250 ± 10	420 ± 40
R54E	330 ± 20	300 ± 10	390 ± 50
Y78H	300 ± 30	290 ± 20	450 ± 50
R94E	390 ± 10	310 ± 20	470 ± 10
E98R	320 ± 10	310 ± 30	400 ± 30
D58A	390 ± 10	290 ± 10	330 ± 30
D58E	360 ± 20	310 ± 30	320 ± 20
D58K	340 ± 30	290 ± 30	320 ± 20
K63A	320 ± 20	290 ± 10	300 ± 20
K63D	300 ± 20	290 ± 20	330 ± 20
K63R	330 ± 30	300 ± 20	330 ± 10

[1]Oxygen evolution rates were measured in the presence of DCBQ, DMBQ and sodium bicarbonate. Data shown are the average of three independent experiments. [2]The standard error have been shown.

3.6.4 Low-temperature 77 K fluorescence emission spectroscopy

To study the effect of single amino acid substitutions in the Psb27 protein on the levels or stoichiometry of the PS I and PS II complexes, low temperature 77 K fluorescence emission spectroscopy measurements were performed. Two different excitation wavelengths (440 nm and 580 nm) were used. The illumination of samples with 440 nm light leads to the excitation of PS II directly, whereas the 580 nm light indirectly excites PS II via the light-harvesting antenna protein complexes providing information on the coupling and energy transfer between the antenna protein complexes and the photosystems (Mullineaux and Emlyn-Jones 2005). The 580 nm excitation gives emission peaks from phycocyanin (PC) (650 nm) and allophycocyanin (APC) (665 nm), while the 685 nm peak corresponds to the antennae pigments (long wavelength terminal emitters of the PBS core) along with emission from the PS II core antenna (usually visible as a 695 nm shoulder); and there is a PS I emission at 725 nm. Excitation with 440 nm results in 685 nm and 695 nm emission peaks from PS II complexes and the emission peak at 725 nm from PS I. The two emission peaks at 685

and 695 nm emissions arise from the CP43 and CP47 core antenna complexes in fully assembled PS II complexes although partially assembled complexes containing only CP43 have also been reported to have a fluorescence emission peak at 695 nm (Murata *et al.* 1966; Vermaas *et al.* 1994; Boehm *et al.* 2011).

The Psb27 control strain, ΔPsb27 and the D14A, R54E, Y78H, R94E and E98R mutants (Fig. 3.11 A and B), when excited at 440 nm displayed typical 725 nm emission, originating from PS I, and the 685 and 695 nm emissions originating from CP43 and CP47, respectively, of PS II. The D14A, E98R, and R54E mutants exhibited a small apparent increase in PS II specific fluorescence relative to their PS I emission compared to the wild type and the Psb27 control strain.

To get insight into the coupling and energy transfer between the PBS and PS II (and possibly PS I), cells were illuminated with a 580 nm light (Fig 3.11 C and D). All strains displayed the typical 725 nm emission originating from PS I; however, the ΔPsb27 strain and the D14A, R54E, Y78H, and R94E cells exhibited slightly lower levels of fluorescence emission from phycocyanin (650 nm), allophycocyanin (665 nm), and the ApcE PBS terminal emitter, respectively when compared to the wild type, the Psb27 control strain and the E98R mutant potentially suggesting efficient coupling of the PBS with the photosystems. Also, a shoulder was visible at 695 nm for the R54E, R94E and Y78H mutants possibly indicating the emission may contain contributions from both the CP43 and CP47 core antennae of PS II as well as the ApcE terminal emitter of the PBS (Joshua and Mullineaux 2004).

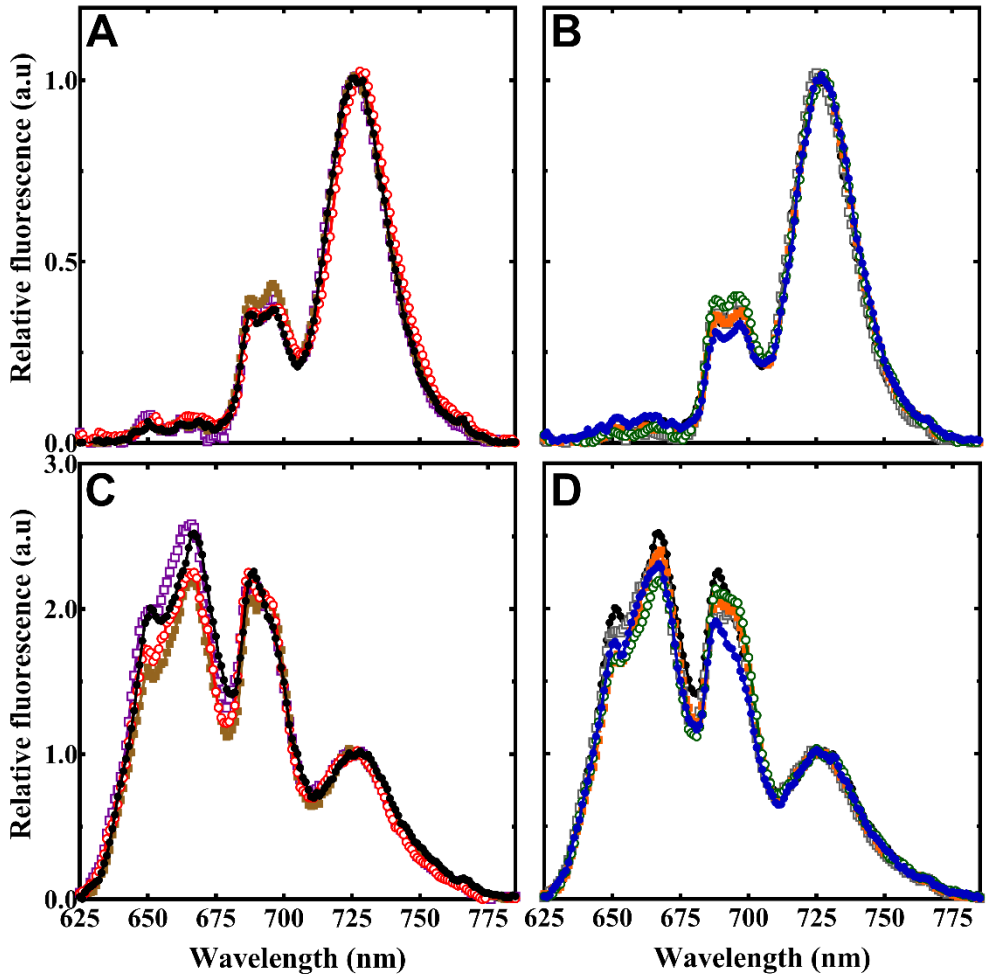

Figure 3.11 Low-temperature fluorescence emission spectra of the strains with amino acid substitutions at Asp-14, Arg-54, Tyr-78, Arg-94 and Glu-98 in Psb27. Panels **(A)** and **(B)** contains the fluorescence emission spectra with an excitation wavelength of 440 nm. Panels **(C)** and **(D)** contains the fluorescence emission spectra with an excitation wavelength of 580 nm. The strains in panels **(A)** and **(C)** are wild type (black, close circles), Psb27 control (red, open circles), D14A (brown, close squares) and E98R (purple, open squares) and the strains in panels **(B)** and **(D)** are wild type (black, close circles), ΔPsb27 (blue, close circles), R54E (green, open circles), R94E (orange, close squares) and Y78H (grey, open squares). Data shown are the average of four independent experiments.

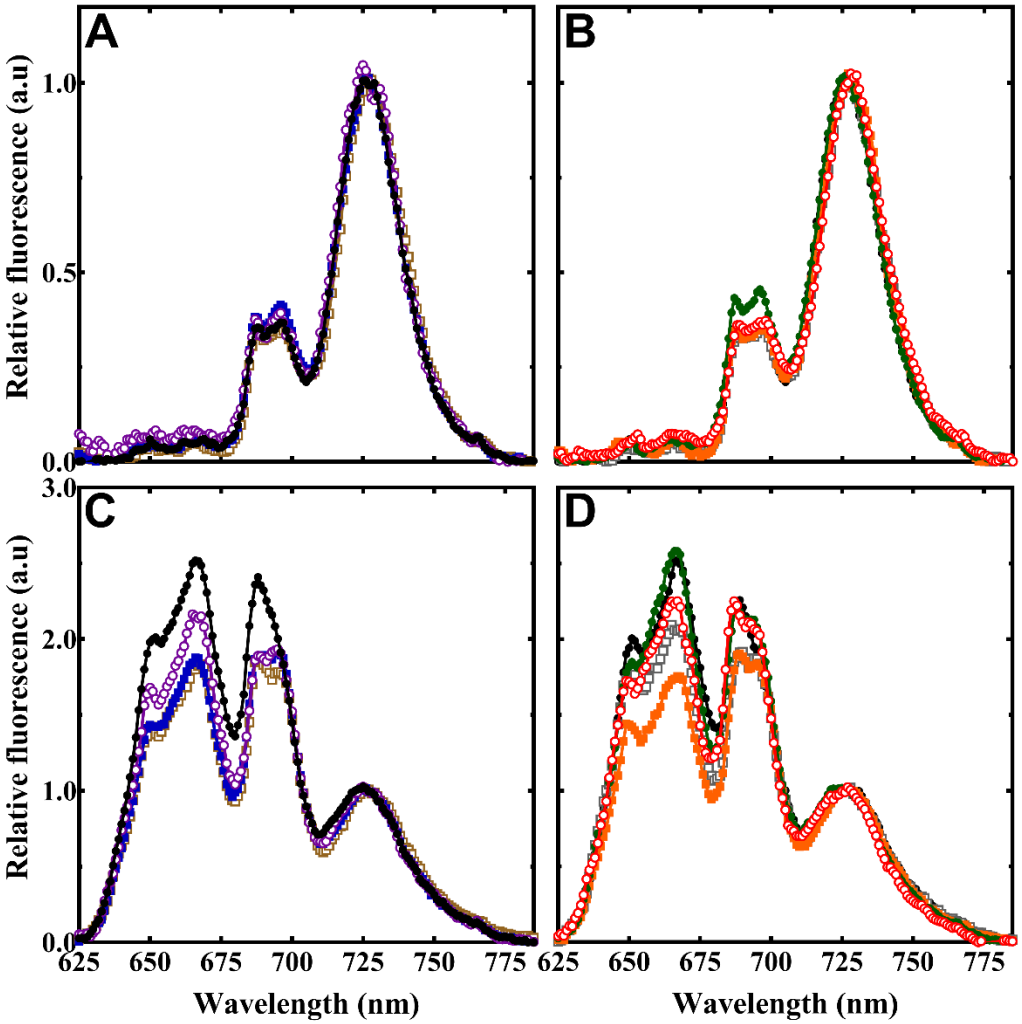

Figure 3.12 Low-temperature fluorescence emission spectra of the strains with amino acid substitutions at Asp-58 and Lys-63 in Psb27 protein. Panels **(A)** and **(B)** contains the fluorescence emission spectra with an excitation wavelength of 440 nm. Panels **(C)** and **(D)** contains the fluorescence emission spectra with an excitation wavelength of 580 nm. The strains in panels **(A)** and **(C)** are wild type (black, close circles), D58A (brown, open squares), D58E (purple, open circles), and D58K (blue, close squares) and the strains in panels **(B)** and **(D)** are wild type (black, close circles), Psb27 control (red, open circles), K63A (green, close circles), K63D (orange, close squares) and K63R (grey, open squares). Data shown are the average of four independent experiments.

Upon excitation of chlorophyll *a* with 440 nm light, strains with amino acid substitutions at Asp58 and Lys63 in Psb27 displayed similar levels of fluorescence emission from PS II (685 nm and 695 nm) and PS I (725 nm) except K63A mutant. In K63A mutant, the relative levels of PS II emission (685 nm and 695 nm) were higher than the wild type (Fig. 3.12 A and B).

Fluorescence emission in these strains was also analysed after excitation with 580 nm light. In the D58A, D58E, D58K, K63D and K63R mutants, the fluorescence emission from phycocyanin (650 nm), allophycocyanin (665 nm) and the ApcE PBS terminal emitter (685 nm) decreased relative to the 725 nm emission from PS I (Fig. 3.12 C and D); however, the K63A mutant was more similar to wild type and the Psb27 control strain. Also, a shoulder was visible at 695 nm in all the strains with amino acid substitutions at Asp58 and Lys63.

3.6.5 Room temperature chlorophyll *a* fluorescence

Measurements of PS II-specific chlorophyll *a* variable fluorescence is a highly sensitive, non-invasive and reliable method to study the rate of electron transfer within PS II (Papageorgiou *et al.* 2007; Stamatakis *et al.* 2007). The fluorescence level increases when the PS II reaction centres are in a closed state (i.e. when the primary plastoquinone electron acceptor, Q_A is reduced) and vice-versa (Vredenberg and Duysens 1963). Two kinds of room temperature chlorophyll *a* fluorescence emission measurements were carried out: chlorophyll *a* fluorescence induction under continuous actinic illumination and the decay of chlorophyll *a* fluorescence following single-turnover actinic flashes**.**

3.6.5.1 Chlorophyll *a* fluorescence Induction

When cyanobacterial cells are exposed to light after dark adaptation, the variable chlorophyll a fluorescence emission from PS II shows a characteristic transient with a series of inflections and maxima designated by the letters O, J, I, P, S, M and T (Fig. 3.13). The minimum fluorescence measured after dark adaptation is the O level; J and I are intermediate inflexions at around 2 and 30 ms after the onset of illumination; P stands for the peak obtained after approximately 1 s of illumination; S is for a semi steady-state level; M for a subsequent maximum, and T is the terminal steady-state level (Govindje 1995). The fast OJIP phase of the induction assay can monitor electron transfer occurring at the acceptor and donor sides of PS II.

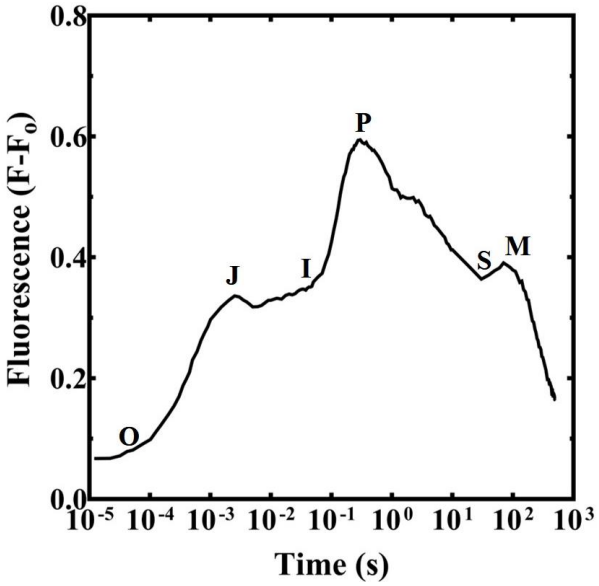

Figure 3.13 Chlorophyll fluorescence induction transients measured in *Synechocystis* 6803.The O, J, I, P, S, M, and T steps, where O is the first measured minimum fluorescence level; P is the peak; S stands for semi-steady state; M for a maximum; and T (not shown) for a terminal steady state level are marked in the diagram.

The D14A and E98R mutants exhibited a lower J level as compared to the wild-type strain and the E98R mutant also had a lower P level (Fig. 3.14 A). The Psb27 control strain displayed a modified IP rise in comparison to the wild type and exhibited a slightly delayed P level (Fig. 3.14 A) as all the mutants were grown in the presence of selective antibiotic i.e. spectinomycin in this case except the wild type. The Y78H strain showed similar fluorescence induction kinetics and a similar P level to those of the wild type; however, the ΔPsb27 strain and the R54E and R94E mutants exhibited an increase in their variable fluorescence emission (Fig. 3.14 B). Nevertheless, the relative kinetics for all strains were similar to the wild type except the delayed P peak in the Psb27 control cells (see insets in Fig. 3.14 A and 3.14 B).

The induction measurements were also carried in the presence of the PS II-specific inhibitor 3-(3,4-dichlorophenyl)-1,1-dimethylurea (DCMU) that blocks the electron transport between the Q_A and Q_B sites in the PS II reaction centre complex. In the presence of DCMU, the maximum $F-F_o$ fluorescence signal is proportional to the number of active PS II centres. The data obtained in the presence of DCMU in Fig 3.14 C was in agreement with Fig. 3.14 A and indicated that there were less assembled PS II centres in the E98R strain and that the Psb27 control strain had modified kinetics

compared to wild type with the maximum fluorescence level being reached following the initial rise in the signal. This difference in the induction curve between the Psb27 control strain and the wild type might arise from changes in absorption cross-section from the movement of the PBS antennae or a decrease in fluorescence quenching due to reduction of the PQ pool in the different strains.

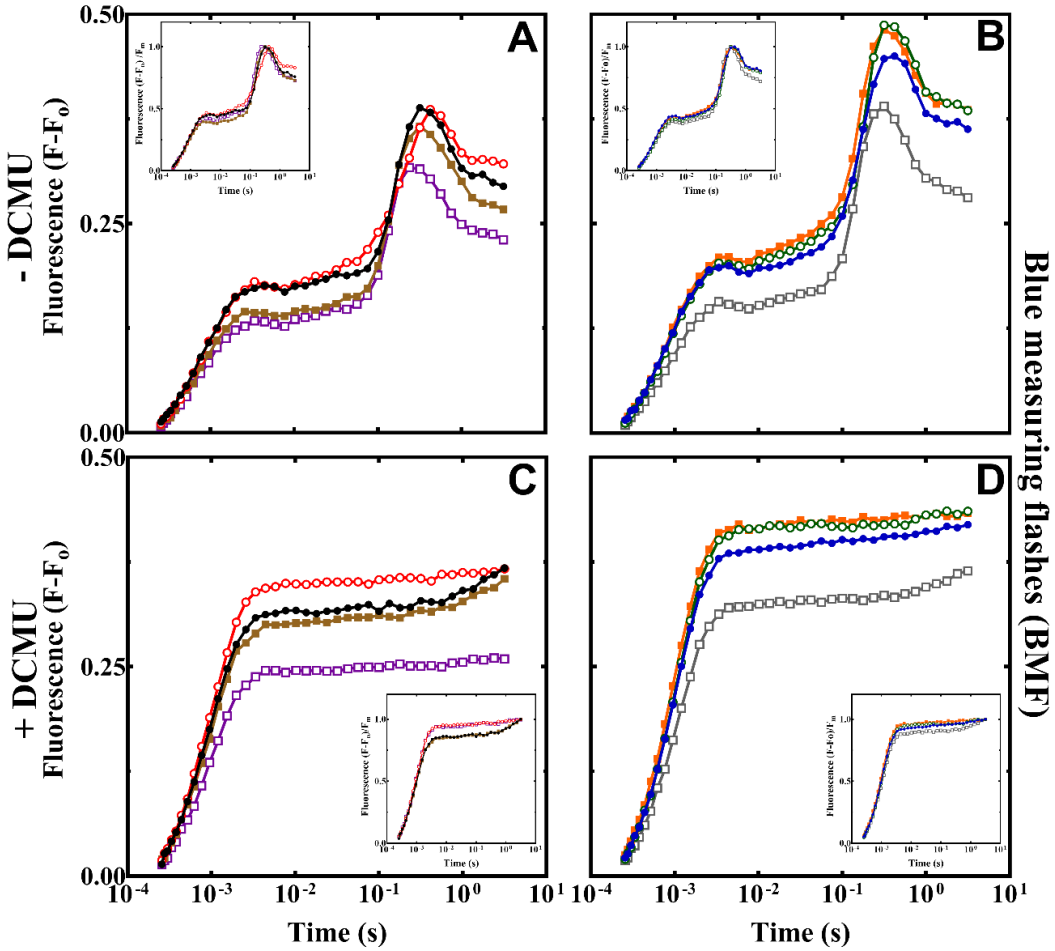

Figure 3.14 Normalised steady-state chlorophyll *a* fluorescence induction in the strains with amino acid substitutions at Asp-14, Arg-54, Tyr-78, Arg-94 and Glu-98 in Psb27.Panels **(A)** and **(B)** contains the measurements in the absence of DCMU and panels **(C)** and **(D)** contains the measurements in the presence of DCMU. The strains in panels **(A)** and **(C)** are wild type (black, close circles), Psb27 control (red, open circles), D14A (brown, close squares) and E98R (purple, open squares), and the strains in panels **(B)** and **(D)** are ΔPsb27 (blue, close circles), R54E (green, open circles), R94E (orange, close squares) and Y78H (grey, open squares). The data normalised to F_m value of each strain has been shown in the insets. Data represented are the average of at least three independent experiments.

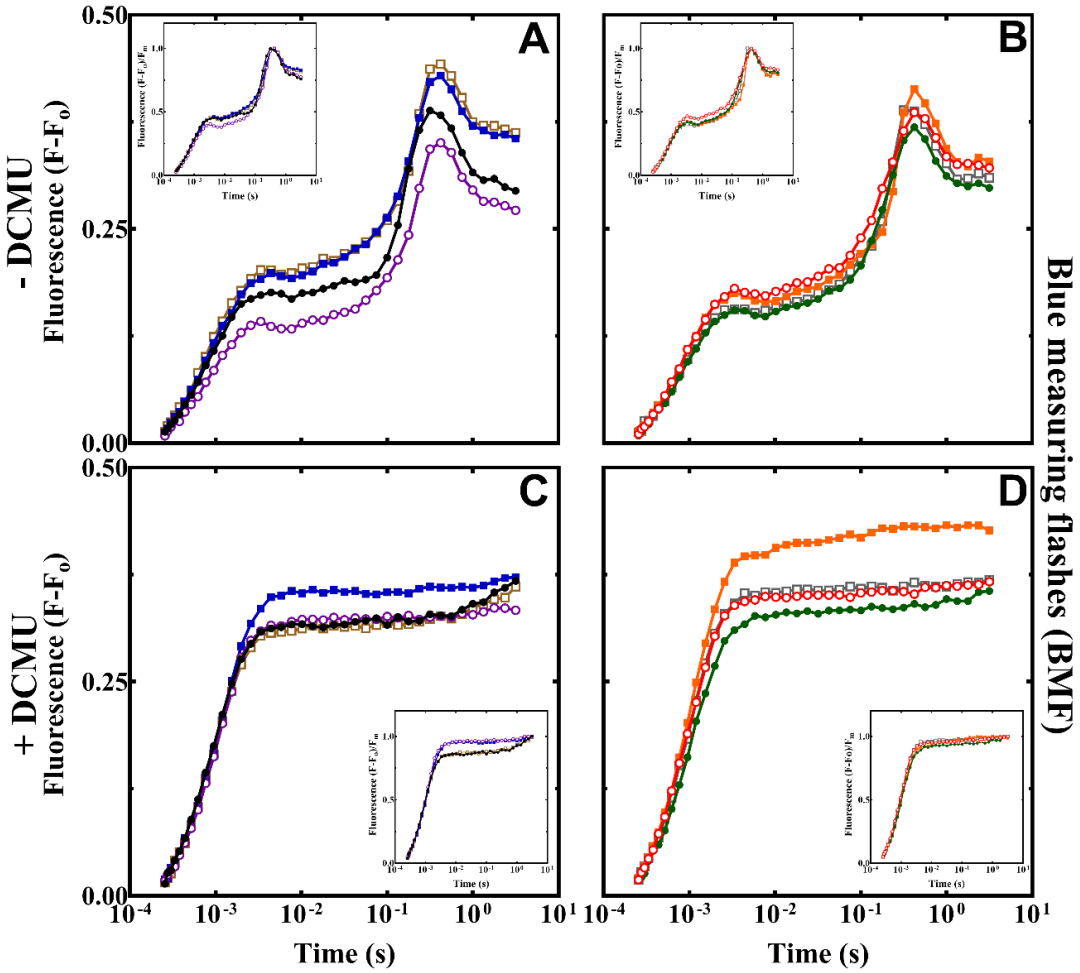

Figure 3.15 Normalised steady-state chlorophyll *a* fluorescence induction in the strains with amino acid substitutions at Asp-58 and Lys-63 in Psb27.Panels **(A)** and **(B)** contains the measurements in the absence of DCMU and panels **(C)** and **(D)** contains the measurements in the presence of DCMU. The strains in panels **(A)** and **(C)** are wild type (black, close circles), D58A (brown, open squares), D58E (purple, open circles), and D58K (blue, close circles) and the strains in panels **(B)** and **(D)** are Psb27 control (red, open circles), K63A (green, close circles), K63D (orange, close squares) and K63R (grey, open squares). The data normalised to F_m value of each strain has been shown in the insets. Data represented are the average of at least three independent experiments.

The D58A and D58K mutants exhibited a greater extent of variable fluorescence with an elevated P peak as compared to the wild type. The induction curve for D58E strain remained below the wild-type trace (Fig. 3.15 A). The K63A and K63R mutants exhibited lower levels for their J and P when compared with both the Psb27 control and the K63D strain (Fig. 3.15 B). All the mutants with the amino acid substitutions at Asp58 and Lys63 exhibited a delayed IP rise relative to the wild-type strain.

To further investigate the differences in the IP rise and P peak of the various Psb27 mutants, the duration of the chlorophyll *a* fluorescence induction assay was increased to ~500 s in the presence and absence of DCMU (Fig. 3.16 and 3.17). The D14A and E98R mutants exhibited similar levels of variable fluorescence except for the IP rise as well as SM rise was higher in the case of D14A cells in comparison to the wild-type strain. As discussed earlier, the Psb27 control strain still displayed a modified IP rise as compared to the wild type and exhibited a slightly delayed P level. The ΔPsb27, R54E and R94E mutants exhibited higher levels of variable fluorescence. However, the SM rise was higher in ΔPsb27 strain (see inset in Fig. 3.16 B). The R54E and R94E mutants displayed a smaller SM rise as compared to the wild type (see inset in Fig. 3.16 B). Also, the Y78H mutant exhibited lower levels of variable fluorescence with a reduced IP rise as compared to the wild type except for elevated O, J inflexion in comparison to the wild type (see inset in Fig. 3.16 B).

Long term fluorescence induction was also carried out in the presence of DCMU (Fig. 3.16 C, D and Fig. 3.17 C, D). The E98R (Fig. 3.16 C) and Y78H (Fig. 3.16 D) mutants exhibited lower variable fluorescence in the presence of DCMU indicating a lower number of assembled PS II centres or presence of unassembled PS II centres. Other possibilities might include the presence of free pigments, or changed energy transfer within CP43.

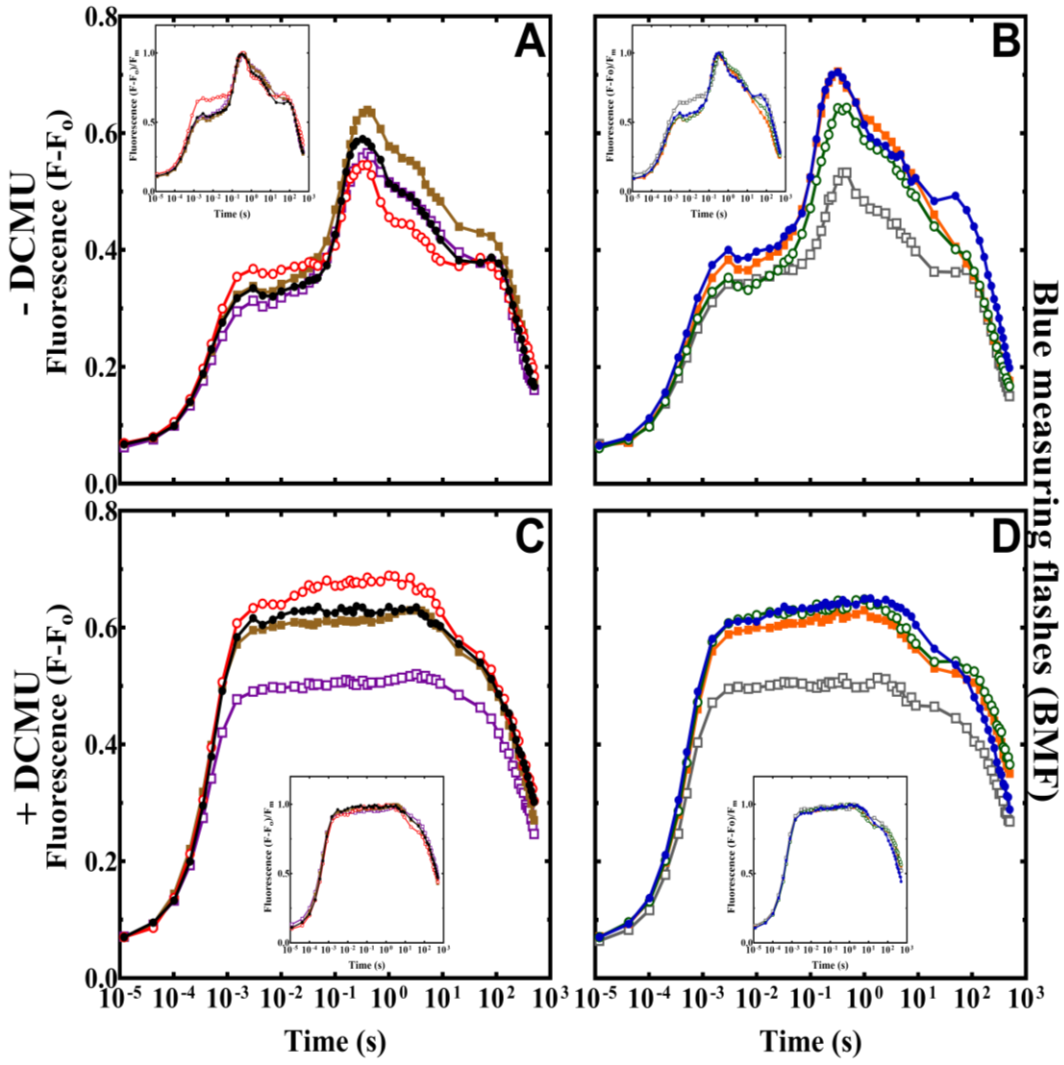

Figure 3.16 Normalised steady-state long-term chlorophyll *a* fluorescence induction (500 s) in strains with amino acid substitutions at Asp-14, Arg-54, Tyr-78, Arg-94 and Glu-98 in Psb27.Panels **(A)** and **(B)** contains the measurements in the absence of DCMU and panels **(C)** and **(D)** contains the measurements in the presence of DCMU. The strains in panels **(A)** and **(C)** are wild type (black, close circles), Psb27 control (red, open circles, D14A (brown, close squares) and E98R (purple, open squares), and the strains in panels **(B)** and **(D)** are ΔPsb27 (blue, close circles), R54E (green, open circles), R94E (orange, close squares) and Y78H (grey, open squares). The data normalised to F_m value of each strain has been shown in the insets. Data represented are the average of at least three independent experiments.

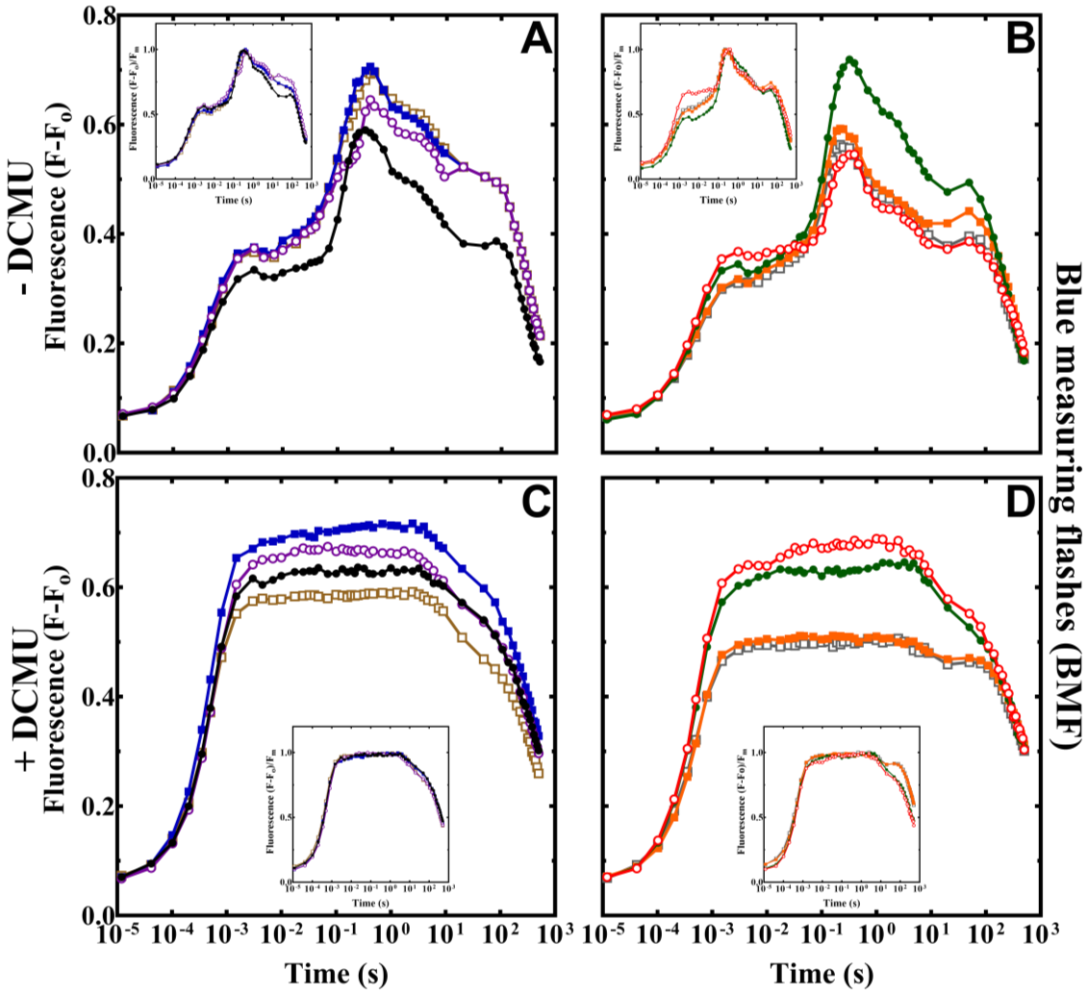

Figure 3.17 Normalised steady-state long-term chlorophyll *a* fluorescence induction (500 s) in strains with amino acid substitutions at Asp-58 and Lys-63 in Psb27.Panels **(A)** and **(B)** contains the measurements in the absence of DCMU and panels **(C)** and **(D)** contains the measurements in the presence of DCMU. The strains in panels **(A)** and **(C)** are wild type (black, close circles), D58A (brown, open squares), D58E (purple, open circles), and D58K (blue, close squares), and the strains in panel **(B)** and **(D)** are Psb27 control (red, open circles), K63A (green, close circles), K63D (orange, close squares) and K63R (grey, open squares). The data normalised to F_m value of each strain has been shown in the insets. Data represented are the average of at least three independent experiments.

All the mutants with the amino acid substitutions at Asp-58 showed higher levels of I, P, S and M positions as compared to the wild type (see Fig. 3.17 A and the inset in Fig. 3.17 A). Also, K63A mutant exhibited higher I, P, S and M levels in comparison to the wild type and the Psb27 control strain (Fig. 3.17 B). The K63D and K63R mutants displayed similar wild-type levels of variable fluorescence in the absence of DCMU. However, the Psb27 control strain, and the D58E, D58K, and K63A mutants exhibited higher levels of variable fluorescence in the presence of DCMU which is in agreement

with the results obtained in the absence of DCMU (Fig. 3.17 C and D). The D58A, K63D and K63R mutants displayed lower levels of assembled PS II centres in the presence of DCMU. Other possibilities might include unassembled PSII centres/free pigments, or changed energy transfer within CP43.

3.6.5.2 Chlorophyll *a* fluorescence decay measurements following single actinic flash

The decay kinetics of chlorophyll *a* fluorescence following single saturating actinic flash were also investigated and compared between wild type and the Psb27 mutants (Fig. 3.18 and 3.19). The kinetics of the chlorophyll *a* fluorescence decay can be used to indicate rates of electron transfer between Q_A^- and Q_B and between Q_A^- and the S_2 state of the oxygen-evolving complex. The model applied in this thesis is based on that developed by Vass and co-workers (Vass *et al.* 1999) and proposes two exponential components and one hyperbolic component (see Chapter 2, Section 2.7.6.2); the initial fast exponential phase (200-400 μs) of the decay reflects electron transfer from Q_A^- to Q_B. The intermediate exponential phase (milliseconds) indicates the binding of the plastoquinone molecule to the Q_B site and the slow hyperbolic phase (seconds) reflects charge recombination between Q_A^- and donor side of the PS II.

All the Psb27 mutants exhibited similar rates of chlorophyll fluorescence decay to the wild-type strain (Fig. 3.17 A, B and Fig. 3.18 A, B), but the decays for the Lys-63 mutants displayed slower forward electron transfer kinetics in comparison to the wild type. Upon analysis, the half-time of the microsecond component of the D14A, D58E, K63A, K63D and K63R mutants was faster than the half-time of the microsecond component of the wild type (Table 3.3). However, the half-time of the microsecond component of R94E, E98R, and D58K mutants was slower than the half-time of the microsecond component of the wild type, but in all cases the changes were small, and the amplitudes were also comparable (Table 3.3). The half-time of the slow component of chlorophyll *a* fluorescence decay, without any addition for most of the Psb27 mutants (ΔPsb27, D14A, Y78H, E98R, D58A, D58E, D58K, K63A, K63D) was faster (~1.7-fold) as compared to the wild type, but this effect was also present in the Psb27 control strain. In addition, the half-time of the slow component without any addition for R54E, R94E, and K63R mutants was similar to the wild type.

The chlorophyll fluorescence decay studies were also carried out in the presence of DCMU (Fig. 3.18 C, D and Fig. 3.19 C, D). The DCMU binds to the Q_B site and blocks the electron transfer between Q_A and Q_B. The traces reflect electron transport and charge recombination pathways between the Q_A^- and the S_2 state (Fufezan *et al.* 2007). All the Psb27 mutants exhibited similar chlorophyll *a* fluorescence decay in the presence of DCMU (Fig. 3.18 C, D and 3.19 C, D). The half-time of the microsecond component of D14A, Y78H, E98R, D58A, D58K mutants was faster than the wild type. Also, the half-time of the fast component of D58E and K63R strains was slower in comparison to the wild type (Table 3.4). The amplitude of the microsecond component of ΔPsb27 strain and the K63D mutant was greater than the amplitude of the microsecond component of the wild type. The R54E and D58A mutants exhibited a smaller millisecond component amplitude as compared to the wild type in the presence of DCMU. Overall, the Psb27 mutants displayed similar back charge recombinant kinetics. However, the increase in the amplitude of the fast component of the ΔPsb27 strain was compensated by the decrease in the amplitude of the slow component of ΔPsb27 strain as compared to the wild type and the Psb27 control strain in the presence of DCMU.

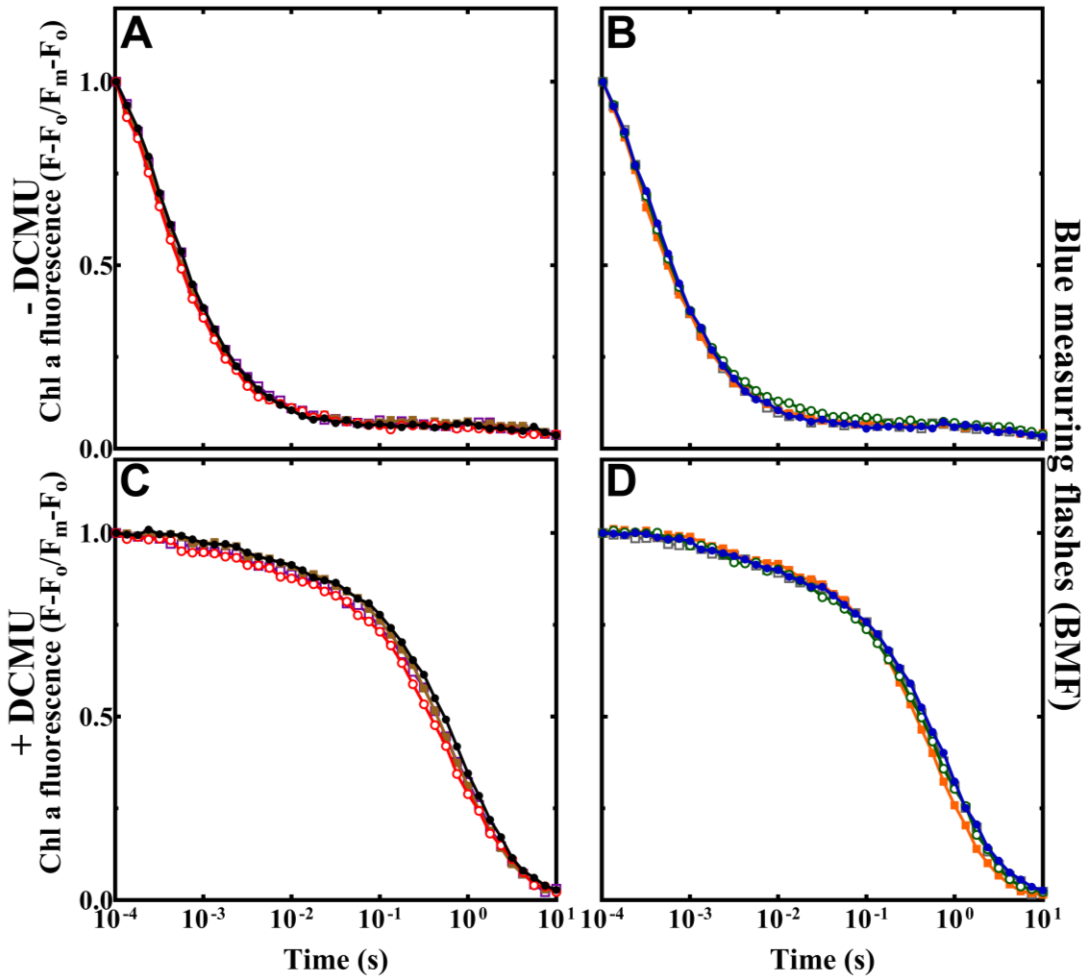

Figure 3.18 Relaxation of chlorophyll *a* fluorescence following single flash in the strains with amino acid substitutions at Asp-14, Arg-54, Tyr-78, Arg-94 and Glu-98 in Psb27.Panels **(A)** and **(B)** contains the measurements in the absence of DCMU. Panel **(C)** and **(D)** contains the measurements in the presence of DCMU. The strains shown in panels **(A)** and **(C)** are wild type (black, close circles), Psb27 control (red, open circles), D14A (brown, close squares) and E98R (purple, open squares), and the strains in panels **(B)** and **(D)** are ΔPsb27 (blue, close circles), R54E (green, open circles), R94E (orange, close squares) and Y78H (grey, open squares). Data represented are the average of at least three independent experiments.

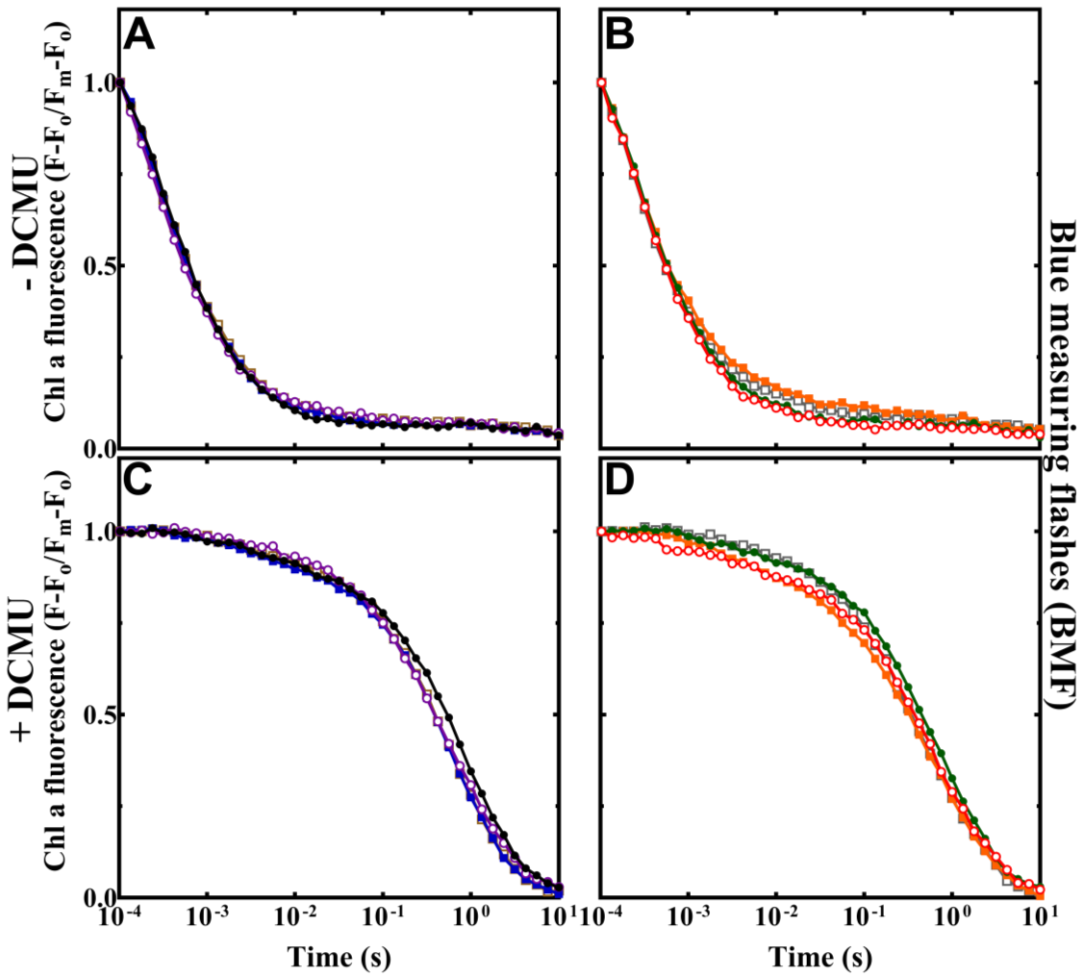

Figure 3.19 Relaxation of chlorophyll *a* fluorescence following single flash in strains with amino acid substitutions at Asp-58 and Lys-63 in Psb27.Panels **(A)** and **(B)** contains the measurements in the absence of DCMU. Panels **(C)** and **(D)** contains the measurements in the presence of DCMU. The strains shown in panels **(A)** and **(C)** are wild type (black, close circles), D58A (brown, open squares), D58E (purple, open circles), and D58K (blue, close squares) and the strains in panels **(B)** and **(D)** are Psb27 control (red, open circles), K63A (green, close circles), K63D (orange, close squares) and K63R (grey, open squares). Data represented are the average of at least three independent experiments.

Table 3.3 Decay kinetics of variable chlorophyll *a* fluorescence following single saturating actinic flash in the absence of DCMU.

Strains	Fast		Intermediate		Slow	
	$T_{1/2}$ (µs)	Amp.	$T_{1/2}$ (ms)	Amp.	$T_{1/2}$ (s)	Amp.
WT	273 ± 16*	62 ± 1	2.8 ± 0.2	30 ± 1	7.5 ± 1.8	8.4 ± 0.2
ΔPsb27	280 ± 9	60 ± 2	2.8 ± 0.2	31 ± 2	4.0 ± 1.0	9.1 ± 0.8
Psb27 control	264 ± 13	62 ± 2	2.9 ± 0.2	29 ± 2	3.8 ± 0.5	9.3 ± 0.1
D14A	245 ± 7	58 ± 1	2.5 ± 0.2	33 ± 1	4.8 ± 1.0	9.2 ± 0.3
R54E	262 ± 11	61 ± 1	3.0 ± 0.3	29 ± 1	6.0 ± 0.5	9.1 ± 0.2
Y78H	264 ± 4	61 ± 1	2.8 ± 0.2	31 ± 1	4.7 ± 0.7	9.1 ± 0.5
R94E	296 ± 11	58 ± 1	3.0 ± 0.2	34 ± 1	6.8 ± 0.4	8.2 ± 0.3
E98R	284 ± 6	60 ± 1	3.0 ± 0.1	31 ± 1	4.9 ± 1.0	9.2 ± 0.6
D58A	264 ± 13	63 ± 2	3.5 ± 0.4	27 ± 2	4.5 ± 0.8	10.1 ± 0.3
D58E	257 ± 14	60 ± 2	3.0 ± 0.3	29 ± 2	4.0 ± 1.0	11.2 ± 1.2
D58K	284 ± 16	59 ± 1	3.2 ± 0.1	31 ± 2	4.8 ± 1.4	10.1 ± 0.6
K63A	258 ± 7	61 ± 1	3.0 ± 0.2	29 ± 1	3.8 ± 0.6	10.1 ± 0.7
K63D	256 ± 9	61 ± 1	3.5 ± 0.4	28 ± 1	3.6 ± 0.1	11.2 ± 0.9
K63R	239 ± 4	60 ± 2	3.3 ± 0.4	30 ± 2	5.0 ± 1.6	11.3 ± 0.4

*The standard error have been shown for the chlorophyll *a* fluorescence decays from four independent experiments.

Table 3.4 Decay kinetics of variable chlorophyll *a* fluorescence following single saturating actinic flash in the presence of DCMU.

Strains	Fast		Slow	
	$T_{1/2}$ (ms)	Amp.	$T_{1/2}$ (s)	Amp.
WT	2.7 ± 0.1*	9.1 ± 0.5	0.4 ± 0.1	91.2 ± 0.5
ΔPsb27	2.3 ± 0.1	13.1 ± 2.0	0.4 ± 0.1	87.2 ± 2.0
Psb27 control	1.8 ± 0.3	9.3 ± 0.2	0.4 ± 0.1	91.3 ± 0.2
D14A	2.0 ± 0.3	8.1 ± 0.5	0.4 ± 0.1	92.1 ± 0.5
R54E	3.0 ± 0.2	6.1 ± 0.7	0.4 ± 0.1	94.4 ± 0.7
Y78H	2.0 ± 0.1	9.2 ± 0.1	0.4 ± 0.1	91.2 ± 0.1
R94E	2.4 ± 0.2	7.1 ± 0.5	0.4 ± 0.1	92.2 ± 0.5
E98R	2.0 ± 0.2	9.1 ± 0.6	0.4 ± 0.1	91.2 ± 0.6
D58A	2.4 ± 0.4	6.3 ± 0.3	0.3 ± 0.1	94.1 ± 0.3
D58E	4.0 ± 1.3	8.4 ± 0.6	0.3 ± 0.1	92.3 ± 0.6
D58K	2.1 ± 0.3	8.1 ± 0.6	0.3 ± 0.1	92.2 ± 0.6
K63A	2.5 ± 0.2	9.1 ± 0.8	0.3 ± 0.1	91.3 ± 0.8
K63D	2.6 ± 0.6	11.2 ± 1.4	0.3 ± 0.1	89.3 ± 1.5
K63R	3.8 ± 1.3	9.3 ± 1.0	0.3 ± 0.1	91.2 ± 1.1

*The standard error have been shown for the chlorophyll *a* fluorescence decays from four independent experiments.

3.6.6 PS II assembly

To investigate the assembly of PS II complexes in the Psb27 mutants, blue native polyacrylamide gel electrophoresis (BN-PAGE) of isolated thylakoid membranes was performed, followed by immunodetection with PS II specific antibodies - D1, D2, CP43 and CP47 proteins (Fig. 3.20). The PS II assembly is a very complicated process, and a series of events takes place in an orderly fashion. The assembly of the mature PS II complex involves the formation of pre-assembly complexes that are assembled in a stepwise manner. The major complexes visible in Fig. 3.2 are the mature PS II dimer and the PS II monomer. Mostly, D1, D2, CP43, and CP47 are involved in the early assembly process of PS II complex assembly (Zhang *et al.* 1999; Rokka *et al.* 2005; Danielsson *et al.* 2006). All the Psb27 mutant strains (ΔPsb27, Psb27 control, D14A, R54E, Y78H, R94E, E98R, D58A, D58E, D58K, K63A, K63D and K63R) displayed similar expression level of the three macromolecular PS II assembly complexes found in wild type (dimers, monomers and RC47) (Fig. 3.20). These data indicate that the assembly of PS II in all strains is similar to wild type. Thus, showing that the introduced point mutations in Psb27, do not perturb PS II assembly.

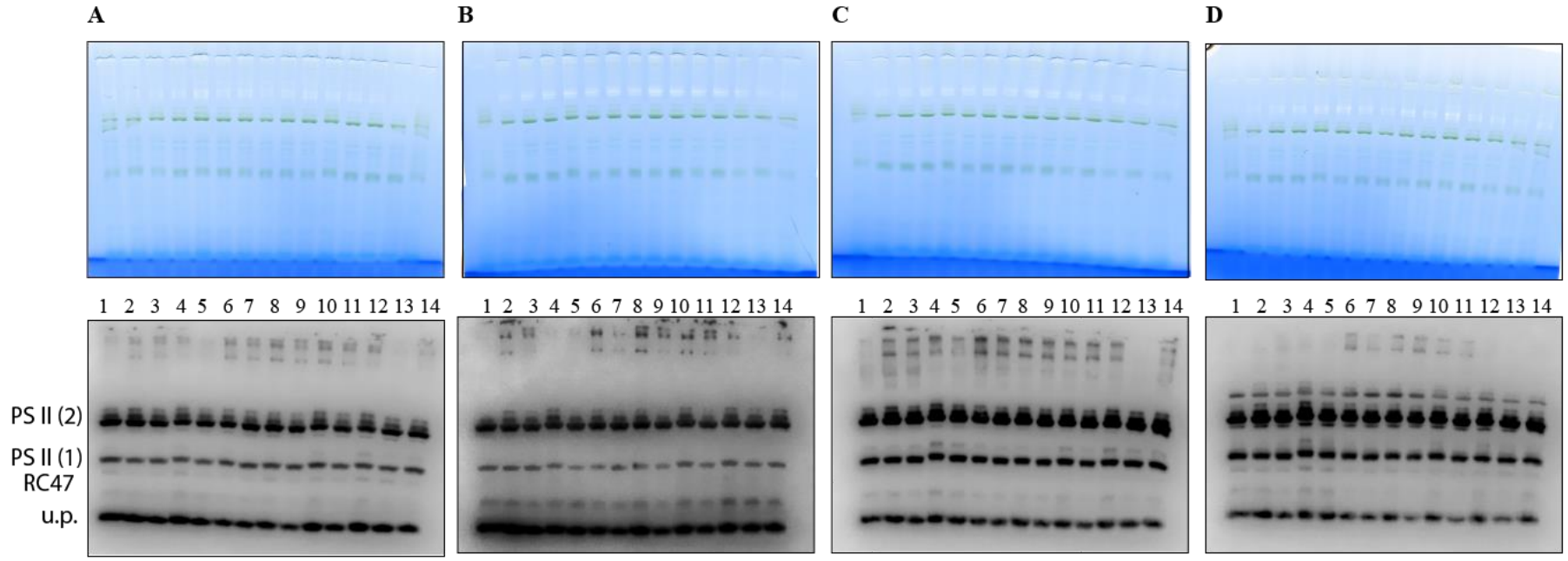

Figure 3.20 PS II assembly analysis. Thylakoid samples run on BN-PAGE followed by the immunodetection of PS II complexes using PS II specific antibodies. (A) D1, (B) D2, (C) CP43 and (D) CP47. 5 µg of chlorophyll was loaded onto 3-12% gradient BN-PAGE. Protein transferred to PVDF membrane for immunodetection through enhanced chemiluminescence (ECL). Lanes are (1) wild type, (2) ΔPsb27, (3) Psb27 control, (4) D14A, (5) R54E, (6) Y78H, (7) R94E, (8) E98R, (9) D58A, (10) D58E, (11) D58K, (12) K63A, (13) K63D and (14) K63R. The complexes are PS II dimer; PS II monomer; RC47, PS II complex without CP43. u.p. means unassembled protein complexes.

.

3.7 Discussion

The *Synechocystis* 6803 Psb27 protein has been shown to interact with the CP43 protein subunit (Liu *et al.* 2011a; Liu *et al.* 2011b; Komenda *et al.* 2012a). In this study, conserved amino acid residues of Psb27 protein potentially involved in protein-protein interactions with other PS II subunits were targeted using site-directed mutagenesis (Fig. 3.2 A). Also, the amino-acid residues of Psb27 that have been proposed to crosslink with the CP43 protein by Pakrasi and co-workers (Liu *et al.* 2011a): i.e. Asp-58 and Lys-63 were also targeted (Fig. 3.2 A).

A Psb27 mutagenesis system was constructed to carry out the studies (Fig. 3.6). The efficiency of the Psb27 mutagenesis system was confirmed by running the isolated thylakoid samples from mutants on SDS-PAGE followed by immunoblotting using Psb27 specific antibodies to test the expression level of Psb27 protein in the constructed mutants (Fig. 3.7). The level of Psb27 expression in the Psb27 control strain, and the R54E* and R94E strains was similar to the wild type. The Psb27 expression was completely absent in the ΔPsb27 strain since the *psb27* gene was deleted in this strain via its replacement with a chloramphenicol-resistance cassette (camR) (Fig. 3.5).

The Psb27 control strain, ΔPsb27 strain and D14A, R54E, Y78H, R94E, E98R, D58A, D58E, D58K, K63A, K63D, and K63R mutants (Fig. 3.8) were able to grow photoautotrophically similar to the wild-type strain (Table 3.1). Most of the Psb27 mutants exhibited wild-type levels of oxygen-evolution activity. However, the Y78H, K63A, and K63D mutants showed lower levels of oxygen evolution, when measured in the presence of PS II specific artificial quinone acceptor DCBQ (Table 3.2). Also, the K63A and D58K mutants exhibited slightly lower levels of oxygen evolution when supported using sodium bicarbonate (Table 3.2).

A similar level of PS II and PS I was displayed by all the Psb27 mutants when excited with the 440 nm light. However, ΔPsb27 strain and D14A, and R54E mutants exhibited higher levels of emission from PS II (685 nm and 695 nm), potentially indicating decrease in the emission maxima of PS I, to which the PS II emissions were normalised potentially due to inhibited chlorophyll *a* biosynthesis. Another possibility could be an increase in the levels of assembled PS II reaction centres in the cells. The ΔPsb27, D14A, D58A, D58E, D58K, K63D, and K63R mutants displayed altered levels of

phycocyanin (650 nm), allophycocyanin (665 nm) and ApcE PBS terminal emitter (685 nm) in comparison to the wild type and the Psb27 control strain potentially suggesting the changes in the energy coupling between PBS and the photosystems (PS II and PS I).

All the Psb27 mutants displayed similar kind of fluorescence induction yields (OJIP) when probed using chlorophyll *a* fluorescence induction assay (Fig. 3.14 A, B and 3.15 A, B). However, the levels of P were lower in Y78H, and D58E mutants and the I and P inflexions were higher in the R54E, R94E, E98R, D58K and D58E cells. All the Psb27 strains exhibited similar variable fluorescence induction traces in the presence of DCMU (Fig. 3.14 C, D and 3.15 C, D). The F_m levels in the presence of DCMU were lower in the R54E and Y78H mutants in comparison to the wild type and the Psb27 control strain potentially suggesting lower numbers of PS II centres. The lower number of assembled PS II centres in the Y78H mutant is a little bit contradictory, as Tyr78 to His was the most conservative amino-acid substitution that was carried out in *Synechocystis* 6803, as most of the algae and higher plants contain Histidine at the 78th position of Psb27 protein. There are different factors that can affect the magnitude and the timing of the events in the chlorophyll *a* fluorescence induction curve (Papageorgiou *et al.* 2007). The differences seen in the induction transients in Psb27 mutants from wild type and Psb27 control strain might arise from changes in absorption cross-section from the movement of the PBS antennae, or a decrease in the fluorescence quenching due to the reduction of the PQ pool in the different strains.

Also, the chlorophyll *a* fluorescence induction assay was repeated with a longer duration of the assay (~500 s) (Fig 3.16 and 3.17) to further investigate the difference in the levels of IP rise and P peak in some of the Psb27 mutants. There was a decrease in the SM rise for R54E, R94E, D58E and D58K cells as compared to the wild type and the Psb27 control strain. The SM phase is usually linked with the transmembrane pH gradient formation and membrane potential and various other non-photochemical quenching processes. Long-term fluorescence induction was also carried out in the presence of DCMU (Fig. 3.16 C, D, and 3.17 C, D). All the Psb27 mutants exhibited similar levels of variable fluorescence in the presence of DCMU (Fig. 3.16 C, D and 3.17 C, D).

Chlorophyll *a* fluorescence decay measurements, following a single actinic flash of dark-adapted cells in the absence of DCMU, showed similar microsecond and

millisecond components in most of the Psb27 mutants as compared to the wild type (Fig. 3.18 A, B and 3.19 A, B). There was no significant difference between the forward electron transfer kinetics in the Psb27 mutants (Table 3.3). The half-time of the slow component for most of the Psb27 mutants (ΔPsb27, Psb27 control, D14A, Y78H, E98R, D58A, D58E, D58K, K63A, and K63D) was faster than the half-time of the slow component of the wild type. The half-time of the fast component of D14A and D58E mutants was faster than the half-time of the fast component of the wild type. Also, the half-time of the fast component of R94E, E98R, and D58K cells was slower than the half-time of the fast component of the wild type. Overall, the forward electron transfer between Q_A and Q_B was looking very much like the wild type.

Chlorophyll *a* fluorescence decay measurements, following a single actinic flash in the presence of DCMU also showed similar millisecond and the second components in most of the Psb27 point mutants as compared to the wild type (Fig. 3.18 C, D and 3.19 C, D). The half-time of the fast component of D14A, Y78H, E98R, D58A, D58K cells was faster than the wild type. Also, the half-time of the fast component of D58E and K63R strains was slower in comparison to the wild type. The amplitude of the fast component of ΔPsb27 and K63D mutants was greater than the amplitude of the fast component of the wild type. The R54E and D58A cells had a lower fast component amplitude as compared to the wild type. Overall, the Psb27 mutants displayed normal back charge recombination through PS II complexes.

The assembly of PS II complexes was also studied in all the Psb27 strains (wild type, ΔPsb27, Psb27 control, D14A, R54E, Y78H, R94E, E98R, D58A, D58E, D58K, K63A, K63D, and K63R strains) (Fig. 3.20). All the Psb27 strains showed that they could assemble the PS II assembly complexes like the wild type. Thus, showing that the PS II assembly is normal in all the Psb27 strains.

None of the substitution mutations of the Psb27 conserved residues (Asp14Ala, Arg54Glu, Tyr78His, Arg94Glu, E98Arg) as well as the Psb27 cross-linking residues Asp-58 and Lys-63 had any major effect on the function of Psb27 interaction with other PS II assembly factors when studied at the gene level. To get more details about the role of the amino-acid residues of Psb27 with the chlorophyll *a*-binding core antenna protein CP43, further studies can be carried out at the protein level

Recently, with MS and cross-linking based methods, the presence of cross-links between Psb27-Lys91 and CP43-Lys381 has been proposed (Cormann *et al.* 2016). It can be in Fig. 3.3, Psb27-Lys91 is highly conserved among the cyanobacteria, algae as well as higher plants. So, studies can be carried out by constructing Psb27-Lys91 mutant also to investigate the effect of this mutation towards the interaction of Psb27 with other PS II intermediate protein complexes. Liu and colleagues proposed that Psb27-Asp58 and Psb27-Lys63 are involved in cross-linking with loop E of CP43 protein (Liu *et al.* 2011a). So, double mutants (Psb27-D58:Psb27-K63) can be constructed in the future to study the effect of the twin point mutation towards the Psb27 protein function.

Recently, it was shown that Psb27 and Psb28-1 are required for the optimal growth especially under intermittent high-light/dark conditions and become components of PS II-PS I supercomplexes (Bečková *et al.* 2017). The formation of this intermediate complex might be an important step in PS II biogenesis, especially under high irradiance. The observed results by Bečková and co-workers, agree with the previously published result showing the Psb27 containing supercomplexes (Komenda *et al.* 2012a), potentially suggesting a role for the super complex in PS II assembly/repair. Previous studies have also indicated a close relationship between Psb27 and Psb28 proteins (Kashino *et al.* 2002b; Liu *et al.* 2011a; Liu *et al.* 2011b; Nowaczyk *et al.* 2012). As the Psb27 is associated with PS II complexes lacking a functional oxygen-evolving complex (Nowaczyk *et al.* 2006), the complexes containing both Psb27 and Psb28 are therefore likely to be involved in *de novo* assembly and repair of PS II.

Chapter Four

A spontaneous mutation at *psbA2*-His252 in *Synechocystis* sp. PCC 6803 blocks electron transfer in the quinone-Fe-acceptor complex of PS II

4.1 Background

In the previous chapter, the role of conserved amino acid residues of Psb27 potentially involved in protein-protein interactions with other PS II subunits was studied by introducing amino acid substitutions employing site-directed mutagenesis in the cyanobacterium *Synechocystis* 6803. All the Psb27 mutants characterised, exhibited a phenotype similar to the wild-type strain. Unexpectedly, a Psb27 mutant (named as R54E*, not discussed in Chapter three) displayed slow photoautotrophic growth, low PS II oxygen-evolving activity, impaired electron transfer between the Q_A and Q_B PS II electron acceptors (as judged by the decay of chlorophyll variable fluorescence after a single turnover flash) and an elevated initial rise in variable chlorophyll *a* fluorescence.

4.2 Objective

This chapter has three goals:

The first was to characterise the phenotype of the R54E* mutant.

The second was to identify the mutation responsible for the R54E* phenotype.

The third was to independently demonstrate that the mutation identified by the second goal was responsible for the observed phenotype.

4.3 Construction of strains required to study the R54E*

4.3.1 Psb27 (R54E*) mutant

The original R54E* mutant was constructed as described for the other Psb27 mutants in Chapter 3, section 3.5.2.

4.3.2 R54E* complementation strain (R54E*:ΔPsb27)

To ascertain if the phenotype of R54E* cells was due to a mutation in Psb27, the R54E* strain was transformed with the pΔPsb27-camR plasmid (discussed in Chapter 3; section 3.5.1) to restore the ΔPsb27 genotype. The complete segregation of R54E* mutant and the R54E*:ΔPsb27 strain is shown in Fig. 4.1. Also, a second R54E strain was constructed again and characterised. The new R54E strain has already been discussed in Chapter 3.

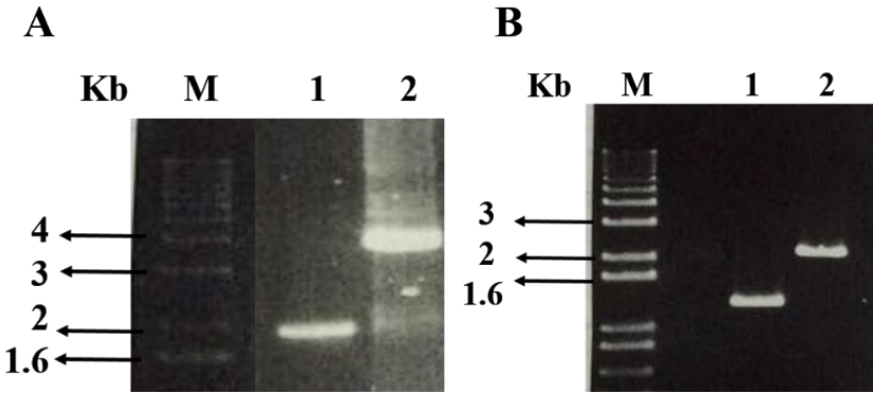

Figure 4.1 Colony PCR of the R54E* mutant and R54E*:ΔPsb27 strain.(A) Confirmation of the complete segregation of R54E* mutant. The lanes are 1, wild type; 2, R54E*. **(B)** Confirmation of the complete segregation of R54E*:ΔPsb27 strain. The lanes are: 1, wild type; 2, R54E*:ΔPsb27. Lane M is the 1 Kb Plus DNA Ladder (Invitrogen, CA), the other lanes contain PCR products corresponding to the segregated mutants.

4.4 Characterisation of the R54E* and R54E*:ΔPsb27 strains

Once complete segregation of the R54E* mutant and R54E*:ΔPsb27 strain was confirmed by sequencing, the phenotypic characterisation of the mutant was performed.

4.4.1 Photoautotrophic growth

The photoautotrophic growth of the R54E* mutant and R54E*:ΔPsb27 strain was measured to investigate the impact of introducing the specific mutation into the Psb27 protein. Fig. 4.2 shows the photoautotrophic growth characteristics of the wild type, the ΔPsb27, and R54E* strains and the R54E*:ΔPsb27 mutant over a period of 168 h. The average doubling time of each strain is presented in Table 4.1.

The R54E* mutant exhibited a doubling time of ~44.2 ± 1.2 h (Fig. 4.2) (Table 4.1). The R54E*:ΔPsb27 strain displayed a doubling time of ~46.4 ± 3.2 h; however, the new R54E strain (already discussed in Chapter 3; section 3.6.2) showed a doubling time similar to the wild-type strain, suggesting that a secondary mutation was present in R54E* cells and this was responsible for the delayed photoautotrophic growth.

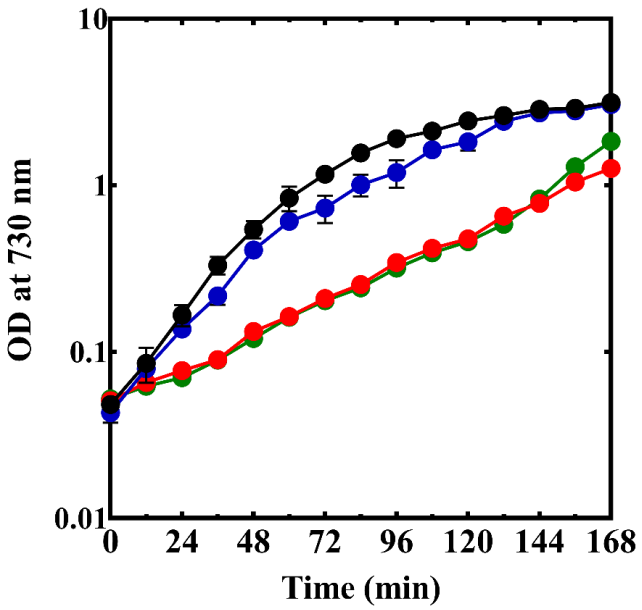

Figure 4.2 Photoautotrophic growth of the wild type, ΔPsb27, R54E* and R54E*:ΔPsb27 strains.The photoautotrophic growth of *Synechocystis* 6803 and the mutants in BG-11 media as measured by optical density at 730 nm. The strains shown are wild type (black), ΔPsb27 (blue), R54E* (red) and R54E*:ΔPsb27 (green). Data shown are the average of three independent experiments. The standard error bars have also been shown

Table 4.1 Photoautotrophic growth of the wild type, ΔPsb27, R54E* and R54E*:ΔPsb27 strains.The doubling time of the wild type and the mutants grown photoautotrophically.

Strain	Doubling time[1] (h)
WT	13.1 ± 0.6[2]
ΔPsb27	15.3 ± 0.4
R54E*	44.2 ± 1.2
R54E*:ΔPsb27	46.4 ± 3.2

[1]The data shown are the mean doubling times over the first 36 h of the growth. Data shown are the average of three independent experiments. [2]The standard error have been shown.

4.4.2 PS II-specific oxygen evolution assay

Oxygen evolution assays were carried out for the wild type, ΔPsb27, R54E* and R54E*:ΔPsb27 strains to assess the impact of the introduced changes on the capacity of PS II to support electron transfer between water and added electron acceptors.

Fig. 4.3 shows the oxygen evolution traces obtained using DCBQ (A), DMBQ (B) and sodium bicarbonate (C). The average oxygen evolution rates for the wild type, ΔPsb27, R54E* and R54E*:ΔPsb27 strains have been presented in Table 4.2.

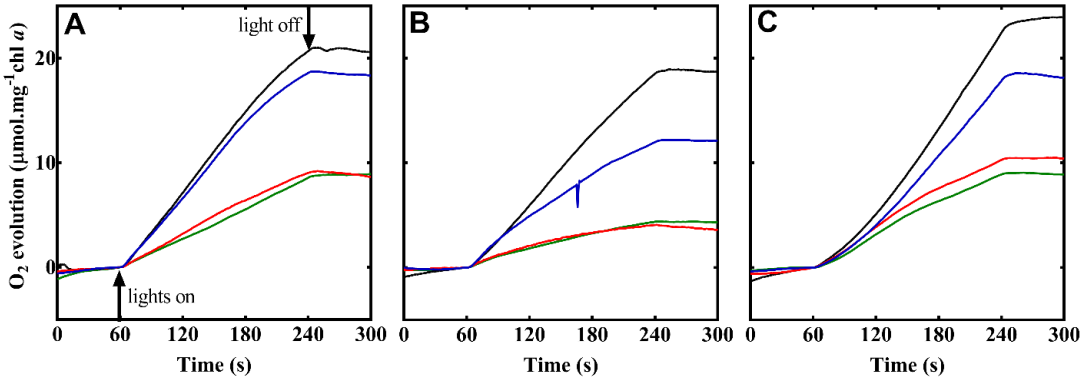

Figure 4.3 Oxygen evolution assay traces for the wild type, ΔPsb27, R54E* and R54E*:ΔPsb27 strains.(A) Oxygen evolution measured in the presence of DCBQ. **(B)** Oxygen evolution measured in the presence of DMBQ. **(C)** Oxygen evolution measured in the presence of sodium bicarbonate. The strains shown are wild type (black), ΔPsb27 (blue), R54E* (red) and R54E*:ΔPsb27 (green). Data shown are the average of three independent experiments. The average values of oxygen evolution rates have been shown in Table 4.2.

The oxygen evolution rates of the R54E* mutant and R54E*:ΔPsb27 strain were ~50% lower than the oxygen-evolution rates of the wild type. The wild type had an oxygen evolution rate of ~380 ± 30 μmol O_2 (mg of chl)$^{-1}$ h^{-1} in the presence of DCBQ, ~290 ± 20 μmol O_2 (mg of chl)$^{-1}$ h^{-1} in the presence of DMBQ and ~460 ± 40 μmol O_2 (mg of chl)$^{-1}$ h^{-1} in the presence of sodium bicarbonate. The oxygen evolution rates of R54E* mutant were ~170 ± 10 μmol O_2 (mg of chl)$^{-1}$ h^{-1} in the presence of DCBQ, ~140 ± 10 μmol O_2 (mg of chl)$^{-1}$ h^{-1} in the presence of DMBQ and ~250 ± 20 μmol O_2 (mg of chl)$^{-1}$ h^{-1} in the presence of sodium bicarbonate. The R54E*:ΔPsb27 strain also had low oxygen evolution rates when supported using different electron acceptors. Overall, both the R54E* mutant and the R54E*:ΔPsb27 strain had altered oxygen-evolving activity.

Table 4.2 Oxygen evolution rates of wild type, ΔPsb27, R54E* and R54E*:ΔPsb27 strain

Strains	Oxygen evolution[1] (μmol O_2 (mg of chl)$^{-1}$ h^{-1})		
	DCBQ	DMBQ	Bicarbonate
WT	380 ± 30[2]	290 ± 20	460 ± 40
ΔPsb27	350 ± 30	300 ± 30	380 ± 10
R54E*	170 ± 10	140 ± 10	250 ± 20
R54E*:ΔPsb27	160 ± 10	130 ± 40	250 ± 20

[1]Oxygen evolution rates were measured in the presence of DCBQ, DMBQ and sodium bicarbonate. Data shown are the average of three independent experiments.
[2]The standard error have been shown.

4.4.3 Low temperature 77 K fluorescence emission spectroscopy

To study the effect of the introduced mutations on the levels or the stoichiometry of the PS I and PS II complexes in the mutants, low temperature 77 K fluorescence emission spectroscopy measurements were performed. The R54E* mutant and R54E*:ΔPsb27 strain displayed normal 725 nm emission, originating from PS I, and the 685 and 695 nm emissions, originating from CP43 and CP47, respectively, of PS II, when excited at 440 nm (Fig. 4.4 A). However, the R54E* mutant exhibited a small apparent increase in PS II-specific fluorescence (685 nm and 695 nm) compared to the wild type. In contrast, the R54E*:ΔPsb27 strain displayed a small apparent decrease in PS II specific fluorescence (685 nm and 695 nm) as compared to the wild type.

To get insight into the coupling and energy transfer between the PBS and PS II (and possibly PS I), cells were illuminated with a 580 nm light (Fig. 4.4 B). The R54E* mutant and the R54E*:ΔPsb27 strain displayed the typical 725 nm emission originating from PS I; however, both the R54E* mutant and the R54E*:ΔPsb27 strain exhibited slightly lower levels of fluorescence emission from phycocyanin (650 nm), allophycocyanin (665 nm) and the ApcE PBS terminal emitter (685 nm), respectively when compared to the wild type potentially suggesting efficient coupling of the PBS with the photosystems. Also, a shoulder was visible at 695 nm for the R54E* mutant and R54E*:ΔPsb27 strain potentially suggesting the emission may contain contributions from both the CP43 and CP47 core antennae of PS II as well as the ApcE terminal emitter of the PBS (Joshua and Mullineaux 2004).

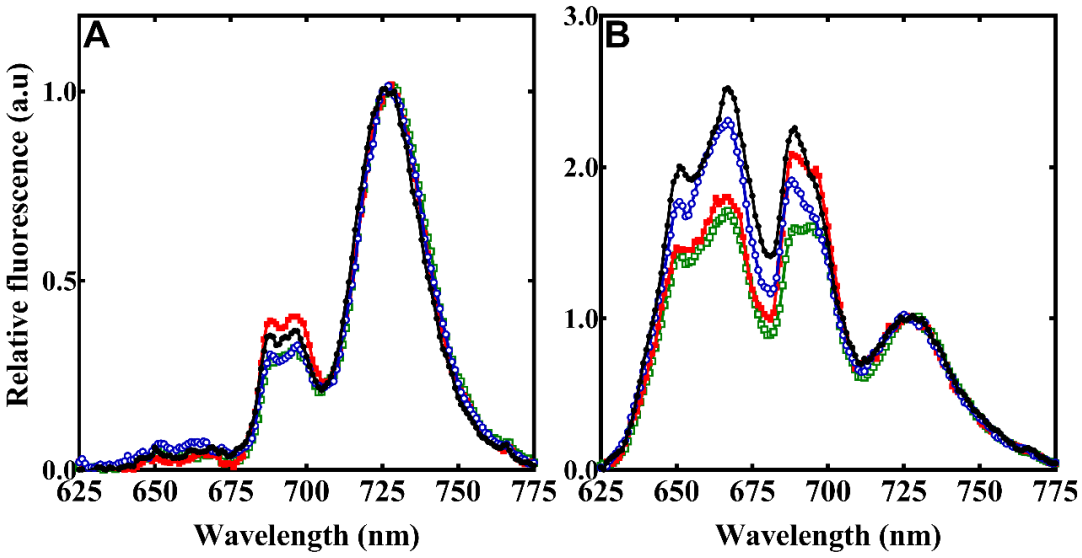

Figure 4.4 Low-temperature fluorescence spectra of wild type, ΔPsb27, R54E* and R54E*: ΔPsb27 strains.Panel **(A)** contains the fluorescence emission spectra with an excitation wavelength of 440 nm. Panel **(B)** contains the fluorescence emission spectra with an excitation wavelength of 580 nm. The strains shown are wild type (black, close circles), ΔPsb27 (blue, open circles), R54E* (red, close squares) and R54E*:ΔPsb27 (green, open squares). Data shown are the average of three independent experiments.

4.4.4 Chlorophyll *a* fluorescence induction

The R54E* mutant and R54E*:ΔPsb27 strain showed a distinct phenotype when the chlorophyll *a* variable fluorescence was compared between the mutant and the wild-type strain in the absence of DCMU (Fig. 4.5 A and see inset in Fig. 4.5 A). The chlorophyll *a* fluorescence induction curve exhibited an initial rapid rise with an elevated J level.

The fluorescence induction measurements were also carried out in the presence of the PS II-specific inhibitor DCMU (Fig. 4.5 B and inset in Fig. 4.5 B). The R54E* mutant and R54E*:ΔPsb27 strain exhibited higher variable fluorescence induction traces in the presence of DCMU (Fig. 4.5 B).

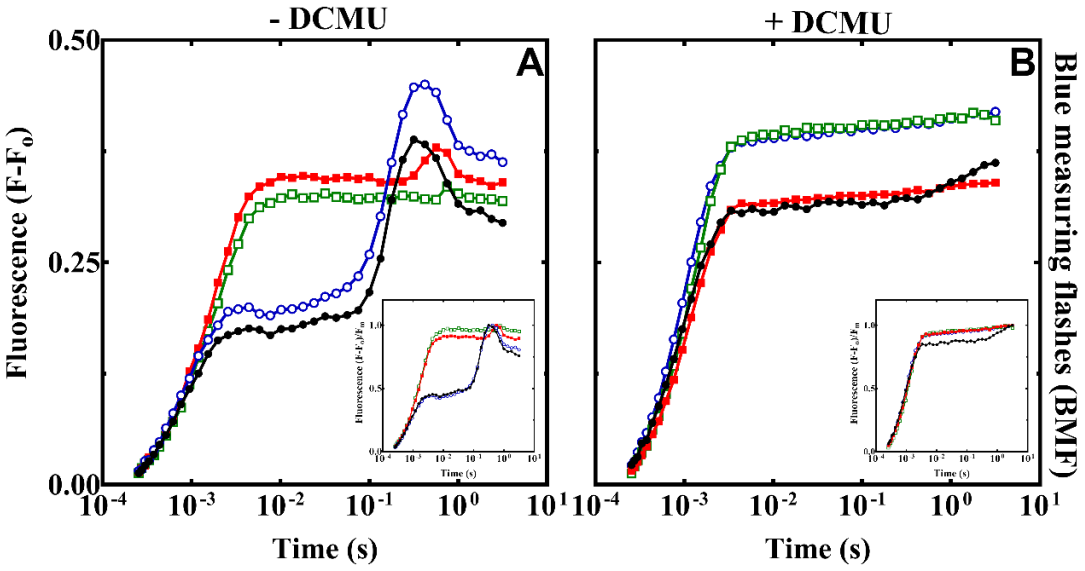

Figure 4.5 Normalised steady-state chlorophyll *a* fluorescence induction in wild type, ΔPsb27, R54E* and R54E*:ΔPsb27 strains.Panel **(A)** contains the measurements in the absence of DCMU and panel **(B)** contains the measurements in the presence of DCMU. The strains shown are wild type (black, close circles), ΔPsb27 (blue, open circles), R54E* (red, close squares) and R54E*:ΔPsb27 (green, open squares). The data normalised to the F_m value of each strain have been shown in the insets. Data shown are average of four independent experiments.

To further investigate the differences in the IP rise and P peak of the R54E* mutant and R54E*:ΔPsb27 strain, the duration of the chlorophyll *a* fluorescence induction assay was increased to ~500 s in the presence and absence of DCMU (Fig. 4.6 A and B). As discussed earlier, the chlorophyll *a* fluorescence induction curve of R54E* strain exhibited an initial rapid rise (Fig. 4.6 A and see inset Fig. 4.6 A). Also, the SM rise was missing in the R54E* strain. The SM phase is usually linked with the transmembrane pH gradient formation and membrane potential and various other non-photochemical quenching processes. The fluorescence rise in the presence of DCMU mostly remained unchanged in the R54E* strain (Fig. 4.6 B).

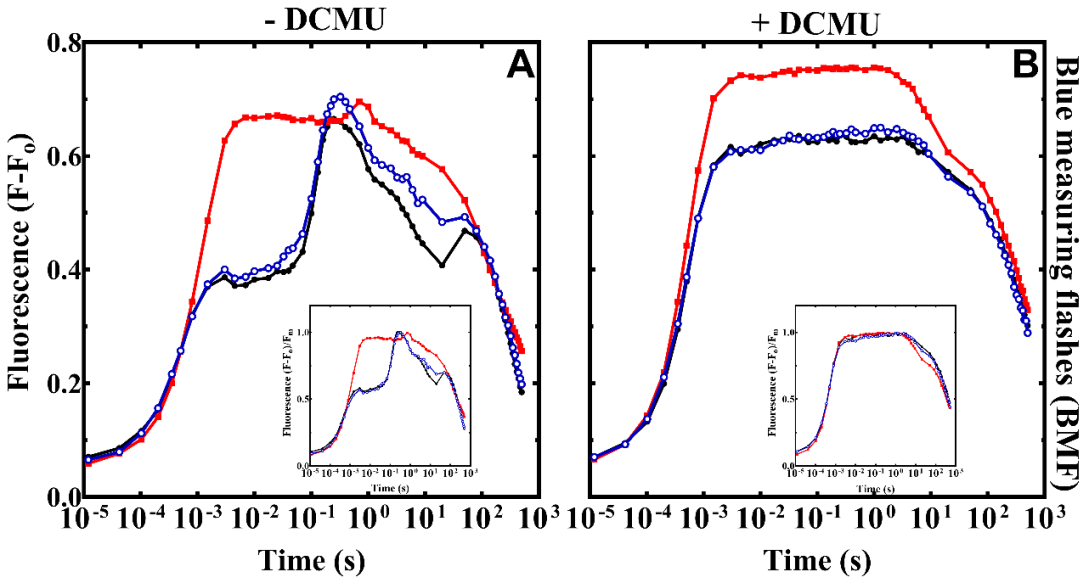

Figure 4.6 Normalised steady-state long-term chlorophyll *a* fluorescence induction (500 s) in wild type, ΔPsb27 and R54E* strains.Panel **(A)** contains the measurements in the absence of DCMU and panel **(B)** contains the measurements in the presence of DCMU. The strains shown are wild type (black, close circles), ΔPsb27 (blue, open circles) and R54E* (red, close squares). The data normalised to the F_m value of each strain have been shown in the insets. Data shown are the average of four independent experiments.

4.4.5 Chlorophyll *a* fluorescence decay following single actinic flash

The decay kinetics of chlorophyll *a* fluorescence following a single saturating actinic flash was also investigated and compared between the strains (Fig. 4.7). The R54E* and R54E*:ΔPsb27 cells exhibited slower forward electron transfer (3-4 times) as compared to the wild type (Fig. 4.7 A). In the R54E* mutant and the R54E*:ΔPsb27 strain, the half-time of the microsecond component was ~630 ± 20 µs and 790 ± 20 µs as compared to ~240 ± 10 µs in wild type (Table 4.3). The half-time of the millisecond component for the R54E* mutant and the R54E*:ΔPsb27 strain was also ~8-9 times slower than the half-time of the millisecond component of the wild type.

The chlorophyll *a* fluorescence decay studies were also carried out in the presence of DCMU (Fig. 4.7 B). The R54E* mutant and R54E*:ΔPsb27 strain displayed similar chlorophyll *a* fluorescence decays in the presence of DCMU (Fig. 4.7 B) (Table 4.4). However, the amplitude of the millisecond component was higher in the R54E* mutant, followed by decreased amplitude of the slower component in comparison to the wild

type. The half-time of the slow component of the R54E* mutant was also slightly faster than the half-time of the wild type.

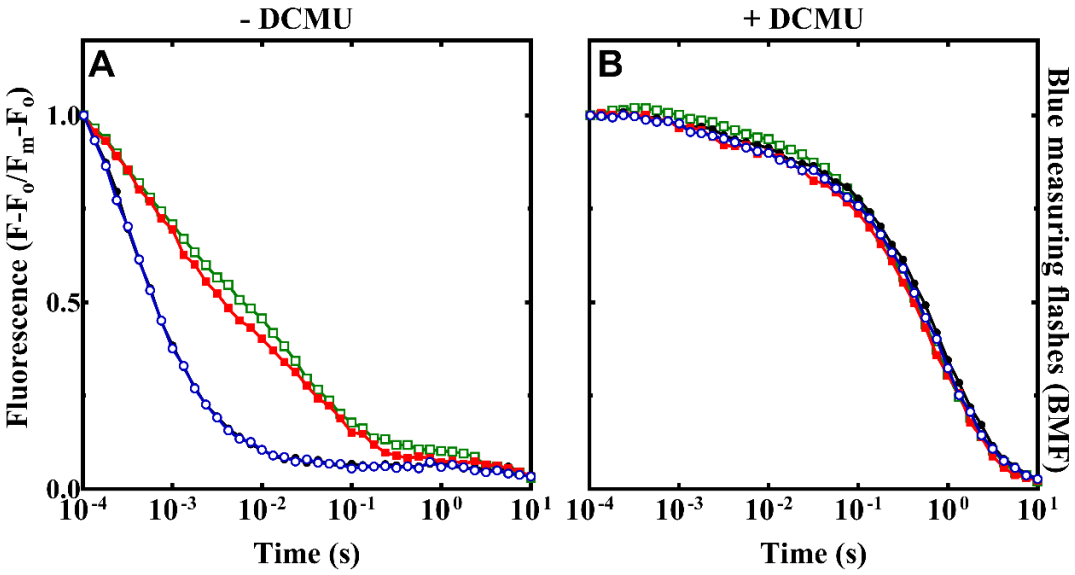

Figure 4.7 Relaxation of chlorophyll *a* fluorescence following single flash in the wild type, ΔPsb27, R54E* and R54E*:ΔPsb27 strains. Panel **(A)** contains the measurements in the absence of DCMU. Panel **(B)** contains the measurements in the presence of DCMU. The strains shown are wild type (black, open circles), ΔPsb27 (blue, close circles), R54E* (red, open squares) and R54E*:ΔPsb27 (green, open squares). Data shown are the average of four independent experiments.

Table 4.3 Decay kinetics of variable chlorophyll *a* fluorescence following single saturating actinic flash in the absence of DCMU.

Strains	Fast		Intermediate		Slow	
	$T_{1/2}$ (µs)	Amp.	$T_{1/2}$ (ms)	Amp.	$T_{1/2}$ (s)	Amp.
WT	240 ± 10*	59 ± 2	3.2 ± 0.3	31 ± 2	4.8 ± 0.6	10.3 ± 1.0
R54E*	630 ± 20	42 ± 1	24.0 ± 0.4	38 ± 2	3.0 ± 0.1	20.2 ± 0.5
R54E*: ΔPsb27	790 ± 20	46 ± 1	29.0 ± 0.9	43 ± 1	2.1 ± 0.2	11.3 ± 0.2

*The standard error have been shown for the chlorophyll *a* fluorescence decays from three independent experiments.

Table 4.4 Decay kinetics of variable chlorophyll *a* fluorescence following single saturating actinic flash in the presence of DCMU.

Strains	Fast		Slow	
	$T_{1/2}$ (µs)	Amp.	$T_{1/2}$ (s)	Amp.
WT	2.8 ± 0.1*	9 ± 1	0.4 ± 0.1	91 ± 1
R54E*	3.1 ± 0.3	18 ± 1	0.6 ± 0.1	81 ± 1
R54E*:ΔPsb27	2.3 ± 0.1	7 ± 1	0.3 ± 0.1	93 ± 1

*The standard error have been shown for the chlorophyll *a* fluorescence decays from three independent experiments.

4.4.6 Chlorophyll *a* fluorescence decay following multiple turnover flashes

Since bicarbonate is an essential ligand to a non-heme iron located between Q_A and Q_B, and as it is important for electron transfer between Q_A and Q_B, the effect of displacing bicarbonate by the addition of formate, as well as adding additional bicarbonate was also examined, on the kinetics of chlorophyll *a* fluorescence decay in R54E* cells and the wild-type cells by using multiple actinic flashes to turn over the two-electron gate and the S-state cycle of the oxygen-evolving complex (Fig. 4.8). It is known that the addition of formate delays the electron transfer from Q_A^- to Q_B (Sedoud *et al.* 2011). In R54E* cells, bicarbonate addition was not able to restore the chlorophyll *a* fluorescence decay kinetics to the wild-type levels (Fig. 4.8). Moreover, the addition of formate also did not appear to induce any significant additional impact on the chlorophyll *a* fluorescence decay of wild type and R54E* cells (Table 4.5). However, the formate was able to inhibit the forward electron transfer kinetics slightly. Table 4.5 shows the characteristic half-time and amplitudes for these chlorophyll *a* fluorescence decay curves in the presence and absence of formate and bicarbonate.

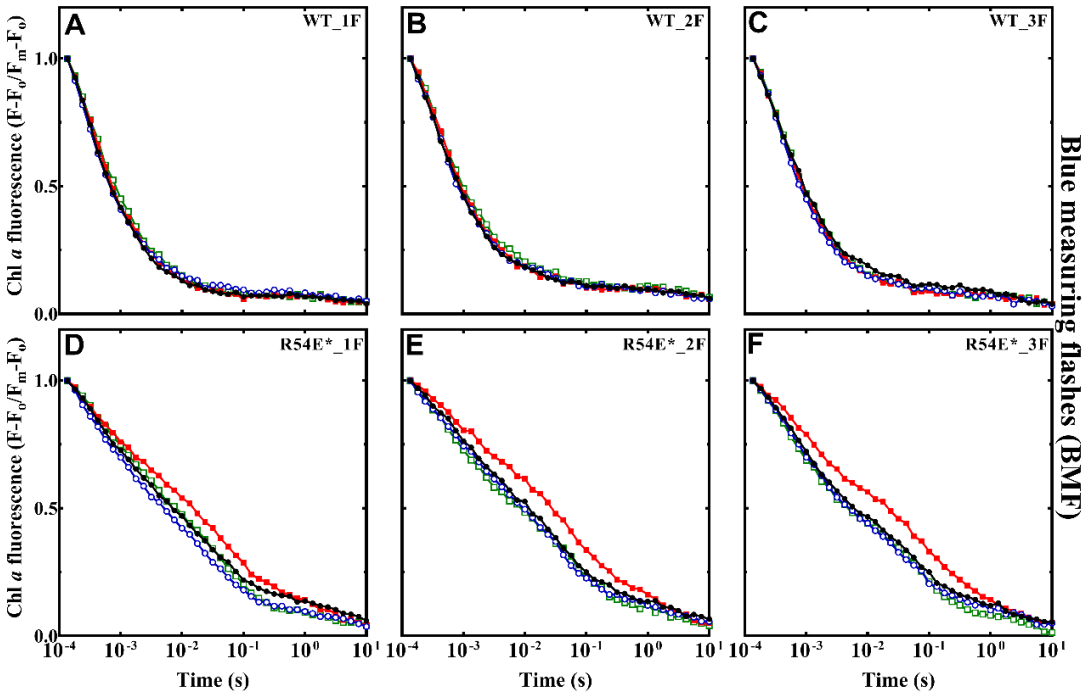

Figure 4.8 Relaxation of chlorophyll *a* fluorescence following multiple turnover flashes in the presence and absence of bicarbonate and sodium formate in the wild type and R54E* strain. Panels **(A)**, **(B)** and **(C)** contains the measurements of wild type after one, two and three actinic flashes. Panels **(D)**, **(E)** and **(F)** contains the measurements of R54E* mutant after one, two and three actinic flashes. The fluorescence yield traces are without formate and bicarbonate (black, close circles), bicarbonate (blue, open circles), formate (red, close squares) and bicarbonate plus formate (green, open squares). Data shown are the average of three independent experiments.

Table 4.5 Decay kinetics of chlorophyll *a* fluorescence after one, two and three actinic flashes in wild type and R54E* cells in presence and absence of sodium formate and sodium bicarbonate.

Strains	Treat-ment	Fast		Intermediate		Slow	
		$T_{1/2}$ (µs)	Amp.	$T_{1/2}$ (ms)	Amp.	$T_{1/2}$ (s)	Amp.
Flash 1							
WT	No addition	250 ± 1*	58 ± 1	2.5 ± 0.2	34 ± 1	5.9 ± 0.3	8.1 ± 0.2
	HCO_3^-	250 ± 1	58 ± 3	3.1 ± 0.2	33 ± 3	7.1 ± 0.7	9.2 ± 0.1
	HCO_2^-	260 ± 20	59 ± 1	3.0 ± 0.3	32 ± 1	5.9 ± 0.6	9.2 ± 0.9
	HCO_2^- + HCO_3^-	310 ± 10	61 ± 2	4.2 ± 0.3	31 ± 2	6.0 ± 0.9	8.3 ± 0.3
R54E*	No addition	610 ± 10	42 ± 1	23.0 ± 0.1	42 ± 2	2.6 ± 0.1	16.1 ± 0.2
	HCO_3^-	600 ± 40	45 ± 2	26.0 ± 5.2	39 ± 3	2.6 ± 0.9	16.4 ± 1.0
	HCO_2^-	590 ± 40	37 ± 1	25.0 ± 2.9	39 ± 2	1.3 ± 0.2	24.1 ± 0.1
	HCO_2^- + HCO_3^-	810 ± 40	42 ± 1	31.0 ± 2.3	44 ± 1	2.1 ± 0.4	14.1 ± 0.2
Flash 2							
WT	No addition	320 ± 20	59 ± 2	3.9 ± 0.7	29 ± 2	8.8 ± 0.4	11.2 ± 0.3
	HCO_3^-	350 ± 20	61 ± 3	5.2 ± 1.4	28 ± 3	8.8 ± 1.6	11.1 ± 0.2
	HCO_2^-	330 ± 20	60 ± 2	4.2 ± 0.6	29 ± 2	7.6 ± 0.7	11.2 ± 0.3
	HCO_2^- + HCO_3^-	370 ± 10	61 ± 1	6.5 ± 0.1	27 ± 1	7.8 ± 0.2	12.1 ± 0.1
R54E*	No addition	750 ± 50	43 ± 2	32.0 ± 3.4	41 ± 1	3.0 ± 0.6	16.4 ± 1.5
	HCO_3^-	810 ± 40	42 ± 2	38.0 ± 7.7	42 ± 1	3.7 ± 0.9	15.4 ± 1.5
	HCO_2^-	790 ± 50	34 ± 2	31.0 ± 2.6	40 ± 1	1.2 ± 0.1	26.3 ± 2.1
	HCO_2^- + HCO_3^-	730 ± 20	43 ± 1	35.1 ± 0.6	40 ± 1	1.6 ± 0.1	17.1 ± 0.1
Flash 3							
WT	No addition	340 ± 40	60 ± 2	3.8 ± 1.0	30 ± 4	4.2 ± 1.6	10.3 ± 1.5
	HCO_3^-	330 ± 10	60 ± 2	3.7 ± 0.1	31 ± 2	5.0 ± 2.1	9.4 ± 0.8
	HCO_2^-	310 ± 40	60 ± 2	3.5 ± 0.7	31 ± 2	5.0 ± 0.3	9.1 ± 0.1

	HCO_2^- + HCO_3^-	340 ± 20	58 ± 1	3.8 ± 0.2	32 ± 0.6	4.0 ± 0.3	10.4 ± 0.5
R54E*	No addition	720 ± 30	49 ± 2	13.0 ± 1.1	36 ± 0.6	2.4 ± 0.5	15.2 ± 2.3
	HCO_3^-	720 ± 20	49 ± 1	40.0 ± 7.0	37 ± 1.1	3.1 ± 0.9	14.1 ± 2.3
	HCO_2^-	770 ± 70	42 ± 3	39.0 ± 3.5	35 ± 0.6	1.1 ± 0.2	24.1 ± 2.9
	HCO_2^- + HCO_3^-	670 ± 30	48 ± 1	37.0 ± 3.5	36 ± 1.1	1.0 ± 0.3	16.4 ± 1.1

*The standard error have been shown for the chlorophyll *a* fluorescence decays from three independent experiments.

The decay kinetics of chlorophyll *a* fluorescence following multiple (flash 1, flash 2, flash 3, flash 4 and flash 5) saturating actinic flashes were also investigated and compared between the wild type and the R54E* mutant (Fig. 4.9). There was no significant effect of the number of flashes as such on the electron transfer between the plastoquinone sites in wild type and the R54E* strain (Table 4.6). However, the millisecond and microsecond component in the R54E* mutant was delayed compared to wild type. Table 4.6 shows the characteristic half-time and amplitudes for these fluorescence decay curves.

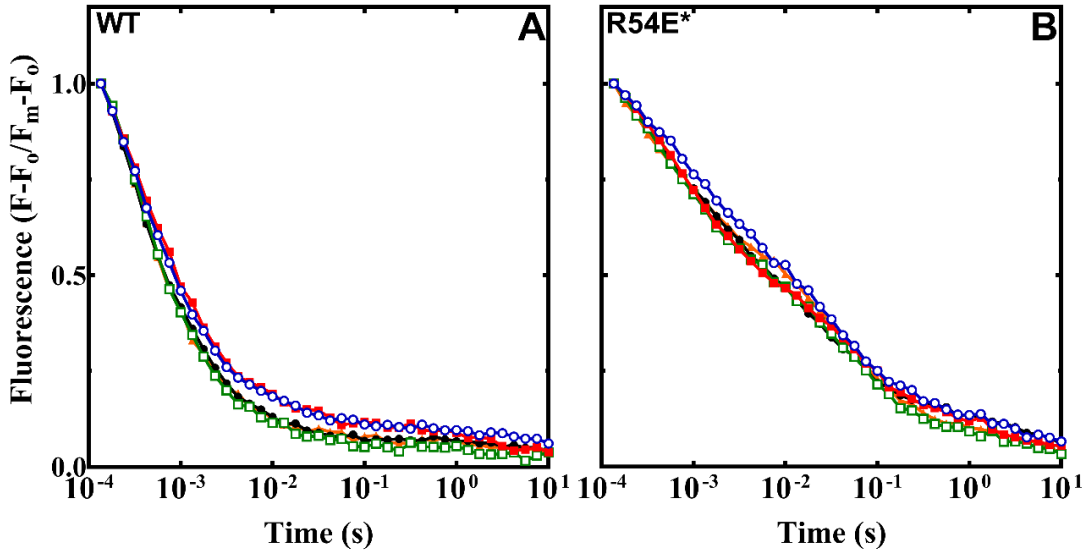

Figure 4.9 Relaxation of chlorophyll *a* fluorescence following multiple turnover flashes (flash one, flash two, flash three, flash four and flash five) in the wild type and R54E* strain. Panel **(A)** contains the measurements of wild type after one, two, three, four and five actinic flashes. Panel **(B)** contains the measurements of R54E* mutant after one, two, three, four and five actinic flashes. The fluorescence yield traces are flash 1 (black, close circles), flash 2 (blue, open circles), flash 3 (red, close squares),

flash 4 (green, open squares) and flash 5 (orange, close triangles). The fluorescence yield traces are without DCMU. Data shown are the average of three independent experiments.

Table 4.6 Decay kinetics of variable chlorophyll *a* fluorescence after one, two, three, four and five actinic flashes in wild type and R54E* cells in the absence of DCMU.

Strain	F	Fast		Intermediate		Slow	
		$T_{1/2}$ (µs)	Amp.	$T_{1/2}$ (ms)	Amp.	$T_{1/2}$ (s)	Amp.
WT	1F	260 ± 12*	58 ± 1	2.6 ± 0.2	34 ± 1	7.7 ± 1.8	8.1 ± 0.2
	2F	320 ± 30	60 ± 2	3.9 ± 0.8	29 ± 2	8.8 ± 0.4	11.2 ± 0.3
	3F	330 ± 30	59 ± 2	3.5 ± 0.7	32 ± 3	4.7 ± 1.2	10.4 ± 1.2
	4F	290 ± 10	64 ± 1	3.1 ± 0.2	30 ± 1	3.4 ± 1.0	6.2 ± 0.3
	5F	280 ± 30	64 ± 2	3.3 ± 0.6	29 ± 2	6.0 ± 1.7	7.1 ± 0.6
R54E*	1F	590 ± 30	43 ± 1	23.0 ± 0.7	41 ± 1	2.1 ± 0.5	15.1 ± 1.7
	2F	700 ± 60	42 ± 2	28.0 ± 0.7	41 ± 2	2.0 ± 0.3	17.2 ± 1.1
	3F	680 ± 50	49 ± 2	34.0 ± 1.3	36 ± 1	2.1 ± 0.5	15.2 ± 1.7
	4F	370 ± 140	31 ± 7	12.0 ± 10.7	33 ± 4	0.5 ± 0.5	35.4 ± 10.4
	5F	320 ± 110	29 ± 6	11.3 ± 10.0	33 ± 5	0.5 ± 0.5	38.3 ± 11.0

*The standard error have been shown for the chlorophyll *a* fluorescence decays from three independent experiments.
F means number of flashes

4.4.7 Photoinhibition and recovery assays

PS II when exposed to light undergoes irreversible damage. This process is also known as photoinhibition (Aro *et al.* 1993b; Adir *et al.* 2003). This irreversible damage can occur even at low intensities, but it affects the photosynthetic electron transport chain only if the rate of damage is more than the rate of PS II repair (Keren *et al.* 1995; Keren *et al.* 1997; Vass 2011; 2012).

4.4.7.1 Oxygen evolution assay

The susceptibility of PS II to light-induced damage and its recovery was also studied by measuring oxygen-evolving activity. The cells were exposed to 45 min of high light treatment (2000 ± 100 µE $m^{-2}s^{-1}$) and allowed to recover under low-light conditions (35 µE $m^{-2}s^{-1}$) for 135 min. The oxygen evolution rates were measured every 15 min in

the presence of different artificial quinone acceptors: DCBQ and DMBQ. Sodium bicarbonate was also used.

Before the high-light exposure, the steady-state oxygen evolution rates of the wild type and the R54E* strain were measured at the time point (T=0 min) in the presence of DCBQ (Fig. 4.10). After T=0 min, the cells were exposed to high-light treatment (2000 ± 100 µE $m^{-2}s^{-1}$) for 45 min. The wild type could acclimatise to the high light, and the oxygen evolution rates were not affected. This indicates that the rate of damage is lower as compared to the rate of repair in the wild-type strain, whereas the oxygen evolution rate of R54E* mutant decreased to 50% of the oxygen evolution rate at T=0, but was able to acclimatise to the high-light damage after 30 mins of incubation. After 45 min of high-light exposure, the cells could recover in standard low-light conditions ~30-35 µE $m^{-2}s^{-1}$ for 135 min.

The oxygen evolution rates of the wild type and the R54E* strain was calculated from the traces and were plotted as a function of time. In Fig. 4.10, the oxygen evolution rates were normalised to the T=0 time point rate for each strain to compare the relative extent of photodamage in each strain directly with respect to the wild type.

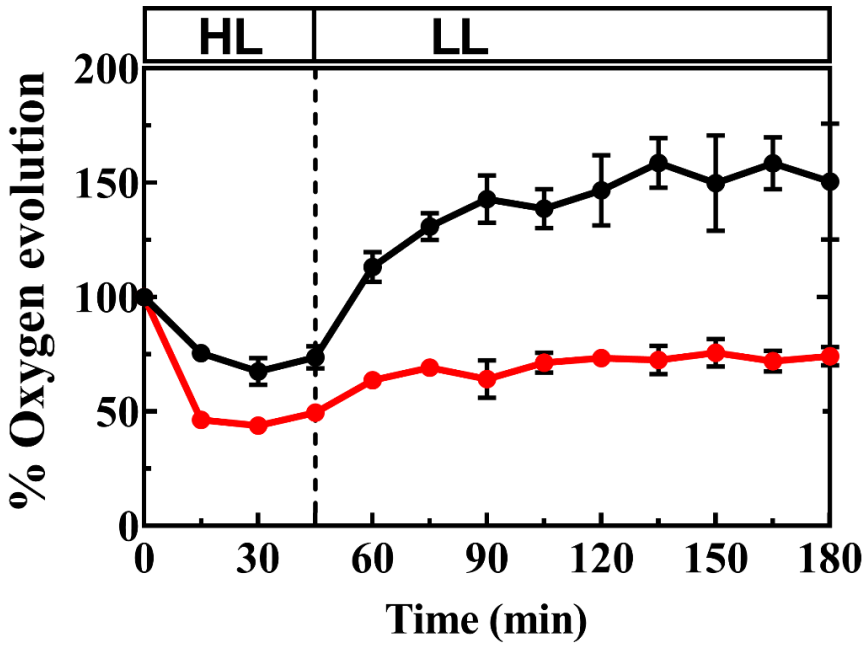

Figure 4.10 Photodamage and recovery of PS II oxygen-evolving activity in the presence of artificial quinone acceptor DCBQ. The cells were suspended to a chlorophyll *a* concentration of 10 µg ml^{-1} and were exposed to high-intensity white light at 2000 µE $m^{-2}s^{-1}$ for 45 min and allowed to recover for 135 min in low-light

conditions at 35 µE $m^{-2}s^{-1}$. The strains shown are wild type (black) and R54E* (red). The data shown are the average of three independent experiments normalised to the initial rate of oxygen evolution from the beginning of the treatment, and standard error have been shown as bars.

The recovery in the case of the wild type even exceeded the initial T=0 oxygen-evolving activity, whereas the R54E* strain could recover upto ~75-80% of the initial oxygen-evolving activity. It appears that the rate of PS II damage was higher than the rate of repair in R54E* strain, leading to an overall decline in PS II oxygen-evolution rates.

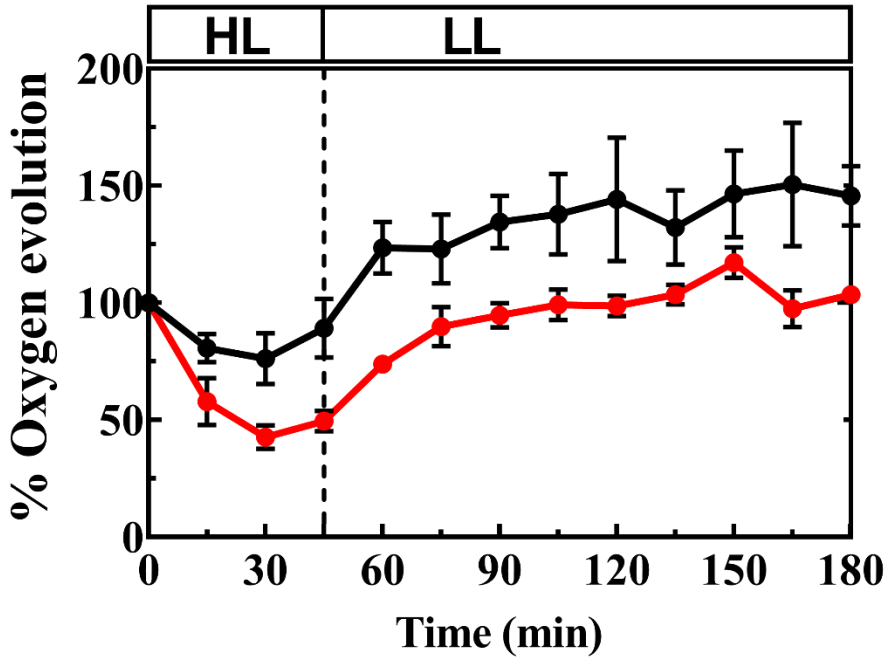

Figure 4.11 Photodamage and recovery of PS II oxygen-evolving activity in the presence of artificial quinone acceptor DMBQ. The cells were suspended to a chlorophyll *a* concentration of 10 µg ml^{-1} and were exposed to high-intensity white light at 2000 µE $m^{-2}s^{-1}$ for 45 min and allowed to recover for 135 min in low-light conditions at 35 µE $m^{-2}s^{-1}$. The strains shown are wild type (black) and R54E* (red). The data represented are the average of three independent experiments normalised to the initial rate of oxygen evolution from the beginning of the treatment and standard errors have been shown as bars.

Oxygen evolution measurements were also carried out in the presence of DMBQ (Fig. 4.11). It was seen that the wild type and the R54E* strain behaved in a similar fashion to the studies carried out in the presence of DCBQ. The wild type could acclimatise under the high-light condition, and the oxygen evolution rates were not greatly affected, whereas, the oxygen-evolution rates of the R54E* mutant decreased to 40% of the

initial rate of oxygen-evolution. Both the strains, however, when allowed to recover in normal low-light conditions of ~30-35 µE $m^{-2}s^{-1}$ after exposure to high light could recover.

Oxygen evolution measurements were also carried out for the wild type and the R54E* strain in the presence of sodium bicarbonate (Fig. 4.12). The wild type and the R54E* strains were able to acclimatise under the high-light condition, and the oxygen evolution rates were not greatly affected.

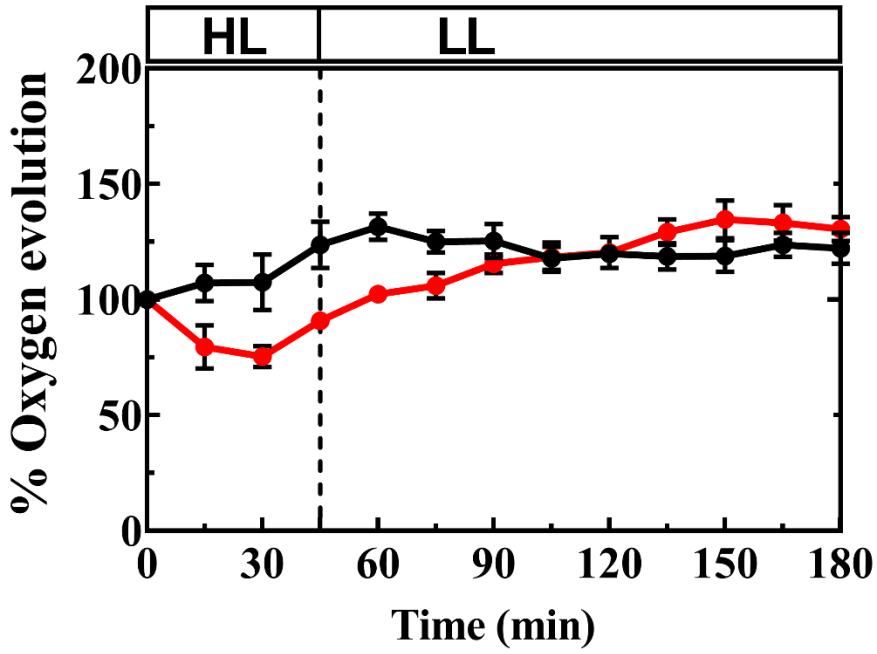

Figure 4.12 Photodamage and recovery of PS II oxygen-evolving activity in the presence of sodium bicarbonate. The cells were suspended to a chlorophyll *a* concentration of 10 µg ml^{-1} and were exposed to high-intensity white light at 2000 µE $m^{-2}s^{-1}$ for 45 min and allowed to recover for 135 min in low-light conditions at 35 µE $m^{-2}s^{-1}$. The strains shown are wild type (black) and R54E* (red). The data represented are the average of three independent experiments normalised to the initial rate of oxygen evolution from the beginning of the treatment and standard errors have been shown as bars.

The extent of photodamage exhibited by both strains when oxygen evolution was supported by the addition of bicarbonate was less evident than when DCBQ and DMBQ were used as electron acceptors. There was a small decrease in the oxygen evolving activity of the R54E* strain (~20-25%) as compared to the wild type during the first 30 min of the high-light incubation. The extent of recovery of PS II oxygen-

evolving activity for the R54E* strain was greater as compared to when DCBQ or DMBQ were used as electron acceptors.

4.4.7.2 Chlorophyll *a* fluorescence decay following single actinic flash

The susceptibility of the decay kinetics of chlorophyll *a* fluorescence to the light-induced damage and the efficiency of the related repair processes were also compared in the wild type and the R54E* strain in the presence and absence of DCMU (Fig. 4.13). The cells were exposed to 75 min of the high-light treatment (2000 µE $m^{-2}s^{-1}$) and were allowed to recover under low-light conditions (35 µE $m^{-2}s^{-1}$) for 100 min. The following time points of 0 min, 75 min and 175 min of the assay are presented in Fig. 4.13 for the wild type and the R54E* strain. The difference between the 0 min and 75 min chlorophyll *a* fluorescence decay curves illustrates the extent of photodamage, due to 75 min of high-light treatment. The 175 min decay curve represents the degree of recovery from the photodamage in each strain after cells have spent ~75 mins in high-light and 100 mins in low-light conditions. In the inset in Fig. 4.13, the fluorescence transients have been normalised as per the ($F-F_o$) to see the effect of the photodamage on the initial fluorescence/number of PS II centres for each strain at different time points of the study. Table 4.7 lists the half-times and the amplitudes of the fluorescence decay in the absence of DCMU.

The recovery in the wild type was much more efficient as compared to the R54E* strain during chlorophyll *a* fluorescence decay measurements in the absence and presence of DCMU (see insets of Fig. 4.13). It was observed that the R54E* strain displayed enhanced susceptibility to photoinhibition (see insets of Fig. 4.13 B and D). Both the wild type and the R54E* mutant could recover from photodamage under low-light conditions. Most of the damage occurs within the first 30-45 min of the assay, as observed by a drop in the initial fluorescence (F_o), fluorescence maximum (F_m) and the variable fluorescence yield (F_v). The R54E* strain, when exposed to high-light, led to the decrease in the initial fluorescence (F_o) and variable fluorescence (F_v), thus indicating that PS II assembly has been compromised due to high light. However, when the cells could recover, the F_o and F_v levels also started improving (see inset of Fig. 4.13). The chlorophyll *a* decay measurements under the high-light and low-light conditions were consistent with the measurements of oxygen evolution (Fig. 4.10, 4.11, and 4.12), which showed a decline in the PS II oxygen-evolving activity within the first

30-45 min, followed by an acclimatisation phase. The extent of photodamage of the R54E* mutant was similar to the wild type in the absence and presence of DCMU. The lower levels of fluorescence yield in high-light susceptible strains denote lower levels of photochemistry as compared to the wild type. The half-time of the fast component in R54E* mutant decreased from 770 ± 10 µs at time 0 min to 620 ± 10 µs at time 75 min. The decrease (~1.5 fold) in the amplitude of the microsecond component of R54E* mutant with the time of the assay could be seen compensating by an increase (~2 fold) in the amplitude of the slow component during forward electron transfer. Also, the amplitude of the microsecond component of R54E* mutant in the presence of DCMU was 3-3.5 times higher than the amplitude of the fast component of the wild type.

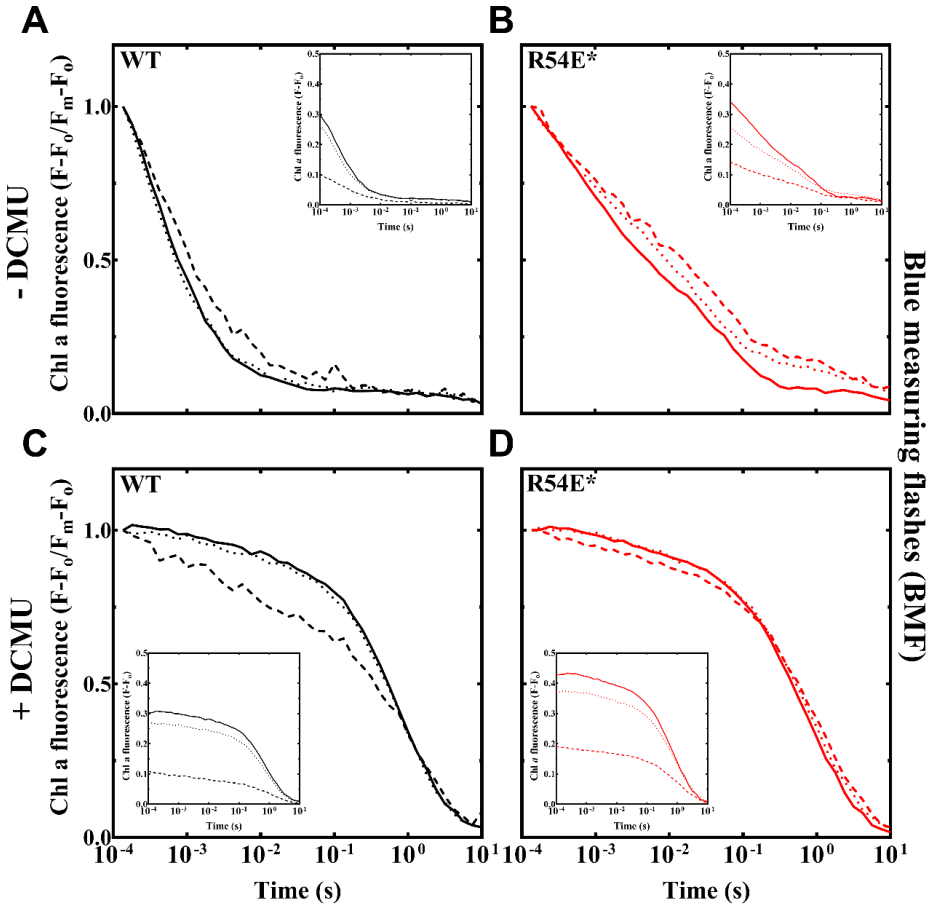

Figure 4.13 Normalised and unnormalised relaxation of chlorophyll *a* fluorescence curves of wild type and R54E* mutant. Normalised and unnormalised chlorophyll *a* fluorescence decay curves of the wild type and the R54E* strain following single turnover actinic flashes at different time points of the photoinhibition assay (T=0 min (low light), T=75 min (high light) and T=175 min (low light)), in the presence (panels **C** and **D**) and absence (panels **A** and **B**) of DCMU. The strains shown are wild type (black) and R54E* (red), where T=0 min (solid), T=75 min (dash) and T=175 min

(dots). The strains were exposed to high light at 2000 µE $m^{-2}s^{-1}$ for 75 min and were allowed to recover for 100 min in low light at 35 µE $m^{-2}s^{-1}$. The data shown are the averages from three independent experiments. The effect of photodamage was measured every 15 min (from 0 min to 175 min) for both the strains.

Table 4.7 Decay kinetics of variable chlorophyll *a* fluorescence following single saturating actinic flash in the absence of DCMU in the high-light and the low-light conditions.

Strain	Treat-ment	Fast		Intermediate		Slow	
		$T_{1/2}$ (µs)	Amp.	$T_{1/2}$ (ms)	Amp.	$T_{1/2}$ (s)	Amp.
WT	T=0 (LL)	310 ± 10*	59 ± 1	2.8 ± 0.3	32 ± 1	5.2 ± 2.0	8.1 ± 0.2
	T=75 (HL)	420 ± 30	58 ± 3	6.0 ± 0.7	31 ± 2	5.7 ± 2.6	11.2 ± 1.5
	T=175 (LL)	270 ± 20	60 ± 1	3.1 ± 0.1	31 ± 1	7.3 ± 0.7	9.1 ± 0.1
R54E*	T=0 (LL)	770 ± 10	48 ± 1	36.0 ± 0.6	42 ± 1	4.4 ± 0.7	10.2 ± 0.3
	T=75 (HL)	620 ± 10	35 ± 1	31.0 ± 0.7	42 ± 1	2.7 ± 0.1	22.4 ± 0.5
	T=175 (LL)	550 ± 30	36 ± 1	22.0 ± 1.3	45 ± 1	3.0 ± 0.3	19.3 ± 0.3

*The standard error have been shown for the chlorophyll *a* fluorescence decays from three independent experiments.

Table 4.8 Decay kinetics of chlorophyll *a* fluorescence following single saturating actinic flash in the presence of DCMU in high-light and low-light conditions.

Strains	Treatment	Fast		Slow	
		$T_{1/2}$ (ms)	Amp.	$T_{1/2}$ (s)	Amp.
WT	T=0 (LL)	13 ± 1*	14 ± 1	0.7 ± 0.1	86.1 ± 0.3
	T=75 (HL)	5 ± 1	28 ± 1	0.8 ± 0.1	72.1 ± 0.1
	T=175 (LL)	20 ± 4	15 ± 1	0.7 ± 0.1	85.1 ± 0.3
R54E*	T=0 (LL)	50 ± 2	24 ± 1	0.7 ± 0.1	76.1 ± 0.3
	T=75 (HL)	30 ± 10	22 ± 1	0.8 ± 0.1	78.2 ± 1.2
	T=175 (LL)	50 ± 10	26 ± 2	0.8 ± 0.1	74.3 ± 1.6

*The standard error have been shown for the chlorophyll *a* fluorescence decays from three independent experiments.

4.4.8 Whole genome sequencing

Since deletion of *psb27* in the R54E* strain could not restore the expected phenotype shown by ΔPsb27 mutant, whole genome sequencing of the R54E* strain was performed to identify the secondary mutations responsible for the phenotype displayed by this mutant. The whole genome sequencing of the R54E* strain was performed using an Illumina HiSeq2500 V4 platform at the New Zealand Genomics Limited (NZGL) as described earlier in Chapter 2, section 2.8. In previous studies, various strains of *Synechocystis* 6803 have already been described (Ikeuchi and Tabata 2001; Trautmann *et al.* 2012).

The R54E* strain used in this study was derived from the GT-O1 (wild type) strain at the University of Otago, Department of Biochemistry, New Zealand. The whole genome sequencing of GT-O1 strain has already been carried out by our lab members in the past. Various other novel single nucleotide polymorphisms (SNPs) and indels (insertions/deletions) were identified in the R54E* strain, that has been introduced since the distribution and usage of the original Williams GT strain (Morris *et al.* 2014).

In the R54E* mutant, ~ 31 novel SNPs and ~3 novel indels were detected. All these variations identified in the R54E* mutant were different and in addition to the already existing mutations in the GT-O1 background strain (Morris *et al.* 2014). Out of the 31 novel SNP`s, 6 SNPs were present in the chromosome of the R54E* genome, and 29 SNPs were present in the pSYSX plasmid. The 2 indels were present in the R54E* chromosome, whereas 1 indel was present in the pSYSX plasmid sequence. Out of 31 SNPs, 9 SNPs were silent mutations. Sixteen SNPs, 1 indel from the genomic sequence and 1 indel from the plasmid sequence were in non-coding regions of the genome of the R54E* strain. The mutations have been discussed in detail in Table 4.9 and Table 4.10.

Table 4.9 List of previously observed mutations detected in parent strain of GT-O1 as compared to the GT-Kazusa chromosome sequence

S.No	Position	Mutation Type	Nucleotide level	Amino acid level	Gene Name	Details
1.	386406	Ins	50 to 60 bps	-	*slr1084* - unknown protein/putative colonic acid biosynthesis; acetyltransferase	US gene: *slr1083* - hypothetical protein DS gene: *slr1085* - probable glycosyltransferase
2.	943495	SNP	G to A	Val604Ile	*slr1834/psaA* – P700 apoprotein subunit/PS I; photosynthesis; metal ion binding	US gene: *sll1730* - unknown protein; hydrolase activity DS gene: *slr1835/psaB* - P700 apoprotein subunit Ib; photosynthesis
3.	1012958	SNP	G to T	-	non-coding region	US gene: *ssl3177/repA* - hypothetical protein; defense response (fungus, bacterium), chitinase activity DS gene: *sll1632/ftsQ*/ hypothetical protein
4.	1364187	SNP	A to G	Leu116Leu	*sll0838/pyrF* – Orotidine 5` monophosphate decarboxylase;	US gene: *sll0837* - periplasmic protein

					pyrimidine ribonucleotide biosynthesis	DS gene: *sll0839* - hypothetical protein
5.	1581467	SNP	G to A	Pro115Ser	*sll1428* – sodium dependent transporter; organic anion transport, bile acid:sodium symporter activity	US gene: *slr1503* - hypothetical protein; oxidoreductase activity DS gene: *ssl2789* - similar to resolvase; transposon-related functions
6.	1819782 1819788	SNP SNP	A to G A to G	Ser70Ser Leu72Leu	*sll1867*/*psbA3* – D1 protein; photosynthesis	US gene: *sll1866* - hypothetical protein DS gene: *sll1868*/*dnaG* - DNA primase; DNA replication, restriction, modification, recombination and repair
7.	2092571	SNP	A to T	Leu313stop codon	*sll0422* – asparaginase; hydrolase activity	US gene: *sll0421*/*purB* - adenylosuccinate lyase; purine ribonucleotide biosynthesis DS gene: *trnN-GUU*/tRNA-Asn (GTT); RNA

8.	2198893	SNP	T to C	Leu689Leu	*sll0142* – probable cation efflux system protein; transport and binding proteins	US gene: *sll0141* - hypothetical protein DS gene: *slr0157* - unknown protein
9.	2204575	Del	CG to C	-	*slr0162*/*pilC* – pilin biogenesis protein; chemotaxis	US gene: *slr0161*/*pilT1* - twitching motility protein PilT; chemotaxis DS gene: *slr0163*/*pilC* - pilin biogenesis protein; chemotaxis
10.	2301721	SNP	A to G	Lys403Glu	*slr0168* – hypothetical protein	US gene: *slr0338* - oxidoreductase DS gene: *ssl0318* - unknown protein
11.	2350285	Ins	T to TA	-	non-coding region	US gene: *sml0001* - PsbI; photosynthesis DS gene: *slr0363* - hypothetical protein
12.	2360245	Ins	G to GC	-	*slr0364* – hypothetical protein	US gene: *slr0363* - hypothetical protein DS gene: *slr0366* - unknown

						protein
13.	2409242	Del	TC to T	-	*sll0762* – hypothetical protein	US gene: *sll0761* - unknown protein DS gene: *sll0763* - hypothetical protein
14.	2419397	Del	AT to A	-	*sll0751/ycf22* – hypothetical protein YCF22	US gene: *slr0782* - amine oxidase; oxidoreductase activity DS gene: *sll0752* - hypothetical protein
15.	2544044	Ins	T to TC	-	*ssl078* – hypothetical protein	US gene: *sll0413* - hypothetical protein DS gene: *ssl0788* - hypothetical protein
16.	2602717 2602734	SNP	C to A T to A	His82Gln Ile88Asn	*slr0468* – unknown protein	US gene: *slr0467/natA* - conserved component of ABC transporter for natural amino acids; transport and binding proteins

						DS gene: *slr0469/rps4* - 30S ribosomal ptn S4; ribosomal proteins: synthesis and modification
17.	2748897	SNP	C to T	-	non-coding region	US gene: *slr0210/hik9* - two-component sensor histidine kinase DS gene: *ssr0332* - hypothetical protein
18.	2807666	SNP	C to T	Ala423Thr	*sll0550/flv3/flv* – flavoprotein; hydrolase activity; oxidoreductase activity; FMN binding	US gene: *sll0549* - hypothetical protein DS gene: *slr0565/SyndsbAB* - hypothetical protein
19.	3096187	SNP	T to C	Ile47Thr	*ssr1175/ISY100v1* – transposase; transposon-related functions	US gene: *sll0676* - hypothetical protein DS gene: *slr0703/ISY523i* - transposase; transposon-related functions

20.	3110189	SNP	G to A	-	non-coding region	US gene: *sll0665*/*ISY523r* - transposase; transposon-related functions DS gene: *sll0666*/*ISY523r* - transposase; transposon-related functions
21.	3110343	SNP	G to T	Pro73Gln	*sll0665*/*ISY523r*/transposase; transposon-related functions	US gene: *sll0664* - unknown protein DS gene: *sll0666*/*ISY523r* - transposase; transposon-related functions
22.	3142651	SNP	A to G	Leu75Leu	*sll0045*/*spsA*/sucrose phosphate synthase; sugars	US gene: *slr0023* - unknown protein DS gene: *slr0022* - hypothetical protein
23.	3260089	Del	TC to T	-	non-coding region	US gene: *sll0528* - hypothetical protein; metalloendopeptidase activity, proteolysis DS gene: *sll0529* - hypothetical protein; aldehyde-lyase activity;

						catalytic activity
24.	3282	SNP	C to T	-	non-coding region; pSYSX	US gene: *slr6001* - Chy46; two-component hybrid sensor and regulator

*US: Upstream; DS: Downstream; SNP: Single nucleotide polymorphism; Ins: Insertion; Del: Deletion.

Table 4.10 List of novel mutations in R54E* mutant.

Sr.No	Position	Mutation Type	Nucleotide level	Amino acid level	Gene Name	Details
1.	7984	SNP	C to A	His252Glu	*slr1311/psbA2* - D1 protein	US gene: *sll1212/gmd/rfb* – GDP-mannose 4,6-dehydratase; catalytic activity; coenzyme binding DS gene: *slr1312/speA/speA1/adc1/adc* – Arginine decarboxylase; arginine catabolic process
2.	291211	SNP	G to C	-	non-coding region	US gene: *ssr2142/ycf19/ylmG* – Ycf19 DS gene: *slr1295/futA1/sufA/sufA1/idiA/futA* – FutA1; iron transport system substrate-binding protein; transport and binding proteins
3.	373250	SNP	C to A	Thr7Lys	*slr1069* - hypothetical	US gene: *slr1068* – hypothetical

					protein	protein DS gene: *slr1070* – unknown protein
4.	488803	SNP	A to T	Gln506Leu	slr1609/*fadD*/*aas* – acyl-ACP synthetase; fatty acid, phospholipid and sterol metabolism	US gene: *sll1500*/cobT – hypothetical protein; cobalamin biosynthetic process; nicotinate-nucleotide-dimethylbenzimidazole phosphoribosyltransferase activity DS gene: *slr1041*/pilG/rre6/taxP3/taxP – putative phototaxis protein; regulation of transcription; two-component signal transduction system
5.	1200306 1200311	SNP SNP	C to A T to G	Pro200Gln Ser202Ala	*slr1862* – unknown protein	US gene: *slr1861* - sigma regulatory factor; RNA synthesis, modification and DNA transcription DS gene: *sll1780*/*ISY203b* – transposase; transposon-related

						functions
6.	1346489	Ins	G to GA	-	*slr0856/ISY100l* – Transposase; transposon-related functions	US gene: *sll0853/cpcU* - hypothetical protein DS gene: *slr0857/ISY100l* – transposase; transposon-related functions
7.	1924068	Ins	T to TTATGTCCTAATCTATGCT	-	non-coding region	US gene: *sll1094* – transposase; transposon-related functions DS gene: *slr1161* – hypothetical protein; catalytic function, hydrolase activity, zinc ion binding
9.	3326 3340 3367 3391 3438 3443 3485	SNP SNP SNP SNP SNP SNP SNP	TTAA to CTAC T to G C to T AAGC to GAGT T to C A to C T to C	-	non-coding region; pSYSX	US gene: *slr6001* – Chy46; regulatory functions; phosphorylation; ATP binding DS gene: *ssr6002* – unknown protein
10.	3573	SNP	TGCA to GGCG	-	*ssr6002* – unknown protein;	US gene: *slr6001* – Chy46; two

	3594 3753	SNP SNP	T to C A to G	Thr30Thr Stop codon to stop codon	pSYSX	component hybrid sensor and regulator DS gene: *ssr6003* – unknown protein
11.	3849	SNP	A to G	-	non-coding region; pSYSX	US gene: *ssr6002* DS gene: *ssr6003*
12.	59363 59411 59420 59457	SNP SNP SNP SNP	T to C CTTA to GCTC G to A T to C	Ala61Ala Val77Val, Leu78Leu Gln80Gln Leu93Leu	*slr6064* – unknown protein; pSYSX	US gene: *slr6063* – unknown protein DS gene: *slr6065* – unknown protein
13.	81876	SNP	G to A	Arg138Arg	*slr6088* – hypothetical protein; pSYSX	US gene: *slr6087* – unknown protein DS gene: *ssr6089* – unknown protein
14.	81962 81967 81975	Del SNP SNP	TAA to TA T to G GTCAGTGACACTGA to CTCAATAACAATGG	-	non-coding region; pSYSX	US gene: *slr6088* DS gene: *ssr6089*

	82000	SNP	CCCGAG to ACCAAC			
	82012	SNP	T to C			
	82025	SNP	GAAAGTA to AAGAATG			
	82036	SNP	G to A			
	82042	SNP	A to G			
	82063	SNP	T to A			
	82195	SNP	C to T			
15.	82299	SNP	G to A	Gly2Arg	*ssr6089* – unknown protein; pSYSX	US gene: *slr6088* DS gene: *slr6090* – unknown protein
	82358	SNP	A to G	Pro21Pro		
	82405	SNP	A to G	Asn37Lys		

*US: Upstream; DS: Downstream; SNP: Single nucleotide polymorphism; Ins: Insertion; Del: Deletion.

4.5 D1-His252 and D1-Ser264 mutants

The whole genome sequencing of the R54E* mutant revealed a C to A substitution in the *psbA2* gene corresponding to a His252 to Gln substitution in the D1 protein of the PS II reaction centre and this residue has been hypothesised to be involved in protonation of Q_B^- in PS II (Crofts *et al.*, 1987). So, to confirm that D1-His252 is responsible for the R54E* mutant phenotype, a series of point mutations were introduced into a *psbA*-deletion strain of *Synechocystis* 6803 strain. Additionally, the D1-Ser264 was also targeted, since D1-Ser264 has also been suggested to be involved in the configuration of the Q_B site and is close to His252 in the X-ray crystallographic structure (Trebst 1991; Umena *et al.* 2011). The following mutants were constructed H252A, H252Q, H252Y, S264A, S264K, S264T and D1 control strain. His252 amino acid is positively charged, so it was mutated to Ala (nonpolar amino acid), Gln (polar amino acid), Tyr (polar aromatic amino acid). Serine amino acid is polar in nature, so it was mutated to Ala (nonpolar amino acid), Lys (positively charged amino acid) and Thre (polar amino acid). The amino acid substitutions was carried out by focussing on the charge reversal mutations or changing the side chains of amino acids of interest thinking that these substitution might prove detrimental for the structural and functional roles of the D1 protein.

4.6 Construction of D1-His252 and D1-Ser264 mutants

The *psbA* triple deletion strain used in this study was originally constructed by Regan Winter in the Eaton-Rye lab (unpublished). The deletion strain and the mutagenesis system for the introduction of targeted mutations into the *psbA2* copy that encodes the D1 protein are described in Appendix, Section A, B, C, D and E. In this *psbA*-triple deletion strain, all the three genes encoding the D1 protein, *psbA*1, *psbA*2, and *psbA*3 were deleted in a step-wise manner. The *psbA1* and *psbA3* were deleted through a markerless deletion strategy, whereas *psbA2* was replaced by inserting a chloramphenicol-resistance cassette respectively. This *psbA*-triple deletion strain can be grown photoheterotrophically using glucose but is incapable of assembling an active PS II complex because of the absence of D1.

4.6.1 *psbA2* mutagenesis system

The following D1 mutations were introduced using the *psbA2* mutagenesis system: D1-His252Ala, D1-His252His (D1 control strain), D1-His252Gln, D1-His252Tyr, D1-Ser264Ala, D1-Ser264Lys, and D1-Ser264Thr. The plasmids containing *psbA2* encoding these amino acid substitutions were introduced into the ΔPsbA deletion strain, and transformants were confirmed by Sanger di-deoxy sequencing. The complete segregation of all strains was confirmed by PCR analysis of each locus (Fig. 4.14).

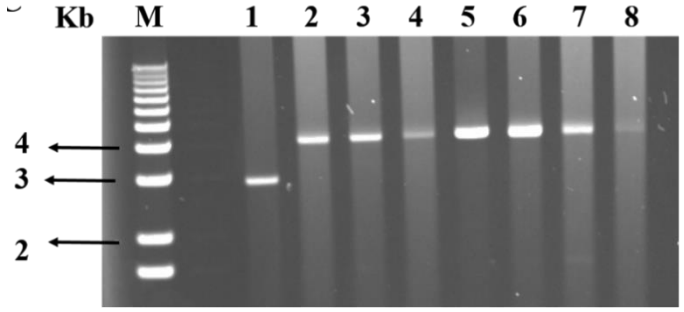

Figure 4.14 Colony PCR of D1-His252 and D1-Ser264 mutants. Confirmation of the complete segregation of D1-His252 and D1-Ser264 mutants. Lane M is the 1 Kb Plus DNA Ladder (Invitrogen, CA), the other lanes contain PCR products corresponding to the segregated mutants. The lanes are 1, wild type; 2, D1-H252A; 3, D1 control strain; 4, D1-H252Q; 5, D1-H252Y; 6, D1-S264A; 7, D1-S264K; 8, D1-S264T.

4.7 Characterisation of *psbA2* mutant strains

4.7.1 PS-II specific oxygen evolution assay

Oxygen evolution assays were carried out for the strains with amino acid substitutions at His252 and Ser264 in the D1 protein and the wild type. Fig. 4.15 shows the oxygen evolution traces obtained using the different PS II-specific artificial quinone acceptors DCBQ (A), DMBQ (B) and sodium bicarbonate (C). The average oxygen evolution rates for each D1 mutant strain have been presented in Table 4.11.

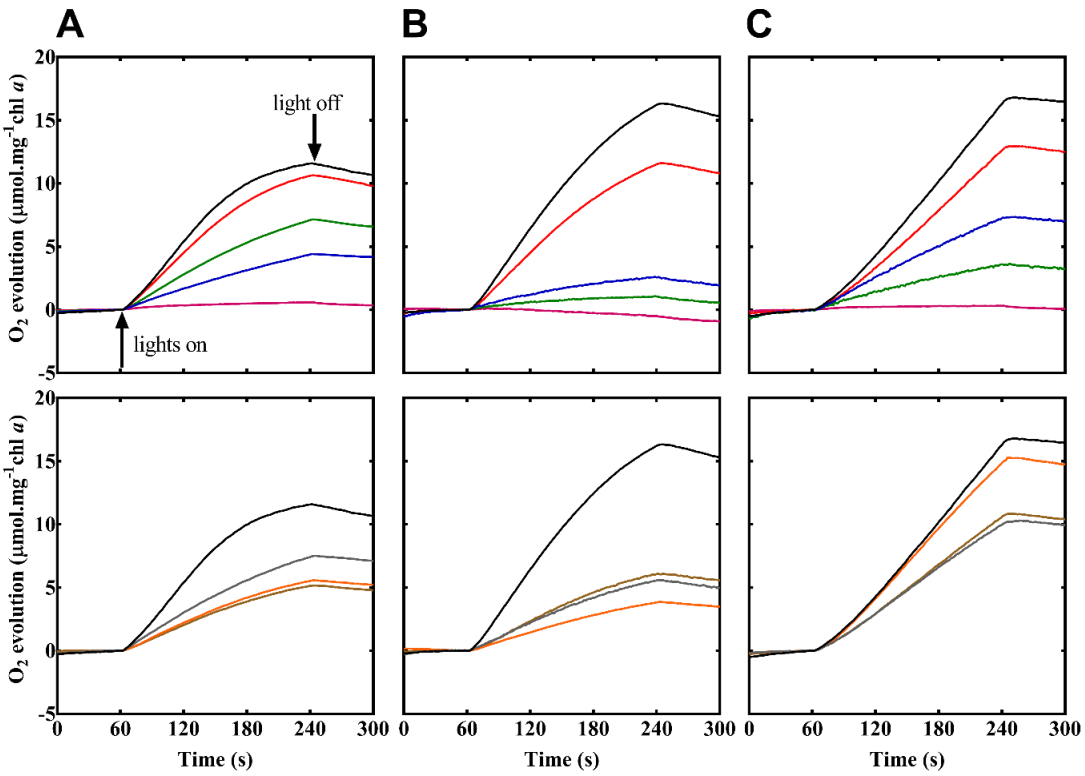

Figure 4.15 Oxygen evolution assay traces for the wild type and the strains with amino acid substitutions at His252 and Ser264 in D1 protein.(A) Oxygen evolution measured in the presence of DCBQ. **(B)** Oxygen evolution measured in the presence of DMBQ. **(C)** Oxygen evolution measured in the presence of sodium bicarbonate. The strains shown are wild type (black), H252A (blue), H252H (red), H252Q (green), and H252Y (pink), S264A (orange), S264K (grey) and S264T (brown). Data shown are the average of three independent experiments. The average values of oxygen evolution rates have been shown in Table 4.11.

The wild type had an oxygen evolution rate of around 320 ± 20 µmol O_2 (mg of chl)$^{-1}$ h^{-1} in the presence of DCBQ, 390 ± 20 µmol O_2 (mg of chl)$^{-1}$ h^{-1} in the presence of DMBQ and 320 ± 10 µmol O_2 (mg of chl)$^{-1}$ h^{-1} in the presence of sodium bicarbonate. The D1:H252Y strain had extremely low oxygen evolution rates in the presence of the PS II specific electron acceptors. The D1 control strain had an oxygen evolution rate around 270 ± 40 µmol O_2 (mg of chl)$^{-1}$ h^{-1} in the presence of DCBQ, 280 ± 50 µmol O_2 (mg of chl)$^{-1}$ h^{-1} in the presence of DMBQ and 250 ± 40 µmol O_2 (mg of chl)$^{-1}$ h^{-1} in the presence of sodium bicarbonate. The oxygen evolution rates of D1:H252A strain were 35% with DCBQ, 21% with DMBQ and 52% with sodium bicarbonate as compared to the oxygen evolution rates of the wild type. The oxygen evolution rates of D1:S264K and D1:S264T mutants were around 44% and 40% with DCBQ, 24% and 33% with DMBQ in comparison to the oxygen evolution rates of the wild type. Overall, the

oxygen-evolving activity of D1-H252A, D1-H252Q, D1-S264A, D1-S264K, and D1-S264T mutants was altered.

Table 4.11 Oxygen evolution rates of wild type and the strains with amino acid substitutions at His252 and Ser264 in D1.

Strains	Oxygen evolution[1] µmol O_2 (mg of chl)$^{-1}$ h^{-1}		
	DCBQ	**DMBQ**	**Bicarbonate**
WT	320 ± 20[2]	390 ± 20	320 ± 10
H252A	110 ± 20	80 ± 20	170 ± 20
H252H	270 ± 40	280 ± 50	250 ± 40
H252Q	170 ± 10	40 ± 10	80 ± 10
H252Y	30 ± 10	10 ± 10	10 ± 10
S264A	190 ± 40	140 ± 20	220 ± 20
S264K	140 ± 10	90 ± 20	320 ± 30
S264T	130 ± 40	130 ± 30	220 ± 20

[1]Oxygen evolution rates were measured in the presence of DCBQ, DMBQ and sodium bicarbonate. Data shown are the average of three independent experiments.
[2]The standard error have been shown.

4.7.2 Low temperature 77 K fluorescence emission spectroscopy

To study the effect of single amino acid substitutions in the D1 protein on the levels or stoichiometry of the PS I and PS II complexes, low temperature 77 K fluorescence emission spectroscopy measurements were performed. The D1-H252A and D1-H252Q, when excited at 440 nm, displayed typical 725 nm emission, originating from PS I (Fig. 4.16 A). However, D1-H252A and D1-H252Q mutants exhibited higher levels of the 685 and 695 nm emissions originating from CP43 and CP47, respectively, of PS II as compared to the wild type (Fig. 4.16 A). The D1-H252Y mutant displayed typical 725 nm emission and a very high merged peak at 685 nm potentially suggesting that D1-H252Y strain is not able to assemble PS II complexes. The D1 control strain exhibited wild-type levels of PS II specific fluorescence relative to their PS I emission (Fig. 4.16 A).

The D1-S264A and D1-S264K mutants displayed typical 725 nm emission, but the 685 and 695 nm emissions originating from CP43 and CP47 were higher as compared to the wild type (Fig. 4.16 B). The D1-S264T mutant exhibited relative wild-type levels of PS II specific fluorescence emission (685 nm and 695 nm) (Fig. 4.16 B).

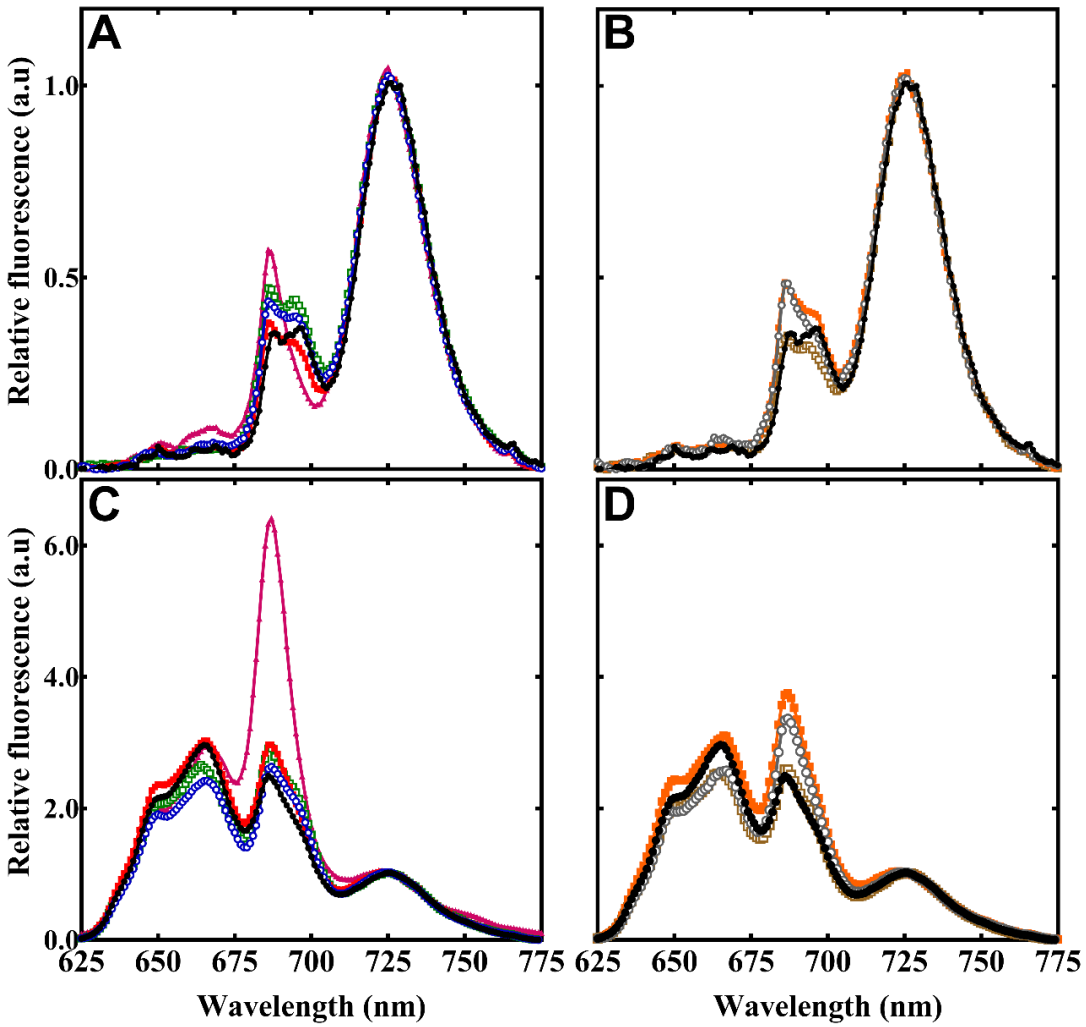

Figure 4.16 Low-temperature fluorescence emission spectra of wild type and the strains with amino acid substitutions at His252 and Ser264 in the D1 protein. Panels **(A)** and **(B)** shows the fluorescence emission spectra with an excitation wavelength of 440 nm. Panels **(C)** and **(D)** show the fluorescence emission spectra with an excitation wavelength of 580 nm. The strains in panels **(A)** and **(C)** are wild type (black, close circles), H252A (blue, open circles), H252H (red, close squares), H252Q (green, open squares), and H252Y (pink, close triangles), and the strains in panel **(B)** and **(D**) are wild type (black, close circles), S264A (orange, close squares), S264K (grey, open circles) and S264T (brown, open squares). Data shown are the average of three independent experiments.

To get insight into the coupling and energy transfer between the PBS and PS II (and possibly PS I), cells were illuminated with a 580 nm light (Fig. 4.16 C and D). The D1-H252A, D1-H252Q mutants and the D1 control strain displayed the typical 725 nm emission originating from PS I; however, the D1-H252Y mutant exhibited high levels of fluorescence emission from allophycocyanin (665 nm) and the ApcE PBS terminal emitter (685 nm), respectively, when compared to the wild type and the D1 control

strain potentially indicating that the PBS are not able to quench the chlorophyll *a* fluorescence efficiently (Fig. 4.16 C).

The D1-S264A and D1-S264K mutants also displayed higher levels of fluorescence emission from allophycocyanin (665 nm) and the ApcE PBS terminal emitter (685 nm), respectively as compared to the wild type and the D1 control strain (Fig. 4.16 D). However, the D1-S264T strain displayed typical 725 nm emission and phycocyanin (650 nm) and allophycocyanin emissions (665 nm) (Fig. 4.16 D).

4.7.3 Chlorophyll *a* fluorescence induction

The D1-H252A and D1-H252Q mutants showed a distinct phenotype when the chlorophyll *a* variable fluorescence was compared between the mutants and the wild type in the absence of DCMU (Fig. 4.17 A). The chlorophyll *a* fluorescence induction curve exhibited an initial rapid rise with an elevated J level. The D1-H252Y strain displayed a collapsed fluorescence transient in the absence of DCMU (Fig. 4.17 A) indicating the absence of PS II specific variable fluorescence.

The chlorophyll *a* fluorescence induction curve of D1-S264A and the D1-S264K mutants also exhibited an initial rapid rise with an elevated J level (Fig. 4.17 B). The fluorescence induction curve of D1-S264T mutant also displayed loss of J-P rise. However, the initial rapid rise and the J level in D1-S264T mutant were similar to the wild type (Fig. 4.17 B).

All the D1 mutants with amino acid substitutions at His252 exhibited higher variable fluorescence induction traces in the presence of DCMU (Fig. 4.17 C). However, the level of fluorescence in case of D1-H252Y mutant was the lowest potentially indicating this strain possesses a lower number of PS II centres (Fig. 4.17 C). The D1-S264A and D1-S264K mutants also exhibited higher levels of variable fluorescence, with D1-S264T displaying similar levels of variable fluorescence to the wild type (Fig. 4.17 D).

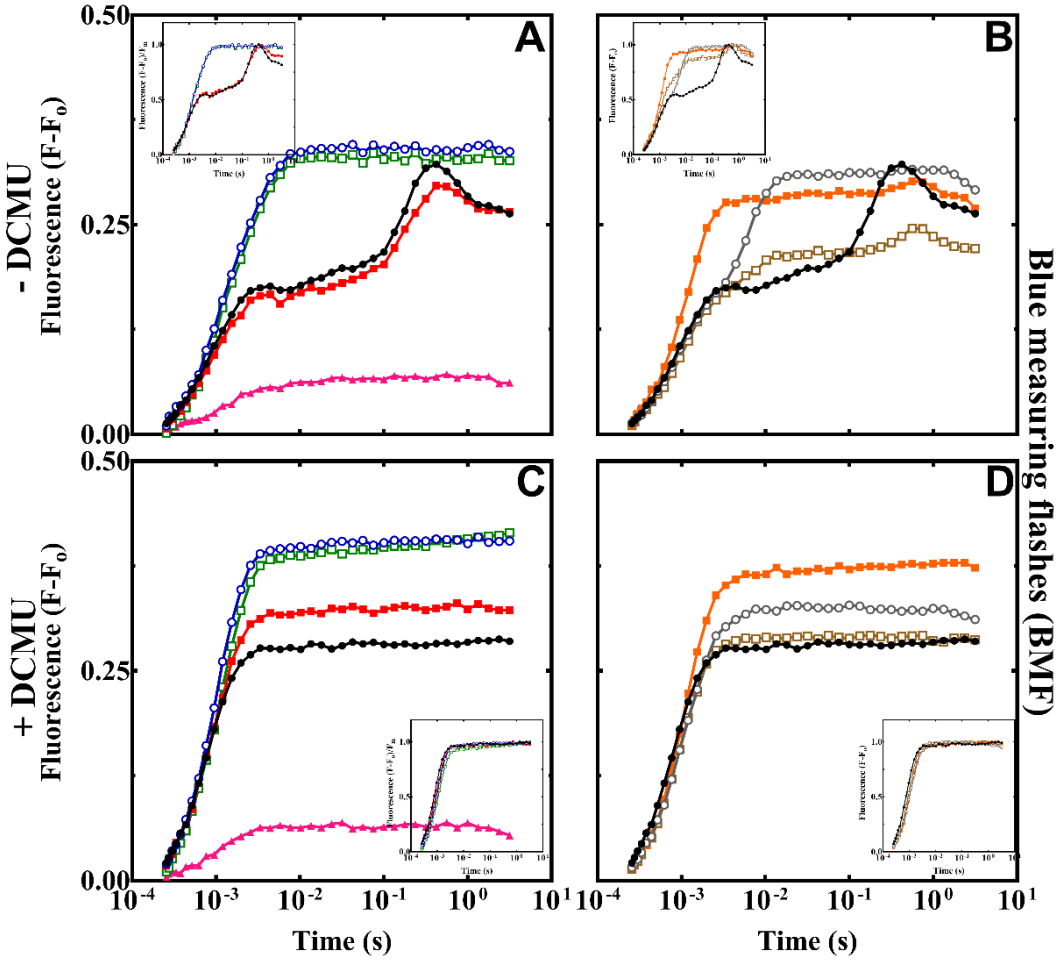

Figure 4.17 Normalised steady-state chlorophyll *a* fluorescence induction in wild type and the strains with amino acid substitutions at His252 and Ser264 in D1 protein.Panels **(A)** and **(B)** contains the measurements in the absence of DCMU and panels **(C)** and **(D)** contains the measurements in the presence of DCMU. The strains in panels **(A)** and **(C)** are wild type (black, close circles), H252A (blue, open circles), H252H (red, close squares), H252Q (green, open squares), and H252Y (pink, close triangles), and the strains in panels **(B)** and **(D)** are wild type (black, close circles), S264A (orange, close squares), S264K (grey, open circles) and S264T (brown, open squares). The data normalised to the F_m value of each strain have been shown in the insets. Data shown are the average of three independent experiments.

To further investigate the differences in the levels of IP rise and P peak in the D1 mutants, the duration of the chlorophyll *a* fluorescence induction assay was increased to ~500 s in the presence and absence of DCMU. The Fig. 4.18 shows the fluorescence induction traces recorded for the strains with amino acid substitutions at His-252 and Ser-264 in D1 protein in the presence and absence of DCMU. The SM rise is missing in all the D1 mutants (H252A, H252Q, H252Y, S264A. S264K and S264T) except the D1 control strain and the wild type. The D1-H252A and D1-H252Q mutants exhibited

higher levels of fluorescence rise in the presence of DCMU in comparison to the wild type. However, the fluorescence levels for the D1 control strain were lower as compared to the wild type in the presence of DCMU. The D1-H252Y mutant exhibited lowest or no fluorescence levels (see Fig. 4.18 C). The D1-S264A, D1-S264K, and D1-S264T mutants exhibited smaller amplitude for the IP rise in comparison to the wild type (see Fig. 4.18 D and inset of Fig. 4.18 D).

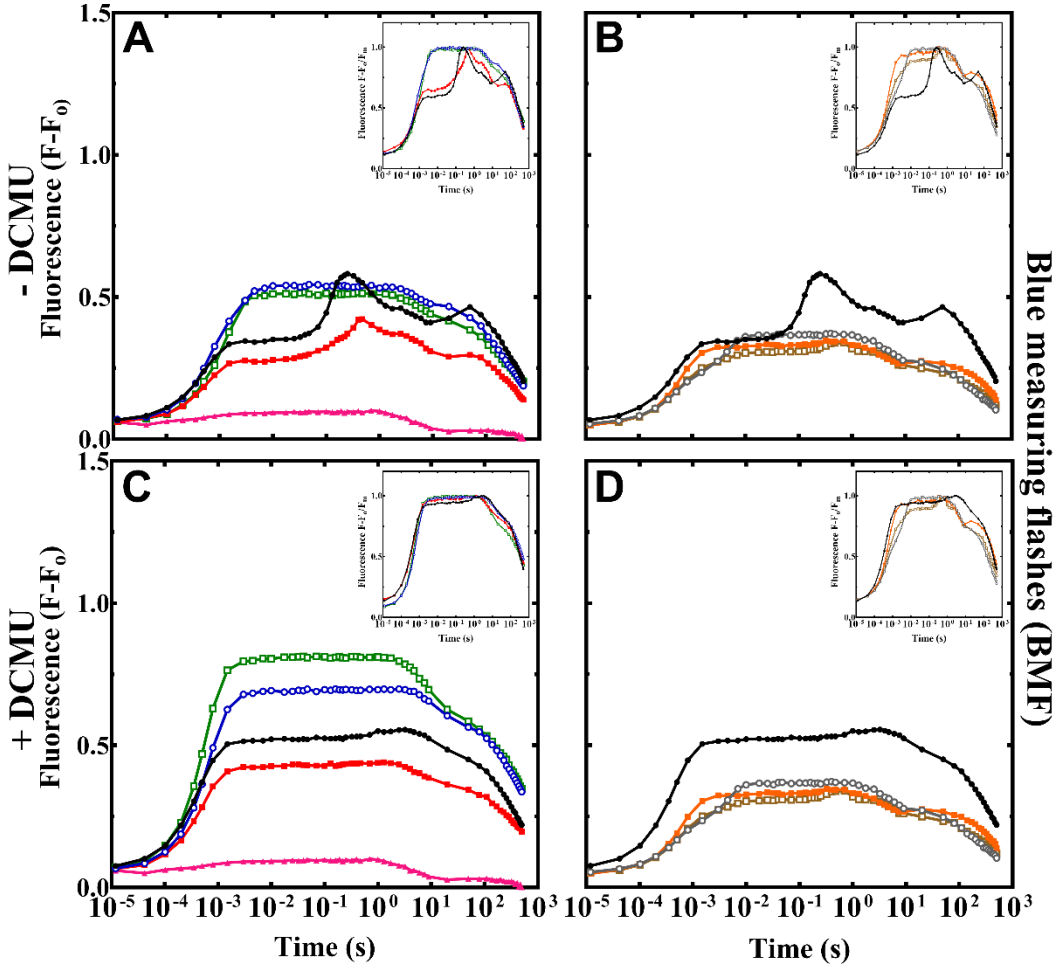

Figure 4.18 Normalised steady-state long-term chlorophyll *a* fluorescence induction (500 s).Panels **(A)** and **(B)** contains the measurements in the absence of DCMU and panels **(C)** and **(D)** contains the measurements in the presence of DCMU. The strains in panels **(A)** and **(C)** are wild type (black, close circles), H252A (blue, open circles), H252H (red, close squares), H252Q (green, open squares), and H252Y (pink, close triangles), and the strains in panels **(B)** and **(D)** are wild type (black, close circles), S264A (orange, close squares), S264K (grey, open circles) and S264T (brown, open squares). The data normalised to the F_m value of each strain have been shown in the insets. Data shown are the average of four independent experiments.

4.7.4 Chlorophyll *a* fluorescence decay following single actinic flash

The decay kinetics of chlorophyll *a* fluorescence following single saturating actinic flash were also investigated and compared between the strains with amino acid substitutions at His-252 and Ser-264 in the D1 protein (Fig. 4.19). All the mutants with amino acid substitution at His-252 and Ser-264 in the D1 protein displayed slower forward electron transfer in comparison to the wild type and the D1 control strain (Fig. 4.19 A and B). In D1-H252A, D1-H252Q and D1-S264K mutants, the half-time of the microsecond component without any addition were ~840 ± 70 µs, ~860 ± 60 µs and 740 ± 10 µs as compared to ~340 ± 10 µs in wild type (Table 4.12). The amplitude of the microsecond component of D1-H252A, D1-H252Q, and D1-S264K mutants was ~24%, 32%, and 18%, respectively, as compared to the 58% in wild type. The half-time of the millisecond component for D1-H252A, D1-H252Q, D1-S264A and D1-S264K mutants was also ~4-5 times slower than the half-time of the millisecond component of the wild type. The amplitude of the slow component of all the D1 mutants except D1 control strain was also higher than the amplitude of the slow component of the wild type.

The chlorophyll fluorescence decay studies were also carried out in the presence of DCMU (Fig. 4.19 C and D). The D1-H252 mutants exhibited similar chlorophyll *a* fluorescence decay in the presence of DCMU, although; the D1-H252Y mutant seemed to have no active PS II centres and hence is not shown in Fig. 4.19 A and C. The amplitude of the microsecond component and millisecond component in D1-S264 mutant varied a lot from the amplitude of the fast component and slow component of the wild type, potentially indicating variations in the charge recombination pathways within the PS II (Fig. 4.19 D) (Table 4.13). The kinetics of the D1-His252 and D1-Ser264 mutants in the presence of DCMU have been presented in Table 4.13.

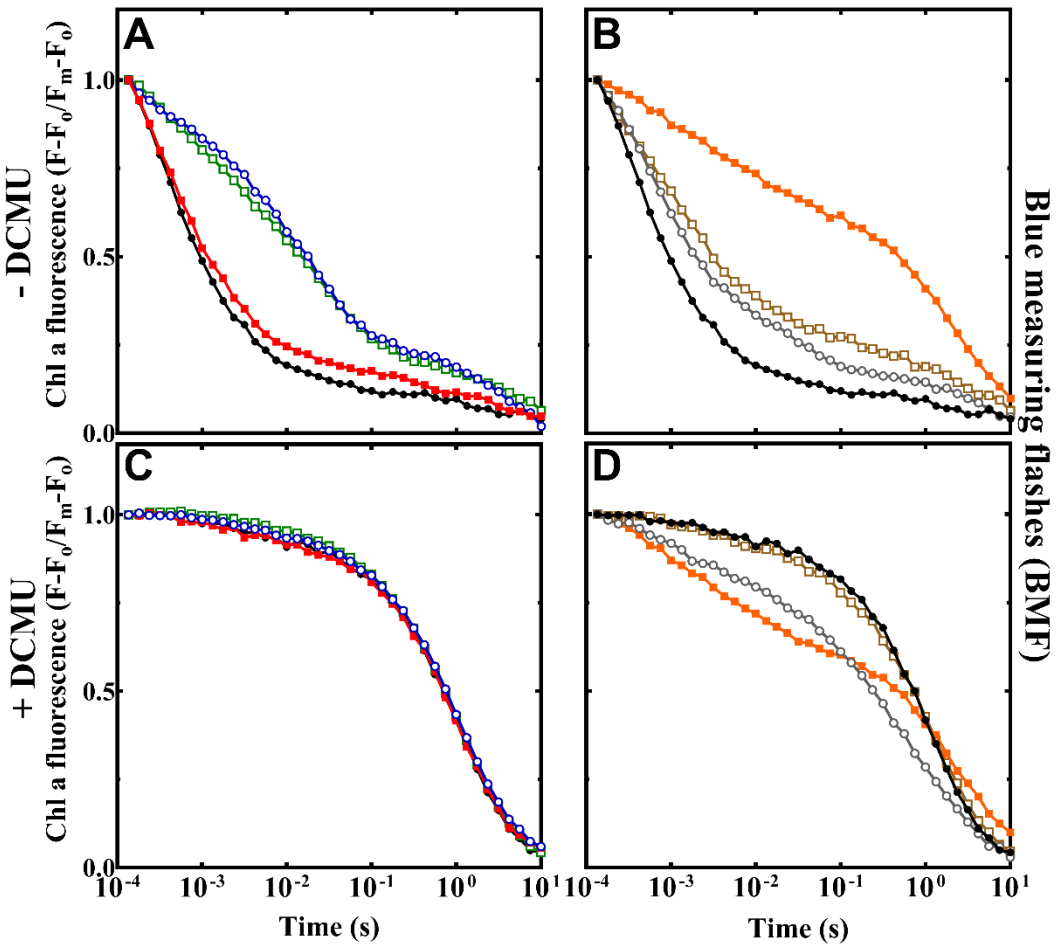

Figure 4.19 Relaxation of chlorophyll *a* fluorescence following single flash in the wild type and the strains with amino acid substitutions at His252 and Ser264 in D1 protein. Panels **(A)** and **(B)** contains the measurements in the absence of DCMU. Panels **(C)** and **(D)** contains the measurements in the presence of DCMU. The strains in panels **(A)** and **(C)** are wild type (black, close circles), H252A (blue, open circles), H252H (red, close squares), and H252Q (green, open squares), and the strains in panels **(B)** and **(D)** are wild type (black, close circles), S264A (orange, close squares), S264K (grey, open circles) and S264T (brown, open squares). Data shown are the average of four independent experiments.

Table 4.12 Decay kinetics of variable chlorophyll *a* fluorescence following single saturating actinic flash in the absence of DCMU.

Strains	Fast		Intermediate		Slow	
	$T_{1/2}$ (µs)	Amp.	$T_{1/2}$ (ms)	Amp.	$T_{1/2}$ (s)	Amp.
WT	340 ± 10*	58 ± 1	4.3 ± 0.2	29 ± 1	2.1 ± 0.2	13.1 ± 0.2
H252A	840 ± 70	24 ± 1	16.0 ± 0.1	47 ± 1	1.2 ± 0.1	28.2 ± 0.3
H252H	340 ± 40	52 ± 4	4.1 ± 0.3	30 ± 3	2.0 ± 0.8	18.4 ± 4.8
H252Q	860 ± 60	32 ± 1	23.5 ± 0.6	44 ± 1	2.7 ± 0.6	23.4 ± 0.9
S264A	570 ± 20	56 ± 4	16.0 ± 0.5	25 ± 1	2.0 ± 0.1	25.1 ± 0.1
S264K	740 ± 10	18 ± 1	13.2 ± 1.4	18 ± 1	1.3 ± 0.1	63.3 ± 1.0
S264T	620 ± 10	47 ± 1	10.0 ± 0.1	26 ± 1	1.8 ± 0.1	27.1 ± 0.2

*The standard error have been shown for the chlorophyll *a* fluorescence decays from three independent experiments.

Table 4.13 Decay kinetics of variable chlorophyll *a* fluorescence following single saturating actinic flash in the presence of DCMU.

Strains	Fast		Slow	
	$T_{1/2}$ (ms)	Amp.	$T_{1/2}$ (s)	Amp.
WT	2.5 ± 0.6*	7 ± 1	0.5 ± 0.1	93.3 ± 0.4
H252A	4.0 ± 1.1	7 ± 1	0.6 ± 0.1	93.2 ± 0.3
H252H	2.6 ± 0.6	8 ± 1	0.5 ± 0.1	92.4 ± 0.7
H252Q	6.1 ± 0.6	6 ± 1	0.5 ± 0.1	94.3 ± 0.6
S264A	3.2 ± 0.6	25 ± 1	0.4 ± 0.1	75.4 ± 0.7
S264K	3.0 ± 0.6	35 ± 1	1.2 ± 0.1	65.2 ± 0.3
S264T	4.1 ± 0.6	11 ± 1	0.6 ± 0.1	89.1 ± 0.1

*The standard error have been shown for the chlorophyll *a* fluorescence decays from three independent experiments.

4.8 Discussion

4.8.1 R54E* mutant and R54E*:ΔPsb27 strain

The R54E* mutant exhibited impaired photoautotrophic growth (Fig. 4.2) (Table 4.1) as compared to the wild type and the other Psb27 mutants that have been discussed in Chapter 3. The transformation of R54E* mutant with Psb27 deletion plasmid (discussed in Chapter 3; section 3.5.1) failed to restore the ΔPsb27 phenotype,

potentially suggesting the presence of a secondary mutation, responsible for the altered characteristics displayed by the R54E* strain. Therefore, the entire genome of the R54E* strain was sequenced, and a secondary mutation was identified in the *psbA2* copy of the gene encoding D1 protein of the PS II reaction centre (resulting in His252 to Gln substitution) in the original R54E* mutant. A second R54E strain was also created without this mutation which was capable of photoautotrophic growth (data shown in Chapter 3, section 3.6.2).

The R54E* mutant and R54E*:ΔPsb27 strain were capable of evolving oxygen, albeit at reduced rates indicating the presence of mixed population of properly assembled and impaired PS II reaction centres (Fig. 4.3) (Table 4.2). The R54E* mutant displayed a small apparent increase in the PS II level (685 nm and 695 nm) when excited with the 440 nm light (Fig. 4.4 A). In contrast, the R54E*:ΔPsb27 strain displayed a small apparent decrease in the PS II level (685 nm and 695 nm) in comparison to the wild type (Fig. 4.4 A). When excited with 580 nm, the emission levels of phycocyanin (650 nm), allophycocyanin (665 nm) and the ApcE PBS terminal emitter (685 nm) in case of R54E* mutant and R54E*:ΔPsb27 strain were lower in comparison to the wild type potentially suggesting differences in PBS coupling to PS II (Fig. 4.4 B). This could be caused due to the increase in the number of PS II reaction centres coupled to PBS and therefore the R54E* mutant and R54E*:ΔPsb27 strain can more efficiently quench the fluorescence as compared to the wild type.

To further investigate the functional impairment of PS II centres in R54E* mutant and R54E*:ΔPsb27 strain, we examined the effect of a single turnover flash on PS II electron transfer (Fig. 4.7, Table 4.3). In R54E* mutant and R54E*:ΔPsb27 strain, there was an increase in the microsecond component as well as the millisecond component of forward electron transfer, suggesting an altered Q_B site (Fig. 4.7 A, Table 4.3). However, the chlorophyll *a* fluorescence decay in the presence of DCMU was similar to the wild type in the R54E* mutant and R54E*:ΔPsb27 strain (Fig. 4.7 B, Table 4.4) indicating normal back reaction kinetics.

As the R54E* cells showed impaired Q_A to Q_B electron transfer during chlorophyll *a* fluorescence decay measurements, the bicarbonate effect was performed to see if bicarbonate is able to help the R54E* mutant in recovering from the inhibited Q_A to Q_B electron transfer (Fig. 4.8 D, E and F). However, in R54E* cells, bicarbonate addition

was not able to restore the forward electron transfer to the wild-type levels. Also, the addition of formate did not appear to induce any significant additional impact on the chlorophyll *a* fluorescence decay of wild type and R54E* cells (Table 4.5). The chlorophyll *a* fluorescence decay measurements, following multiple turnover actinic flashes of dark-adapted cells in the absence of DCMU, showed delayed microsecond and millisecond component in the R54E* mutant as compared to the wild type (Fig. 4.9) (Table 4.6)

The R54E* cells as compared to the wild-type cells were susceptible to photodamage during oxygen evolution measurements (Fig. 4.10, 4.11 and 4.12). The oxygen evolution rate for the R54E* mutant reduced to 50% of its initial oxygen evolution rate under high-light exposure of 30 min in the presence of DCBQ and DMBQ (Fig. 4.10 and Fig. 4.11). However, from 45 min onwards, the R54E* mutant acclimatised to the high-light conditions and then started recovering like the wild-type cells. However, the activity rapidly decreased during the assay indicating an enhanced sensitivity to photoinactivation. One possible explanation is that the PS II centres might be receiving too much light as a result of an increased antenna to PS II centre ratio. The extent of photodamage in R54E* mutant was lower in case of sodium bicarbonate (Fig. 4.12) as compared to the extent of photodamage in DCBQ and DMBQ.

The effect of light stress on chlorophyll *a* fluorescence decay kinetics were also studied in the presence and absence of DCMU (Fig. 4.13) (Table 4.7 and 4.8). In the presence of high light, the initial fluorescence (F_o) and variable fluorescence (F_v) of the wild type and R54E* cells decreased, thus showing that PS II assembly was perturbed due to high light. However, when the cells were allowed to recover, the F_o and F_v levels started improving (see inset of Fig. 4.16).

4.8.2 D1-His252 and D1-Ser264 strains

The confirmation that a His to Gln substitution at position 252 was responsible for the R54E* phenotype was obtained by constructing point mutants in *psbA2* in *psbA*-deletion strain of *Synechocystis* 6803. The D1-Ser264 mutants were also constructed as D1-H252 and D1-S264 are suggested to play a supportive role in the stabilisation of the Q_B site (Saito *et al.* 2013). The D1 and D2 reaction centre proteins are encoded by small multiple gene families of *psbA* and *psbD* (Golden 1995), whereas in higher

plants, only one copy of the *psbA* is present (Cardona 2015; Cardona *et al.* 2015). The different forms of *psbA* and *psbD* play an important role towards acclimatisation to various stressful conditions (Summerfield *et al.* 2008; Mulo *et al.* 2009; Cardona *et al.* 2015).

Three forms of D1 are present in *Synechocystis* 6803*:* PsbA1 (*slr1181*), PsbA2 (*slr1311*) and PsbA3 (*sll1867*). The PsbA2 and PsbA3 are the dominant forms of D1 protein expressed under normal growth conditions; with *psbA2* making ~80-90% of the transcript while *psbA3* makes up to ~10-20%. Both become overexpressed under high-light conditions, whereas *psbA1* is expressed only under micro-aerobic conditions, and is named D1′ (Summerfield *et al.* 2008; Mulo *et al.* 2009). The D1 protein consists of five transmembrane α helices (named as A to E) with an extended DE-loop between joining helices D and E on the stromal (or cytosolic) side of the membrane and a lumenal loop joining helices C and D (Fig. 4.20).

Mutagenesis studies targeting several conserved residues in the DE loop region have proven to be deleterious towards PS II function (Kless *et al.* 1994). However, mutations in conserved residues of other loop regions of D1 had insignificant effects on the photoautotrophic growth, electron transfer parameters and modification of affinities of PS II inhibitors (Maenpaa *et al.* 1993; Kless *et al.* 1994). Mutations targeting the coordination sphere of Mn_4O_5Ca cluster were, however, found to prevent PS II activity. Recent studies have suggested that the most of the ligands of the manganese cluster (D1-Asp170, D1-Glu189, D1-His332, D1-Glu333, D1-Asp342 and D1-Ala344) and calcium ions are amino acids from the D1 proteins (Debus *et al.* 2000a; Debus *et al.* 2000b; Murray *et al.* 2008). The D1-Asp170 mutant was unable to assemble manganese cluster or evolve oxygen (Nixon and Diner 1992). The D1-Glu189 mutant led to decreased oxidation of water (Chu *et al.* 1995; Clausen *et al.* 2001). The mutation at D1-His332 resulted in lower oxygen-evolution rates (Nixon and Diner 1994; Chu *et al.* 1995). The D1-Glu333 mutant was not able to grow photoautotrophically nor could assemble manganese cluster (Chu *et al.* 1995). Even the D1-Asp342 mutant was not able to grow photoautotrophically (Nixon and Diner 1994; Chu *et al.* 1995).

Figure 4.20 Structure of cyanobacterial D1 protein. Plastoquinone acceptors (Q_A and Q_B) (pink), Mn_4CaO_5 cluster (Mn cluster), bicarbonate ligand (BCT), haem iron (Fe), water molecules (red spheres)

The oxygen evolution rate of the D1-H252Y mutant was the lowest amongst the D1 mutants tested in the presence of DCBQ, DMBQ, and the sodium bicarbonate (Fig. 4.15) (Table 4.11). All the other D1 mutants exhibited lower oxygen-evolving rates in comparison to the wild type and the D1 control strain. The amino acid substitutions at His252 and Ser264 in the D1 protein did have a pronounced effect on the oxygen evolution rates potentially indicating the unhealthy state of the mature PS II core holoenzyme in the mutants due to an impaired PS II acceptor side (Fig. 4.15).

The D1-H252Y, D1-S264A and D1-S264K mutants displayed an increase in PS II fluorescence compared to the wild type during low temperature 77 K fluorescence emission spectroscopy measurements when excited by 440 nm light, potentially indicating defective assembly of PS II complexes (Fig. 4.16 A and B). The D1-H252Y, D1-S264A, and D1-S264K mutants also displayed higher levels of fluorescence emission in the form of a single peak from the PS II fluorescence levels (685 nm and 695 nm) relative to the PS I (725 nm), when excited at 580 nm light (Fig. 4.16 C and D). The D1 control strain showed similar level of fluorescence levels in comparison to the wild type.

The chlorophyll *a* fluorescence induction curves of D1-H252A, D1-H252Q, D1-S264A and D1-S264K cells exhibited an initial rapid rise and elevated J levels in the absence

of DCMU (Fig. 4.17 A and B). The D1-H252Y displayed very lower levels of variable fluorescence in the absence of DCMU. All the D1 mutants exhibited higher levels of variable fluorescence in the presence of DCMU (Fig. 4.17 C and D) except the D1-S264T mutant which exhibited wild-type levels of variable fluorescence. Also, the level of variable fluorescence in case of D1-H252Y was the lowest potentially indicating that a lower number of PS II centres are present in this strain.

The chlorophyll *a* fluorescence decay measurements, following single actinic flashes applied to dark-adapted cells in the absence of DCMU, showed a delayed microsecond component as well as a delayed millisecond component in the D1-H252A, D1-H252Q, D1-S264A, D1-S264K and D1-S264T mutants as compared to the wild type (Fig. 4.19 A and B) (Table 4.12). In the presence of DCMU, the D1-H252A and D1-H252Q mutants exhibited a similar phenotype to that of wild type, whereas the D1-S264A, D1-S264K and D1-S264T mutants displayed faster backward chlorophyll *a* fluorescence decay as compared to the wild type (Fig. 4.19 C and D) (Table 4.13).

The mutation of D1-His252 led to substantial changes in the stability of the PS II complex, inhibited electron transfer from Q_A^- to Q_B potentially suggesting a role of D1-His252 in the stabilisation of the Q_B and Q_B proton transfer. The examination of the primary structure of the D1 polypeptide shows that His252 is a highly conserved residue in the DE loop and is present near the Q_B binding site. Already, different computational modelling as well as simulations studies have hypothesised a role of D1-His252 and D1-Ser264 in modulating the dynamics of plastoquinone binding pocket and plastoquinol-plastoquinone exchange by interacting with each other. The D1-His252K mutant constructed by Diner and co-workers (Diner *et al.* 1991) in *Chlamydomonas reinhardtii* also displayed inhibited electron transfer to Q_B. Lupinkova and co-workers (Lupinkova *et al.* 2002) constructed D1-His252Leu mutant to carry out the studies regarding the involvement of D1-His252 residue of PS II D1 protein in light-induced cross-linking of the polypeptide with the α subunit of cytochrome b_{559}. The D1-His252Leu mutation caused inhibition of the electron transfer between the PS II acceptors Q_A and Q_B and exhibited impaired PS II oxygen-evolving activity. Hence, it can be suggested that the D1-His252 residue might play a pivotal role in electron transfer between the PS II electron acceptors Q_A and Q_B. However, the D1-H252Y mutant seemed to have no PS II centres. One possible reason might be that conversion of D1-His252 to Tyr disturbed the interaction of the D1-His252 completely with its

surrounding environment. Other reason might be that a secondary mutation might have cropped up to cope up with the stress of D1-His252 to Tyr mutation. So, to confirm the real genotype of the D1-H252 mutant, either whole genome sequencing of the strain can be performed, or complementation test can be carried out using a plasmid containing the wild-type gene cop of *psbA2* to revert the D1-His252Tyr mutation to the wild type.

The inhibited forward electron transfer exhibited by D1-Ser264 mutants potentially indicated an altered Q_B binding site. Previous studies related to computer modelling and simulations showed that the D1-Ser264 might play a pivotal role in the stabilisation of Q_B binding site. Furthermore, the relevance of the D1-Ser264 residue has long been evidenced in naturally occurring and genetically modified plants, algae and cyanobacteria presenting a remarkable resistance to different classes of herbicides also (Trebst 1991; Oettmeier 1999). Previous studies carried out on D1-Ser264 mutants were also found to inhibit the electron transfer between Q_A and Q_B (Sundby *et al.* 1993; Srivastava *et al.* 1995). Recently quantum mechanical/molecular mechanical (QM/MM) calculations have also indicated the involvement of the D1-Ser264 in the first protonation of the reduced Q_B (Saito *et al.* 2013). Hence, it looks like D1-His252 and D1-Ser264 both might play a role in the stabilisation of Q_B binding site (Fig. 4.21). The D1-His252 and D1-Ser264 might also participate in the protonation of the Q_B^- semi-quinone during the turnover of the two-electron gate.

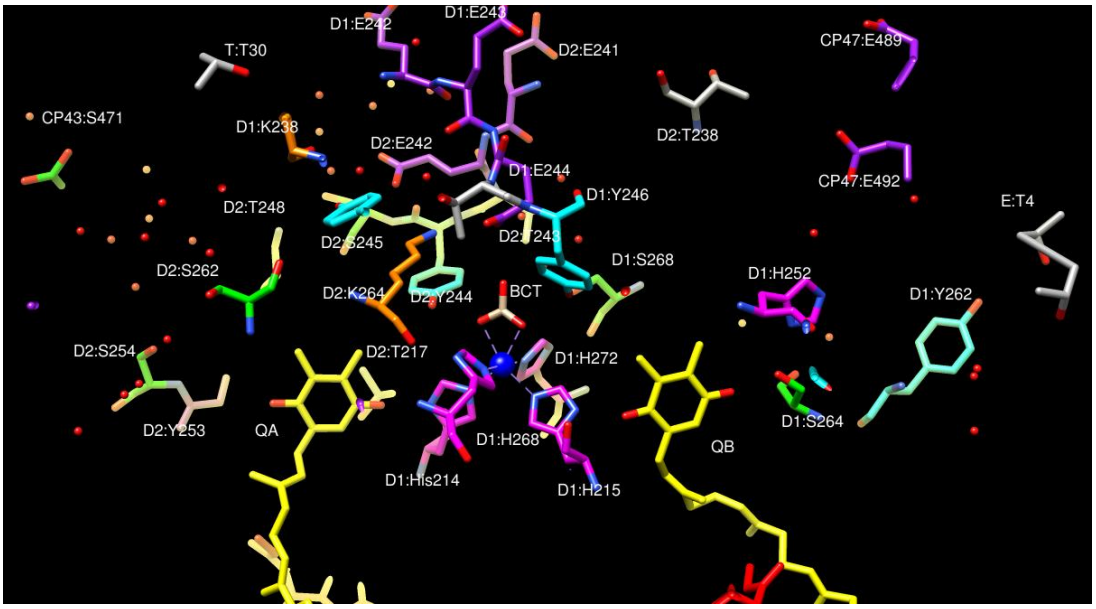

Figure 4.21 Important amino acids network around plastoquinone acceptors (Q_A and Q_B), Haem iron and bicarbonate. The possible flow of protons towards the Q_B molecule. One of the protons may be picked up through D1:H252 and D1:S264 to protonate Q_B^-, while the second one may be transferred through bicarbonate, D1:H272, and D1-H215 to Q_B. Water molecules are shown as red spheres. Figure based on data of Suga and co-workers (Suga *et al.* 2015a).

Recently, studies have been performed by constructing D1-Ser264Lys mutant in *Chlamydomonas reinhardtii* which indicated an important role of D1-Ser264 in coordinating the dynamics of the plastoquinone binding pocket and plastoquinol–plastoquinone exchange via its interaction with D1-His252 residue (Zobnina *et al.* 2017)

Chapter Five

Characterisation of the low-molecular-weight proteins of the CP43 pre-assembly complex

5.1 Introduction

The CP43 pre-assembly complex possesses additional low molecular weight (LMW) proteins: membrane spanning Psb30 (3 kDa), PsbK (4 kDa), PsbZ (9 kDa) and the lumenal-located hydrophilic Psb27 (12 kDa) (Ferreira *et al.* 2004; Komenda *et al.* 2004; Guskov *et al.* 2009). These LMW proteins also help in the stabilisation of CP43 sub-complexes. (Nowaczyk *et al.* 2006; Liu *et al.* 2011a; Liu *et al.* 2011b; Komenda *et al.* 2012a).

The CP43 protein consists of six transmembrane α helices and binds ~13 chlorophyll molecules along with several β-carotene in the cyanobacterial PS II core complex (Umena *et al.* 2011). Typically, four carotenoids are associated with CP43, located at the interfaces between CP43 and the PsbK and PsbZ proteins (Umena *et al.* 2011). As discussed earlier in Chapter 1, the CP43 protein acts as a light-harvesting antenna (Bricker and Frankel 2002), and it also helps in the stabilisation of the Mn_4CaO_5 cluster (Ferreira *et al.* 2004).

5.2 Objective

There are various LMW proteins in the final PS II core complex whose functions are still unknown. The biogenesis of PS II involves the stepwise assembly of the reaction centre sub-complex together with the sequential addition of the two chlorophyll-binding core antenna proteins CP43 and CP47 (Komenda *et al.* 2012a). As Psb27 interacts with the lumenal region of CP43 during biogenesis and the CP43 pre-assembly complex consists of additional transmembrane LMW proteins (Boehm *et al.* 2012b), the study was extended to investigate the role of all the known subunits of the CP43 pre-complex. The additional LMW proteins of the CP43 pre-assembly complex are Psb30, PsbK, and PsbZ and in this chapter single deletions of each of these subunits are investigated along with double mutants for each of these proteins that additionally lack Psb27.

5.3 Construction of mutants

5.3.1 Single deletion mutants (ΔPsb27, ΔPsb30, ΔPsbK, and ΔPsbZ)

5.3.1.1 *psb27* deletion strain

The construction of the ΔPsb27 strain was described in Chapter 3, section 3.5.1.

5.3.1.2 *psb30/ycf12* deletion strain

To construct the ΔPsb30 strain, a plasmid was generated using fusion PCR, in which most of the *psb30* gene was deleted and replaced by a kanamycin-resistance cassette (kanR) (Fig. 5.1). The plasmid was named pΔPsb30-kanR (Fig. 5.1). To construct the ΔPsb30 plasmid, upstream (~927 bps) and downstream (~873 bps) flanking regions of *psb30* were amplified using primers (Chapter 2, Table 2.1). The primers with overhangs complementary to the sequence of a kanamycin-resistance cassette were also used. The kanamycin-resistance cassette was amplified in a separate PCR reaction. The resulting fusion PCR product was ligated into a pJET cloning vector (Promega. Madison, USA) and verified by sequencing. The final cloned PCR product was used to transform wild-type *Synechocystis* cells. The complete segregation of all the strains was confirmed by PCR analysis (Fig. 5.4).

5.3.1.3 *psbK* deletion strain

To construct the ΔPsbK strain, a plasmid was generated using fusion PCR, in which most of the *psbK* gene was deleted and replaced by a kanamycin-resistance cassette (Fig. 5.2). The plasmid was named pΔPsbK-kanR (Fig. 5.2). To construct the ΔPsbK plasmid, upstream (~1001 bps) and downstream (~968 bps) flanking regions of *psbK* were amplified with the primers (Chapter 2, Table 2.1). The kanamycin-resistance cassette was amplified in a separate PCR reaction. The resulting fusion PCR product was ligated into a pJET cloning vector (Promega. Madison, USA) and verified by sequencing. The final cloned PCR product was used to transform wild-type *Synechocystis* cells. The complete segregation of all the strains was confirmed by PCR analysis (Fig. 5.4).

5.3.1.4 *psbZ/ycf9* deletion strain

To construct the ΔPsbZ strain, a plasmid was generated using fusion PCR, in which most of the *psbZ* gene was deleted and replaced by a kanamycin-resistance cassette (Fig. 5.3). The plasmid was named pΔPsbZ-kanR (Fig. 5.3). To construct the ΔPsbZ plasmid, upstream (~1052 bps) and downstream (~877 bps) flanking regions of *psbZ* were amplified with the primers (Chapter 2, Table 2.1). The kanamycin-resistance cassette was amplified in a separate PCR reaction. The resulting fusion PCR product was ligated into a pJET cloning vector (Promega. Madison, USA) and verified by sequencing. The final cloned PCR product was used to transform wild-type *Synechocystis* cells. The complete segregation of all the strains was confirmed by PCR analysis (Fig. 5.4).

5.3.2 Double deletion mutants (ΔPsb27:ΔPsb30, ΔPsb27:ΔPsbK and ΔPsb27:ΔPsbZ)

The ΔPsb30, ΔPsbK and ΔPsbZ mutants were transformed with ΔPsb27 plasmid to make double deletion strains. The complete segregation of all the double deletion strains was confirmed by PCR analysis.

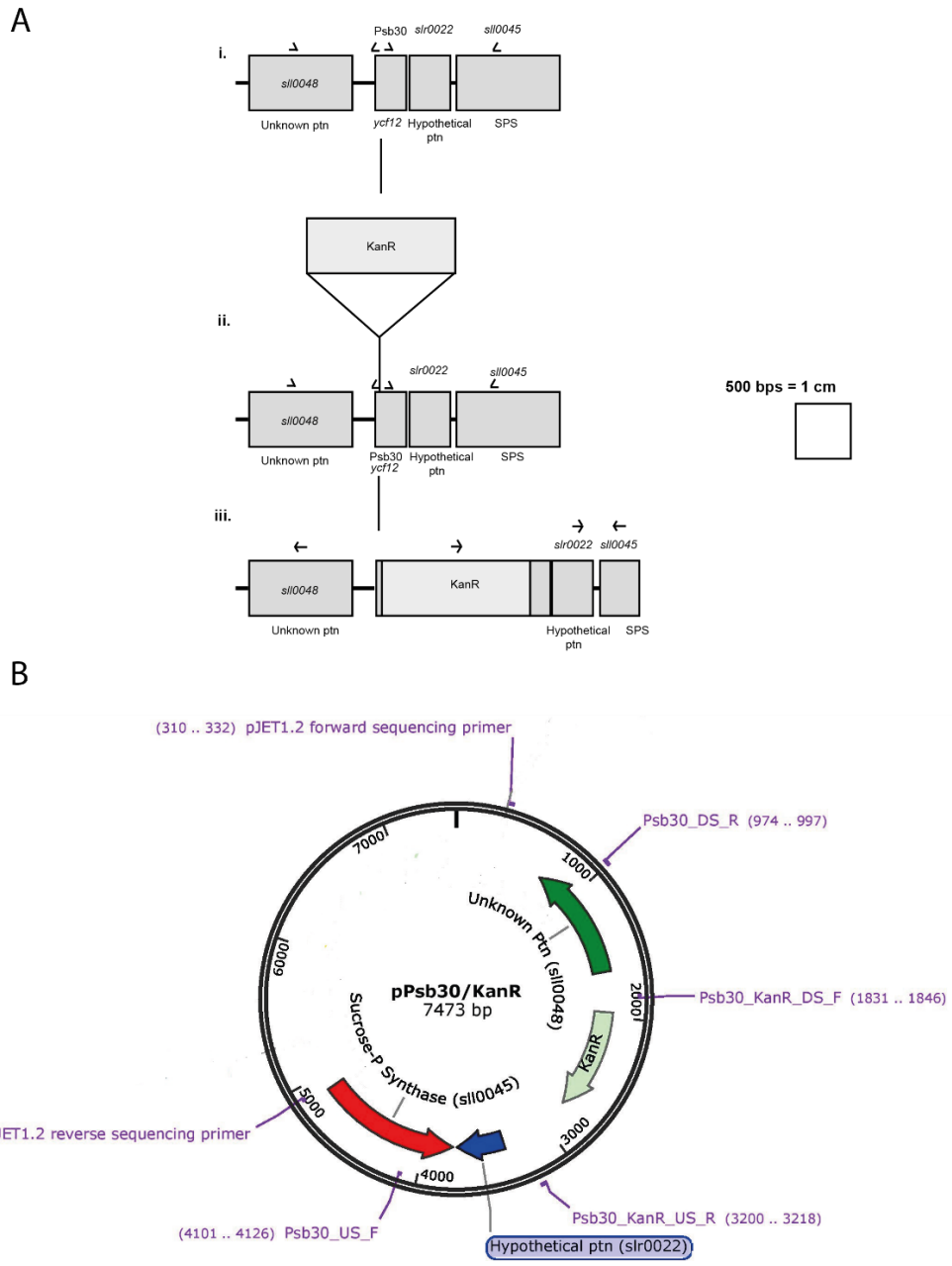

Figure 5.1 Construction of *Synechocystis* 6803 *psb30* deletion strain.(A) Insertion of a ~1.2 kb kanamycin-resistance cassette between the left flanking region and right flanking region of *psb30*. One cm corresponds to 500 bp. **(B)** Plasmid map of pΔPsb30 kanamycin plasmid. This plasmid was used for transforming wild-type *Synechocystis* 6803 to produce the ΔPsb30 strain. The mutant was grown and segregated on kanamycin-containing selective media.

A

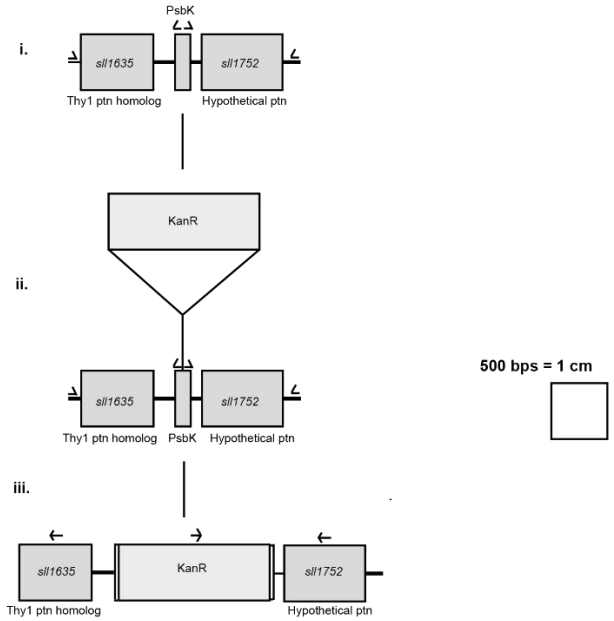

B

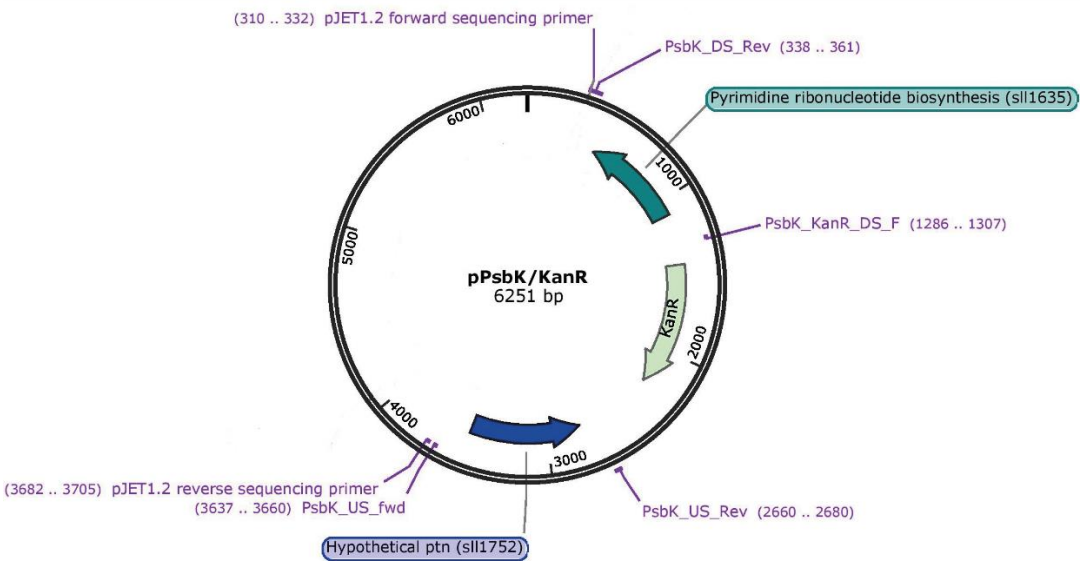

Figure 5.2 Construction of *Synechocystis* 6803 *psbK* deletion strain.(A) Insertion of a ~1.2 kb kanamycin-resistance cassette between the left flanking region and right flanking region of *psbK*. One cm corresponds to 500 bp **(B)** Plasmid map of pΔPsbK kanamycin plasmid. This plasmid was used for transforming wild-type *Synechocystis* 6803 to produce the ΔPsbK strain. The mutant was grown and segregated on kanamycin-containing selective media.

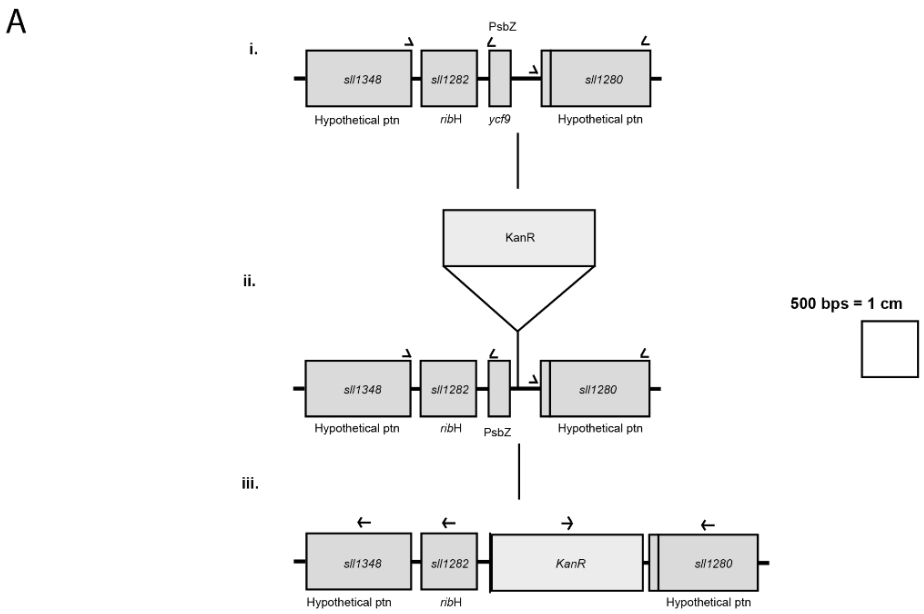

B

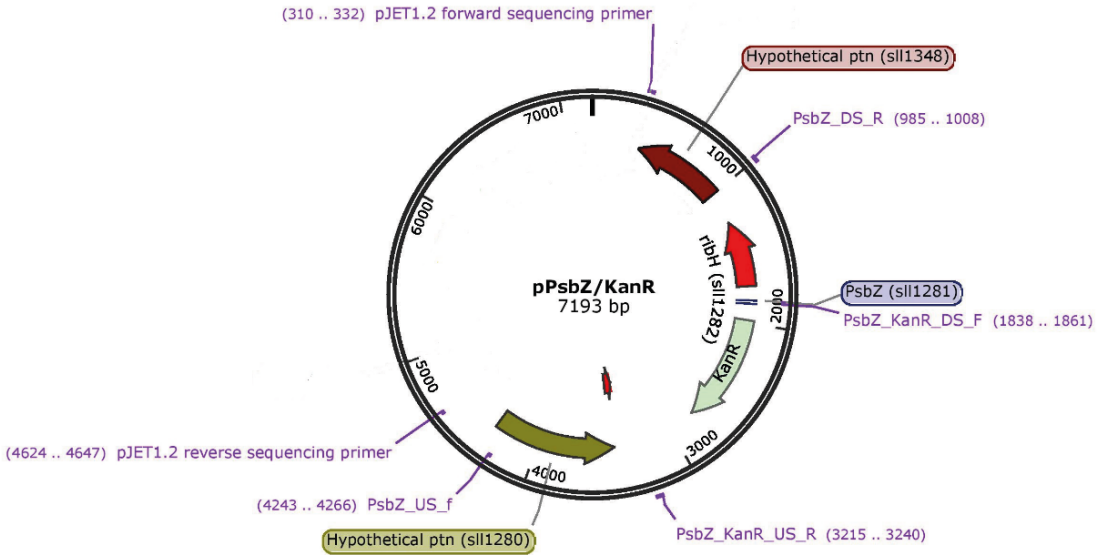

Figure 5.3 Construction of *Synechocystis* 6803 *psbZ* deletion strain.(A) Insertion of a ~1.2 kb kanamycin-resistance cassette between the left flanking region and right flanking region of *psbZ*. One cm corresponds to 500 bp **(B)** Plasmid map of pΔPsbZ kanamycin plasmid. This plasmid was used for transforming wild-type *Synechocystis* 6803 to produce the ΔPsbZ strain. The mutant strain was grown and segregated on kanamycin-containing selective media.

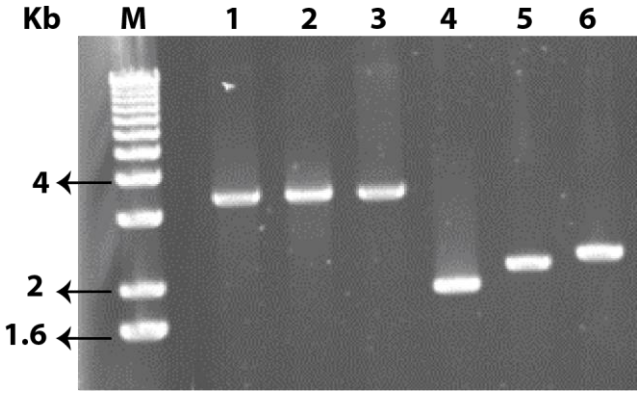

Figure 5.4 Colony PCR of the ΔPsb30, ΔPsbK and ΔPsbZ strains. Confirmation of the complete segregation of ΔPsb30, ΔPsbK, and ΔPsbZ cells with the help of the colony PCR. Lane M is the 1 Kb Plus DNA Ladder (Invitrogen, CA), the other lanes contain PCR products corresponding to the segregated mutants. The lanes are: 1, ΔPsb30; 2, ΔPsbK; 3, ΔPsbZ; 4, wild type (Psb30); 5, wild type (PsbK); 6, wild type (PsbZ).

5.4 Characterisation of the single and double deletion strains

Once complete segregation of the targeted mutants was confirmed by sequencing, the phenotypic characterisation of the cells was carried out.

5.4.1 Photoautotrophic growth

To investigate the impact of deletion of the *psb27*, *psb30*, *psbK*, and *psbZ* single mutants and double deletion mutants, photoautotrophic growth curves were initially performed (Fig. 5.5). Fig. 5.5 shows the photoautotrophic growth characteristics of the wild type, ΔPsb27, ΔPsb30, ΔPsbK, ΔPsbZ, ΔPsb27:ΔPsb30, ΔPsb27:ΔPsbK and ΔPsb27:ΔPsbZ mutants over a period of 168 h. The average doubling time of each strain has been listed in Table 5.1. The doubling time of wild type was around ~13.1 ± 0.6 h, whereas the doubling time of ΔPsbK was ~29.1 ± 2.4 h. Interestingly, in the ΔPsb27:ΔPsbK strain, the doubling time can be seen reducing from ~29.1 ± 2.4 h to ~21.1 ± 2.1 h. The increase in the doubling time shows that, in ΔPsbK strain, the PS II assembly is more impaired as compared to the ΔPsb27:ΔPsbK strain. The doubling time of ΔPsbZ was also higher (~19.2 ± 0.9 h) as compared to ΔPsb27:ΔPsbZ (~16.2 ± 1.0 h) strain. The ΔPsb27, ΔPsb30, and ΔPsb27:ΔPsb30 strains could grow photoautotrophically similar to the wild type. The single deletion of *psbK* and *psbZ* is more deleterious as compared to the corresponding double deletion strains (ΔPsb27:ΔPsbK and ΔPsb27:ΔPsbZ).

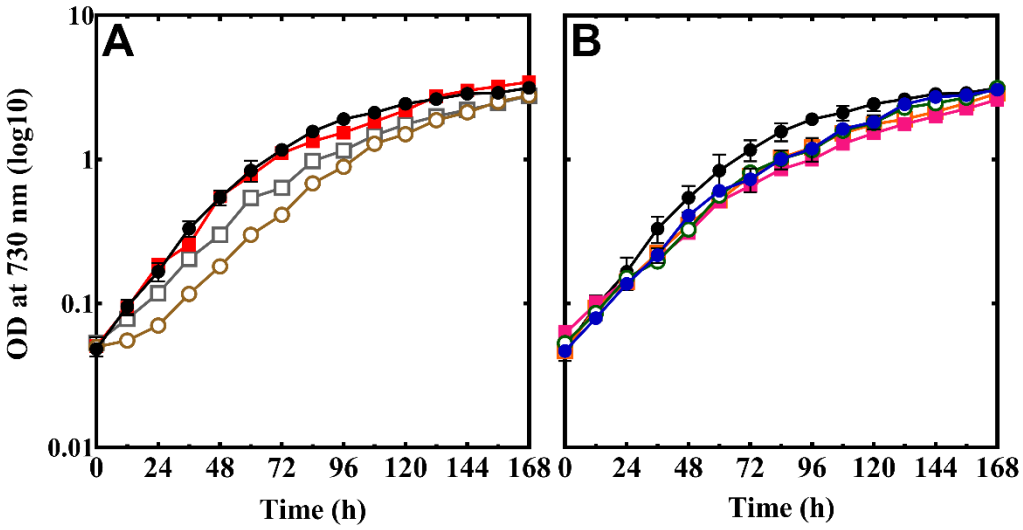

Figure 5.5 Photoautotrophic growth of the wild type and the LMW protein deletion strains. The photoautotrophic growth of *Synechocystis* 6803 and the LMW protein deletion strains in BG-11 media as measured by optical density at 730 nm. The strains shown in panel **(A)** are wild type (black, close circles), ΔPsb30 (brown, open circles), ΔPsbK (red, close squares) and ΔPsbZ (grey, open squares) and the strains shown in panel **(B)** are wild type (black, close circles), ΔPsb27 (blue, close circles), ΔPsb27:ΔPsb30 (green, open circles), ΔPsb27:ΔPsbK (pink, close squares) and ΔPsb27:ΔPsbZ (orange, open squares). Data shown are the average of three independent experiments. The standard error bars have also been shown.

Table 5.1 Photoautotrophic growth of the wild type and the LMW protein deletion strains. The doubling time of the wild type, ΔPsb27, ΔPsb30, ΔPsbK, ΔPsbZ, ΔPsb27:ΔPsb30, ΔPsb27:ΔPsbK and ΔPsb27:ΔPsbZ strains grown photoautotrophically.

Strain	Doubling time[1] (h)
WT	13.1 ± 0.6[2]
ΔPsb30	15.3 ± 0.9
ΔPsbK	29.1 ± 2.4
ΔPsbZ	19.2 ± 0.8
ΔPsb27	16.4 ± 0.4
ΔPsb27:ΔPsb30	19.2 ± 0.9
ΔPsb27:ΔPsbK	21.1 ± 2.1
ΔPsb27:ΔPsbZ	16.2 ± 1.0

[1]The data shown are the mean doubling times over the first 36 h of the growth. Data shown are the average of three independent experiments.
[2]The standard error have been shown.

5.4.2 PS II-specific oxygen evolution assay

Oxygen evolution assays were carried out for the wild type, ΔPsb27, ΔPsb30, ΔPsbK, ΔPsbZ, ΔPsb27:ΔPsb30, ΔPsb27:ΔPsbK and ΔPsb27:ΔPsbZ strains to assess the impact of the deletion of the genes on the capacity of PS II to support electron transfer between water and the added electron acceptor.

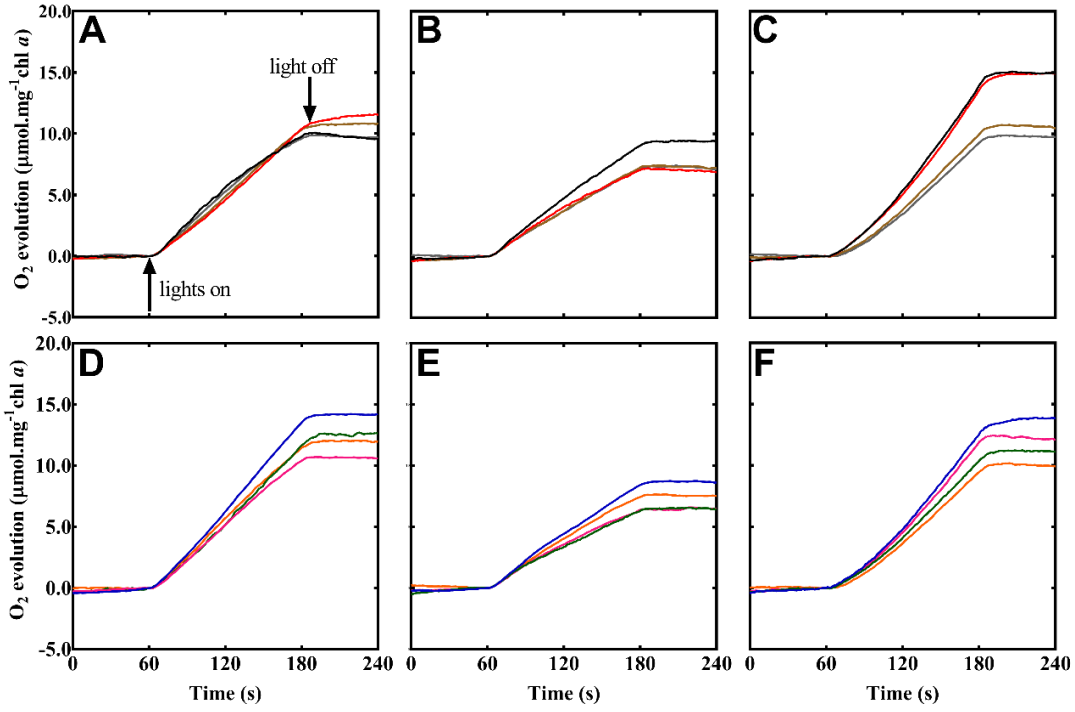

Figure 5.6 Oxygen evolution assay traces for the LMW protein single and double deletion strains using different electron acceptors.(A) Oxygen evolution measured in the presence of DCBQ **(B)** Oxygen evolution measured in the presence of DMBQ. **(C)** Oxygen evolution measured in the presence of sodium bicarbonate. The strains shown in panels **(A)**, **(B)** and **(C)** are wild type (black), ΔPsb30 (red), ΔPsbK (brown) and ΔPsbZ (grey) and strains shown in panels **(D)**, **(E)** and **(F)** are ΔPsb27 (blue), ΔPsb27:ΔPsb30 (green), ΔPsb27:ΔPsbK (pink) and ΔPsb27:ΔPsbZ (orange). Data shown are the average of three independent experiments. The average values of oxygen evolution rates have been shown in Table 5.2.

Fig. 5.6 shows the oxygen evolution traces obtained using the different PS-II specific acceptors: DCBQ (A), DMBQ (B) and the sodium bicarbonate (C). The average oxygen evolution rates for each mutant strain has been presented in Table 5.2.

Table 5.2 Oxygen evolution rates of LMW protein single and double deletion strains.

Strains	Oxygen evolution[1] (µmol O_2 (mg of chl)$^{-1}$ h^{-1})		
	DCBQ	**DMBQ**	**Bicarbonate**
WT	420 ± 30[2]	310 ± 20	420 ± 10
ΔPsb27	350 ± 20	280 ± 20	380 ± 10
ΔPsb30	350 ± 10	250 ± 20	400 ± 30
ΔPsbK	300 ± 10	230 ± 20	340 ± 10
ΔPsbZ	360 ± 20	280 ± 20	320 ± 10
ΔPsb27: ΔPsb30	330 ± 20	280 ± 30	340 ± 10
ΔPsb27: ΔPsbK	330 ± 40	280 ± 20	390 ± 20
ΔPsb27: ΔPsbZ	320 ± 20	270 ± 20	330 ± 20

[1]Oxygen evolution rates were measured in the presence of DCBQ, DMBQ and sodium bicarbonate. Data shown are average of three independent experiments.
[2]The standard error have been shown.

The wild type had an oxygen evolution rate of around 420 ± 30 µmol O_2 (mg of chl)$^{-1}$ h^{-1} in the presence of DCBQ, 310 ± 20 µmol O_2 (mg of chl)$^{-1}$ h^{-1} in the presence of DMBQ and 420 ± 10 µmol O_2 (mg of chl)$^{-1}$ h^{-1} in the presence of sodium bicarbonate. The ΔPsbK had lower oxygen evolution rate of 300 ± 10 µmol O_2 (mg of chl)$^{-1}$ h^{-1} with DCBQ and 230 ± 20 µmol O_2 (mg of chl)$^{-1}$ h^{-1} with DMBQ as compared to the wild type. The oxygen evolution rates of ΔPsb27:ΔPsbK was higher as compared to the ΔPsbK strain in the presence of DCBQ, DMBQ, and the sodium bicarbonate. The ΔPsb30, ΔPsbZ, ΔPsb27:ΔPsb30 and ΔPsb27:ΔPsbZ deletion strains had similar rates of oxygen evolution as compared to the wild type.

5.4.3 Low-temperature 77 K fluorescence emission spectroscopy

To study the effect of deletion of LMW proteins of CP43 pre-assembly complex on the levels or the stoichiometry of the PS I and PS II complexes, low temperature 77 K fluorescence emission spectroscopy measurements were performed. The ΔPsb30, ΔPsbK, ΔPsbZ, ΔPsb27, and ΔPsb27:ΔPsb30 mutants (Fig. 5.7 A and B), when excited at 440 nm displayed typical 725 nm emission, originating from PS I, and the 685 and 695 nm emissions originating from CP43 and CP47, respectively, of PS II. The ΔPsb27:ΔPsbK and ΔPsb27:ΔPsbZ mutants exhibited a small apparent increase in PS II specific fluorescence relative to their PS I emission compared to the wild type.

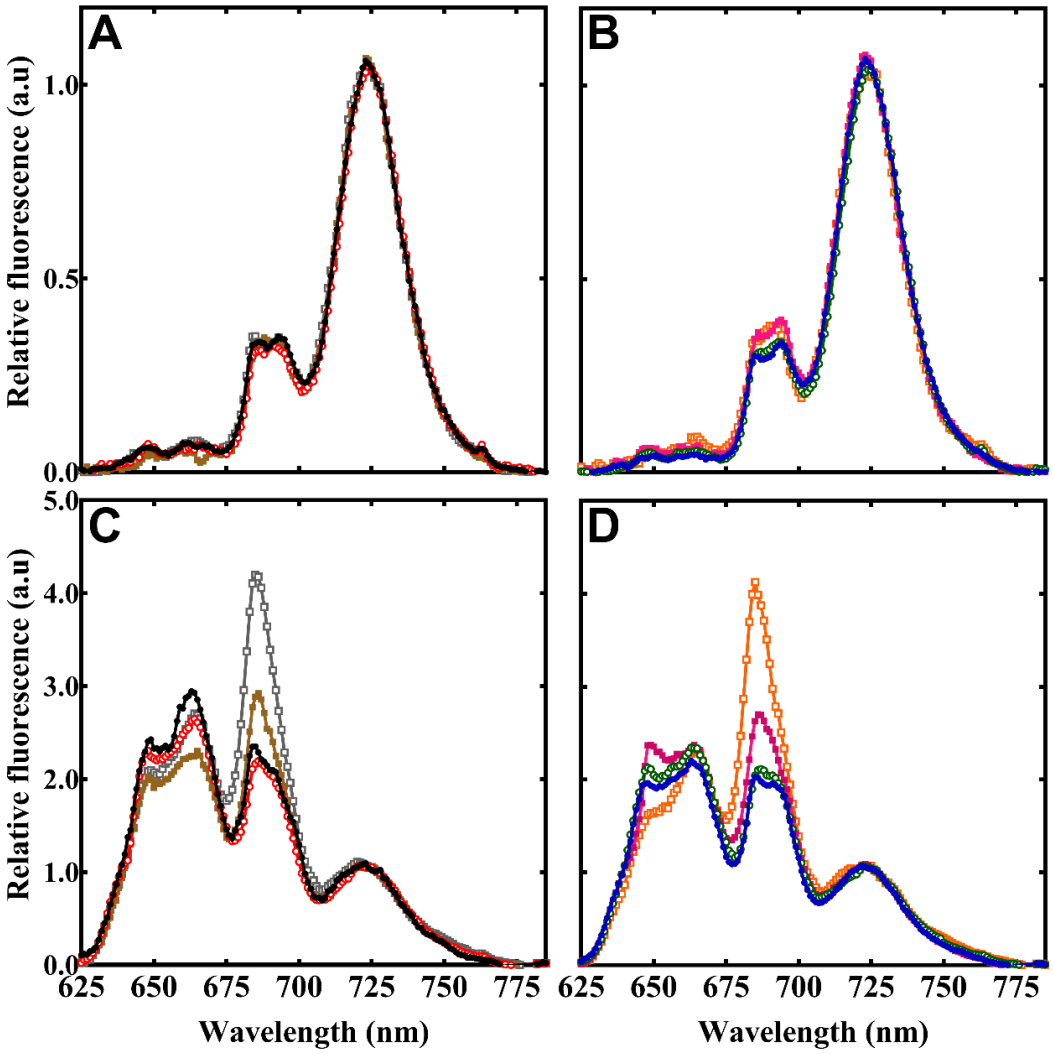

Figure 5.7 Low-temperature fluorescence emission spectra of wild type and the LMW protein deletion strains. Panels **(A)** and **(B)** contains the fluorescence emission spectra with an excitation wavelength of 440 nm. Panels **(C)** and **(D)** contains the fluorescence emission spectra with an excitation wavelength of 580 nm. The strains shown in panels **(A)** and **(C)** are wild type (black, close circles), ΔPsb30 (red, open circles), ΔPsbK (brown, close squares) and ΔPsbZ (grey, open squares) and the strains shown in panels **(B)** and **(D)** are ΔPsb27 (blue, close circles), ΔPsb27:ΔPsb30 (green, open circles), ΔPsb27:ΔPsbK (pink, close squares) and ΔPsb27:ΔPsbZ (orange, open squares). Data shown are the average of three independent experiments.

To get insight into the coupling and energy transfer between the PBS and PS II (and possibly PS I), cells were illuminated with a 580 nm light (Fig. 5.7 C and D). All strains displayed the typical 725 nm emission originating from PS I; however ΔPsb27, ΔPsbK ΔPsb27:ΔPsb30, ΔPsb27:ΔPsbK, and ΔPsb27:ΔPsbZ mutants exhibited lower levels of fluorescence emission from phycocyanin (650 nm), allophycocyanin (665 nm) and the ApcE PBS terminal emitter (685 nm), respectively when compared to the wild

type. Also, a shoulder was visible at 695 nm for the ΔPsb27, ΔPsb30, and ΔPsb27:ΔPsb30 strains potentially suggesting the emission may contain contributions from both the CP43 and CP47 core antennae of PS II as well as the ApcE terminal emitter of the PBS (Joshua and Mullineaux 2004). In addition, ΔPsbK, ΔPsbZ, ΔPsb27:ΔPsbK and ΔPsb27:ΔPsbZ cells exhibited a higher and merged peak at 680 nm.

5.4.4 Chlorophyll *a* fluorescence induction

The ΔPsb30, ΔPsbK and ΔPsbZ strains exhibited a higher J level as compared to the wild-type strain (see inset of Fig. 5.8 A) and had a lower P level (Fig. 5.8 A). The ΔPsb30, ΔPsbK and ΔPsbZ strains also displayed a modified IP rise in comparison to the wild type (see inset of Fig. 5.8 A), with ΔPsbZ displaying a broader IP peak as well as early IP rise as compared to the wild type.

The ΔPsb27:ΔPsb30, ΔPsb27:ΔPsbK and ΔPsb27:ΔPsbZ strains also exhibited a higher J level as compared to the wild type (see inset of Fig. 5.8 C) and had a lower P level (Fig. 5.8 C). Nevertheless, the relative kinetics for all strain were similar to the wild type except for the early P peak in the ΔPsb27, ΔPsb27:ΔPsbK and ΔPsb27:ΔPsbZ strains (see insets in Fig. 5.8 C).

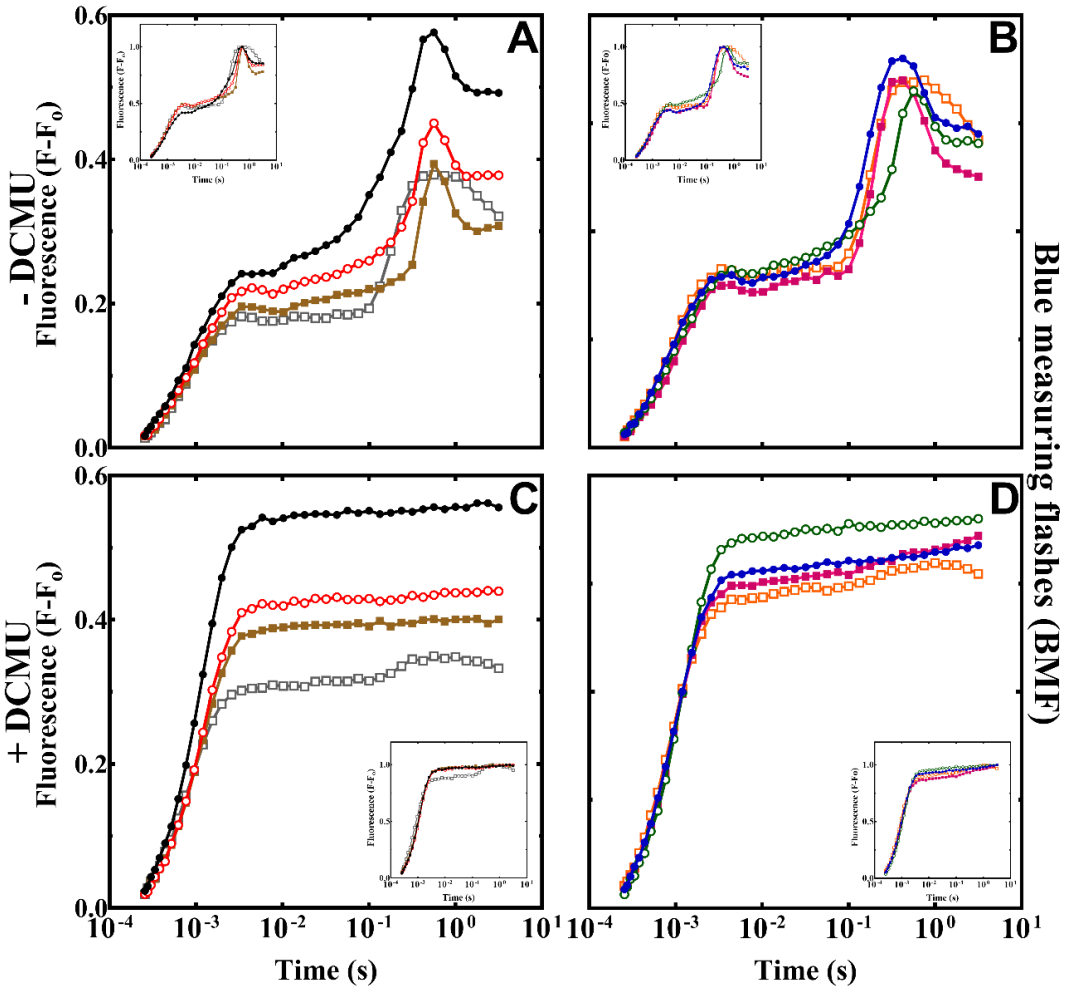

Figure 5.8 Steady-state chlorophyll *a* fluorescence induction in wild type and the LMW deletion strains. Panels **(A)** and **(B)** contains the measurements in the absence of DCMU and panels **(C)** and **(D)** contains the measurements in the presence of DCMU. The strains shown in panels **(A)** and **(C)** are wild type (black, close circles), ΔPsb30 (red, open circles), ΔPsbK (brown, close squares) and ΔPsbZ (grey, open squares) and the strains shown in panels **(B)** and **(D)** are ΔPsb27 (blue, close circles), ΔPsb27:ΔPsb30 (green, open circles), ΔPsb27:ΔPsbK (pink, close squares) and ΔPsb27:ΔPsbZ (orange, open squares). The data normalised to the F_m value of each strain has been shown in the insets. Data represented are the average of at least four independent experiments.

The induction measurements were also carried in the presence of the PS II-specific inhibitor DCMU that blocks the electron transport between the Q_A and Q_B sites in the PS II reaction centre complex. In the presence of DCMU the maximum $F-F_o$ fluorescence signal is proportional to the number of active PS II centres. The data obtained in the presence of DCMU indicated that there were less assembled PS II centres in all the single and double deletion strains (Fig. 5.8 C and D). The ΔPsbZ, ΔPsb27:ΔPsbK and ΔPsb27:ΔPsbZ strains had modified kinetics compared to wild type

with the maximum fluorescence level being reached following the initial rise in the signal (see inset of Fig. 5.8 C and D). This difference in the induction curve between the ΔPsbZ, ΔPsb27:ΔPsbK, ΔPsb27:ΔPsbZ strains and the wild type, might arise from changes in absorption cross-section from the movement of the PBS antennae, or a decrease in fluorescence quenching due to reduction of the PQ pool in the different strains.

To further investigate the differences in the IP rise and P peak of the various LMW protein deletion mutants, the duration of the chlorophyll *a* fluorescence induction assay was increased to ~500 s in the presence and absence of DCMU (Fig. 5.9). The ΔPsb30 and ΔPsbZ mutants exhibited similar levels of variable fluorescence except the IP rise was modified and SM rise was higher in case of ΔPsb30 cells in comparison to the wild-type strain (Fig. 5.9 A and inset of Fig. 5.9 A). On the other hand, ΔPsbK cells exhibited a lower level of the IP rise while the SM rise was also early and higher as compared to the wild type (Fig. 5.9 A and inset of Fig. 5.9 A).

The ΔPsb27:ΔPsb30 and ΔPsb27:ΔPsbK mutants exhibited similar levels of variable fluorescence (Fig. 5.9 B). The ΔPsb27 and ΔPsb27:ΔPsbK strains displayed an early SM rise and higher levels of variable fluorescence (Fig. 5.9 B and see inset of Fig. 5.9 B). Also, the IP peak was modified in the case of ΔPsb27:ΔPsbK and ΔPsb27:ΔPsbZ mutants when compared to the wild type (Fig. 5.9 B).

Long term fluorescence induction was also carried out in the presence of DCMU (Fig. 5.9 C and D). The ΔPsb30, ΔPsbK and ΔPsbZ mutants exhibited lower variable fluorescence in the presence of DCMU indicating that lower number of assembled PS II centres was present in these mutants (Fig. 5.9 C).

The ΔPsb27 and ΔPsb27:ΔPsb30 mutants displayed similar wild-type levels of variable fluorescence in the presence of DCMU. However, the ΔPsb27:ΔPsbK, and ΔPsb27:ΔPsbZ mutants exhibited lower levels of variable fluorescence in the presence of DCMU which is in agreement with the results obtained in the absence of DCMU (Fig. 5.9 D).

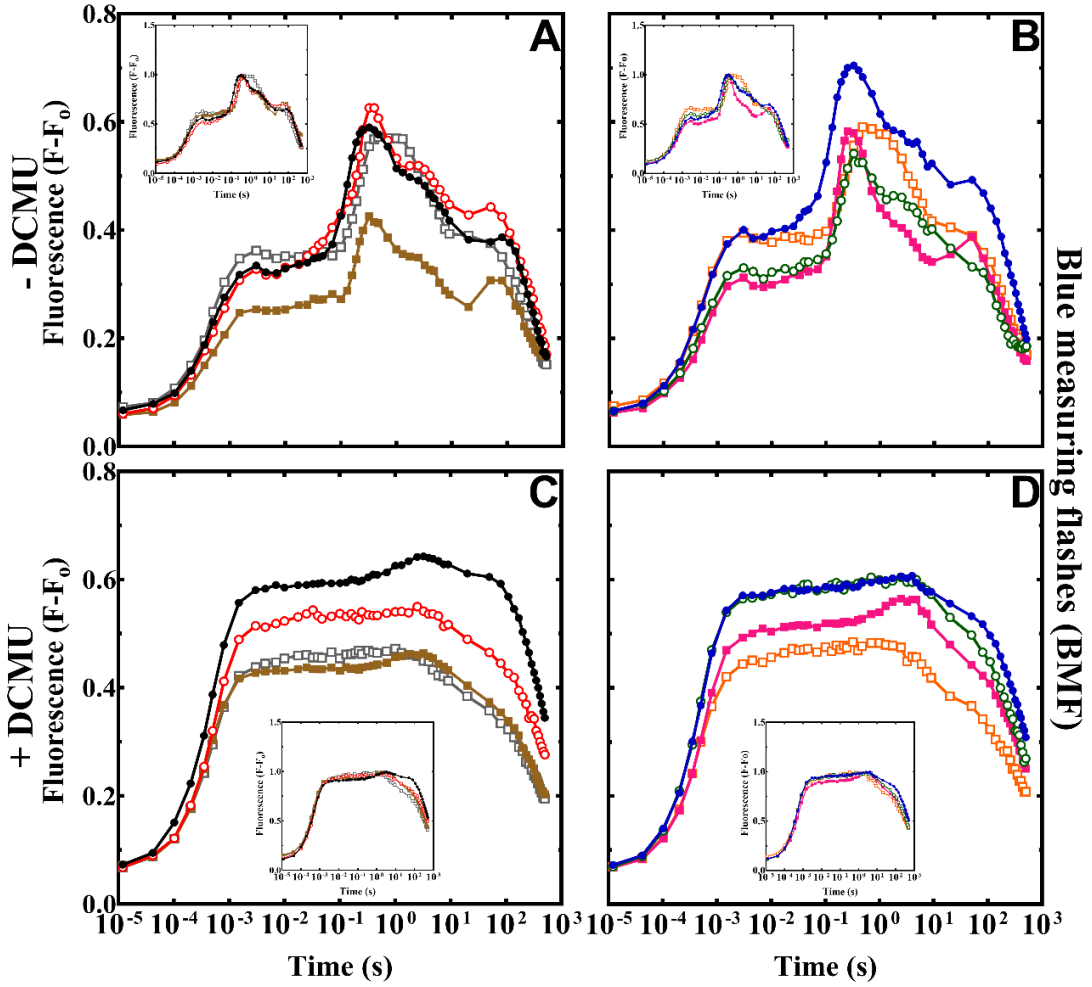

Figure 5.9 Steady-state long-term chlorophyll *a* fluorescence induction (500 s) in wild type and the LMW deletion strains. Panels **(A)** and **(B)** contains the measurements in the absence of DCMU and panels **(C)** and **(D)** contains the measurements in the presence of DCMU. The strains shown in panels **(A)** and **(C)** are wild type (black, close circles), ΔPsb30 (red, open circles), ΔPsbK (brown, close squares) and ΔPsbZ (grey, open squares) and the strains shown in panels **(B)** and **(D)** are ΔPsb27 (blue, close circles), ΔPsb27:ΔPsb30 (green, open circles), ΔPsb27:ΔPsbK (pink, close squares) and ΔPsb27:ΔPsbZ (orange, open squares). The data normalised to the F_m value of each strain has been shown in the insets. Data represented are the average of at least four independent experiments.

5.4.4.1 Chlorophyll *a* fluorescence decay following single actinic flash

The decay kinetics of chlorophyll *a* fluorescence following single saturating actinic flash were also investigated and compared between wild type and the LMW protein deletion strains (Fig. 5.10).

The ΔPsb27, ΔPsb30, ΔPsb27:ΔPsb30 and ΔPsb27:ΔPsbK mutants exhibited similar rates of chlorophyll fluorescence decay to the wild-type strain (Fig. 5.10 A and B), but

the decays for the ΔPsbK, ΔPsbZ, and ΔPsb27:ΔPsbZ mutants exhibited slower forward electron transfer kinetics in comparison to the wild type. Upon analysis, the half-time of the microsecond component of the chlorophyll fluorescence decay in the ΔPsbK, ΔPsbZ, and ΔPsb27:ΔPsbZ mutants was slower than the half-time of the microsecond component of the wild type (Table 5.3). However, the half-time of the microsecond component of ΔPsb27:ΔPsbK mutant was faster than the half-time of the microsecond component of the wild type, but in all cases the changes were small, and the amplitudes were also comparable (Table 5.3). The half-time of the slow component of chlorophyll *a* fluorescence decay, without any addition for most of the LMW protein deletion mutants (ΔPsb27, ΔPsbK, ΔPsbZ, ΔPsb27:ΔPsb30, ΔPsb27:ΔPsbK and ΔPsb27:ΔPsbZ) was faster (~2-3 fold) as compared to the wild type. In addition, the half-time of the slow component without any addition for ΔPsb30 was similar to the wild type.

The chlorophyll *a* fluorescence decay studies were also carried out in the presence of DCMU (Fig. 5.10 C and D). The ΔPsb27, ΔPsb30, ΔPsbK, and ΔPsb27:ΔPsb30 mutants exhibited similar chlorophyll *a* fluorescence decay in the presence of DCMU (Fig. 5.10 C and D) except ΔPsbZ, ΔPsb27:ΔPsbK and ΔPsb27:ΔPsbZ strains. The half-time of the microsecond component of ΔPsb27, ΔPsb30, ΔPsbK, ΔPsbZ, and ΔPsb27:ΔPsbZ mutants was faster than the wild type (Table 5.4). The amplitude of the microsecond component of all the LMW protein deletion strains was greater than the amplitude of the microsecond component of the wild type except for the ΔPsb30 strain. The ΔPsb27, ΔPsbK, ΔPsbZ, ΔPsb27:ΔPsbK and ΔPsb27: ΔPsbZ mutants exhibited a smaller microsecond component amplitude as compared to the wild type. Overall, the LMW protein deletion mutants displayed similar back charge recombinant kinetics. However, the increase in the amplitude of the fast component of the strains was compensated by the decrease in the amplitude of the slow component of the strain as compared to the wild type.

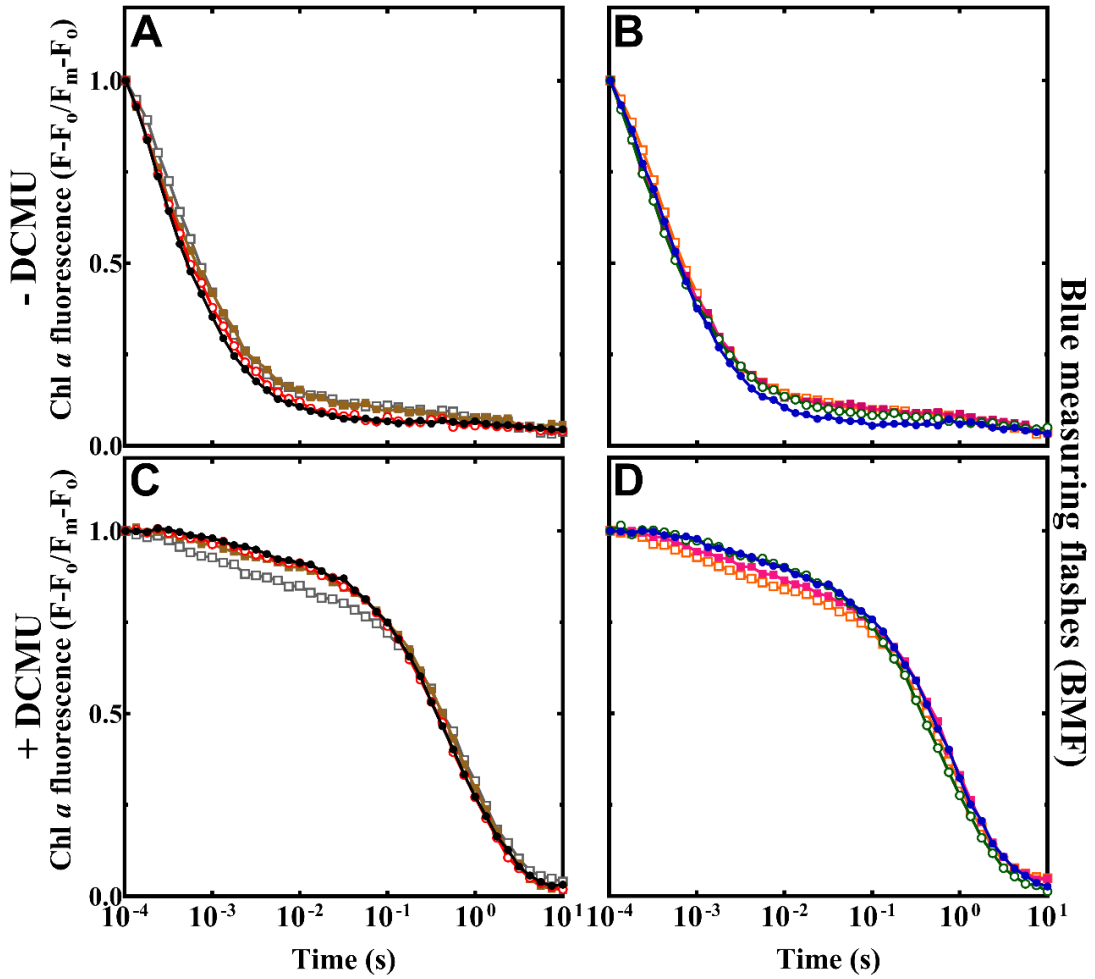

Figure 5.10 Relaxation of chlorophyll *a* fluorescence following single flash in the wild type and the LMW protein deletion strains.Panels **(A)** and **(B)** contains the measurements in the absence of DCMU. Panels **(C)** and **(D)** contains the measurements in the presence of DCMU. The strains shown in panels **(A)** and **(C)** are wild type (black, close circles), ΔPsb30 (red, open circles), ΔPsbK (brown, close squares) and ΔPsbZ (grey, open squares) and the strains shown in panels **(B)** and **(D**) are ΔPsb27 (blue, close circles), ΔPsb27:ΔPsb30 (green, open circles), ΔPsb27:ΔPsbK (pink, close squares) and ΔPsb27:ΔPsbZ (orange, open squares). Data represented are the average of at least three independent experiments.

Table 5.3 Decay kinetics of variable chlorophyll *a* fluorescence following single saturating actinic flash in the absence of DCMU.

Strains	Fast		Intermediate		Slow	
	$T_{1/2}$ (µs)	Amp.	$T_{1/2}$ (ms)	Amp.	$T_{1/2}$ (s)	Amp.
WT	260 ± 10*	59 ± 2	2.7 ± 0.2	33 ± 2	7.5 ± 2.1	8.4 ± 0.9
ΔPsb27	290 ± 10	60 ± 1	3.8 ± 0.1	29 ± 1	3.0 ± 0.5	11.3 ± 0.6
ΔPsb30	280 ± 10	56 ± 1	3.1 ± 0.1	35 ± 1	6.9 ± 1.3	9.4 ± 2.3
ΔPsbK	310 ± 50	55 ± 2	3.5 ± 0.4	33 ± 1	4.8 ± 1.1	10.2 ± 0.3
ΔPsbZ	370 ± 20	56 ± 2	3.0 ± 0.3	32 ± 2	2.3 ± 0.1	12.2 ± 0.4
ΔPsb27: ΔPsb30	260 ± 20	54 ± 3	3.2 ± 0.2	35 ± 1	4.0 ± 1.4	11.4 ± 1.5
ΔPsb27: ΔPsbK	250 ± 10	50 ± 1	2.5 ± 0.1	39 ± 1	4.1 ± 0.2	11.1 ± 0.1
ΔPsb27: ΔPsbZ	400 ± 20	61 ± 2	3.6 ± 0.3	28 ± 2	2.7 ± 0.3	11.1 ± 0.2

*The standard error have been shown for the chlorophyll *a* fluorescence decays from three independent experiments.

Table 5.4 Decay kinetics of variable chlorophyll *a* fluorescence following single saturating actinic flash in the presence of DCMU.

Strains	Fast		Slow	
	$T_{1/2}$ (ms)	Amp.	$T_{1/2}$ (s)	Amp.
WT	2.5 ± 0.2*	7 ± 1	0.4 ± 0.1	93.3 ± 0.6
ΔPsb27	1.6 ± 0.1	11 ± 1	0.4 ± 0.1	89.1 ± 0.1
ΔPsb30	1.8 ± 0.1	8 ± 1	0.4 ± 0.1	92.4 ± 1.0
ΔPsbK	1.9 ± 0.4	10 ± 2	0.5 ± 0.1	90.4 ± 1.5
ΔPsbZ	1.5 ± 0.1	14 ± 1	0.5 ± 0.1	86.4 ± 0.9
ΔPsb27: ΔPsb30	2.1 ± 0.2	10 ± 2	0.4 ± 0.1	90.3 ± 1.3
ΔPsb27: ΔPsbK	2.2 ± 0.2	13 ± 1	0.6 ± 0.1	87.3 ± 1.0
ΔPsb27: ΔPsbZ	1.5 ± 0.1	14 ± 1	0.5 ± 0.1	86.4 ± 1.0

*The standard error have been shown for the chlorophyll *a* fluorescence decays from three independent experiments. .

5.4.5 Photoinhibition and recovery assays

5.4.5.1 Oxygen evolution assay

The susceptibility of PS II to light-induced damage and its recovery was also studied by measuring oxygen evolving activity (Fig. 5.11 and 5.12). The cells were exposed to 45 min of high light treatment (2000 ± 100 µE $m^{-2}s^{-1}$) and allowed to recover under low-light conditions (35 µE $m^{-2}s^{-1}$) for 135 min. The oxygen evolution rates were measured every 15 min in the presence of different quinone acceptors: DCBQ and DMBQ. Sodium bicarbonate was also used.

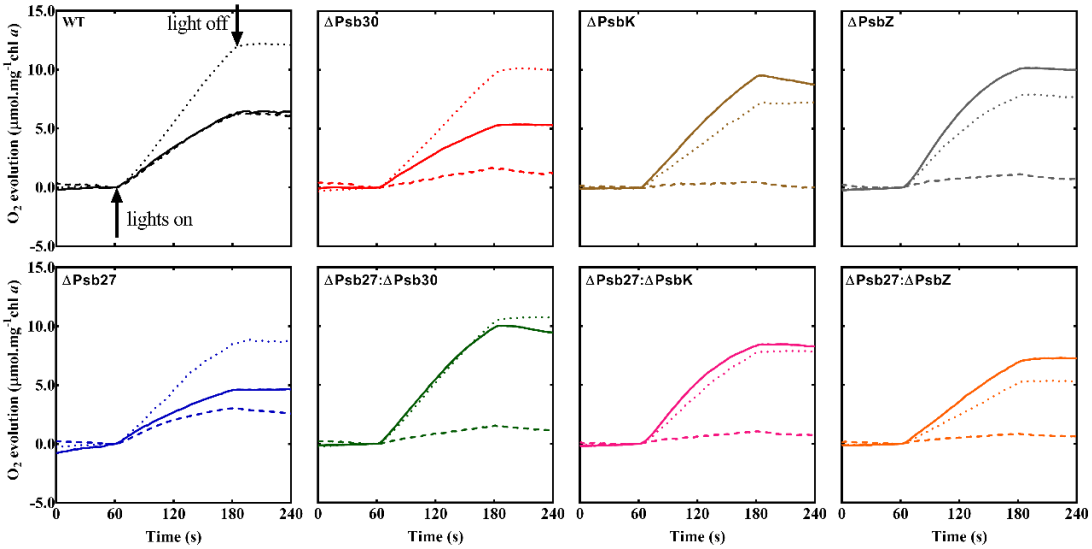

Figure 5.11 PS II oxygen evolving traces from whole cells during the photodamage and recovery assay in the presence of DCBQ. The traces shown represents the different time points of photoinhibition assay: T=0 min (low light), T=45 min (high light) and T=180 min (low light). The strains shown are wild type (black), ΔPsb30 (red), ΔPsbK (brown), ΔPsbZ (grey), ΔPsb27 (blue), ΔPsb27:ΔPsb30 (green), ΔPsb27:ΔPsbK (pink) and ΔPsb27:ΔPsbZ (orange), where T=0 min (solid), T=45 min (dash) and T=180 min (dots).

Before the high-light exposure, wild-type cells, and the LMW protein deletion strains displayed a steady state of oxygen evolution rates at the time point (T=0 min) in the presence of DCBQ (Fig. 5.11 and Fig. 5.12). After T=0 min, the cells were exposed to high light treatment (2000 ± 100 µE m^{-2} s^{-1}) for 45 min. The wild type, as well as the ΔPsb27 strain, could acclimatise to the high-light and the oxygen-evolution rates were

not affected that much. This indicates that the rate of damage is lower as compared to the rate of repair in the wild type and the ΔPsb27 strain, whereas the oxygen evolution rates of all the other strains: ΔPsb30, ΔPsbK, ΔPsbZ, ΔPsb27:ΔPsb30, ΔPsb27:ΔPsbK and ΔPsb27:ΔPsbZ decreased, potentially suggesting that the rate of damage is higher than the rate of repair in these mutants. After 45 min of high-light exposure, the cells were allowed to recover in low light conditions ~30-35 µE $m^{-2}s^{-1}$ for 135 min. Afterward, the oxygen evolution rates of the wild type and the mutants were calculated from the traces and were plotted as a function of time. In Fig. 5.12, the oxygen evolution rates were normalised to the T=0 oxygen evolution rates for each strain to compare the relative extent of photodamage in each strain directly with respect to the wild type.

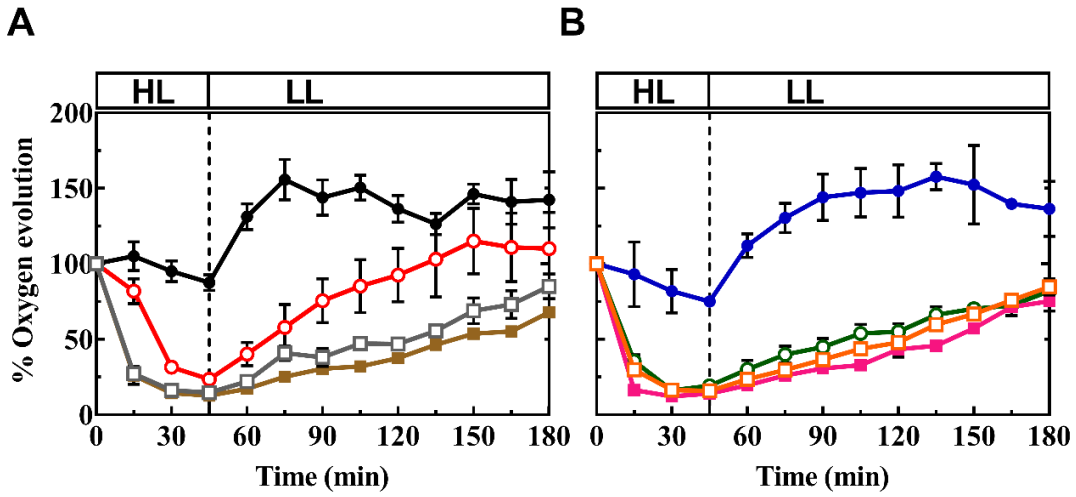

Figure 5.12 Photodamage and recovery of the PS II oxygen-evolving activity in the presence of artificial quinone acceptor DCBQ. The cells were suspended to a chlorophyll *a* concentration of 10 µg.ml^{-1} and were exposed to high-intensity white light at 2000 µE $m^{-2}s^{-1}$ for 45 min and allowed to recover for 135 min in low light conditions at 35 µE $m^{-2}s^{-1}$. The strains shown are **(A)** wild type (black, close circles), ΔPsb30 (red, open circles), ΔPsbK (brown, close squares) and ΔPsbZ (grey, open squares), **(B)** ΔPsb27 (blue, close circles), ΔPsb27:ΔPsb30 (green, open circles), ΔPsb27:ΔPsbK (pink, close squares) and ΔPsb27:ΔPsbZ (orange, open squares). The data represented are the average of three independent experiments normalised to the initial rate of oxygen evolution from the beginning of the treatment, and standard error have been shown as bars.

It can be seen in Fig. 5.12, there was a rapid decrease in the oxygen evolving activity of all the single and double deletion strains in the presence of DCBQ, except the wild type and the ΔPsb27 strain during the first 30 min of the high light stress. The oxygen

evolution rates of the ΔPsb30, ΔPsbK, ΔPsbZ, ΔPsb27:ΔPsb30, ΔPsb27:ΔPsbK and ΔPsb27:ΔPsbZ cells decreased to ~20-25% of their initial oxygen evolution rates. The rate of inhibition was slower in ΔPsb30 mutant as compared to the other single and double deletion strains except for the wild type and the ΔPsb27 strain. However, all the strains could acclimatise to the high-light treatment, thus preventing any further decline in the oxygen-evolving activity of PS II. The ΔPsb30 strain was able to recover fully to the initial T=0 time point of oxygen evolving activity, whereas other single and double deletion strains were able to recover upto ~80-90% of the initial state of oxygen evolving activity. It appears that the rate of PS II damage was higher than the rate of repair in these mutants, leading to an overall decline in PS II oxygen evolution rates.

Oxygen evolution measurements were also carried out in the presence of DMBQ (Fig. 5.13 and Fig. 5.14). It was seen that the cells behaved in a similar fashion to the studies done in the presence of DCBQ. The wild type, as well as the ΔPsb27 strain, could acclimatise under the high-light conditions, and the oxygen evolution rates were not affected considerably. In contrast, the oxygen evolution rates of the ΔPsb30, ΔPsbK, ΔPsbZ, ΔPsb27:ΔPsb30, ΔPsb27:ΔPsbK and ΔPsb27:ΔPsbZ cells decreased. All the strains, when allowed to recover in normal low-light conditions ~30-35 µE $m^{-2}s^{-1}$ after exposure to high light could improve their oxygen evolution rates (Fig. 5.13).

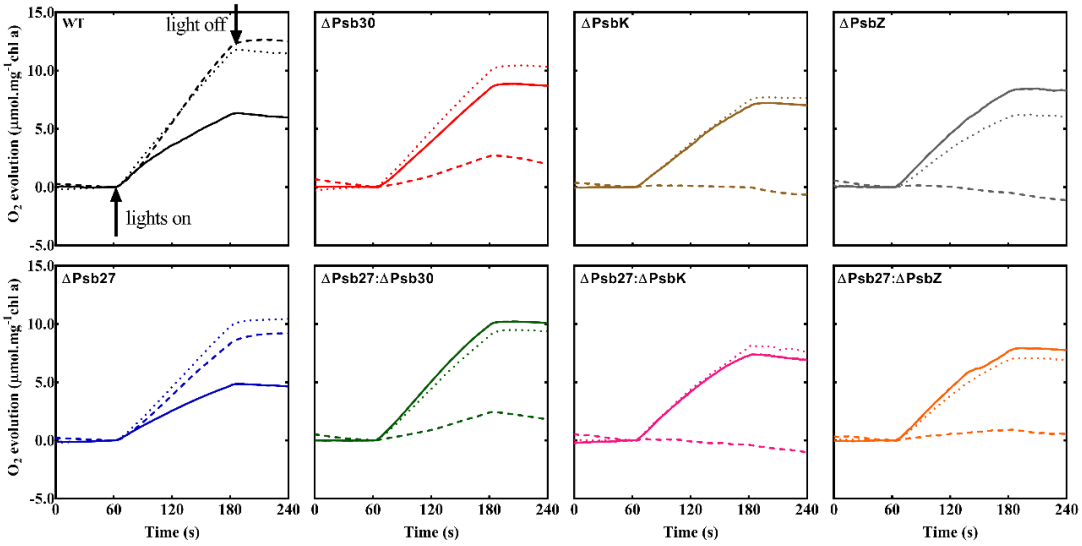

Figure 5.13 PS II oxygen evolving traces from whole cells during the photodamage and recovery assay in the presence of DMBQ. The traces shown represents the different time points of photoinhibition assay: T=0 min (low light), T=45 min (high light) and T=180 min (low light). The strains shown are wild type (black), ΔPsb30 (red), ΔPsbK (brown), ΔPsbZ (grey), ΔPsb27 (blue), ΔPsb27:ΔPsb30 (green),

ΔPsb27:ΔPsbK (pink) and ΔPsb27:ΔPsbZ (orange), where T=0 min (solid), T=45 min (dash) and T=180 min (dots).

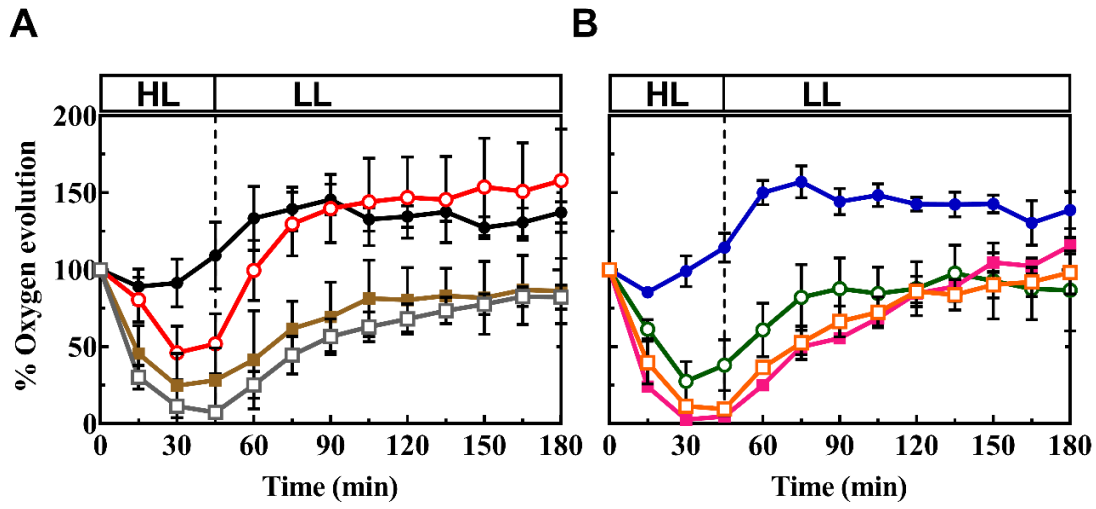

Figure 5.14 Photodamage and recovery of PS II oxygen-evolving activity in the presence of artificial quinone acceptor DMBQ. The cells were suspended to a chlorophyll *a* concentration of 10 μg.ml^{-1} and were exposed to high-intensity white light at 2000 μE m^{-2}s^{-1} for ~45 min and allowed to recover for ~135 min in low light conditions at 35 μE m^{-2}s^{-1}. The strains shown are **(A)** wild type (black, close circles), ΔPsb30 (red, open circles), ΔPsbK (brown, close squares) and ΔPsbZ (grey, open squares), **(B)** ΔPsb27 (blue, close circles), ΔPsb27:ΔPsb30 (green, open circles), ΔPsb27:ΔPsbK (pink, close squares) and ΔPsb27:ΔPsbZ (orange, open squares). The data represented are the average of three independent experiments normalised to the initial rate of oxygen evolution from the beginning of the treatment, and standard error have been shown as bars.

The oxygen evolution rates of the wild type and the mutant in the presence of DMBQ were also calculated from the traces and plotted as a function of time to 180 min after the initiation of the experiment. In Fig. 5.14, the oxygen evolution rates were again normalised to the T=0 oxygen evolution rate for each strain. The extent of photodamage in the case of DMBQ for some of the deletion strains was greater as compared to the DCBQ traces. It can be seen in Fig. 5.14, there was a rapid decrease in the oxygen evolving activity of all the single and double deletion strains, except the wild type and the ΔPsb27 strain during the first 30 min of the high-light stress. The oxygen evolution rates of the ΔPsb30 decreased to ~50%, for ΔPsbK to 75%, for ΔPsbZ to 90%, for ΔPsb27:ΔPsb30 to 60-70%, for ΔPsb27:ΔPsbK and ΔPsb27:ΔPsbZ to ~90-95% in comparison to their initial T=0 oxygen evolution rates. The ΔPsb30 and ΔPsb27:ΔPsb30 can be seen acclimatising to the photodamage after 30 mins of high-light exposure. The extent of photodamage in ΔPsbZ, ΔPsb27:ΔPsbK and

ΔPsb27:ΔPsbZ strains was greater as compared to the DCBQ conditions. The degree of recovery of ΔPsb30, ΔPsbK, ΔPsbZ, ΔPsb27:ΔPsb30, ΔPsb27:ΔPsbK and ΔPsb27:ΔPsbZ strains was higher as compared to the DCBQ conditions.

Oxygen evolution measurements were also carried out for the mutants in the presence of sodium bicarbonate (Fig. 5.15 and Fig. 5.16). The wild type, ΔPsb27, ΔPsb30, ΔPsbK, ΔPsb27: ΔPsb30 strain were able to acclimatise with the high light, and the oxygen-evolution rates were not affected. In contrast, the oxygen-evolution rates of the ΔPsbZ, ΔPsb27:ΔPsbK and ΔPsb27:ΔPsbZ cells were lowered as compared to the wild type. All the strains were able to recover under low-light conditions (Fig. 5.15).

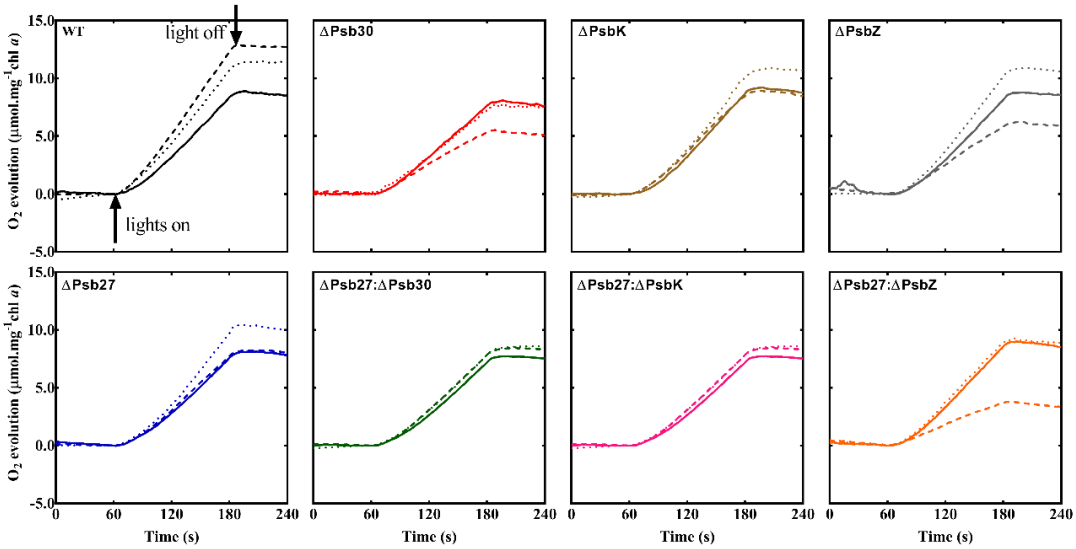

Figure 5.15 PS II oxygen evolving traces from whole cells during the photodamage and recovery assay in the presence of sodium bicarbonate. The traces shown represents the different time points of photoinhibition assay: T=0 min (low light), T=45 min (high light) and T=180 min (low light), in the presence of sodium bicarbonate. The strains shown are wild type (black), ΔPsb30 (red), ΔPsbK (brown), ΔPsbZ (grey), ΔPsb27 (blue), ΔPsb27:ΔPsb30 (green), ΔPsb27:ΔPsbK (pink) and ΔPsb27:ΔPsbZ (orange), where T=0 min (solid), T=45 min (dash) and T=180 min (dots).

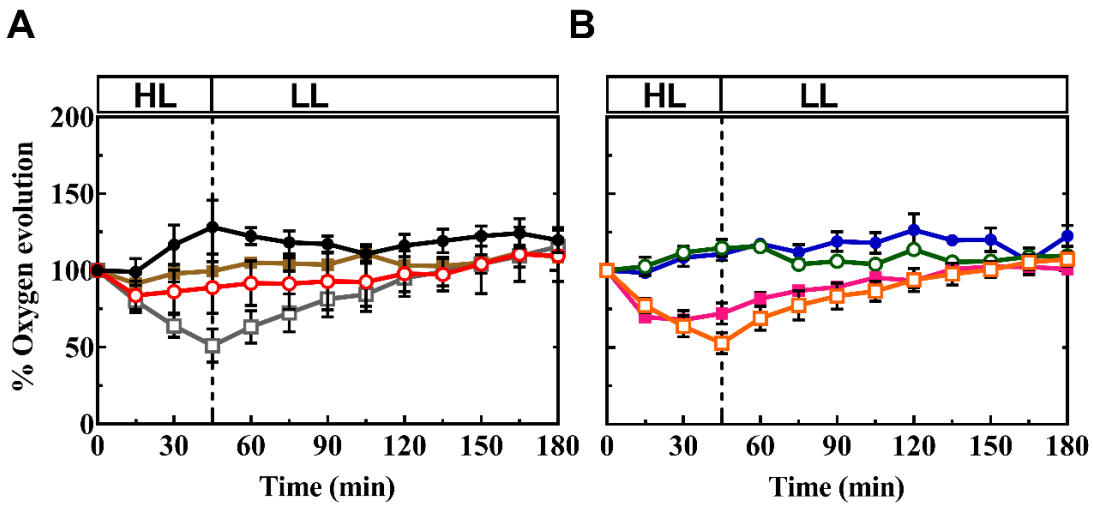

Figure 5.16 Photodamage and recovery of PS II oxygen-evolving activity in the presence of sodium bicarbonate. The cells were suspended to a chlorophyll *a* concentration of 10 µg.ml^{-1} and were exposed to high-intensity white light at 2000 µE m^{-2}s^{-1} for 45 min and allowed to recover for 135 min in low light conditions at 35 µE m^{-2}s^{-1}. The strains shown are **(A)** wild type (black, close circles), ΔPsb30 (red, open circles), ΔPsbK (brown, close squares) and ΔPsbZ (grey, open squares), **(B)** ΔPsb27 (blue, close circles), ΔPsb27:ΔPsb30 (green, open circles), ΔPsb27:ΔPsbK (pink, close squares) and ΔPsb27:ΔPsbZ (orange, open squares). The data represented are the average of three independent experiments normalised to the initial rate of oxygen evolution from the beginning of the treatment, and standard error have been shown as bars.

The oxygen evolution rates of the strains were plotted as a function of time to determine their oxygen-evolution rates. The rates were normalised to the T=0 time point rate for each strain, to compare the relative extent of photodamage with respect to the wild type (Fig. 5.16). The extent of photodamage when oxygen evolution was supported by bicarbonate was less than observed in the presence of DCBQ and DMBQ as electron acceptors. There was an insignificant decrease in the oxygen evolving activity of ΔPsbZ, ΔPsb27:ΔPsbK and ΔPsb27:ΔPsbZ strains in comparison to the wild type and the other mutant strain during the first 30-45 min of the high light incubation. The oxygen evolution rates of the ΔPsbZ and ΔPsb27:ΔPsbZ decreased to ~50%, in comparison to their initial T=0 oxygen evolution rates. All the other strains did not show any reduction in the oxygen evolving activity under high light conditions.

5.4.5.2 Chlorophyll *a* fluorescence decay following single actinic flash

The susceptibility of the decay kinetics of chlorophyll *a* fluorescence to the light-induced damage and the efficiency of the related repair processes were also compared

to the wild type, and the mutants in the absence and presence of DCMU (Fig. 5.17 and Fig. 5.18). The cells were exposed to 45 min of the high-light treatment (2000 µE $m^{-2}s^{-1}$) and were allowed to recover under low-light conditions (35 µE $m^{-2}s^{-1}$) for 75 min. The following time points: 0 min, 45 min and 120 min of the assay are presented in Fig. 5.17 and Fig. 5.18 for the wild type and the mutants. The difference between the 0 min and 45 min chlorophyll *a* fluorescence decay curves illustrates the extent of photodamage, due to 45 min of high light treatment. The 120 min decay curve represents the degree of recovery from the photodamage in each strain after cells have spent ~45 min in high-light and 75 min in low-light conditions. In the insets in Fig. 5.17 and Fig. 5.18), the fluorescence transients have been normalised as per the ($F-F_o$) to see the effect of the photodamage on the initial fluorescence/number of PS II centres for each strain at different time points of the study. Table 5.5 lists the half-times and the amplitudes of the fluorescence decay in the absence of the DCMU.

The recovery in the wild type was much more efficient as compared to the other mutants during chlorophyll *a* fluorescence decay measurements in the absence of DCMU. It was observed that the removal of Psb30, PsbK, PsbZ proteins enhanced the susceptibility to the photoinhibition. The removal of Psb27 in the Psb30, PsbK and PsbZ background did result in the enhancement of the sensitivity to the photodamage as compared to the single deletion mutants. All the mutants could recover from the photodamage in low-light conditions. Most of the damage occurs within the first 30-45 min of the assay, which can be observed as a drop in the initial fluorescence (F_o), fluorescence yield (F_m) and the variable fluorescence yield (F_v). The decrease in the initial fluorescence (F_o) and variable fluorescence (F_v) during the high-light treatment potentially indicates that the PS II assembly has been affected. However, when the cells could recover, the F_o and F_v levels also started recovering from the photodamage. The chlorophyll *a* fluorescence decay measurements under the high and low light conditions were consistent with the measurements of oxygen evolution (Fig. 5.12, Fig. 5.14 and Fig. 5.16), which showed a rapid decline in the PS II evolving activity within the first 30-45 min, followed by acclimatisation phase. The extent of photodamage was greater in ΔPsbK, ΔPsbZ, ΔPsb27:ΔPsb30, ΔPsb27:ΔPsbK and the ΔPsb27:ΔPsbZ strains in the absence of DCMU. The half-time of the fast component in ΔPsbZ cells increased from ~340 ± 10 µs at time 0 min to ~500 ± 80 µs at time 45 min. Also in the ΔPsb27:ΔPsbZ strain the half-time of fast component increased from ~370 µs ± 2 (T=0

min) to ~500 ± 90 µs (T=45 min). The half-time of the slow component of ΔPsb27:ΔPsb30 mutant was the fastest as compared to the wild type and the other strains.

The susceptibility of the decay kinetics of chlorophyll *a* fluorescence to light-induced damage and the efficiency of the related repair processes were also compared to the wild type and the mutant strains in the presence of DCMU. Table 5.6 lists the half-times and the amplitudes of the fluorescence decay in the presence of the DCMU to indicate the Q_A^- reoxidation rates in each strain. As seen before, the removal of Psb30, PsbK, PsbZ subunits enhanced the susceptibility to the photoinhibition in the presence of DCMU. The removal of Psb27 in combination with Psb30, PsbK, and PsbZ background lead to the increase in the extent of photodamage as compared to the single deletion strains. All the mutant strains could recover from the photoinhibition in low light conditions. The recovery in the wild type was more efficient as compared to the other mutants during the variable chlorophyll *a* fluorescence decay measurements in the presence of DCMU. The extent of photodamage was greater in ΔPsbK, ΔPsbZ, ΔPsb27:ΔPsbK and the ΔPsb27:ΔPsbZ strains with DCMU. The amplitude of the fast component in ΔPsbK and ΔPsb27:ΔPsbK mutants increased from 14% (T=0 min) and 18% (T=0) to 40% (T=45 min) and 48% (T=45). For ΔPsbZ and ΔPsb27:ΔPsbZ cells also, the amplitude of the fast component increased from 15% (T=0 min) and 16% (T=0) to 47% (T=45 min) and 51% (T=45 min). The amplitude of the slow component of the ΔPsbZ and ΔPsb27:ΔPsbZ cells decreased from 85% (T=0 min) and 84% (T=0 min) to 53% (T=45 min) and 48% (T=45 min).

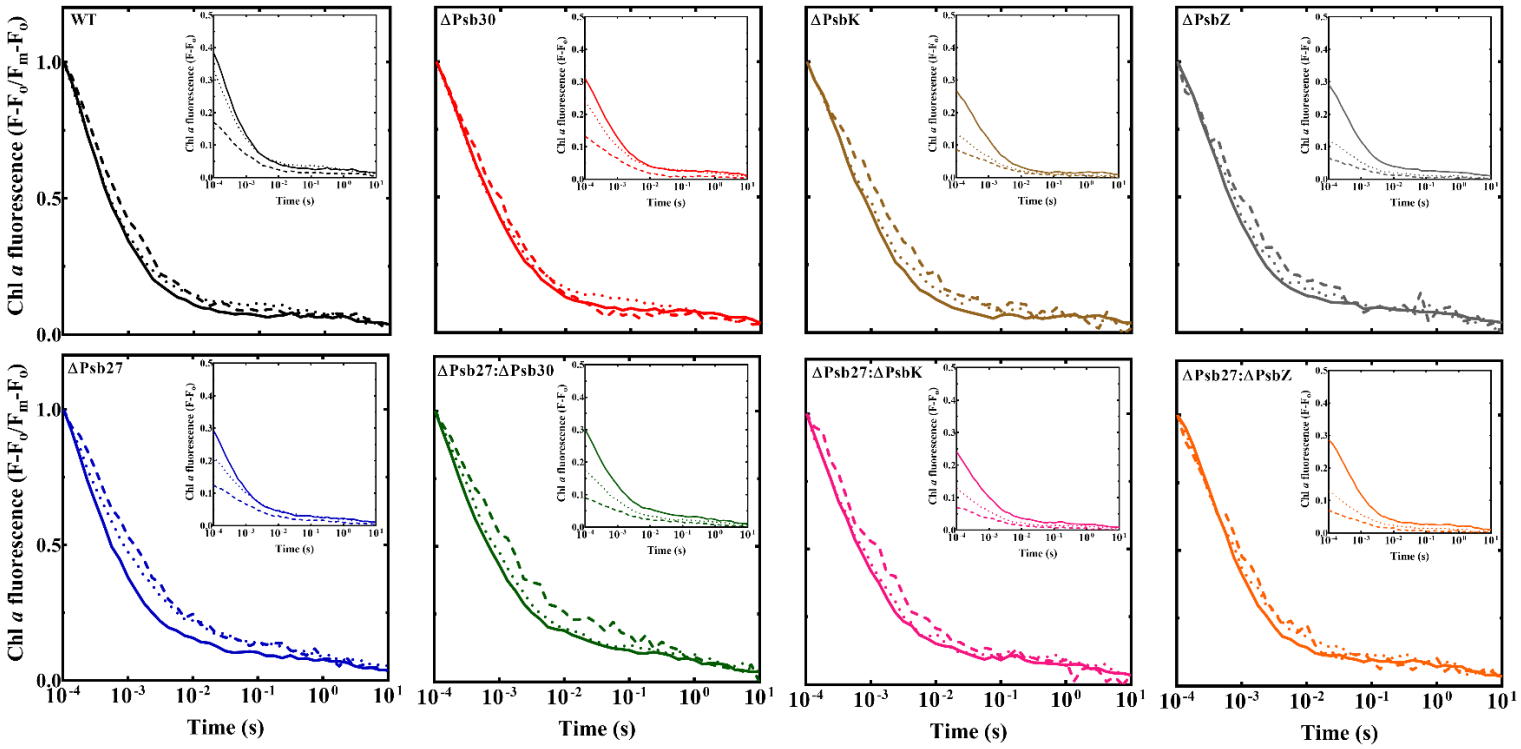

Figure 5.17 Normalised and unnormalised relaxation of chlorophyll *a* fluorescence curves of wild type and the cells in the absence of DCMU.Normalised and unnormalised chlorophyll *a* fluorescence decay curves of the wild type and the LMW protein deletion strains following single turnover actinic flash at different time points of photoinhibition assay (T=0 min (low light), T=45 min (high light) and T=120 min (low light)), in the absence of DCMU. The strains shown are wild type (black), ΔPsb27 (blue), ΔPsb30 (red), ΔPsbK (brown), ΔPsbZ (grey), ΔPsb27:ΔPsb30 (green), ΔPsb27:ΔPsbK (pink) and ΔPsb27:ΔPsbZ (orange), where T=0 min (solid), T=45 min (dash) and T=120 min (dots). The strains were exposed to high light at 2000 µE $m^{-2}s^{-1}$ for 45 min and were allowed to recover for 75 min in low light at 35 µE $m^{-2}s^{-1}$. The cells suspensions contain 2.5 µg of chlorophyll *a* per ml and the data shown are the averages from three independent experiments. The effect of photodamage was measured every 15 min (from 0 min to 120 min) for all the strains.

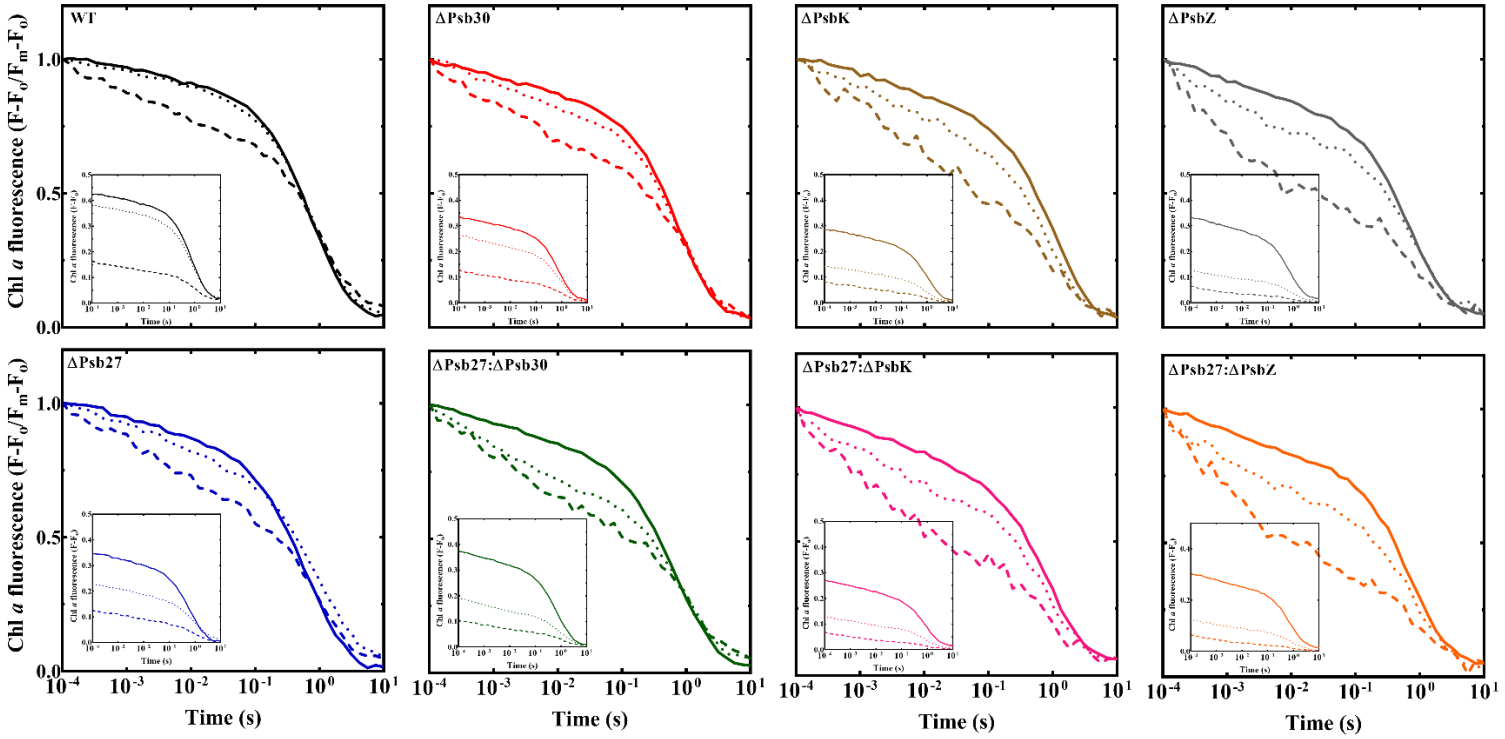

Figure 5.18 Normalised and unnormalised relaxation of chlorophyll *a* fluorescence decay curves of wild type and the mutant cells in the presence of DCMU.Normalised and unnormalised chlorophyll *a* fluorescence decay curves of the wild type and the mutants following single turnover actinic flash at different time points of photoinhibition assay (T=0 min (low light), T=45 min (high light) and T=120 min (low light)), in the presence of DCMU. The strains shown are wild type (black), ΔPsb27 (blue), ΔPsb30 (red), ΔPsbK (brown), ΔPsbZ (grey), ΔPsb27:ΔPsb30 (green), ΔPsb27:ΔPsbK (pink) and ΔPsb27:ΔPsbZ (orange), where T=0 min (solid), T=45 min (dash) and T=175 min (dots). The strains were exposed to high light at 2000 µE $m^{-2}s^{-1}$ for 45 min and were allowed to recover for 75 min in low light at 35 µE $m^{-2}s^{-1}$. The cells suspensions contain 2.5 µg of chlorophyll *a* per ml and the data shown are the averages from three independent experiments. The effect of photodamage was measured every 15 min (from 0 min to 120 min) for all the strains.

Table 5.5 Decay kinetics of variable chlorophyll *a* fluorescence following single saturating actinic flash in the absence of DCMU in the high-light and the low-light conditions.

Strains	Time (min)	Fast		Intermediate		Slow	
		$T_{1/2}$ (µs)	Amp.	$T_{1/2}$ (ms)	Amp.	$T_{1/2}$ (s)	Amp.
WT	T=0	260 ± 10*	60 ± 1	2.8 ± 0.2	32 ± 1	6.4 ± 0.2	8.1 ± 0.1
	T=45	290 ± 4	53 ± 1	3.4 ± 0.2	37 ± 1	4.6 ± 0.5	10.1 ± 0.2
	T=120	240 ± 1	56 ± 1	2.4 ± 0.1	32 ± 1	2.2 ± 0.1	12.1 ± 0.1
ΔPsb27	T=0	290 ± 10	61 ± 1	3.8 ± 0.2	28 ± 1	2.8 ± 0.1	11.1 ± 0.1
	T=45	400 ± 20	48 ± 1	5.1 ± 0.6	37 ± 1	1.5 ± 0.2	15.3 ± 1.0
	T=120	320 ± 40	53 ± 3	5.5 ± 1.0	33 ± 2	3.0 ± 0.6	15.2 ± 0.6
ΔPsb30	T=0	310 ± 10	55 ± 1	3.4 ± 0.1	36 ± 1	5.8 ± 0.1	9.2 ± 0.1
	T=45	360 ± 10	51 ± 1	4.4 ± 0.1	41 ± 1	3.6 ± 0.5	8.3 ± 0.7
	T=120	250 ± 20	50 ± 3	3.0 ± 0.4	37 ± 2	2.1 ± 0.6	13.4 ± 1.0
ΔPsbK	T=0	370 ± 20	56 ± 2	3.9 ± 0.2	37 ± 2	8.2 ± 0.7	7.1 ± 0.1
	T=45	500 ± 80	49 ± 3	5.8 ± 0.5	39 ± 2	1.1 ± 0.1	12.4 ± 0.5
	T=120	370 ± 50	55 ± 3	4.9 ± 0.8	36 ± 4	2.5 ± 0.6	10.2 ± 0.2
ΔPsbZ	T=0	340 ± 10	58 ± 1	3.1 ± 0.1	32 ± 1	3.3 ± 0.1	10.1 ± 0.1
	T=45	500 ± 80	56 ± 7	8.0 ± 0.9	32 ± 5	2.4 ± 0.9	12.4 ± 1.8
	T=120	390 ± 40	59 ± 5	4.3 ± 0.6	30 ± 4	2.0 ± 0.6	11.4 ± 1.3
ΔPsb27: ΔPsb30	T=0	260 ± 10	52 ± 2	3.4 ± 0.3	34 ± 2	1.7 ± 0.2	14.2 ± 0.2
	T=45	300 ± 40	37 ± 5	3.3 ± 0.5	41 ± 2	0.7 ± 0.2	22.4 ± 3.2
	T=120	340 ± 40	53 ± 3	4.6 ± 0.7	33 ± 3	3.0 ± 0.1	14.1 ± 0.2
ΔPsb27: ΔPsbK	T=0	280 ± 10	53 ± 1	3.2 ± 0.1	36 ± 1	2.8 ± 0.1	11.2 ± 0.3
	T=45	300 ± 20	43 ± 1	4.1 ± 0.1	42 ± 1	0.8 ± 0.1	14.1 ± 0.3
	T=120	240 ± 10	46 ± 1	2.9 ± 0.1	42 ± 1	3.2 ± 0.1	12.1 ± 0.1
ΔPsb27: ΔPsbZ	T=0	370 ± 2	59 ± 1	3.3 ± 0.1	31 ± 1	3.6 ± 0.3	10.3 ± 0.6
	T=45	500 ± 90	59 ± 4	7.7 ± 2.2	31 ± 3	9.2 ± 6.0	10.3 ± 1.1
	T=120	320 ± 10	54 ± 1	3.9 ± 0.2	33 ± 1	2.7 ± 0.9	13.3 ± 0.8

*The standard error have been shown for the chlorophyll *a* fluorescence decays from three independent experiments. .

Table 5.6 Decay kinetics of variable chlorophyll *a* fluorescence following single saturating actinic flash in the presence of DCMU in high light and low light conditions.

Strains	Time (min)	Fast		Slow	
		$T_{1/2}$ (µs)	Amp.	$T_{1/2}$ (s)	Amp.
Plus DCMU					
WT	T=0	1.7 ± 0.6*	7.1 ± 0.1	0.5 ± 0.1	93.1 ± 0.1
	T=45	2.5 ± 0.6	24 .1± 0.1	0.8 ± 0.1	76.2 ± 0.1
	T=120	2.0 ± 0.6	9.1 ± 0.1	0.5 ± 0.1	91.1 ± 0.1
ΔPsb27	T=0	1.6 ± 0.6	11.1 ± 0.1	0.4 ± 0.1	89.1 ± 0.1
	T=45	3.1 ± 0.6	31.3 ± 3.5	0.5 ± 0.6	69.3 ± 3.4
	T=120	3.8 ± 0.6	20.1 ± 0.1	0.6 ± 0.1	80.2 ± 0.1
ΔPsb30	T=0	1.6 ± 0.6	11.4 ± 0.6	0.5 ± 0.1	89.3 ± 0.6
	T=45	2.7 ± 0.6	31.2 ± 0.1	0.6 ± 0.1	68.1 ± 0.1
	T=120	1.8 ± 0.6	17.3 ± 0.7	0.5 ± 0.1	83.4 ± 0.7
ΔPsbK	T=0	2.7 ± 0.6	14.4 ± 0.5	0.6 ± 0.1	86.3 ± 0.5
	T=45	3.5 ± 0.6	40.4 ± 1.4	0.5 ± 0.5	60.4 ± 1.4
	T=120	3.4 ± 0.6	40.3 ± 1.4	0.5 ± 0.1	60.3 ± 1.4
ΔPsbZ	T=0	1.8 ± 0.6	15.2 ± 0.1	0.5 ± 0.1	85.1 ± 0.1
	T=45	1.1 ± 0.6	47.1 ± 2.0	0.5 ± 0.1	53.2 ± 2.0
	T=120	1.1 ± 0.6	47.1 ± 2.0	0.5 ± 0.1	53.1 ± 2.0
ΔPsb27: ΔPsb30	T=0	1.8 ± 0.6	13.1 ± 0.1	0.4 ± 0.1	87.2 ± 0.1
	T=45	2.7 ± 0.6	38.2 ± 1.0	0.7 ± 0.1	62.3 ± 1.0
	T=120	1.8 ± 0.6	28.3 ± 0.9	0.6 ± 0.1	72.3 ± 0.9
ΔPsb27: ΔPsbK	T=0	2.9 ± 0.6	18.1 ± 0.3	0.6 ± 0.1	82.1 ± 0.3
	T=45	2.2 ± 0.6	48.1 ± 0.1	0.5 ± 0.1	52.1 ± 0.1
	T=120	1.5 ± 0.6	27.3 ± 1.0	0.6 ± 0.1	73.3 ± 1.0
ΔPsb27: ΔPsbZ	T=0	1.6 ± 0.6	16.1 ± 0.1	0.5 ± 0.1	84.1 ± 0.1
	T=45	1.5 ± 0.6	51.3 ± 1.0	0.5 ± 0.1	48.4 ± 1.0
	T=120	1.4 ± 0.6	31.1 ± 0.1	0.5 ± 0.1	69.2 ± 0.1

*The standard error have been shown for the chlorophyll *a* fluorescence decays from three independent experiments. .

5.4.6 PS II assembly

The assembly of PS II complexes was studied in the single and double deletion strains (wild type, ΔPsb27, ΔPsb30, ΔPsbK, ΔPsbZ, ΔPsb27:ΔPsb30, ΔPsb27:ΔPsbK and ΔPsb27:ΔPsbZ) with BN-PAGE, followed by immunoblotting using D1, D2, CP43 and CP47 specific antibodies (Fig. 5.19). Multiple bands could be seen, representing different assembly intermediates of the PS II complex. The bands could be identified as PS II dimers, PS II monomers, RC47 complexes and some unassembled protein complexes. The PS II dimer bands were present in all the mutant strains. The ΔPsb30, ΔPsbZ, ΔPsb27:ΔPsb30 and ΔPsb27:ΔPsbZ strains showed less intense PS II dimer bands (PS II (2)) as well as PS II monomer (PS II (1)) as compared to the wild type when probed with the CP43 antibody. The intensity of the PS II dimer and PS II monomer bands was higher in ΔPsb27:ΔPsbZ as compared to ΔPsbZ. The ΔPsb30 and ΔPsb27:ΔPsb30 strains, when probed with the CP47 antibody, displayed a reduced intensity of PS II dimer bands as compared to the wild type. The ΔPsbZ and ΔPsb27:ΔPsbZ strains showed less intense bands of PS II monomers. The ΔPsb30, ΔPsbZ, and ΔPsb27:ΔPsbZ strains also displayed lighter bands of the RC47 complex. In the presence of D1 antibody, ΔPsb30, ΔPsbZ, and ΔPsb27:ΔPsb30 strains showed lower levels of PS II dimer bands. In the case of ΔPsbZ and ΔPsb27:ΔPsbZ strains, the PS II monomer bands were lighter. The ΔPsb30, ΔPsbK, and ΔPsb27:ΔPsbK mutants displayed some intermediate bands between PS II dimer and PS II monomer as compared to the wild type. Removal of the LMW proteins in these deletion mutants might cause an accumulation of intermediate complexes involved in PS II assembly. The BN-PAGE analysis showed that PS II assembly was possible in all the mutants.

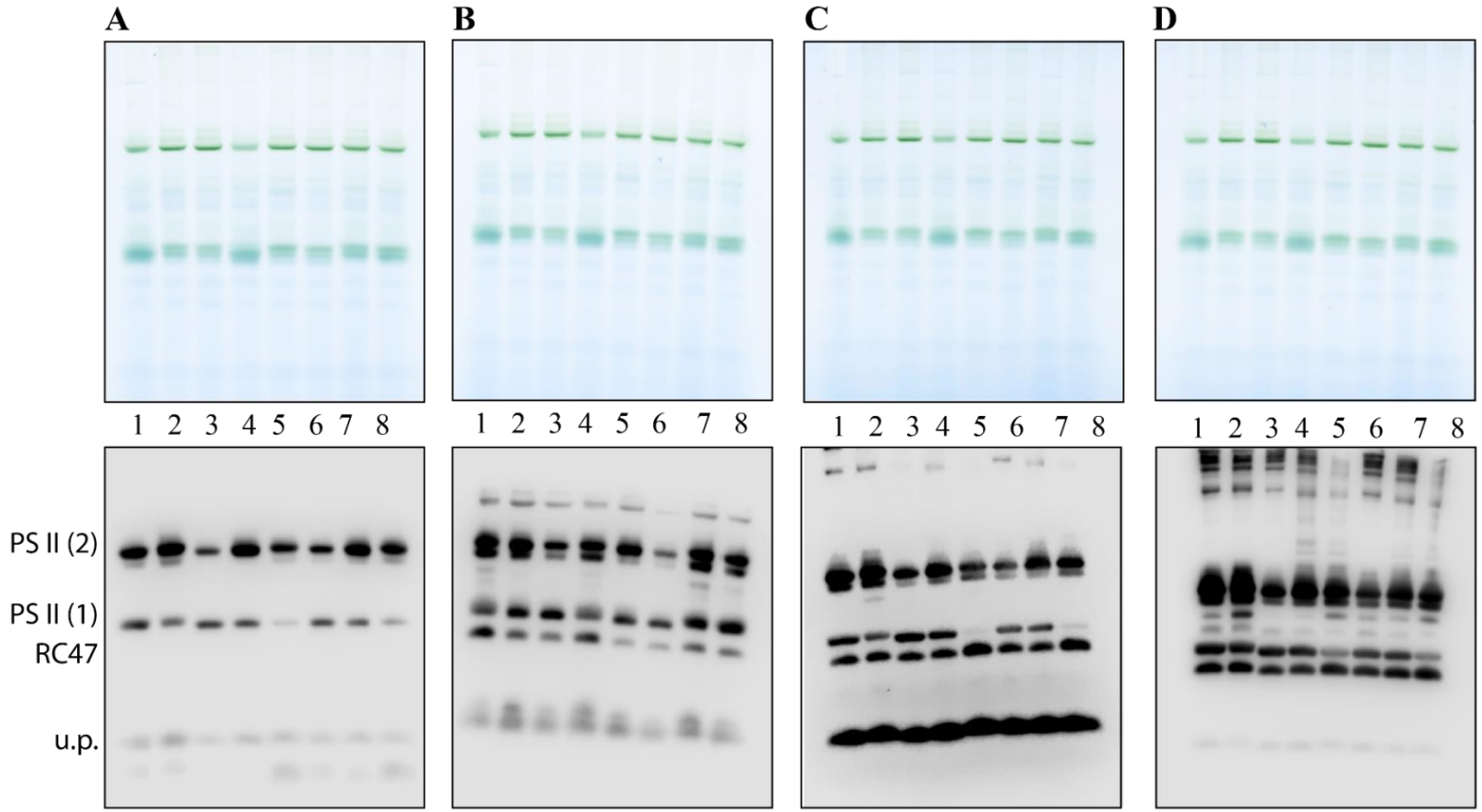

Figure 5.19 PS II assembly analysis. Thylakoid samples run on BN-PAGE followed by Immunodetection of PS II complexes using PS II specific antibodies. **(A)** CP43, **(B)** CP47, **(C)** D1 and **(D)** D2. 5 µg of chlorophyll was loaded onto 3-12% gradient BN-PAGE. The proteins were transferred to PVDF membrane for immunodetection through enhanced chemiluminescence (ECL). Lanes are (1) wild type, (2) ΔPsb27, (3) ΔPsb30, (4) ΔPsbK, (5) ΔPsbZ, (6) ΔPsb27:ΔPsb30, (7) ΔPsb27:ΔPsbK, (8) ΔPsb27:ΔPsbZ. The complexes are PS II dimer; PS II monomer; RC47, PS II complex without CP43. u.p. means unassembled protein complexes

5.5 Whole genome sequencing

Once all the single and double deletion strains were fully characterised, whole genome sequencing of ΔPsbK and ΔPsbZ mutants was performed to establish the genotypes of these two deletion strains. All the strains used in this study were derived from the GT-O1 (wild type) strain at the University of Otago, Department of Biochemistry, New Zealand. The whole genome sequencing of GT-O1 strain has already been carried out by our lab members. Various other novel single nucleotide polymorphisms (SNPs) and indels (insertions/deletions) were identified in these strains, that might have generated since the distribution and usage of the original Williams GT strain (Morris *et al.* 2014).

In ΔPsbK, ~10 novel SNPs and 4 unique indels were detected, whereas, in ΔPsbZ, 11 novel SNPs and 1 novel indel were detected. All these mutations identified in the ΔPsbK (Table 5.7) and ΔPsbZ (Table 5.8) mutants were in addition to the already existing variations in GT-O1 background strain (Morris *et al.* 2014). Out of the 10 novel SNPs in ΔPsbK mutant, 5 SNPs were silent mutations. In ΔPsbZ strain, all the 11 SNPs detected were silent mutations. Silent mutations are mutations in DNA that do not significantly alter the phenotype of the organism in which they occur. Silent mutations either do not result in a change to the amino acid sequence of a protein or lead to the insertion of an alternative amino acid with similar properties to that of the original amino acid; in either case, there is no significant change in phenotype.

Table 5.7 List of novel mutations detected in ΔPsbK mutant.

Sr.No	Position	Mutation Type	Nucleotide level	Amino acid level	Gene Name	Details
1.	373250	SNP	C to A	Thr7Lys	*slr1069* - hypothetical protein	US gene: s*lr1068* - hypothetical protein DS gene: *slr1070* - unknown protein
2.	488803	SNP	A to T	Gln506Leu	*slr1609/fadD* - hypothetical protein (acyl-ACP synthetase), phospholipid and sterol metabolism	US gene: *sll1501* - cobyrinic acid a, c-diamide synthase DS gene: *slr1043* – cheW/ chemotaxis protein
3.	1346489	Ins	G to GA	-	*slr0856* - Putative transposase/*ISY100l*	US gene: *sll0853*/*cpcU* - hypothetical protein DS gene: *slr0857* - Putative transposase/*ISY100l*
4.	117274	Ins	50-60 bps	-	*sll5130* – hypothetical protein; pSYSM	US gene: *ssl5129* - hypothetical protein DS gene: *sll5131* - putative transposase (*ISY203j*)

5.	3753	SNP	A to G	Stop to Stop	*ssr6002* - unknown protein; pSYSX	US gene: *slr6001* - Chy46/two-component hybrid sensor and regulator DS gene: *ssr6003* - unknown protein
6.	26972 27017 27056	SNP SNP Ins	G to A T to A C to CAGT	Thr76Thr Thr91Thr -	*slr6029* - hypothetical protein; pSYSX	US gene: *slr6028* - unknown protein DS gene: *ssr6030* - unknown protein
7.	59363	SNP	T to C	Ala100Ala	*slr6064* - unknown protein; pSYSX	US gene: *slr6063* - unknown protein DS gene: *slr6065* - unknown protein
8.	81876	SNP	G to A	Arg138Arg	*slr6088* - hypothetical protein; pSYSX	US: *slr6087* - unknown protein DS: *ssr6089* - unknown protein
9.	82299 82357 82358	SNP SNP SNP	G to A C to T A to G	- - -	*ssr6089* – unknown protein; pSYSX	US: *slr6088* - hypothetical protein DS: *slr6090* - unknown protein

*US: Upstream; DS: Downstream; SNP: Single nucleotide polymorphism; Ins: Insertion; Del: Deletion.

Table 5.8 List of novel mutations in ΔPsbZ strain.

Sr.No	Position	Mutation Type	Nucleotide level	Amino acid level	Gene Name	Details
1.	858747	SNP	G to A	Phe1040Phe	*sll1787:* rpoB RNA polymerase β subunit; RNA synthesis, modification and DNA transcription	US gene: *sll1786* - tatD putative deoxyribonuclease DS gene: *sll1789* - rpoC2/RNA polymerase beta prime subunit
2.	1827496	SNP	G to A	Arg80Arg	*slr1470* - hypothetical protein	US gene: slr1469 – rnpA/RNase P DS gene: *slr1471/alb3/oxa1/ synyidC* - hypothetical protein
3.	117276	Ins	More than 100 bps	-	*sll5130* - hypothetical protein; pSYSM	US gene: *sll5131* - putative transposase (*ISY203j*) DS gene: *ssl15129* - hypothetical protein
4.	3594 3753	SNP SNP	T to C A to G	Thr30Thr Stop to Stop	*ssr6002* - unknown protein; pSYSX	US gene: *slr6001* - Chy46/two-component hybrid sensor and regulator

						DS gene: *ssr6003* - unknown protein
5.	59363 59411 59420 59457 59489 59492 59495	SNP - SNP SNP SNP SNP SNP	T to C CTTA to GCTC G to A T to C C to G A to G T to C	Ala100Ala Val116Val, Leu117Leu Gln119Gln Leu132Leu Val141Val Lys143Lys Phe144Phe	*slr6064* - unknown protein pSYSX	US gene: *slr6063* - unknown protein DS gene: *slr6065* - unknown protein
6.	81876	SNP	G to A	Arg138Arg	*slr6088* - hypothetical protein; pSYSX	US gene: *slr6087* - unknown protein DS gene: *ssr6089* - unknown protein

*US: Upstream; DS: Downstream; SNP: Single nucleotide polymorphism; Ins: Insertion; Del: Deletion.

5.6 Discussion

The LMW proteins of the CP43 pre-assembly complex (Psb30, PsbK, and PsbZ) were targeted to understand the role played by these subunits towards the function, assembly and the repair mechanism of PS II. The Psb27 protein was also included along with these LMW proteins, as the Psb27 protein in *Synecocystis* 6803 has been shown to interact with CP43 (Liu *et al.* 2011b; Komenda *et al.* 2012a).

The ΔPsb27, ΔPsb30, and ΔPsb27:ΔPsbZ mutants, when grown photoautotrophically, exhibited doubling times relatively similar to the wild type (Table 5.1). This phenotype shown here agrees with the photoautotrophic growth displayed in studies carried out on strains lacking Psb27 (Roose and Pakrasi 2008) and Psb30 (Inoue-Kashino *et al.* 2008) in *Synechocystis* 6803. The ΔPsbK, ΔPsbZ, ΔPsb27:ΔPsbK, and ΔPsb27:ΔPsbZ cells showed an extended doubling time as compared to the wild type. This phenotype displayed by the ΔPsbK strain is in agreement with the delayed photoautotrophic growth exhibited by the *psbK* deletion strain, characterised by Ikeuchi and coworkers (Ikeuchi *et al.* 1991) in *Synechocystis* 6803, whereas, the phenotype shown by the *psbZ* deletion strain here is in contrast with the studies conducted by Bishop and colleagues (Bishop *et al.* 2007), as the ΔPsbZ strain constructed by them in *Synechocystis* 6803 did not have altered photoautotrophic growth characteristics. The doubling time of our ΔPsbK strain was the slowest, followed by the ΔPsb27:ΔPsbK, ΔPsbZ, and ΔPsb27:ΔPsb30 strains as compared to the doubling time of wild type. Unexpectedly, it would appear that the single deletion strains lacking PsbK and PsbZ were hampering photoautotrophic growth and potentially PS II activity more as compared to the corresponding double deletion mutants.

The oxygen evolution assay was carried out using different PS II-specific quinone acceptors and sodium bicarbonate (Fig. 5.6, Table 5.2). The oxygen-evolution rates of the ΔPsb27, ΔPsb30, ΔPsbZ, ΔPsb27:ΔPsb30 and ΔPsb27:ΔPsbZ strains were similar to the wild type in the presence of DCBQ. The ΔPsbK strain had a lower oxygen evolution rate in the presence of DCBQ and DMBQ as compared to the wild type and the other strains. The deletion of the *psb27* along with *psb30*, *psbK*, and *psbZ* genes did not have much effect on the oxygen-evolution rates. All the mutants displayed good levels of oxygen evolution activity, thus supporting the healthy state of the mature PS II core holoenzyme in the mutants.

Low temperature 77 K fluorescence emission spectroscopy measurements were also performed to study the effect of LMW deletion strains on the levels or stoichiometry of the PS I and PS II complexes (Fig. 5.7). The ΔPsb27:ΔPsbK and ΔPsb27:ΔPsbZ strains displayed a small apparent increase in the PS II level when excited by the 440 nm light (Fig. 5.7 B). This changed ratios of PS II to PS I of fluorescence might be the result of an accumulation of CP43 or CP47 subcomplexes or due to the defects in the incorporation of CP43/CP47 proteins. The ΔPsbK, ΔPsbZ, ΔPsb27:ΔPsbK and ΔPsb27:ΔPsbZ cells exhibited a higher and merged peak at 680 nm (Fig. 5.7 C and D), when excited with 580 nm light potentially suggesting a lower number of PS II centres were present to use the energy; hence the excess energy is released from the PBS because of the weak quenching of chlorophyll *a* fluorescence via energy transfer to the PS II light-harvesting protein complexes (CP43 and CP47).

The ΔPsb30, ΔPsbK and ΔPsbZ and ΔPsb27:ΔPsbZ strains displayed lower P levels as compared to the wild type and the other mutants in the absence of DCMU (Fig. 5.8 A and B). The ΔPsbZ and ΔPsb27:ΔPsbZ strains exhibited an altered IP rise as compared to the wild type and the other strains in the absence of DCMU (Fig. 5.8 A and B). All the single and double deletion strains exhibited similar variable fluorescence induction traces in the presence of DCMU (Fig. 5.8 C and D). Although the F_m level were lower for the ΔPsb30, ΔPsbK and ΔPsbZ strains in the presence of DCMU, potentially signalling towards a lower number of PS II centres in the strains. Ikeuchi and co-workers (Ikeuchi *et al.* 1991) also observed a decrease in the number of PS II reaction centres in variable fluorescence analysis for ΔPsbK strain.

The chlorophyll *a* fluorescence decay measurements, following single actinic flashes applied to dark-adapted cells in the absence of DCMU for ΔPsbK, ΔPsbZ and ΔPsb27:ΔPsbZ strains showed slower microsecond component as compared to the wild type (Fig. 5.10 A and B) (Table 5.3). All the single and double deletion strains had slower microsecond component except ΔPsb27:ΔPsbK mutant. The second fast component of all the mutants was faster as compared to the wild type. The millisecond component of chlorophyll *a* fluorescence decay measurements for ΔPsb27, ΔPsb30, ΔPsbK, ΔPsbZ, and ΔPsb27:ΔPsbZ strains in the presence of DCMU were faster as compared to the wild type (Table 5.4). There were no differences in the second component for the strains in the presence of DCMU. The mutants displayed normal back charge recombination rates and amplitudes.

All the single and double deletion strains were susceptible to photodamage except the ΔPsb27 strain during oxygen-evolution measurements. The extent of photodamage towards the oxygen-evolving capacity of PS II was greatest in the presence of DMBQ (Fig. 5.14) as compared to the DCBQ (Fig. 5.12) and was the lowest with sodium bicarbonate (Fig. 5.16) as the electron acceptor. The oxygen evolution rates of the ΔPsb30, ΔPsbK, ΔPsbZ, ΔPsb27:ΔPsb30, ΔPsb27:ΔPsbK and ΔPsb27:ΔPsbZ mutants decreased to ~20-25% of their initial oxygen evolution rates in the presence of DCBQ, whereas, in the presence of DMBQ; the oxygen evolution rates of ΔPsb30 decreased to ~50%, ΔPsbK to 75%, ΔPsbZ to 90%, ΔPsb27:ΔPsb30 to 60-70%, ΔPsb27:ΔPsbK and ΔPsb27:ΔPsbZ to ~90-95% of their initial oxygen evolution rates. The DCBQ quinone acceptor is suggested to accept electrons directly from Q_A (Graan and Ort 1986), whereas DMBQ quinone acceptor accepts electrons from Q_B (Graan and Ort 1986). These findings suggest a role for the LMW proteins belonging to CP43-precomplex in optimising PS II activity under high-light intensities. Furthermore, the greater susceptibility of the single and double deletion strains towards high-light, suggests that the LMW proteins play a photoprotective role towards the PS II complex by structural and functional stabilisation.

The effect of light stress on chlorophyll *a* fluorescence decay kinetics were also studied in the presence and absence of DCMU in all the mutants (Fig. 5.17 and Fig. 5.18) (Table 5.5 and Table 5.6). All the single and double deletion strains were sensitive to the photodamage as compared to the wild type and the ΔPsb27 strain. The ΔPsb27:ΔPsb30, ΔPsb27:ΔPsbK and ΔPsb27:ΔPsbZ deletion strains were more susceptible to the photodamage than the single deletion mutants (ΔPsb30, ΔPsbK, and ΔPsbZ). The chlorophyll *a* decay measurements under the high light and low light conditions were consistent with the measurements of oxygen evolution, which also showed a rapid decline in the PS II- evolving activity within the first 30-45 min, followed by acclimatisation phase.

The assembly of PS II complexes was also studied in all the LMW deletion strains with the help of 3-12% BN-PAGE, followed by immunoblotting using D1, D2, CP43, and CP47 specific antibodies (Fig. 5.19). All the strains showed that they could assemble the PS II complexes at similar levels to the wild type. Thus, showing that the PS II assembly is normal in all the Psb27 mutants.

The ΔPsbK, ΔPsbZ, ΔPsb27:ΔPsbK and ΔPsb27:ΔPsbZ strains of *Synechocystis* 6803 were sensitive to the combined condition of glucose and light, suggesting that PsbK and PsbZ may have a role in the protection of PS II (Kobayashi *et al.* 2005a). It looks like the LMW protein plays an important part in the attachment of the CP43 complex to RC47 complex.

Some of the phenotypic traits shown by ΔPsbK and ΔPsbZ mutants were in disagreement to the previous studies carried out by other research groups. So, to confirm the genotype of these deletion strains, whole genome sequencing of ΔPsbK and ΔPsbZ strains was conducted. In the GTO1 parent strain, 17 SNP and 8 indels were already present (Chapter 4, Table . The details of the mutations have been discussed in Chapter 4, Table 4.9). The mutations present in ΔPsbK and ΔPsbZ strains has also been shown in Table 5.7 and 5.8.

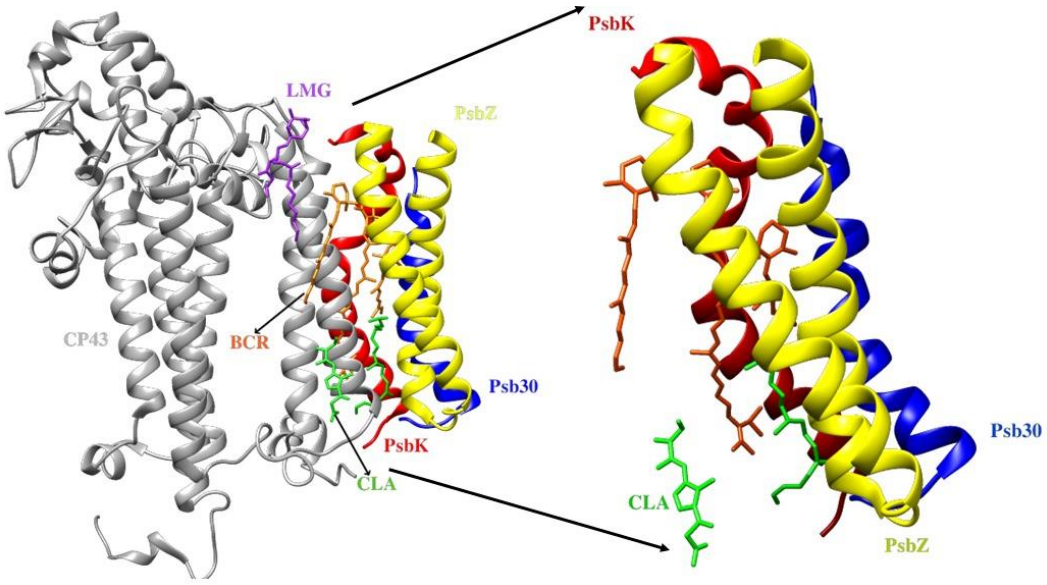

Figure 5.20 Structures around Psb30, PsbK and PsbZ subunit in PS II. The following subunits have been shown: CP43 (grey), Psb30 (blue), PsbK (red) and PsbZ (yellow). Psb30 and PsbK are single helices whereas PsbZ consists of two helixes. The carotenoids have been depicted within a distance of 3 Å of PsbK and PsbZ: Beta-carotene (orange), LMG (purple) and CLA (green). The figures were drawn with UCSF Chimera with PDB: 3BZ1.

The proximity of carotenoids to Psb30, PsbK, and PsbZ suggests that these subunits may play a role in photoprotection during PS II assembly and repair. Carotenoids are poly-isoprenoid compounds that can play pivotal roles in the regulation of light-

harvesting energy transfer, quenching of chlorophyll triplet states, scavenging of singlet oxygen species and stabilisation of the structure (Sozer *et al.* 2011).

Further studies can be carried out by the construction of mutants lacking different LMW protein combinations to explore these LMW interactions in more detail. All the single and double deletion strains were highly susceptible to photodamage, so further studies should be carried out to understand it in more detail. The protein assembly of the LMW deletion strains can be explored further by employing different antibodies, and two-dimensional gels can be performed in combination with mass spectrometry to study the composition of different intermediate PS II complexes.

Chapter Six

Discussion

6.1 Overview

The CP43 pre-assembly complex plays an important role during the early stages of the assembly process of the oxygen-evolving PS II core complex. In addition to the chlorophyll-binding CP43 protein, the pre-complex possesses at least three additional membrane-spanning low-molecular-weight (LMW) proteins: these are the single helix Psb30 and PsbK, and the two-helix PsbZ (Boehm *et al.* 2012b). Psb27 also associates with the CP43 subunit of PS II during photosystem biogenesis. Several models have been proposed for the interaction between Psb27 and CP43 (Liu *et al.* 2011b; Komenda *et al.* 2012a).

The objective of this project was to contribute to the current understanding of the structural and functional roles of the LMW proteins (Psb27, Psb30, PsbK, and PsbZ) associated with the CP43 pre-assembly complex involved in the assembly and repair of PS II.

6.2 Psb27 protein - Site-directed mutagenesis system in *Synechocystis* 6803

6.2.1 Conservation of Psb27

The Psb27 protein is evolutionarily conserved between higher plants and cyanobacteria (Fig. 3.3), potentially indicating the functional importance of the protein (Roose *et al.* 2007b; Fagerlund and Eaton-Rye 2011a). Little is known about the functional roles of the conserved amino acid residues of the Psb27 protein in the interaction with other protein subunits of the PS II complex. A few highly conserved amino acid residues were identified on the surface of the Psb27 protein to study the role of Psb27 in PS II assembly (Fig. 3.4). The amino-acid residues of Psb27 involved in cross-linking between Psb27 and CP43 that are implicated in protein-protein interactions in the studies outlined in the literature were also targeted (Liu *et al.* 2011a). Eleven variants of the Psb27 subunit were introduced into the *Synechocystis* 6803 Psb27 protein using targeted mutagenesis of *psb27* (Fig. 3.2 A). The following amino acid residues were selected in these mutagenesis studies: Asp-14, Arg-54, Tyr-78, Arg-94, Glu-98, Asp-58, and Lys-63. It was anticipated that the amino acid substitutions in Psb27 would confer a phenotype different from the wild type.

A *Synechocystis* 6803 strain was constructed in which the *psb27* gene was deleted (Fig. 3.5). A complementary mutagenesis vector system was created to introduce mutations into the wild-type copy of *psb27* gene (Fig. 3.6). A Psb27 control strain was generated containing a wild-type copy of *psb27* with a spectinomycin-resistance cassette introduced downstream of the *psb27* gene without hindering the upstream and downstream neighbouring genes of *psb27*. Care was taken to maintain the wild-type expression level of the *psb27* gene while analysing the potential contribution of the Psb27 protein towards the cells. The efficiency of the Psb27 mutagenesis system was confirmed by running the isolated thylakoid samples from mutants on SDS-PAGE followed by immunoblotting using a Psb27-specific antibody to test the expression level of Psb27 protein in the constructed mutants (Fig. 3.7). The expression levels of Psb27 protein in the Psb27 control strain, R54E* mutant and the R94E strain was similar to the wild type. The Psb27 expression was completely absent in ΔPsb27 strain, as in the *psb27* deletion mutant, the open-reading frame was replaced by a chloramphenicol-resistance cassette.

6.2.2 Effect of deletion of LMW proteins on photoautotrophic growth and PS II oxygen-evolving activity

In this study, the mutation of the amino acids in the Psb27 protein and the removal of LMW proteins of CP43 preassembly complex did affect the photoautotrophic growth of the cells (Table 3.1, Table 5.1). The Psb27 control strain, ΔPsb27, D14A, R54E, Y78H, R94E, E98R, D58A, D58E, D58K, K63A, K63D, K63R mutants (Fig. 3.8) displayed the doubling time similar to the wild type suggesting that there were no major functional abnormalities in PS II assembly, as PS II function is crucial for the photoautotrophic growth of cells. In the previous studies also, the deletion of Psb27 did not affect the photoautotrophic growth in the *Synechocystis* 6803 (Roose and Pakrasi 2008). The ΔPsbK cells exhibited delayed photoautotrophic growth characteristics in comparison to the ΔPsbZ mutant (Table 5.1) which is in agreement with the higher doubling time displayed by the ΔPsbK strain in *Synechocystis* 6803 constructed by Ikeuchi and coworkers (Ikeuchi *et al.* 1991). The ΔPsbZ also displayed higher doubling time is also in agreement with the delayed photoautotrophic growth exhibited by ΔPsbZ mutant in *Synechocystis* 6803 (Bishop *et al.* 2007). The normal photoautotrophic growth seen in ΔPsb30 is also in agreement with photoautotrophic growth

characteristics displayed by a ΔPsb30 *in Synechocystis* 6803 (Inoue-Kashino *et al.* 2008).

The interesting observation was that the deletion of *psb27* gene along with the *psbK* and *psbZ* gene could reduce the inhibitory effect on the photoautotrophic growth of cells. However, the ΔPsb27, ΔPsb30, ΔPsb27:ΔPsb30, ΔPsb27:ΔPsbZ deletion strain displayed the doubling time similar to the wild-type strain suggesting the mutants were able to assemble PS II. Surprisingly, ΔPsbK, ΔPsbZ, ΔPsb27:ΔPsbK and ΔPsb27:ΔPsbZ mutants exhibited extended doubling time when grown in the presence of glucose in contrast to wild type (data not shown). Photomixotrophic growth conditions lead to excess photooxidative damage (Sonoike *et al.* 2001) which can, in turn, be avoided by dispersal of the excess excitation energy through different photoprotection mechanisms, which are linked to the xanthophyll cycle in plants. However, cyanobacteria cannot perform the xanthophyll cycle (Demmig-Adams and Adams 1990); a further reason might be that the PQ pool is more reduced in the presence of glucose. A similar kind of observation related to the sensitivity of the growth in the presence of glucose has also been seen for a ΔPsbK strain of *Synechocystis* 6803 (Kobayashi *et al.* 2005b).

The mutations in the Psb27 protein did little to alter the oxygen-evolving activity of the PS II reaction centre complex (Table 3.2). The photoautotrophic growth characteristics and oxygen-evolving activity exhibited by the ΔPsb27 strain in *Synechocystis* 6803 is in agreement with the previous studies performed in *Arabidopsis thaliana* and *Synechocystis* 6803 (Chen *et al.* 2006; Roose and Pakrasi 2008).

The ΔPsb27, ΔPsb30, ΔPsbK, ΔPsbZ, ΔPsb27:ΔPsb30, ΔPsb27:ΔPsbK and ΔPsb27:ΔPsbZ cells were able to evolve oxygen similar to the wild-type levels (Table 5.2). The oxygen-evolving activity displayed by ΔPsb30 and ΔPsbZ mutants are in agreement with the levels of oxygen-evolution activity shown by ΔPsb30 mutants constructed by Inoue-Kashino and colleagues (Inoue-Kashino *et al.* 2008) and ΔPsbZ mutant constructed by Bishop and colleagues in *Synecocystis* 6803 (Bishop *et al.* 2007). However, the oxygen-evolution activity seen in ΔPsbK strain disagrees with the observation of Ikeuchi (Ikeuchi *et al.* 1991) and Katoh (Katoh and Ikeuchi 2001). No additive effects were observed upon removal of Psb27 in combination with the deletion of the PsbK and PsbZ proteins on the oxygen-evolving activity of PS II complex.

Hence, it can be suggested that Psb27 acts independently of the LMW proteins and as such do not seem to play any functional role in enhancing the efficiency of oxygen evolution. The results of this study support the hypothesis that during the assembly or recovery processes, Psb27 binds to inactive PS II pre-complexes but dissociates from PS II before the subunits of the oxygen-evolving complex bind and the functional complex are formed (Nowaczyk *et al.* 2006). The Psb27 subunit is, therefore absent from functional PS II complexes.

6.2.3 The deletion of LMW proteins affect the PBS energy coupling efficiency in cells

The relative ratios of the fluorescence emission from PS II (685 nm and 695 nm) and PS I (725 nm) were similar to the wild type, the Psb27 control strain, as well as the R54E, Y78H, E98R, D58A, D58E, D58K, K63D and K63R cells (Fig. 3.11 and 3.12). However, the PS II fluorescence levels (685 nm and 695 nm) were higher for the D14A, K63A strains and the PS II fluorescence levels (685 nm and 695 nm) were lower for the ΔPsb27 strain. Nevertheless, the ΔPsb27, R54E, R94E, Y78H, D58A, D58E, D58K, K63D and K63R strains displayed more efficient coupling and energy transfer between the antenna protein complexes and the photosystems (PS I and PS II) relative to the wild type, Psb27 control strain, and the D14A, E98R and K63A mutants. This observation might suggest that the deletion/mutation of the Psb27 protein leads to altered PS II structural interactions, as the energy transfer from the PBS to PS II was more efficient in the D14A, D58E, D58K and K63D cells which can also be supported by the elevated fluorescence levels displayed by D58E, D58K and K63D cells in the presence of DCMU during chlorophyll *a* fluorescence induction measurements. The reason might be an accumulation of bound PBS, because of disturbances in the assembly of PS II complex. Another explanation could be that because of the higher number of PS II centres, more PBS can bind, and therefore the absorbed energy is transferred more efficiently to PS II resulting in better quenching of the fluorescence.

All the LMW protein single and double deletion strains were able to assemble similar levels of PS II in comparison to the wild- type cells (Fig. 5.7 A and B). In the case of ΔPsb30 mutant, it is in agreement with the studies related to the ratio of PS II to PS I, measured by 77K fluorescence emission spectroscopy (Inoue-Kashino *et al.* 2008). However, the removal of PsbK and PsbZ was shown to increase PBS fluorescence

indicating lower numbers of PS II centres in these strains (Fig. 5.7 C). The increased PBS fluorescence displayed by ΔPsbK and ΔPsbZ mutants is also supporting the stabilisation function of PsbK and PsbZ towards the CP43 pre-assembly complex; as another reason for this sharp peak could be the accumulation of subcomplexes or disturbance of the incorporation of CP43. In comparison, the ΔPsb27:ΔPsbK and ΔPsb27:ΔPsbZ mutants led to the relative lowering of the PBS fluorescence emission but showing the same merged peak (685 nm) as the ΔPsbK and ΔPsbZ mutants, indicating a perturbation in PS II assembly.

6.2.4 The deletion of LMW proteins affect the PS I levels in the cells

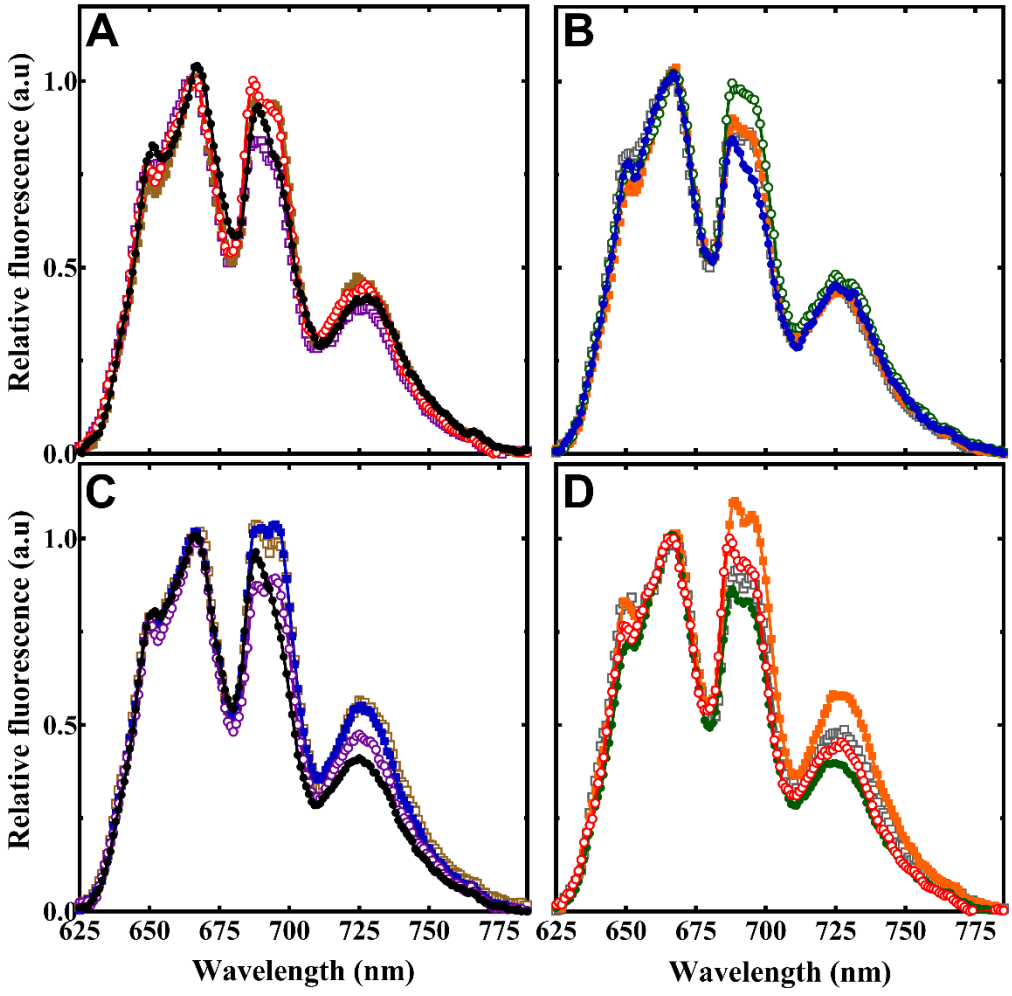

Figure 6.1 Low-temperature (77K) fluorescence absorption spectroscopy of Psb27 mutants. The strains shown in panel **(A)** are wild type (black, close circles), Psb27 control (red, open circles, D14A (brown, close squares), E98R (purple, open squares); panel **(B)** are ΔPsb27 (blue, close circles), R54E (green, open circles), R94E (orange, close squares), Y78H (grey, open squares); panel **(C)** are wild type (black, close circles), D58A (brown, open squares), D58E (purple, open circles), and D58K (blue,

close squares), and panel **(D)** are Psb27 control (red, open circles), K63A (green, close circles), K63D (orange, close squares) and K63R (grey, open squares). Spectra obtained using 580 nm excitation light. Spectra shown are the average of four independent experiments are shown normalised to 665 nm emission maxima of phycocyanin.

In Fig. 6.1, the 77 K emission spectra obtained using 580 nm light excitation has been presented. All the traces have been normalised to the 665 nm peak (allophycocyanin) to gain more insight towards the effect of Psb27 mutations and deletion of LMW proteins toward the levels of PS I in the cells. It can be seen that introduction of specific mutations in the Psb27 protein resulted in a considerable variation in the fluorescence emission at 725 nm (PS I). Interestingly, the D14A, R54E, D58A, D58E, D58K, K63D and K63R strains displayed higher levels of PS I emission in comparison to the wild type and the Psb27 control strain. This observation is interesting as the Psb27 protein has already been suggested to play a role in interactions with the PS I. Recently, evidence for an interaction between Psb27 and PS I was observed by yeast two-hybrid analyses using the split-ubiquitin system (Pasch *et al.* 2005; Komenda *et al.* 2012a). These data provide insight into an association of Psb27 with PS I via the PsaB subunit. The mutations in Psb27 did alter the efficiency of oxygen-evolving activity of the whole photosynthetic electron transport chain in comparison to the wild type and the Psb27 control strain.

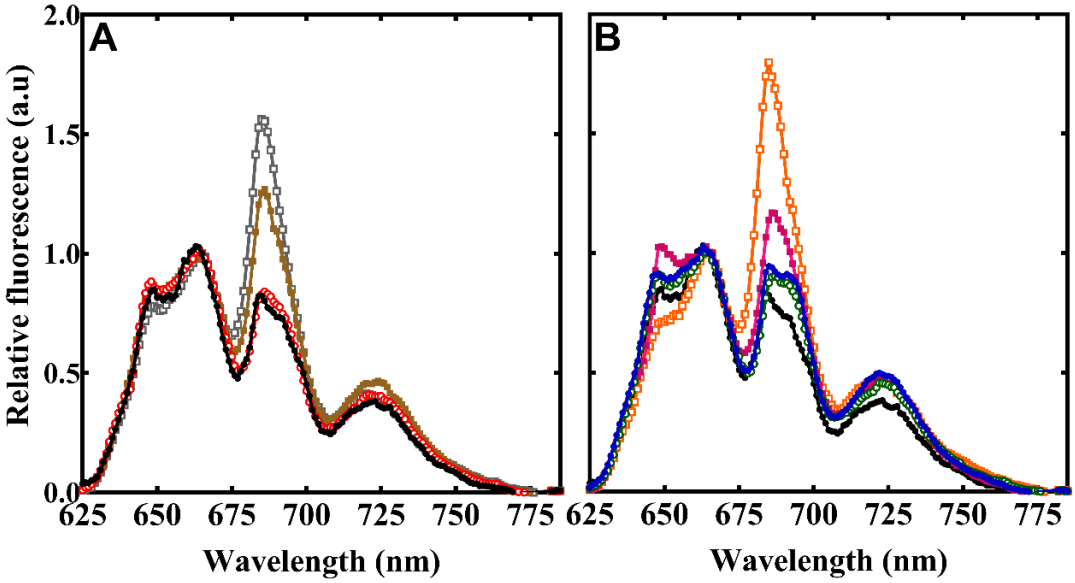

Figure 6.2 Low-temperature (77K) fluorescence absorption spectroscopy of LMW protein deletion strains. The strains shown in panel **(A)** are wild type (black, close circles), ΔPsb30 (red, open circles, ΔPsbK (brown, close squares), and ΔPsbZ (grey, open squares); panel **(B)** are wild type (black, close circles), ΔPsb27 (blue, close

circles), ΔPsb27:ΔPsb30 (green, open circles), ΔPsb27:ΔPsbK (pink, close squares), and ΔPsb27:ΔPsbZ (orange, open squares). Spectra obtained using 580 nm excitation light. Spectra shown are the average of four independent experiments are shown normalised to 665 nm emission maxima of phycocyanin.

6.2.5 Effect of deletion of LMW proteins on the electron transfer kinetics

Analysis of the room temperature steady-state fluorescence induction displayed some differences between the Psb27 mutants and the wild type (Fig. 3.14 and 3.15). The Psb27 control, ΔPsb27, R54E, R94E, D58A, D58K, K63A, K63D and K63R strains exhibited the typical fluorescence induction curve (OJIP) similar to the wild type, potentially indicating standard electron transfer at the acceptor and donor sides of PS II. However, the D14A and E98R mutants exhibited an early IP rise as compared to the wild type and the Psb27 control strain. The increase in IP peak corresponds to the reduction of the PQ pool which depends on the PS II centres with both a Q_B site and an active manganese cluster to provide electrons required for the saturation of the acceptor side. The ΔPsb27 strain, and the R54E, R94E, D58K and K63D mutants displayed a pronounced effect on the fluorescence induction curves in the presence of DCMU (Fig. 3.14 C, D and Fig. 3.15 C, D). These strains exhibited a higher F_m level in comparison to the wild type. The higher fluorescence (F_m) levels in the presence of DCMU corresponds to the higher number of PS II centres. However, the E98R strain exhibited an apparent lower number of PS II centres in comparison to the wild type.

No effect was seen on chlorophyll *a* fluorescence decay kinetics upon removal of Psb27 indicating that Psb27 does not directly affect the donor-side or acceptor-side functions of PS II (Table 3.3 and 3.4). However, the Psb27 control strain and the Psb27 mutants exhibited faster half-time for the slow component of the forward reaction of chlorophyll *a* fluorescence decay in the absence of DCMU. The half-time of the slow component is influenced by the midpoint potentials of the Q_A/Q_A^- couple and that of the S_2 state of the manganese cluster or oxygen-evolving complex as well as the equilibrium for the sharing of an electron between Q_A and Q_B. This lag in the slower phase exhibited by Psb27 mutants was also observed previously in the isolated Psb27-containing early PS II assembly complexes with processed D1 carboxyl terminus. However, this increased half time for the slower component was not found for the Psb27-containing early PS II assembly complexes with an unprocessed carboxyl terminus of D1 (Liu *et al.* 2011a). All the Psb27 mutants exhibited similar variable fluorescence traces in the presence of

DCMU potentially indicating normal electron transport and charge recombination pathways between the S_2 or Q_A^- species within PS II (Fufezan *et al.* 2007). Previous studies based on EPR spectroscopy and flash-induced variable fluorescence also displayed that the Psb27 protein does not affect the acceptor side or donor side of PS II in *Thermosynechococcus elongatus* (Mamedov *et al.* 2007).

The OJIP rise in the absence of DCMU remains unchanged in the ΔPsb30, ΔPsbK, ΔPsbZ, ΔPsb27:ΔPsb30, ΔPsb27:ΔPsbK and ΔPsb27:ΔPsbZ mutants (Fig. 5.8 A and B), suggesting that the electron transfer between the manganese cluster and Q_A is unaffected. However, the ΔPsb30, ΔPsbK, and ΔPsbZ cells exhibited a decrease in the levels of the OJIP rise, indicating inhibition of the accumulation of reduced PQ. The perturbation in the structure-function interactions of the oxygen-evolving complex has been shown to relate with the quenching of the IP rise resulting in a decline of F_m levels (Boisvert *et al.* 2006). The IP peak was broader in ΔPsbZ and ΔPsb27:ΔPsbZ strains. Interestingly, the ΔPsb30, ΔPsbK, and ΔPsbZ mutants displayed lower levels of F_m or decreased number of PS II centres in the presence of DCMU in comparison to the wild type and the ΔPsb27, ΔPsb27:ΔPsb30, ΔPsb27:ΔPsbK and ΔPsb27:ΔPsbZ cells (Fig. 5.8 C and D). The ΔPsb30, ΔPsbK, and ΔPsbZ strains exhibited an early SM rise (Fig. 5.9 A) indicating state transitions (Papageorgiou and Govindjee 2011; Kana *et al.* 2012). State transitions (Bonaventura and Myers 1969; Murata and Sugahara 1969; Forti and Caldiroli 2005; Mullineaux and Emlyn-Jones 2005) are known to balance absorbed energy between the two photosystems by mobilising specific light-harvesting pigment protein antenna complexes (Takahashi *et al.* 2006; Peers *et al.* 2009).

There was no significant impairment in the functioning of the donor side or acceptor side reactions of PS II in the ΔPsb27, ΔPsb30, ΔPsbK, ΔPsbZ, ΔPsb27:ΔPsb30, ΔPsb27:ΔPsbK, ΔPsb27:ΔPsbZ strains, as measured by chlorophyll *a* fluorescence decay measurements (Table 5.3 and 5.4). The fluorescence relaxation rate in the ΔPsbK, ΔPsbZ, and ΔPsb27:ΔPsbZ strains was slower than wild type, indicating a slower transfer from Q_A^- to Q_B. This might be caused by a lower occupancy of the Q_B site in the dark-adapted cells.

6.2.6 Psb27 mutants affect state transitions in PS II?

The OJIPSM rise in the absence of DCMU, mostly remained unchanged in the Psb27 control strain as well as the D14A, Y78H, E98R, D58E, K63D and K63A mutants, suggesting that the electron transfer between the manganese complex and Q_A is unaffected (Fig. 3.16 and 3.17). However, the SM peak was lower in R54E, R94E, D58A and D58K cells as compared to the wild type. The SM phase is linked with state 2 (low fluorescence; a larger antenna in PS I) to state 1 (high fluorescence; a larger antenna in PS II) transition. State transitions are light-acclimated processes that enlarge or diminish the size of light-harvesting antennae that feed excitation to the core complexes of PS II and PS I. In the PBS/chlorophyll *a* containing cyanobacteria it involves putative translational and orientational movements of extramembrane PBS that favour one or the other photosystem. The state transitions are regulated by the redox potential of the PQ pool (Williams and Allen 1987; Allen and Forsberg 2001). According to the mobile PBS model (Kirilovsky 2015), the transition to state 2 occurs when PBS dissociates from PS II and migrates along the cytoplasmic face of the thylakoid to bind to PS I. The redistribution of phycobilin absorbed excitation energy during state transitions can be explained by the mobility of PBS. However, still, it is hard to describe the occurrence of the spillover mechanism (Bruce *et al.* 1989; Salehian and Bruce 1992; McConnell *et al.* 2002). The variation in energy transfer efficiency from PBS to PS I and energy spill over from PS II to PS I are proposed to play a role in controlling the state transitions (McConnell *et al.* 2002). The photosystem arrangement and changes in the PBS can mediate the redistribution of excitation energy transfer. In state 1, PS II particles are suggested to be organised into rows as opposed to the more random configuration of state 2 (Olive *et al.* 1986; Olive *et al.* 1997; Folea *et al.* 2008). The spill over of excitation energy from PS II to PS I decreases when PS II is organised into rows in state 1 due to loss of PS II–PS I connections (Yang *et al.* 2007).

The K63A strain exhibited higher F_m level as compared to the wild type in the presence of DCMU. The Psb27 control strain, ΔPsb27, D14A, R54E, R94E mutants and all the strains with amino acid substitutions at Asp58 exhibited similar variable fluorescence induction traces in the presence of DCMU, but the F_m level were lower in the E98R, Y78H mutants and the strains with amino acid substitutions at Lys63 as compared to the wild type, potentially indicating lower number of PS II centres. The Psb27 knockout

mutants in *Arabidopsis thaliana* have also been proposed to display highly accelerated state transitions (Hou *et al.* 2015).

6.2.7 PS II assembly in LMW protein deletion mutants

Analysis of native PS II complexes showed wild-type levels of abundance of the three macromolecular PS II assembly complexes (i.e., the RC47 pre-complex, the PS II monomers and the PS II dimers) in the Psb27 control, ΔPsb27 and the Psb27 strains when probed with the four PS II-specific antibodies against the D1, D2, CP43 and CP47 proteins (Fig. 3.20). The following strains: D14A, R54E, Y78H, D58E, K63A, K63D, and K63R, when probed with the CP43 antibody, displayed bands of high-molecular-weight complexes (bands between PS II dimer and PS II monomer) of the PS II monomer complex potentially indicating disturbances of the PS II biogenesis process. It is possible that the extra PS II monomer band displayed by these strains might be an incompletely assembled PS II complex or intermediate PS II assembly complex, as the *Synechocystis* 6803 Psb27 protein has been shown to interact with the CP43 protein subunit (Liu *et al.* 2011a; Liu *et al.* 2011b; Komenda *et al.* 2012a). Also, the Psb27 protein has been shown to be associated with PS II complexes lacking a functional oxygen-evolving complex (Nowaczyk *et al.* 2006). It is more likely to be a result of misassembly in PS II biogenesis indicating Psb27 is playing a role in the assembly of PS II as well. Another possibility might be that these particular mutations in the Psb27 protein induce changes in the structure/interactions of the Psb27 protein leading to the impaired assembly of the PS II monomer. However, as noted above, any changes in the assembly process did not affect the capacity of the strains for photoautotrophic growth.

It is hard to study the function of the Psb27 protein *in vivo*, as Psb27 deletion strains are phenotypically similar to the wild-type strain (Roose and Pakrasi 2008). Although Psb27 is highly conserved among plants, algae, and cyanobacteria, there are some differences seen between Psb27 protein sequences of plants, green algae, and cyanobacteria. These differences in the sequence can explain the differences in the phenotype observed between the Psb27 mutants of *Arabidopsis thaliana* and *Synechocystis* 6803, as it is possible that Psb27 has different functional roles in the cyanobacteria and higher plant systems (Fig. 3.3). Furthermore, BN-PAGE and immunoblot analysis revealed less PS II dimers and PS II monomers in the ΔPsb30,

ΔPsbZ, ΔPsb27:ΔPsb30 and ΔPsb27:ΔPsbZ strains relative to the wild type (Fig. 5.19). These results suggest that the lack of Psb30 and PsbZ protein results in lower numbers of PS II dimers and PS II monomers.

6.2.8 Models related to the Psb27-Asp14, Psb27-Glu98, Psb27-Asp58, and Psb27-Lys63 residues

According to the Psb27 structures (PDB: 2KMF and 2Y6X), Psb27-Asp14 is proposed to stabilise the protein folding of Psb27 by forming hydrogen bonds with the N-terminal end of Psb27 protein and Psb27-Glu98 is placed on the surface of the Psb27. However, the Psb27 structure (PDB: 2KND) suggests that the Psb27-Glu98 is instead embedded in the Psb27 protein and does not, therefore, have an interaction with Psb27-Asp14. In this study, the substitution mutants Psb27-D14A and Psb27-E98R were constructed and characterised. The Psb27-D14A mutant exhibited an extended doubling time, lower oxygen-evolution activity when measured using PS II-specific artificial quinone acceptors and displayed a lower number of PS II centres. In contrast, the Psb27-E98R mutant exhibited wild-type levels of photoautotrophic growth, PS II assembly and oxygen-evolution. The results of this thesis reveal, the effect of mutating Psb27-Glu98 to be much smaller than expected for reversal of a buried charge in protein. Therefore, I would like to support the idea that the Psb27-Glu98 is surface-exposed and is consistent with the model proposed by the two Psb27 structures (Michoux *et al.* 2012; Mabbitt *et al.* 2014). The Psb27-Glu98 is a surface exposed amino acid and using 2KMF, or 2Y6X Psb27 models will support more reliable models of the interaction of Psb27 with CP43.

All the Psb27-Asp58 and Psb27-Lys63 mutants did exhibit slower photoautotrophic growth. The D58K, K63A, K63D and K63R mutants displayed altered oxygen evolution rates. The K63D and K63R showed lower F_m levels with DCMU and altered phycocyanin levels as well as altered chlorophyll *a* fluorescence decay kinetics.

6.2.9 The Psb30, PsbK, and PsbZ plays photoprotective role

This study has also shown that the removal of Psb30, PsbK, and PsbZ increases the susceptibility of cells to photodamage indicating that these proteins might play an essential photoprotective role (Fig. 5.12, 5.14 and 5.16). The Psb30, PsbK, and PsbZ

proteins are in close association with the carotenoids (Fig. 5.20). Carotenoids play an important role in photoprotection through the non-photochemical quenching of the excitation energy. Therefore, the deletion of Psb30, PsbK, and PsbZ might disrupt carotenoid binding, potentially inhibiting the energy quenching ability of PS II and increasing the photodamage to PS II. The oxygen-evolution activity of ΔPsb30, ΔPsbK, ΔPsbZ, ΔPsb27:ΔPsb30, ΔPsb27:ΔPsbK and ΔPsb27:ΔPsbZ mutants were lower with DCBQ as the electron acceptor than with DMBQ as the electron acceptor. The ΔPsb27:ΔPsb30 mutant exhibited higher susceptibility to photoinhibition in comparison to the ΔPsb30 strain. Our results on the function of the *psb27* gene product in *Synechocystis* 6803, indicate that Psb27 is likely to be a temporary structural factor that guides PS II assembly and facilitates PS II repair after photoinhibition. Moreover, Psb27 has been shown to be involved in acclimation to fluctuating light conditions in Arabidopsis thaliana (Hou *et al.* 2015). The ΔPsb27 strain exhibited slower PS II recovery from photoinhibition in *Synechocystis* 6803 (Roose and Pakrasi 2008).

Previous studies in *Synechocystis* 6803 double mutants lacking Psb27 and PsbM has been suggested to play an important role in the PS II biogenesis in the ΔPsb27:ΔPsbM mutant and in the recovery of the photodamaged PS II in the ΔPsb27:ΔPsbTc (F.K. Bentley, H. Luo 2008). Studies based on The Psb27-H1 mutant in *Arabidopsis thaliana* exhibited decreased D1 protein levels and PS II activity, when exposed to high light, suggesting that the Psb27 protein is required for the efficient recovery of damaged PS II from photoinhibition (Chen *et al.* 2006).

The chlorophyll *a* fluorescence decay kinetics of LMW single, as well as double deletion strains, was found to be more susceptible to the light-induced damage in comparison to the wild type (Table 5.5 and 5.6). The recovery in the wild type was much more efficient as compared to the LMW proteins single and double deletion strains in the presence and absence of DCMU. However, an insignificant additive effect was seen on susceptibility to photoinhibition by the deletion of the *psb27* gene along with the deletion or inactivation of the *psb30, psbK*, and *psbZ* genes.

Furthermore, BN-PAGE and immunoblot analysis revealed less PS II dimers and PS II monomers in the ΔPsb30, ΔPsbZ, ΔPsb27:ΔPsb30 and ΔPsb27:ΔPsbZ strains relative to the wild type (Fig. 5.19). These results suggest that the lack of Psb30 and PsbZ protein results in lower numbers of PS II dimers and PS II monomers. The relevant

findings of Psb27 mutants and LMW protein deletion strains have been presented in Appendix, Table A-1 briefly.

6.3 A spontaneous mutation discovered at D1-His252 in *Synechocystis* sp. PCC 6803 blocks electron transfer in the quinone-Fe-acceptor complex of PS II

While studying the effects of site-directed mutagenesis of the conserved and cross-linking amino acid residues on the protein-protein interaction of the Psb27 protein with other PS II subunits in the cyanobacterium *Synechocystis* 6803, a Psb27 mutant line, R54E*, exhibited a robust phenotype that was substantially different from the wild type and the other Psb27 mutants. The R54E* strain displayed slow photoautotrophic growth, low PS II oxygen-evolving activity, impaired electron transfer between the Q_A and Q_B primary and secondary electron acceptors of PS II and an elevated and accelerated rise in chlorophyll *a* variable fluorescence. In addition, the BN-PAGE indicated regular PS II assembly in the R54E* mutant and complementation failed to restore the wild-type phenotype. In the past, also, Psb27 deletion strains or Psb27 mutant strains were found to have a high susceptibility to suppressor/secondary mutations (Bentley *et al.* 2008b; Jackson *et al.* 2014). Development of secondary mutations often suggests an alternate way for a cell to cope with the stress experienced because of the introduction of the primary mutation. Therefore, further work to identify the secondary mutation was carried out by performing whole genome sequencing of the R54E* strain. The whole genome sequencing of the R54E* strain revealed a C to A substitution in the *psbA2* gene corresponding to a His252 to Gln substitution in the *psbA2* copy of the D1 PS II reaction centre protein. Therefore, the confirmation that D1:His252 was responsible for the phenotype displayed by R54E* mutant was confirmed by introducing a series of point mutations into a *psbA*-deletion mutant of *Synechocystis* 6803.

6.3.1 R54E* mutant – Impaired photoautotrophic growth and PS II oxygen-evolution

The R54E* mutant and the R54E* complement strain (R54E*:ΔPsb27) displayed a doubling time three times slower than the wild type (Table 4.1), potentially suggesting the presence of impaired PS II centres in the mutants. The oxygen-evolving activity

rates of the R54E* mutant and R54E*:ΔPsb27 strain were found to be inhibited upto 55-60% of the wild-type levels of oxygen evolution in the presence of the both PS II-specific quinone acceptors (DCBQ and DMBQ) suggesting modifications to the Q_B site of PS II. Both of the strains were able to evolve 50-55% of wild-type levels of oxygen evolution in the presence of bicarbonate (Table 4.2).

The ΔPsb27 strain and R54E*:ΔPsb27 mutant displayed more efficient coupling and energy transfer between the antenna protein complexes and the photosystems (PS I and PS II) relative to the wild type potentially suggesting altered PS II structural interactions, as the efficiency of energy transfer from the PBS to PS II was potentially increased. Other reason might be an increase in the number of PS II centres in ΔPsb27 strain and R54E*:ΔPsb27 mutant.

6.3.2 R54E* mutant - Altered PS II acceptor side kinetics

The chlorophyll *a* fluorescence induction curve of the R54E* mutant and the R54E*:ΔPsb27 strain exhibited an initial rapid rise and loss of the J-P levels in the absence of photosynthetic electron transport inhibitor (DCMU) (Fig. 4.5 A). These results suggested that electron transfer between the primary plastoquinone acceptor (Q_A) and the secondary plastoquinone electron acceptor (Q_B) was impaired. The IP rise in R54E* mutant and R54E*:ΔPsb27 strain was higher in comparison to the wild type and the ΔPsb27 strain. It is already known that high levels of chlorophyll *a* fluorescence in the presence of DCMU is due to the closed PS II reaction centre, caused by the presence of high concentration of Q_A^-. The PS II-specific inhibitor, DCMU, binds to the Q_B site and displaces Q_B, and, thus, inhibits electron transport from reduced Q_A to the PQ pool. Another reason for the altered IP rise might be due to increase in the energy transfer from PBS to PS II leading to induction of a high fluorescence state 1 transition (Tsimilli-Michael *et al.* 2009; Kana *et al.* 2012; Stamatakis and Papageorgiou 2014). The SM rise was also absent in the R54E* strain. The SM phase is linked with the state 2 (low fluorescence; a larger antenna in PS I) to state 1 (high fluorescence; a larger antenna in PS II) transition.

While investigating the decay kinetics of chlorophyll *a* fluorescence following single saturating actinic flash, the R54E* mutant and R54E*:ΔPsb27 strain displayed apparently slower electron transfer kinetics between Q_A and Q_B (acceptor side) as

compared to the wild type in the absence of DCMU (Table 4.3 and 4.4). The half-time of the microsecond, as well as the millisecond components, were slower than the wild type. Also, the inhibition of cells by DCMU exhibited near wild-type rates of recombination of Q_A^- with the donor side of PS II potentially indicating that the redox potential of Q_A^-/Q_A couple may not have been changed in R54E* mutant and R54E*:ΔPsb27 strain. However, forward electron transfer was impaired, and therefore parameters governing electron transport to Q_B were altered in both the strains.

6.3.3 R54E*-The role of bicarbonate on the acceptor side of PS II

The effect of displacing bicarbonate by the addition of formate, as well as adding additional bicarbonate on the kinetics of Q_A^- oxidation in R54E* cells and the wild type was investigated by using multiple actinic flashes to turn over the two-electron gate and the S-state cycle of the oxygen-evolving complex. These measurements did not appear to reveal any significant additional impact on the chlorophyll *a* fluorescence decay kinetics of wild type and R54E* cells (Table 4.5). A bicarbonate effect on acceptor-side of electron transport has been known for many years (Govindjee and van Rensen 1978; Shevela *et al.* 2012). Bicarbonate enhances the Hill reaction and also, reverses formate-induced inhibition of electron flow from Q_A^- to the Q_B (Govindjee and van Rensen 1978). Also, there was no major effect of the number of flashes as such on the electron transfer between the plastoquinone sites in wild type and R54E* strains. Overall, there was no change observed in the chlorophyll fluorescence decay kinetics in the presence of bicarbonate.

6.3.4 The susceptibility of R54E* cells to high light

The R54E* strain was found to be more susceptible to high-light stress in the presence of DCBQ and DMBQ in comparison to the wild-type strain (Fig. 4.10 and 4.11). However, both the strains could acclimatise to the stress of the high-light treatment, thus preventing any further decline in the oxygen-evolving activity of PS II. The ability to acclimate under high-light stress has been attributed to *de novo* synthesis of D1 protein and its insertion into inactive intermediates of PS II (Tyystjarvi *et al.* 2001). Reduction in rates of oxygen evolution arises from photodamage of the D1 subunit impairing PS II-specific electron transport. As of a result of a high turnover rate of D1, an efficient repair mechanism has evolved in organisms capable of oxygenic

photosynthesis. New D1 protein precursors are synthesised, processed and inserted into CP43-less monomers reactivating PS II. During the repair process in low light, an enhanced rate of oxygen evolution was observed in wild-type cells potentially suggesting the occurrence of increased protein synthesis during high-light stress. Removal of the high light allowed the synthesis of D1 to recede to normal levels. However, the presence of bicarbonate appeared to protect wild type and the R54E* strain from photoinactivation (Fig. 4.12). The bicarbonate ion may donate protons to the Q_B site, therefore, speeding up the protonation required for complete reduction and dissociation of PQH_2 (Eaton-Rye and Govindjee 1988). Additionally, the presence of bicarbonate may confer increased stability between the Q_A and Q_B sites of PS II facilitating electron transport.

The chlorophyll *a* fluorescence decay kinetics in R54E* strain were also found to be more susceptible to the light-induced damage in comparison to the wild type (Table 4.7 and Table 4.8). The recovery in the wild type was much more efficient as compared to the R54E* strain in the presence and absence of DCMU. The BN-PAGE indicated wild-type levels of PS II assembly in the R54E* mutant (data not shown).

6.3.5 PS I levels in R54E* mutant and R54E*:ΔPsb27 strain

In Fig. 6.2, the 77 K emission spectra obtained using 580 nm light excitation has been presented. All the traces have been normalised to the 665 nm peak (allophycocyanin) to gain more insight towards the effect on the levels of PS I in R54E* mutant and R54E*:ΔPsb27 strain. It can be seen that the PS I levels increased in R54E* mutant and R54E*:ΔPsb27 strain in comparison to the wild type potentially suggesting variations in the PS II to PS I ratio.

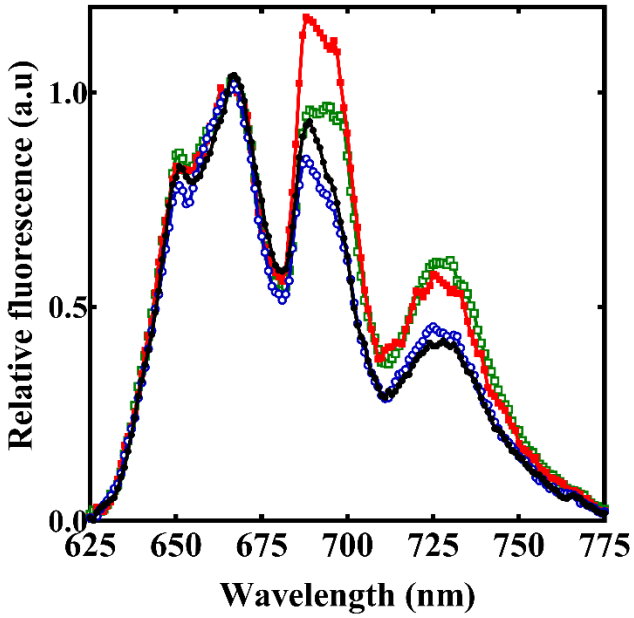

Figure 6.3 Low-temperature (77K) fluorescence absorption spectroscopy of Psb27 mutants. The strains shown are wild type (black, close circles), ΔPsb27 (blue, open circles), R54E* (red, close squares), and R54E*:ΔPsb27 (red, open squares. Spectra obtained using 580 nm excitation light. Spectra shown are the average of four independent experiments are shown normalised to 665 nm emission maxima of phycocyanin.

6.4 Characterisation of a spontaneous mutation affecting the electron transfer in the quinone-Fe-acceptor complex of PS II

6.4.1 Strains with amino acid substitutions at His252 and Ser264 in D1 protein

The confirmation that D1:His252 was responsible for the phenotype displayed by the R54E* mutant was obtained by constructing point mutants in *psbA2* in a *psbA*-deletion strain of *Synechocystis* 6803. Additionally, the D1-Ser264 was also targeted, since D1-Ser264 has also been suggested to be involved in the configuration of the Q_B site and is close to His252 in the X-ray crystallographic structure (Trebst 1991; Umena *et al.* 2011). The D1-H252 and D1-S264 are also suggested to play a supportive role in the stabilisation of the Q_B site (Shevela *et al.* 2012).

An already constructed *Synechocystis* 6803 strain (ΔPsbA) was present in the lab in which each of the members of the *psbA* gene family was deleted. A mutagenesis vector was created to allow the introduction of mutations into the *psbA2* gene copy. The D1 control strain was generated containing a wild-type copy of *psbA2* with a kanamycin-

resistance cassette introduced downstream of the *psbA2* gene. The D1 control strain exhibited a phenotype similar to the wild type strain.

6.4.2 The lower levels of oxygen evolution of D1-His252 and D1-Ser264 mutants

D1-His252 mutants

The oxygen evolution rates were readily inhibited in strains with amino acid substitution at His252 in D1 protein without high-light treatment when the PS II-specific electron acceptors DCBQ and DMBQ were used (Table 4.11). Previously, Lupinkova and co-workers (Lupinkova *et al.* 2002) constructed a D1-H252K mutant in *Synechocystis* 6803, to carry out the studies regarding the involvement of D1-His252 residue of PS II D1 protein in light-induced cross-linking of the polypeptide with the α subunit of cytochrome b_{559}. The D1-His252Leu mutation caused inhibition of the electron transfer between the PS II acceptors Q_A and Q_B and exhibited impaired PS II oxygen-evolving activity. According to our data, the oxygen-evolution rates were inhibited to ~70-80% in the presence of PS II electron acceptor DMBQ in D1-H252 strains in comparison to the wild type and the D1 control strain. The strains with mutations at D1-His252 also exhibited low oxygen-evolution rates with bicarbonate as the electron acceptor, potentially suggesting a modification of the bicarbonate binding in D1-H252 strains due to conformational changes leading to the decreased stability between the Q_A and Q_B sites of PS II facilitating electron transport. However, the oxygen evolution was completely abolished in the case of D1-H252Y strain suggesting non-assembly of PS II reaction centres.

D1-Ser264 mutants

The D1-Ser264 mutants also exhibited inhibited oxygen-evolution activity with PS II-specific artificial quinone acceptors (DCBQ and DMBQ). Interestingly, D1-S264 mutants displayed better oxygen-evolution rates with bicarbonate as the PS II electron acceptor.

6.4.3 D1-His252 and D1-Ser264 mutants - PS II to PS I ratio and energy coupling

In the 77 K fluorescence emission spectra, the mutants D1-H252Y, D1-S264K and D1-S264T cells, when excited with 440 nm light, displayed a merged peak at 685-690 nm

with an increased amplitude, without showing the distinct peaks for emission from CP43 and CP47 (Fig. 4.16 A and B). This peak could be caused by an accumulation of subcomplexes or disturbance of the incorporation of the CP43 protein. The D1-His252Y, D1-Ser264K and D1-Ser264T mutations seem to have a high impact on the correct assembly of PS II. The D1-H252Y, D1-S264K and D1-S264T mutants when excited with 580 nm light (Fig. 4.16 C and D), exhibited increased levels of emission at 685 nm, suggesting an enhanced emission from the terminal emitter of the PBS in the cells and indicating a lower number of PS II centres. This may reflect partial decoupling of the PBS resulting in increased fluorescence from the terminal phycobilin emitters in the PS II mutants and to a lesser extent in the wild type.

6.4.4 D1-His252 and D1-Ser264 mutants – Inhibited electron transfer between Q_A and Q_B site of PS II

The chlorophyll *a* fluorescence induction curve of D1-H252A, D1-H252Q, D1-S264A and D1-S264K cells exhibited an initial rapid rise and loss of the J to P rise in the absence of photosynthetic electron transport inhibitor (DCMU), suggesting impaired electron transfer between the Q_A and Q_B site (Fig. 4.17 A and B). The D1-S264T had low variable fluorescence potentially indicating less PS II centres or damaged PS II centres. The F_m levels in D1-H252A, D1-H252Q, D1-S264A and D1-S264K strain in the presence of DCMU were higher in comparison to the wild type and D1 control strain suggesting an elevated number of closed PS II reaction centres, caused by the presence of high concentrations of Q_A^- (Fig. 4.17 C and D). The SM rise was also low in all the D1-His252 and D1-Ser264 mutant strains compared to wild type and the D1 control strain (Fig. 4.18 A and B). As noted above, the SM phase is linked with state 2 (low fluorescence; a larger antenna in PS I) to state 1 (high fluorescence; a larger antenna in PS II) transition.

The decay kinetics of chlorophyll *a* fluorescence following single saturating actinic flash in the D1-His252, and D1-S264 strains displayed slower electron transfer between Q_A and Q_B site (acceptor side) as compared to the wild type and the D1 control strain in the absence of DCMU (Table 4.12). The microsecond, as well as millisecond component, was higher than the wild type. Also, the D1-His252 mutants exhibited near wild-type rates of recombination of Q_A^- with the donor side of PS II in the presence of DCMU (Table 4.13). The D1-S264A and the D1-S264K mutants displayed impaired

rates of recombination of Q_A^- with the donor side of PS II in the presence of DCMU (Table 4.13). This suggests that the redox potential of Q_A^-/Q_A couple may not have been changed in D1-His252 strains, but may have been altered in the D1-Ser264 mutants. However, forward electron transfer was impaired, and therefore parameters governing electron transport to Q_B were altered in both the strains with amino acid substitutions at His252 and Ser264 in D1 protein.

6.4.4.1 Do D1-His252 and D1-Ser264 potentially play a important role in protonation of Q_B site

The Q_B forms hydrogen bonds with D1-His215 which is seen as a ligand for the non-haem iron and D1-Ser264. The Q_B site is located in a hydrophobic environment formed by D1-Phe211, D1-Met214, D1-Phe255, D1-Phe265 of D1, D2-pheophytin and lipids. Many hydrogen-bond networks are found linking the bicarbonate ion to the stromal (or cytosolic) solution and are expected to be present for the transfer of protons. The amino acid residues D1-Tyr246, D1-Ser268, D1-His272 and D1-His215 surrounding the bicarbonate ion have been hypothesised to play an important role in the transfer of protons via water molecules to the site of bicarbonate and the reduced Q_B (Linke and Ho 2014). Any changes in any these residues might lead to the disturbance of the positions of the water molecules, and the disruption of the hydrogen-bond networks (Takahashi *et al.* 2009; Saito *et al.* 2013). Also, it is suggested that D1-His252 and D1-Ser264 forms a hydrogen bond network with the Q_B site. As D1-His252 is located in a hydrophilic area, protons might be transferred to Q_B through D1-His252 and D1-Ser264. It can be proposed that the first proton to protonate Q_B^- is taken up through D1-His252 and D1-Ser264, and the second proton is transferred via bicarbonate to D1-His272 and D1-His215, and, finally to Q_B through the hydrogen bond network (Shevela *et al.* 2012; Saito *et al.* 2013). Therefore, further functional studies need to be performed to analyse the order of these protonation events. Recently, it was shown that there might be an alternative proton paths newly created due to conformational changes. Recent high-resolution structures of PS II by Suga and coworkers (Suga *et al.* 2017) led to the observation of visible changes around the Q_B/non-haem iron. The changes around the Q_B/non-haem iron region reflected the electron and proton transfers induced by the two-flash illumination (Suga *et al.* 2017).

Characterisation of the D1-His252 and D1-Ser264 mutants *in vivo* revealed a block of the electron transfer between the PS II electron acceptors Q_A and Q_B probably indicating a general requirement of the histidine residue at the position 252 and serine residue in the position 264 for the proper function of the PS II acceptor side. PS II utilises light to drive oxidation of water and reduction of plastoquinone (PQ). Reduction of PQ involves working of Q_A and Q_B (PQ cofactors), in series. Q_A is a one-electron carrier, whereas Q_B forms QBH_2 by undergoing sequential reduction and protonation. The QBH_2 then exchanges with PQ from the pool in the membrane. Based on the atomic coordinates of the PS II crystal structure and the different computational models and simulations proposed about the route of the proton transfer at the acceptor side of PS II, we would like to suggest that the initial proton transfer to Q_B might occur from the protonated, D1-His252 to Q_B^- via D1-Ser264. The second proton transfer might occur from D1-His215 to $Q_B^{2-}(H^+)$ via a hydrogen bond, resulting in the formation of Q_BH_2. The pathway for reprotonation of D1-His215 might involve D1-Tyr246, bicarbonate, and water in the vicinity of the Q_B site. The relevant findings of strains with amino acid substitutions at D1-His252 and D1-Ser264, in brief, has been presented in Appendix, Table A-2.

6.5 Conclusion and future perspectives

The amino acid substitutions of conserved as well as cross-linking residues in Psb27 protein displayed normal photoautotrophic growth and oxygen-evolving activity. However, the Psb27 mutants showed insignificantly lower oxygen-evolving activity in the presence of bicarbonate suggesting PS I levels may have been altered, so as to affect whole chain rates. A further reason might be that these mutations are affecting the PS I levels or the activity of PS I, as recently an interaction between Psb27 and PS I was observed by yeast two-hybrid analyses using the split-ubiquitin system (Pasch *et al.* 2005; Komenda *et al.* 2012a). The Psb27 point mutants displayed more efficient coupling and energy transfer between the antenna protein complexes and the photosystems (PS I and PS II) suggesting an accumulation of bound PBS or higher number of PS II centres. The Psb27 strains exhibited wild-type levels of fluorescence induction kinetics as well as chlorophyll *a* fluorescence decay kinetics, potentially indicating normal electron transfer at the acceptor and donor sides of PS II. It will be useful to isolate PS II from Psb27 mutants with conserved amino acid or cross-linking

amino acid substitutions and to probe for LMW proteins surrounding CP43 protein to study if the deletion of Psb27 affects the composition of the other polypeptides belonging to the CP43-precomplex.

The CP43 protein complex and recombinant Psb27 can be isolated to study the structural basis of the interaction. The CP43 protein can be his-tagged followed by purification from the Psb27 deletion strain or Psb27 mutants of *Synechocystis* 6803 (Boehm *et al.* 2011). However, the R54E, R94E, D58A and D58K strains were believed to alter the light acclimation processes that enlarge or diminish the size of light-harvesting antennae that feed excitation to the core complexes of PS II and PS I. Overall, the Psb27 protein was found to be dispensable for the normal functioning and assembly of PS II in *Synechocystis* 6803. Photodamage and recovery assays should be carried out for Psb27 mutants using pulse-chase radiolabelling experiments enabling us the direct visualisation of D1-turnover during the assays and will provide insights into the effect of these specific amino acid substitutions towards the photoinhibition and recovery process of PS II. Further experiments should focus on the creation of Psb27 mutants containing a combination of critical amino acid substitutions (Psb27-Asp58 and Psb27-Lys63) to contribute to further understanding of the Psb27 protein-protein interactions in PS II assembly and repair mechanism. Some putative high-molecular-weight PS II assembly intermediates were identified in the D14A, R54E, Y78H, D58E, K63A, K63D and K63R *Synechocystis* 6803 mutants through the separation of native protein complexes by BN-PAGE. The protein composition of these potential assembly intermediates needs to be assessed through separation in the second dimension to gain a better understanding of the role of Psb27 protein in the assembly process of cyanobacterial PS II.

Analysis of D1-His252 and D1-Ser264 mutants indicated impaired oxygen-evolving capacity as compared to the wild type and the D1 control strain. The mutations at D1-His252 and D1-Ser264 lead to perturbed photosynthetic electron transport. Future research could investigate the mechanism of the susceptibility to the photodamage in these D1-His252 and Ser-264 mutants. The assembly of PS II complexes should be studied with the help of BN-PAGE. The His252 to Tyr mutation in the D1-H252Y mutant was found to be lethal with very low PS II assembly. Therefore, to confirm the phenotype whole genome sequencing of D1-H252Y strain can be performed or wild-type copy of *psbA2* can be introduced again through a complementation test.

In *Synechocystis* 6803, the ΔPsbK and ΔPsbZ strains exhibited delayed photoautotrophic growth in comparison to the ΔPsb27:ΔPsbK and ΔPsb27:ΔPsbZ mutants. The removal of LMW proteins did little to alter the oxygen-evolving activity of PS II. There was no impairment in the donor side or acceptor side reactions of PS II in the ΔPsb30, ΔPsbK and ΔPsbZ mutants nor in the corresponding double mutants lacking Psb27 as measured by chlorophyll *a* fluorescence decay studies. Requirements for the Psb30, PsbK and PsbZ subunits are less strict, and the main functional requirements for these proteins appear to be in protecting PS II from the photoinhibitory damage of high light. Further experiments should focus on the creation of mutants lacking different combinations of the LMW proteins of the CP43 pre-assembly complex to contribute to further understanding of the protein-protein and protein-cofactor interactions in this complex. In particular, it will be interesting to explore the reduced levels of PS II monomers in the ΔPsbZ and ΔPsb27:ΔPsbZ strain.

References

Adir N, Zer H, Shochat S, Ohad I. 2003. Photoinhibition - a historical perspective. *Photosynth Res* 76: 343-370.

Ago H, et al. 2016. Novel Features of Eukaryotic Photosystem II Revealed by Its Crystal Structure Analysis from a Red Alga. *J Biol Chem* 291: 5676-5687.

Allen JF, Forsberg J. 2001. Molecular recognition in thylakoid structure and function. *Trends Plant Sci* 6: 317-326.

Anbudurai PR, Mor TS, Ohad I, Shestakov SV, Pakrasi HB. 1994. The *ctpA* gene encodes the C-terminal processing protease for the D1 protein of the photosystem II reaction center complex. *Proc Natl Acad Sci U S A* 91: 8082-8086.

Aoi M, Kashino Y, Ifuku K. 2014. Function and association of CyanoP in photosystem II of *Synechocystis* sp. PCC 6803. *Res Chem Intermediat* 40: 3209-3217.

Aro EM, McCaffery S, Anderson JM. 1993a. Photoinhibition and D1 Protein Degradation in Peas Acclimated to Different Growth Irradiances. *Plant Physiol* 103: 835-843.

Aro EM, Virgin I, Andersson B. 1993b. Photoinhibition of Photosystem II. Inactivation, protein damage and turnover. *Biochim Biophys Acta* 1143: 113-134.

Balint I, Bhattacharya J, Perelman A, Schatz D, Moskovitz Y, Keren N, Schwarz R. 2006. Inactivation of the extrinsic subunit of photosystem II, PsbU, in *Synechococcus* PCC 7942 results in elevated resistance to oxidative stress. *FEBS Lett* 580: 2117-2122.

Barber J. 2006. Photosystem II: an enzyme of global significance. *Biochem Soc Trans* 34: 619-631.

Barry BA, Babcock GT. 1987. Tyrosine radicals are involved in the photosynthetic oxygen-evolving system. *Proc Natl Acad Sci U S A* 84: 7099-7103.

Bečková M, Gardian Z, Yu J, Konik P, Nixon PJ, Komenda J. 2017. Association of Psb28 and Psb27 Proteins with PS II-PS I Supercomplexes upon Exposure of *Synechocystis* sp. PCC 6803 to High Light. *Mol Plant* 10: 62-72.

Bentley FK, Luo H, Dilbeck P, Burnap RL, Eaton-Rye JJ. 2008a. Effects of Inactivating *psbM* and *psbT* on Photodamage and Assembly of Photosystem II in *Synechocystis* sp. PCC 6803. *J Biochem* 47: 11637-11646.

Bialek W, Wen S, Michoux F, Beckova M, Komenda J, Murray JW, Nixon PJ. 2013. Crystal structure of the Psb28 accessory factor of *Thermosynechococcus elongatus* photosystem II at 2.3 A. *Photosynth Res* 117: 375-383.

Birnboim HC, Doly J. 1979. A rapid alkaline extraction procedure for screening recombinant plasmid DNA. *Nucleic Acids Res* 7: 1513-1523.

Bishop CL, Ulas S, Baena-Gonzalez E, Aro EM, Purton S, Nugent JH, Maenpaa P. 2007. The PsbZ subunit of Photosystem II in *Synechocystis* sp. PCC 6803 modulates electron flow through the photosynthetic electron transfer chain. *Photosynth Res* 93: 139-147.

Boehm M, Romero E, Reisinger V, Yu J, Komenda J, Eichacker LA, Dekker JP, Nixon PJ. 2011. Investigating the early stages of photosystem II assembly in *Synechocystis* sp. PCC 6803: isolation of CP47 and CP43 complexes. *J Biol Chem* 286: 14812-14819.

Boehm M, Yu J, Krynicka V, Barker M, Tichy M, Komenda J, Nixon PJ, Nield J. 2012a. Subunit organization of a *Synechocystis* hetero-oligomeric thylakoid FtsH complex involved in photosystem II repair. *Plant Cell* 24: 3669-3683.

Boehm M, Yu J, Reisinger V, Beckova M, Eichacker LA, Schlodder E, Komenda J, Nixon PJ. 2012b. Subunit composition of CP43-less photosystem II complexes of *Synechocystis* sp. PCC 6803: implications for the assembly and repair of photosystem II. *Philos Trans R Soc Lond B Biol Sci* 367: 3444-3454.

Boisvert S, Joly D, Carpentier R. 2006. Quantitative analysis of the experimental O-J-I-P chlorophyll fluorescence induction kinetics. Apparent activation energy and origin of each kinetic step. *FEBS J* 273: 4770-4777.

Bolivar F. 1978. Construction and characterization of new cloning vehicles. III. Derivatives of plasmid pBR322 carrying unique *Eco* RI sites for selection of *Eco* RI generated recombinant DNA molecules. *Gene* 4: 121-136.

Bonaventura C, Myers J. 1969. Fluorescence and oxygen evolution from C*hlorella pyrenoidosa*. *Biochim Biophys Acta* 189: 366-383.

Bricker TM, Frankel LK. 2002. The structure and function of CP47 and CP43 in Photosystem II. *Photosynth Res* 72: 131-146.

Bricker TM, Roose JL, Fagerlund RD, Frankel LK, Eaton-Rye JJ. 2012. The extrinsic proteins of Photosystem II. *Biochim Biophys Acta* 1817: 121-142.

Bruce D, Brimble S, Bryant DA. 1989. State transitions in a phycobilisome-less mutant of the cyanobacterium *Synechococcus* sp. PCC 7002. *Biochim Biophys Acta* 974: 66-73.

Burnap RL, Shen JR, Jursinic PA, Inoue Y, Sherman LA. 1992. Oxygen yield and thermoluminescence characteristics of a cyanobacterium lacking the manganese-stabilizing protein of photosystem II. *J Biochem* 31: 7404-7410.

Burnap RL, Sherman LA. 1991. Deletion mutagenesis in *Synechocystis* sp. PCC6803 indicates that the Mn-stabilizing protein of photosystem II is not essential for O_2 evolution. *J Biochem* 30: 440-446.

Cai YP, Wolk CP. 1990. Use of a conditionally lethal gene in *Anabaena* sp. strain PCC 7120 to select for double recombinants and to entrap insertion sequences. *J Bacteriol* 172: 3138-3145.

Cardona T. 2015. A fresh look at the evolution and diversification of photochemical reaction centers. *Photosynth Res* 126: 111-134.

Cardona T, Murray JW, Rutherford AW. 2015. Origin and Evolution of Water Oxidation before the Last Common Ancestor of the Cyanobacteria. *Mol Biol Evol* 32: 1310-1328.

Cardona T, Sedoud A, Cox N, Rutherford AW. 2012. Charge separation in photosystem II: a comparative and evolutionary overview. *Biochim Biophys Acta* 1817: 26-43.

Chen H, Zhang D, Guo J, Wu H, Jin M, Lu Q, Lu C, Zhang L. 2006. A Psb27 homologue in Arabidopsis thaliana is required for efficient repair of photodamaged photosystem II. *Plant Mol Biol* 61: 567-575.

Chu HA, Nguyen AP, Debus RJ. 1995. Amino acid residues that influence the binding of manganese or calcium to photosystem II. 2. The carboxy-terminal domain of the D1 polypeptide. *J Biochem* 34: 5859-5882.

Cinco RM, McFarlane Holman KL, Robblee JH, Yano J, Pizarro SA, Bellacchio E, Sauer K, Yachandra VK. 2002. Calcium EXAFS establishes the Mn-Ca cluster in the oxygen-evolving complex of photosystem II. *J Biochem* 41: 12928-12933.

Clausen J, Winkler S, Hays AM, Hundelt M, Debus RJ, Junge W. 2001. Photosynthetic water oxidation in *Synechocystis* sp. PCC6803: mutations D1-E189K, R and Q are without influence on electron transfer at the donor side of photosystem II. *Biochim Biophys Acta* 1506: 224-235.

Cormann KU, Bangert JA, Ikeuchi M, Rogner M, Stoll R, Nowaczyk MM. 2009. Structure of Psb27 in solution: implications for transient binding to photosystem II during biogenesis and repair. *J Biochem* 48: 8768-8770.

Cormann KU, Bartsch M, Rogner M, Nowaczyk MM. 2014. Localization of the CyanoP binding site on photosystem II by surface plasmon resonance spectroscopy. *Front Plant Sci* 5: 595.

Cormann KU, Moller M, Nowaczyk MM. 2016. Critical Assessment of Protein Cross-Linking and Molecular Docking: An Updated Model for the Interaction Between Photosystem II and Psb27. *Front Plant Sci* 7: 157.

Cser K, Vass I. 2007. Radiative and non-radiative charge recombination pathways in Photosystem II studied by thermoluminescence and chlorophyll fluorescence in the cyanobacterium *Synechocystis* 6803. *Biochim Biophys Acta* 1767: 233-243.

Danielsson R, Suorsa M, Paakkarinen V, Albertsson PA, Styring S, Aro EM, Mamedov F. 2006. Dimeric and monomeric organization of photosystem II. Distribution of five distinct complexes in the different domains of the thylakoid membrane. *J Biol Chem* 281: 14241-14249.

De Marais DJ. 2000. Evolution. When did photosynthesis emerge on Earth? *Sci* 289: 1703-1705.

de Paula JC, Li PM, Miller AF, Wu BW, Brudvig GW. 1986. Effect of the 17- and 23-kilodalton polypeptides, calcium, and chloride on electron transfer in photosystem II. *J Biochem* 25: 6487-6494.

Debus RJ, Barry BA, Babcock GT, McIntosh L. 1988a. Site-directed mutagenesis identifies a tyrosine radical involved in the photosynthetic oxygen-evolving system. *Proc Natl Acad Sci U S A* 85: 427-430.

Debus RJ, Barry BA, Sithole I, Babcock GT, McIntosh L. 1988b. Directed mutagenesis indicates that the donor to P^{+}_{680} in photosystem II is tyrosine-161 of the D1 polypeptide. *J Biochem* 27: 9071-9074.

Debus RJ, Campbell KA, Peloquin JM, Pham DP, Britt RD. 2000a. Histidine 332 of the D1 polypeptide modulates the magnetic and redox properties of the manganese cluster and tyrosine $Y_{(Z)}$ in photosystem II. *J Biochem* 39: 470-478.

Debus RJ, Campbell KA, Pham DP, Hays AM, Britt RD. 2000b. Glutamate 189 of the D1 polypeptide modulates the magnetic and redox properties of the manganese cluster and tyrosine $Y_{(Z)}$ in photosystem II. *J Biochem* 39: 6275-6287.

Demmig-Adams B, Adams WW, 3rd. 1990. The carotenoid zeaxanthin and 'high-energy-state quenching' of chlorophyll fluorescence. *Photosynth Res* 25: 187-197.

Diner BA, Petrouleas V, Wendoloski JJ. 1991. The iron-quinone electron-acceptor complex of photosystem II. *Physiologia Plantarum* 81: 423-436.

Diner BA, Rappaport F. 2002. Structure, dynamics, and energetics of the primary photochemistry of photosystem II of oxygenic photosynthesis. *Annu Rev Plant Biol* 53: 551-580.

Dismukes GC, Siderer Y. 1981. Intermediates of a polynuclear manganese center involved in photosynthetic oxidation of water. *Proc Natl Acad Sci U S A* 78: 274-278.

Dobakova M, Sobotka R, Tichy M, Komenda J. 2009. Psb28 protein is involved in the biogenesis of the photosystem II inner antenna CP47 (PsbB) in the cyanobacterium *Synechocystis* sp. PCC 6803. *Plant Physiol* 149: 1076-1086.

Dobakova M, Tichy M, Komenda J. 2007. Role of the PsbI protein in photosystem II assembly and repair in the cyanobacterium *Synechocystis* sp. PCC 6803. *Plant Physiol* 145: 1681-1691.

Eaton-Rye JJ, Govindjee. 1988. Electron transfer through the quinone acceptor complex of Photosystem II in bicarbonate-depleted spinach thylakoid membranes as a function of actinic flash number and frequency. *Biochim Biophys Acta - Bioenergetics* 935: 237-247.

Eaton-Rye JJ, Shand JA, Nicoll WS. 2003. pH-dependent photoautotrophic growth of specific photosystem II mutants lacking lumenal extrinsic polypeptides in *Synechocystis* PCC 6803. *FEBS Lett* 543: 148-153.

Enami I, Okumura A, Nagao R, Suzuki T, Iwai M, Shen JR. 2008. Structures and functions of the extrinsic proteins of photosystem II from different species. *Photosynth Res* 98: 349-363.

Enami I, Yoshihara S, Tohri A, Okumura A, Ohta H, Shen J-R. 2000. Cross-Reconstitution of Various Extrinsic Proteins and Photosystem. *Plant and Cell Physiol* 41: 1354-1364.

Ermakova-Gerdes S, Vermaas W. 1999. Inactivation of the open reading frame *slr0399* in *Synechocystis* sp. PCC 6803 functionally complements mutations near the $Q_{(A)}$ niche of photosystem II. A possible role of Slr0399 as a chaperone for quinone binding. *J Biol Chem* 274: 30540-30549.

Fagerlund RD, Eaton-Rye JJ. 2011a. The lipoproteins of cyanobacterial photosystem II. *J Photochem Photobiol B* 104: 191-203.

Ferreira KN, Iverson TM, Maghlaoui K, Barber J, Iwata S. 2004. Architecture of the photosynthetic oxygen-evolving center. *Sci* 303: 1831-1838.

Fey H, Piano D, Horn R, Fischer D, Schmidt M, Ruf S, Schröder WP, Bock R, Büchel C. 2008. Isolation of highly active photosystem II core complexes with a His-tagged Cyt b_{559} subunit from transplastomic tobacco plants. *Biochim Biophys Acta - Bioenergetics* 1777: 1501-1509.

Folea IM, Zhang P, Aro EM, Boekema EJ. 2008. Domain organization of photosystem II in membranes of the cyanobacterium *Synechocystis* PCC6803 investigated by electron microscopy. *FEBS Lett* 582: 1749-1754.

Forti G, Caldiroli G. 2005. State transitions in *Chlamydomonas reinhardtii*. The role of the Mehler reaction in state 2-to-state 1 transition. *Plant Physiol* 137: 492-499.

Frazao C, Enguita FJ, Coelho R, Sheldrick GM, Navarro JA, Hervas M, De la Rosa MA, Carrondo MA. 2001. Crystal structure of low-potential cytochrome c_{549} from *Synechocystis* sp. PCC 6803 at 1.21 A resolution. *J Biol Inorg Chem* 6: 324-332.

Fufezan C, Gross CM, Sjodin M, Rutherford AW, Krieger-Liszkay A, Kirilovsky D. 2007. Influence of the redox potential of the primary quinone electron acceptor on photoinhibition in photosystem II. *J Biol Chem* 282: 12492-12502.

Funk C. 2000. Functional analysis of the PsbX protein by deletion of the corresponding gene in *Synechocystis* sp. PCC 6803. *Plant Mol Biol* 44: 815-827.

Funk C, Vermaas W. 1999. A cyanobacterial gene family coding for single-helix proteins resembling part of the light-harvesting proteins from higher plants. *J Biochem* 38: 9397-9404.

Garrison E, Marth G. 2012. [Haplotype-based variant detection from short-read sequencing]. *Genomics*.

Gau AE, Thole HH, Sokolenko A, Altschmied L, Hermann RG, Pistorius EK. 1998. PsbY, a novel manganese-binding, low-molecular-mass protein associated with photosystem II. *Mol Gen Genet* 260: 56-68.

Gay P, Le Coq D, Steinmetz M, Berkelman T, Kado CI. 1985. Positive selection procedure for entrapment of insertion sequence elements in gram-negative bacteria. *J Bacteriol* 164: 918-921.

Gay P, Le Coq D, Steinmetz M, Ferrari E, Hoch JA. 1983. Cloning structural gene sacB, which codes for exoenzyme levansucrase of *Bacillus subtilis*: expression of the gene in *Escherichia coli*. *J Bacteriol* 153: 1424-1431.

Golden SS. 1995. Light-responsive gene expression in cyanobacteria. *J Bacteriol* 177: 1651-1654.

Goremykin VV, Hirsch-Ernst KI, Wolfl S, Hellwig FH. 2003. Analysis of the Amborella trichopoda chloroplast genome sequence suggests that *Amborella* is not a basal angiosperm. *Mol Biol Evol* 20: 1499-1505.

Govindje e. 1995. Sixty-Three Years Since Kautsky: Chlorophyll <I>a</I> Fluorescence. *Functional Plant Biol* 22: 131-160.

Govindjee, van Rensen JJ. 1978. Bicarbonate effects on the electron flow in isolated broken chloroplasts. *Biochim Biophys Acta* 505: 183-213.

Graan T, Ort DR. 1986. Quantitation of 2,5-dibromo-3-methyl-6-isopropyl-p-benzoquinone binding sites in chloroplast membranes: evidence for a functional dimer of the cytochrome b_6f complex. *Arch Biochem Biophys* 248: 445-451.

Grossman AR, Bhaya D, Apt KE, Kehoe DM. 1995. Light-harvesting complexes in oxygenic photosynthesis: diversity, control, and evolution. *Annu Rev Genet* 29: 231-288.

Guskov A, Kern J, Gabdulkhakov A, Broser M, Zouni A, Saenger W. 2009. Cyanobacterial photosystem II at 2.9-Å resolution and the role of quinones, lipids, channels and chloride. *Nat Struct Mol Biol* 16: 334-342.

Hakala M, Tuominen I, Keranen M, Tyystjarvi T, Tyystjarvi E. 2005. Evidence for the role of the oxygen-evolving manganese complex in photoinhibition of Photosystem II. *Biochim Biophys Acta* 1706: 68-80.

Hankamer B, Morris E, Nield J, Carne A, Barber J. 2001. Subunit positioning and transmembrane helix organisation in the core dimer of photosystem II. *FEBS Lett* 504: 142-151.

He Q, Dolganov N, Bjorkman O, Grossman AR. 2001. The high light-inducible polypeptides in *Synechocystis* PCC6803. Expression and function in high light. *J Biol Chem* 276: 306-314.

Henmi T, Iwai M, Ikeuchi M, Kawakami K, Shen JR, Kamiya N. 2008. X-ray crystallographic and biochemical characterizations of a mutant photosystem II complex from *Thermosynechococcus vulcanus* with the *psbTc* gene inactivated by an insertion mutation. *J Synchrotron Radiat* 15: 304-307.

Hernandez-Prieto MA, Semeniuk TA, Giner-Lamia J, Futschik ME. 2016. The Transcriptional Landscape of the Photosynthetic Model Cyanobacterium *Synechocystis* sp. PCC6803. *Sci Rep* 6: 22168.

Hohmann-Marriott MF, Blankenship RE. 2011. Evolution of photosynthesis. *Annu Rev Plant Biol* 62: 515-548.

Homann PH. 2002. Chloride and calcium in Photosystem II: from effects to enigma. *Photosynth Res* 73: 169-175.

Hou X, Fu A, Garcia VJ, Buchanan BB, Luan S. 2015. PSB27: A thylakoid protein enabling *Arabidopsis* to adapt to changing light intensity. *Proc Natl Acad Sci U S A* 112: 1613-1618.

Ifuku K, Ido K, Sato F. 2011. Molecular functions of PsbP and PsbQ proteins in the photosystem II supercomplex. *J Photochem Photobiol B: Biol* 104: 158-164.

Ikeuchi M, Eggers B, Shen GZ, Webber A, Yu JJ, Hirano A, Inoue Y, Vermaas W. 1991. Cloning of the *psbK* gene from *Synechocystis* sp. PCC 6803 and characterization of photosystem II in mutants lacking PS II-K. *J Biol Chem* 266: 11111-11115.

Ikeuchi M, Inoue Y. 1988. A new photosystem II reaction center component (4.8 kDa protein) encoded by chloroplast genome. *FEBS Lett* 241: 99-104.

Ikeuchi M, Koike H, Inoue Y. 1989. N-terminal sequencing of low-molecular-mass components in cyanobacterial photosystem II core complex Two components correspond to unidentified open reading frames of plant chloroplast DNA. *FEBS Lett* 253: 178-182.

Ikeuchi M, Shukla VK, Pakrasi HB, Inoue Y. 1995a. Directed inactivation of the *psbI* gene does not affect photosystem II in the cyanobacterium *Synechocystis* sp. PCC 6803. *Mol. Gen. Genet*. 249: 622-628

Ikeuchi M, Tabata S. 2001. *Synechocystis* sp. PCC 6803 - a useful tool in the study of the genetics of cyanobacteria. *Photosynth Res* 70: 73-83.

Inagaki N, Yamamoto Y, Satoh K. 2001. A sequential two-step proteolytic process in the carboxyl-terminal truncation of precursor D1 protein in *Synechocystis* sp. PCC6803. *FEBS Lett* 509: 197-201.

Inoue-Kashino N, Kashino Y, Satoh K, Terashima I, Pakrasi HB. 2005. PsbU provides a stable architecture for the oxygen-evolving system in cyanobacterial photosystem II. *J Biochem* 44: 12214-12228.

Inoue-Kashino N, Kashino Y, Takahashi Y. 2011. Psb30 is a photosystem II reaction center subunit and is required for optimal growth in high light in C*hlamydomonas reinhardtii*. *J Photochem Photobiol B* 104: 220-228.

Inoue-Kashino N, Takahashi T, Ban A, Sugiura M, Takahashi Y, Satoh K, Kashino Y. 2008. Evidence for a stable association of Psb30 (Ycf12) with photosystem II core complex in the cyanobacterium *Synechocystis* sp. PCC 6803. *Photosynth Res* 98: 323-335.

Ivleva TP, Merzhanov AG. 2001. Structure and variability of spinning reaction waves in three-dimensional excitable media. *Phys Rev E Stat Nonlin Soft Matter Phys* 64: 036218.

Iwai M, Katoh H, Katayama M, Ikeuchi M. 2004. PS II-Tc protein plays an important role in dimerization of photosystem II. *Plant Cell Physiol* 45: 1809-1816.

Iwai M, Suzuki T, Dohmae N, Inoue Y, Ikeuchi M. 2007. Absence of the PsbZ subunit prevents association of PsbK and Ycf12 with the PSII complex in the thermophilic cyanobacterium *Thermosynechococcus elongatus* BP-1. *Plant Cell Physiol* 48: 1758-1763.

Iwai M, Suzuki T, Kamiyama A, Sakurai I, Dohmae N, Inoue Y, Ikeuchi M. 2010. The PsbK subunit is required for the stable assembly and stability of other small subunits in the PSII complex in the thermophilic cyanobacterium *Thermosynechococcus elongatus* BP-1. *Plant Cell Physiol* 51: 554-560.

Jackson SA, Eaton-Rye JJ. 2015. Characterization of a *Synechocystis* sp. PCC 6803 double mutant lacking the CyanoP and Ycf48 proteins of Photosystem II. *Photosyn Res* 124: 217-229.

Jackson SA, Hervey JRD, Dale AJ, Eaton-Rye JJ. 2014. Removal of both Ycf48 and Psb27 in *Synechocystis* sp. PCC 6803 disrupts Photosystem II assembly and alters Q_A^- oxidation in the mature complex. *FEBS Lett* 588: 3751-3760.

Joshua S, Mullineaux CW. 2004. Phycobilisome diffusion is required for light-state transitions in cyanobacteria. *Plant Physiol* 135: 2112-2119.

Kamiya N, Shen JR. 2003. Crystal structure of oxygen-evolving photosystem II from *Thermosynechococcus vulcanus* at 3.7-Å resolution. *Proc Natl Acad Sci U S A* 100: 98-103.

Kana R, Kotabova E, Komarek O, Sediva B, Papageorgiou GC, Govindjee, Prasil O. 2012. The slow S to M fluorescence rise in cyanobacteria is due to a state 2 to state 1 transition. *Biochim Biophys Acta* 1817: 1237-1247.

Kaneko T, Matsubayashi T, Sugita M, Sugiura M. 1996a. Physical and gene maps of the unicellular cyanobacterium *Synechococcus* sp. strain PCC6301 genome. *Plant Molr Biol* 31: 193-201.

Kaneko T, Nakamura Y, Sasamoto S, Watanabe A, Kohara M, Matsumoto M, Shimpo S, Yamada M, Tabata S. 2003. Structural Analysis of Four Large Plasmids Harboring in a Unicellular Cyanobacterium, *Synechocystis* sp. PCC 6803. *DNA Res* 10: 221-228.

Kaneko T, et al. 1996b. Sequence analysis of the genome of the unicellular cyanobacterium *Synechocystis* sp. strain PCC 6803. II. Sequence determination of the entire genome and assignment of potential protein-coding regions. *DNA Res* 3: 109-136.

Kashino Y, Koike H, Yoshio M, Egashira H, Ikeuchi M, Pakrasi HB, Satoh K. 2002a. Low-molecular-mass polypeptide components of a photosystem II preparation from the thermophilic cyanobacterium *Thermosynechococcus vulcanus*. *Plant Cell Physiol* 43: 1366-1373.

Kashino Y, Lauber WM, Carroll JA, Wang Q, Whitmarsh J, Satoh K, Pakrasi HB. 2002b. Proteomic analysis of a highly active photosystem II preparation from the cyanobacterium *Synechocystis* sp. PCC 6803 reveals the presence of novel polypeptides. *J Biochemistry* 41: 8004-8012.

Kashino Y, Takahashi T, Inoue-Kashino N, Ban A, Ikeda Y, Satoh K, Sugiura M. 2007. Ycf12 is a core subunit in the photosystem II complex. *Biochim Biophys Acta* 1767: 1269-1275.

Kasting JF, Siefert JL. 2002. Life and the evolution of Earth's atmosphere. *Sci* 296: 1066-1068.

Katoh H, Ikeuchi M. 2001. Targeted disruption of *psbX* and biochemical characterization of photosystem II complex in the thermophilic cyanobacterium *Synechococcus elongatus*. *Plant Cell Physiol* 42: 179-188.

Keren N, Berg A, van Kan PJ, Levanon H, Ohad I. 1997. Mechanism of photosystem II photoinactivation and D1 protein degradation at low light: the role of back electron flow. *Proc Natl Acad Sci U S A* 94: 1579-1584.

Keren N, Gong H, Ohad I. 1995. Oscillations of reaction center II-D1 protein degradation in vivo induced by repetitive light flashes. Correlation between the level of RCII-Q_B^- and protein degradation in low light. *J Biol Chem* 270: 806-814.

Keren N, Ohkawa H, Welsh EA, Liberton M, Pakrasi HB. 2005. Psb29, a conserved 22-kD protein, functions in the biogenesis of Photosystem II complexes in *Synechocystis* and *Arabidopsis*. *Plant Cell* 17: 2768-2781.

Kerfeld CA, Sawaya MR, Bottin H, Tran KT, Sugiura M, Cascio D, Desbois A, Yeates TO, Kirilovsky D, Boussac A. 2003. Structural and EPR characterization of the soluble form of cytochrome *c*-550 and of the *psbV2* gene product from the cyanobacterium *Thermosynechococcus elongatus*. *Plant Cell Physiol* 44: 697-706.

Kern J, Renger G. 2007. Photosystem II: structure and mechanism of the water:plastoquinone oxidoreductase. *Photosynth Res* 94: 183-202.

Kim SH, Gregor W, Peloquin JM, Brynda M, Britt RD. 2004. Investigation of the calcium-binding site of the oxygen evolving complex of photosystem II using 87Sr ESEEM spectroscopy. *J Am Chem Soc* 126: 7228-7237.

Kimura A, Eaton-Rye JJ, Morita EH, Nishiyama Y, Hayashi H. 2002. Protection of the oxygen-evolving machinery by the extrinsic proteins of photosystem II is essential for development of cellular thermotolerance in *Synechocystis* sp. PCC 6803. *Plant Cell Physiol* 43: 932-938.

Kirilovsky D. 2015. Modulating energy arriving at photochemical reaction centers: orange carotenoid protein-related photoprotection and state transitions. *Photosynth Res* 126: 3-17.

Kless H, Oren-Shamir M, Malkin S, McIntosh L, Edelman M. 1994. The D-E region of the D1 protein is involved in multiple quinone and herbicide interactions in photosystem II. *J Biochem* 33: 10501-10507.

Klinkert B, Ossenbuhl F, Sikorski M, Berry S, Eichacker L, Nickelsen J. 2004. PratA, a periplasmic tetratricopeptide repeat protein involved in biogenesis of photosystem II in *Synechocystis* sp. PCC 6803. *J Biol Chem* 279: 44639-44644.

Kobayashi M, Okada K, Ikeuchi M. 2005a. A suppressor mutation in the alpha-phycocyanin gene in the light/glucose-sensitive phenotype of the *psbK*-disruptant of the cyanobacterium *Synechocystis* sp. PCC 6803. *Plant Cell Physiol* 46: 1561-1567.

Kok B, Forbush B, McGloin M. 1970. Cooperation of charges in photosynthetic O_2 evolution-I. A linear four step mechanism. *Photochem Photobiol* 11: 457-475.

Komenda J, Barber J. 1995. Comparison of *psbO* and *psbH* deletion mutants of *Synechocystis* PCC 6803 indicates that degradation of D1 protein is regulated by the Q_B site and dependent on protein synthesis. *J Biochem* 34: 9625-9631.

Komenda J, Barker M, Kuvikova S, de Vries R, Mullineaux CW, Tichy M, Nixon PJ. 2006. The FtsH protease slr0228 is important for quality control of photosystem II in the thylakoid membrane of *Synechocystis* sp. PCC 6803. *J Biol Chem* 281: 1145-1151.

Komenda J, Knoppova J, Kopecna J, Sobotka R, Halada P, Yu J, Nickelsen J, Boehm M, Nixon PJ. 2012a. The Psb27 assembly factor binds to the CP43 complex of photosystem II in the cyanobacterium *Synechocystis* sp. PCC 6803. *Plant Physiol* 158: 476-486.

Komenda J, Lupinkova L, Kopecky J. 2002. Absence of the *psbH* gene product destabilizes photosystem II complex and bicarbonate binding on its acceptor side in *Synechocystis* PCC 6803. *Eur J Biochem* 269: 610-619.

Komenda J, Nickelsen J, Tichy M, Prasil O, Eichacker LA, Nixon PJ. 2008. The cyanobacterial homologue of HCF136/YCF48 is a component of an early photosystem II assembly complex and is important for both the efficient assembly and repair of photosystem II in *Synechocystis* sp. PCC 6803. *J Biol Chem* 283: 22390-22399.

Komenda J, Reisinger V, Muller BC, Dobakova M, Granvogl B, Eichacker LA. 2004. Accumulation of the D2 protein is a key regulatory step for assembly of the photosystem II reaction center complex in *Synechocystis* PCC 6803. *J Biol Chem* 279: 48620-48629.

Komenda J, Sobotka R, Nixon PJ. 2012b. Assembling and maintaining the Photosystem II complex in chloroplasts and cyanobacteria. *Curr Opin Plant Biol* 15: 245-251.

Komenda J, Tichy M, Prasil O, Knoppova J, Kuvikova S, de Vries R, Nixon PJ. 2007. The exposed N-terminal tail of the D1 subunit is required for rapid D1 degradation during photosystem II repair in *Synechocystis* sp PCC 6803. *Plant Cell* 19: 2839-2854.

Krieger-Liszkay A. 2005. Singlet oxygen production in photosynthesis. *J Exp Bot* 56: 337-346.

Krieger-Liszkay A, Fufezan C, Trebst A. 2008. Singlet oxygen production in photosystem II and related protection mechanism. *Photosynth Res* 98: 551-564.

Kruk J, Trebst A. 2008. Plastoquinol as a singlet oxygen scavenger in photosystem II. *Biochim Biophys Acta* 1777: 154-162.

Kruse O, Rupprecht J, Mussgnug JH, Dismukes GC, Hankamer B. 2005. Photosynthesis: a blueprint for solar energy capture and biohydrogen production technologies. *Photochem Photobiol Sci* 4: 957-970.

Kunkel TA. 1985. Rapid and efficient site-specific mutagenesis without phenotypic selection. *Proc Natl Acad Sci U S A* 82: 488-492.

Kuvikova S, Tichy M, Komenda J. 2005. A role of the C-terminal extension of the photosystem II D1 protein in sensitivity of the cyanobacterium *Synechocystis* PCC 6803 to photoinhibition. *Photochem Photobiol Sci* 4: 1044-1048.

Kyle DJ, Ohad I, Arntzen CJ. 1984. Membrane protein damage and repair: Selective loss of a quinone-protein function in chloroplast membranes. *Proc Natl Acad Sci U S A* 81: 4070-4074.

Kyte J, Doolittle RF. 1982. A simple method for displaying the hydropathic character of a protein. *J Mol Biol* 157: 105-132.

Li H, Durbin R. 2009. Fast and accurate short read alignment with Burrows-Wheeler transform. *Bioinformatics* 25: 1754-1760.

Li H, Handsaker B, Wysoker A, Fennell T, Ruan J, Homer N, Marth G, Abecasis G, Durbin R, Genome Project Data Processing S. 2009. The Sequence Alignment/Map format and SAMtools. *Bioinformatics* 25: 2078-2079.

Lind LK, Shukla VK, Nyhus KJ, Pakrasi HB. 1993. Genetic and immunological analyses of the cyanobacterium *Synechocystis* sp. PCC 6803 show that the protein encoded by the *psbJ* gene regulates the number of photosystem II centers in thylakoid membranes. *J Biol Chem* 268: 1575-1579.

Linke K, Ho FM. 2014. Water in Photosystem II: structural, functional and mechanistic considerations. *Biochim Biophys Acta* 1837: 14-32.

Liu H, Chen J, Huang RY, Weisz D, Gross ML, Pakrasi HB. 2013a. Mass spectrometry-based footprinting reveals structural dynamics of loop E of the chlorophyll-binding protein CP43 during photosystem II assembly in the cyanobacterium *Synechocystis* 6803. *J Biol Chem* 288: 14212-14220.

Liu H, Huang RY, Chen J, Gross ML, Pakrasi HB. 2011a. Psb27, a transiently associated protein, binds to the chlorophyll binding protein CP43 in photosystem II assembly intermediates. *Proc Natl Acad Sci U S A* 108: 18536-18541.

Liu H, Roose JL, Cameron JC, Pakrasi HB. 2011b. A genetically tagged Psb27 protein allows purification of two consecutive photosystem II (PSII) assembly intermediates in *Synechocystis* 6803, a cyanobacterium. *J Biol Chem* 286: 24865-24871.

Liu H, Weisz DA, Pakrasi HB. 2015. Multiple copies of the PsbQ protein in a cyanobacterial photosystem II assembly intermediate complex. *Photosynth Res* 126: 375-383.

Liu H, Zhang H, Weisz DA, Vidavsky I, Gross ML, Pakrasi HB. 2014. MS-based cross-linking analysis reveals the location of the PsbQ protein in cyanobacterial photosystem II. *Pro Natl Acad Sci* 111: 4638-4643.

Loll B, Kern J, Saenger W, Zouni A, Biesiadka J. 2005. Towards complete cofactor arrangement in the 3.0 Å resolution structure of photosystem II. *Nature* 438: 1040-1044.

Lupinkova L, Metz JG, Diner BA, Vass I, Komenda J. 2002. Histidine residue 252 of the Photosystem II D1 polypeptide is involved in a light-induced cross-linking of the polypeptide with the alpha subunit of cytochrome *b*-559: study of a site-directed mutant of *Synechocystis* PCC 6803. *Biochim Biophys Acta* 1554: 192-201.

Mabbitt PD, Eaton-Rye JJ, Wilbanks SM. 2013. Mutational analysis of the stability of Psb27 from *Synechocystis* sp. PCC 6803: implications for models of Psb27 structure and binding to CP43. *Eur Biophys Jl* 42: 787-793.

Mabbitt PD, Rautureau GJ, Day CL, Wilbanks SM, Eaton-Rye JJ, Hinds MG. 2009. Solution structure of Psb27 from cyanobacterial photosystem II. *J Biochem* 48: 8771-8773.

Mabbitt PD, Wilbanks SM, Eaton-Rye JJ. 2014. Structure and function of the hydrophilic Photosystem II assembly proteins: Psb27, Psb28 and Ycf48. *Plant Physiol Biochem* 81: 96-107.

Maenpaa P, Kallio T, Mulo P, Salih G, Aro EM, Tyystjarvi E, Jansson C. 1993. Site-specific mutations in the D1 polypeptide affect the susceptibility of *Synechocystis* 6803 cells to photoinhibition. *Plant Mol Biol* 22: 1-12.

Mamedov F, Nowaczyk MM, Thapper A, Rögner M, Styring S. 2007. Functional Characterization of Monomeric Photosystem II Core Preparations from *Thermosynechococcus elongatus* with or without the Psb27 Protein. *J Biochem* 46: 5542-5551.

Mayes SR, Dubbs JM, Vass I, Hideg E, Nagy L, Barber J. 1993. Further characterization of the psbH locus of *Synechocystis* sp. PCC 6803: Inactivation of *psbH* impairs Q_A to Q_B electron transport in photosystem II. *J Biochem* 32: 1454-1465.

McConnell MD, Koop R, Vasil'ev S, Bruce D. 2002. Regulation of the distribution of chlorophyll and phycobilin-absorbed excitation energy in cyanobacteria. A structure-based model for the light state transition. *Plant Physiol* 130: 1201-1212.

Meetam M, Keren N, Ohad I, Pakrasi HB. 1999. The PsbY Protein Is Not Essential for Oxygenic Photosynthesis in the Cyanobacterium *Synechocystis* sp. PCC 6803. *Plant Physiol* 121: 1267-1272.

Michoux F, Takasaka K, Boehm M, Komenda J, Nixon PJ, Murray JW. 2012. Crystal structure of the Psb27 assembly factor at 1.6 Å: implications for binding to Photosystem II. *Photosynth Res* 110: 169-175.

Morris JN, Crawford TS, Jeffs A, Stockwell PA, Eaton-Rye JJ, Summerfield TC. 2014. Whole genome re-sequencing of two 'wild-type' strains of the model cyanobacterium *Synechocystis* sp. PCC 6803. *N Z J Bot* 52: 36-47.

Muh F, Renger T, Zouni A. 2008. Crystal structure of cyanobacterial photosystem II at 3.0 Å resolution: a closer look at the antenna system and the small membrane-intrinsic subunits. *Plant Physiol Biochem* 46: 238-264.

Mullineaux CW, Emlyn-Jones D. 2005. State transitions: an example of acclimation to low-light stress. *J Exp Bot* 56: 389-393.

Mulo P, Sicora C, Aro EM. 2009. Cyanobacterial *psbA* gene family: optimization of oxygenic photosynthesis. *Cell Mol Life Sci* 66: 3697-3710.

Murata N, Miyao M, Hayashida N, Hidaka T, Sugiura M. 1988. Identification of a new gene in the chloroplast genome encoding a low-molecular-mass polypeptide of photosystem II complex. *FEBS Lett* 235: 283-288.

Murata N, Nishimura M, Takamiya A. 1966. Fluorescence of chlorophyll in photosynthetic systems. 3. Emission and action spectra of fluorescence--three emission bands of chlorophyll a and the energy transfer between two pigment systems. *Biochim Biophys Acta* 126: 234-243.

Murata N, Sugahara K. 1969. Control of excitation transfer in photosynthesis. 3. Light-induced decrease of chlorophyll a fluorescence related to photophosphorylation system in spinach chloroplasts. *Biochim Biophys Acta* 189: 182-192.

Murata N, Takahashi S, Nishiyama Y, Allakhverdiev SI. 2007. Photoinhibition of photosystem II under environmental stress. *Biochim Biophys Acta* 1767: 414-421.

Murray JW, Maghlaoui K, Kargul J, Sugiura M, Barber J. 2008. Analysis of xenon binding to photosystem II by X-ray crystallography. *Photosynth Res* 98: 523-527.

Nagao R, Tomo T, Noguchi T. 2015. Effects of Extrinsic Proteins on the Protein Conformation of the Oxygen-Evolving Center in Cyanobacterial Photosystem II As Revealed by Fourier Transform Infrared Spectroscopy. *J Biochem* 54: 2022-2031.

Nakamura Y, et al. 2003. Complete genome structure of *Gloeobacter violaceus* PCC 7421, a cyanobacterium that lacks thylakoids. *DNA Res* 10: 181-201.

Nelson N, Ben-Shem A. 2004. The complex architecture of oxygenic photosynthesis. *Nat Rev Mol Cell Biol* 5: 971-982.

Nelson N, Yocum CF. 2006. Structure and function of photosystems I and II. *Annu Rev Plant Biol* 57: 521-565.

Neufeld S, Zinchenko V, Stephan DP, Bader KP, Pistorius EK. 2004. On the functional significance of the polypeptide PsbY for photosynthetic water oxidation in the cyanobacterium *Synechocystis* sp. strain PCC 6803. *Mol Genet Genomics* 271: 458-467.

Nixon PJ, Diner BA. 1992. Aspartate 170 of the photosystem II reaction center polypeptide D1 is involved in the assembly of the oxygen-evolving manganese cluster. *J Biochem* 31: 942-948.

Nixon PJ, Diner BA. 1994. Analysis of water-oxidation mutants constructed in the cyanobacterium *Synechocystis* sp. PCC 6803. *Biochem Soc Trans* 22: 338-343.

Nixon PJ, Michoux F, Yu J, Boehm M, Komenda J. 2010. Recent advances in understanding the assembly and repair of photosystem II. *Ann Bot* 106: 1-16.

Nixon PJ, Trost JT, Diner BA. 1992. Role of the carboxy terminus of polypeptide D1 in the assembly of a functional water-oxidizing manganese cluster in photosystem II of the cyanobacterium *Synechocystis* sp. PCC 6803: assembly requires a free carboxyl group at C-terminal position 344. *J Biochem* 31: 10859-10871.

Nowaczyk MM, Hebeler R, Schlodder E, Meyer HE, Warscheid B, Rogner M. 2006. Psb27, a cyanobacterial lipoprotein, is involved in the repair cycle of photosystem II. *Plant Cell* 18: 3121-3131.

Nowaczyk MM, Krause K, Mieseler M, Sczibilanski A, Ikeuchi M, Rogner M. 2012. Deletion of *psbJ* leads to accumulation of Psb27-Psb28 photosystem II complexes in *Thermosynechococcus elongatus*. *Biochim Biophys Acta* 1817: 1339-1345.

Nowaczyk MM, Sander J, Grasse N, Cormann KU, Rexroth D, Bernat G, Rogner M. 2010. Dynamics of the cyanobacterial photosynthetic network: communication and modification of membrane protein complexes. *Eur J Cell Biol* 89: 974-982.

Oettmeier W. 1999. Herbicide resistance and supersensitivity in photosystem II. *Cell Mol Life Sci* 55: 1255-1277.

Ohnishi N, Allakhverdiev SI, Takahashi S, Higashi S, Watanabe M, Nishiyama Y, Murata N. 2005. Two-step mechanism of photodamage to photosystem II: step 1 occurs at the oxygen-evolving complex and step 2 occurs at the photochemical reaction center. *J Biochem* 44: 8494-8499.

Ohnishi N, Takahashi Y. 2001. PsbT polypeptide is required for efficient repair of photodamaged photosystem II reaction center. *J Biol Chem* 276: 33798-33804.

Olive J, Ajlani G, Astier C, Recouvreur M, Vernotte C. 1997. Ultrastructure and light adaptation of phycobilisome mutants of *Synechocystis* PCC 6803. *Biochim Biophys Acta - Bioenergetics* 1319: 275-282.

Olive J, M'Bina I, Vernotte C, Astier C, Wollman FA. 1986. Randomization of the EF particles in thylakoid membranes of *Synechocystis* 6714 upon transition from state I to state II. *FEBS Lett* 208: 308-312.

Pakrasi HB, De Ciechi P, Whitmarsh J. 1991. Site directed mutagenesis of the heme axial ligands of cytochrome b_{559} affects the stability of the photosystem II complex. *EMBO J* 10: 1619-1627.

Pakrasi HB, Nyhus KJ, Granok H. 1990. Targeted deletion mutagenesis of the beta subunit of cytochrome b_{559} protein destabilizes the reaction center of photosystem II. *Z Naturforsch C* 45: 423-429.

Papageorgiou GC, Govindjee. 2011. Photosystem II fluorescence: slow changes--scaling from the past. *J Photochem Photobiol B* 104: 258-270.

Papageorgiou GC, Tsimilli-Michael M, Stamatakis K. 2007. The fast and slow kinetics of chlorophyll a fluorescence induction in plants, algae and cyanobacteria: a viewpoint. *Photosynth Res* 94: 275-290.

Pasch JC, Nickelsen J, Schunemann D. 2005. The yeast split-ubiquitin system to study chloroplast membrane protein interactions. *Appl Microbiol Biotechnol* 69: 440-447.

Peers G, Truong TB, Ostendorf E, Busch A, Elrad D, Grossman AR, Hippler M, Niyogi KK. 2009. An ancient light-harvesting protein is critical for the regulation of algal photosynthesis. *Nature* 462: 518-521.

Peloquin JM, Britt RD. 2001. EPR/ENDOR characterization of the physical and electronic structure of the OEC Mn cluster. *Biochim Biophys Acta* 1503: 96-111.

Peltier JB, et al. 2002. Central functions of the lumenal and peripheral thylakoid proteome of *Arabidopsis* determined by experimentation and genome-wide prediction. *Plant Cell* 14: 211-236.

Philbrick JB, Diner BA, Zilinskas BA. 1991. Construction and characterization of cyanobacterial mutants lacking the manganese-stabilizing polypeptide of photosystem II. *J Biol Chem* 266: 13370-13376.

Pizarro SA, et al. 2004. Chloride ligation in inorganic manganese model compounds relevant to photosystem II studied using X-ray absorption spectroscopy. *J Biol Inorg Chem* 9: 247-255.

Plucken H, Muller B, Grohmann D, Westhoff P, Eichacker LA. 2002. The HCF136 protein is essential for assembly of the photosystem II reaction center in *Arabidopsis thaliana*. *FEBS Lett* 532: 85-90.

Pospisil P. 2011. Enzymatic function of cytochrome b_{559} in photosystem II. *J Photochem Photobiol B* 104: 341-347.

Prentki P, Krisch HM. 1984. In vitro insertional mutagenesis with a selectable DNA fragment. *Gene* 29: 303-313.

Rajalahti T, Huang F, Klement MR, Pisareva T, Edman M, Sjostrom M, Wieslander A, Norling B. 2007. Proteins in different *Synechocystis* compartments have distinguishing N-terminal features: a combined proteomics and multivariate sequence analysis. *J Proteome Res* 6: 2420-2434.

Rappaport F, Diner BA. 2008. Primary photochemistry and energetics leading to the oxidation of the $(Mn)_4Ca$ cluster and to the evolution of molecular oxygen in Photosystem II. *Coord Chem Rev* 252: 259-272.

Raszewski G, Diner BA, Schlodder E, Renger T. 2008. Spectroscopic properties of reaction center pigments in photosystem II core complexes: revision of the multimer model. *Biophys J* 95: 105-119.

Regel RE, Ivleva NB, Zer H, Meurer J, Shestakov SV, Herrmann RG, Pakrasi HB, Ohad I. 2001. Deregulation of electron flow within photosystem II in the absence of the PsbJ protein. *J Biol Chem* 276: 41473-41478.

Rehman AU, Cser K, Sass L, Vass I. 2013. Characterization of singlet oxygen production and its involvement in photodamage of Photosystem II in the cyanobacterium *Synechocystis* PCC 6803 by histidine-mediated chemical trapping. *Biochim Biophys Acta* 1827: 689-698.

Renger G, Renger T. 2008. Photosystem II: The machinery of photosynthetic water splitting. *Photosynth Res* 98: 53-80.

Rippka R, Deruelles J, Waterbury JB, Herdman M, Stanier RY. 1979. Generic Assignments, Strain Histories and Properties of Pure Cultures of Cyanobacteria. *Microbiol* 111: 1-61.

Rokka A, Suorsa M, Saleem A, Battchikova N, Aro EM. 2005. Synthesis and assembly of thylakoid protein complexes: multiple assembly steps of photosystem II. *Biochem J* 388: 159-168.

Roose JL, Kashino Y, Pakrasi HB. 2007a. The PsbQ protein defines cyanobacterial Photosystem II complexes with highest activity and stability. *Proc Natl Acad Sci U S A* 104: 2548-2553.

Roose JL, Pakrasi HB. 2004. Evidence that D1 processing is required for manganese binding and extrinsic protein assembly into photosystem II. *J Biol Chem* 279: 45417-45422.

Roose JL, Pakrasi HB. 2008. The Psb27 protein facilitates manganese cluster assembly in photosystem II. *J Biol Chem* 283: 4044-4050.

Roose JL, Wegener KM, Pakrasi HB. 2007b. The extrinsic proteins of Photosystem II. *Photosynth Res* 92: 369-387.

Ruf S, Biehler K, Bock R. 2000. A small chloroplast-encoded protein as a novel architectural component of the light-harvesting antenna. *J Cell Biol* 149: 369-378.

Saito K, Rutherford AW, Ishikita H. 2013. Mechanism of proton-coupled quinone reduction in Photosystem II. *Proc Natl Acad Sci U S A* 110: 954-959.

Sakata S, Mizusawa N, Kubota-Kawai H, Sakurai I, Wada H. 2013. Psb28 is involved in recovery of photosystem II at high temperature in *Synechocystis* sp. PCC 6803. *Biochim Biophys Acta* 1827: 50-59.

Salehian O, Bruce D. 1992. Distribution of excitation energy in photosynthesis: quantification of fluorescence yields from intact cyanobacteria. *J Lumin* 51: 91-98.

Sambrook J, Russell DW. 2006. Preparation of Plasmid DNA by Alkaline Lysis with SDS: Midipreparation. *CSH Protoc* 2006.

Satoh K, Oh-hashi M, Kashino Y, Koike H. 1995. Mechanism of Electron Flow through the QB Site in Photosystem II. 1. Kinetics of the Reduction of Electron Acceptors at the Q_B and Plastoquinone Sites in Photosystem II Particles from the Cyanobacterium *Synechococcus vulcanus*. *Plant Cell Physiol* 36: 597-605.

Satoh K, Yamamoto Y. 2007. The carboxyl-terminal processing of precursor D1 protein of the photosystem II reaction center. *Photosynth Res* 94: 203-215.

Sawaya MR, Krogmann DW, Serag A, Ho KK, Yeates TO, Kerfeld CA. 2001. Structures of cytochrome c-549 and cytochrome c-6 from the cyanobacterium *Arthrospira maxima*. *J Biochem* 40: 9215-9225.

Schottkowski M, Gkalympoudis S, Tzekova N, Stelljes C, Schunemann D, Ankele E, Nickelsen J. 2009a. Interaction of the periplasmic PratA factor and the PsbA (D1) protein during biogenesis of photosystem II in *Synechocystis* sp. PCC 6803. *J Biol Chem* 284: 1813-1819.

Schottkowski M, Ratke J, Oster U, Nowaczyk M, Nickelsen J. 2009b. Pitt, a novel tetratricopeptide repeat protein involved in light-dependent chlorophyll biosynthesis and thylakoid membrane biogenesis in *Synechocystis* sp. PCC 6803. *Mol Plant* 2: 1289-1297.

Sedoud A, Kastner L, Cox N, El-Alaoui S, Kirilovsky D, Rutherford AW. 2011. Effects of formate binding on the quinone-iron electron acceptor complex of photosystem II. *Biochim Biophys Acta* 1807: 216-226.

Sedoud A, Lopez-Igual R, Ur Rehman A, Wilson A, Perreau F, Boulay C, Vass I, Krieger-Liszkay A, Kirilovsky D. 2014. The Cyanobacterial Photoactive Orange Carotenoid Protein Is an Excellent Singlet Oxygen Quencher. *Plant Cell* 26: 1781-1791.

Seidler A. 1996. The extrinsic polypeptides of Photosystem II. *Biochimica et Biophysica Acta - Bioenergetics* 1277: 35-60.

Shen J-R, Ikeuchi M, Inoue Y. 1992. Stoichiometric association of extrinsic cytochrome c_{550} and 12 kDa protein with a highly purified oxygen-evolving photosystem II core complex from *Synechococcus vulcanus*. *FEBS Lett* 301: 145-149.

Shen JR. 2015. The Structure of Photosystem II and the Mechanism of Water Oxidation in Photosynthesis. *Annu Rev Plant Biol* 66: 23-48.

Shen JR, Burnap RL, Inoue Y. 1995. An independent role of cytochrome c-550 in cyanobacterial photosystem II as revealed by double-deletion mutagenesis of the *psbO* and *psbV* genes in *Synechocystis* sp. PCC 6803. *J Biochem* 34: 12661-12668.

Shen JR, Ikeuchi M, Inoue Y. 1997. Analysis of the *psbU* gene encoding the 12-kDa extrinsic protein of photosystem II and studies on its role by deletion mutagenesis in *Synechocystis* sp. PCC 6803. *J. Biol. Chem*. 272: 17821.

Shen JR, Inoue Y. 1993. Binding and functional properties of two new extrinsic components, cytochrome c-550 and a 12-kDa protein, in cyanobacterial photosystem II. *J Biochem* 32: 1825-1832.

Shevela D, Eaton-Rye JJ, Shen J-R, Govindjee. 2012. Photosystem II and the unique role of bicarbonate: A historical perspective. *Biochim Biophys Acta - Bioenergetics* 1817: 1134-1151.

Shi L-X, Kim SJ, Marchant A, Robinson C, Schröder WP. 1999. Characterisation of the PsbX protein from Photosystem II and light regulation of its gene expression in higher plants. *Plant Mol Biol* 40: 737-744.

Silva P, Thompson E, Bailey S, Kruse O, Mullineaux CW, Robinson C, Mann NH, Nixon PJ. 2003. FtsH is involved in the early stages of repair of photosystem II in *Synechocystis* sp PCC 6803. *Plant Cell* 15: 2152-2164.

Sirpio S, Allahverdiyeva Y, Suorsa M, Paakkarinen V, Vainonen J, Battchikova N, Aro EM. 2007. TLP18.3, a novel thylakoid lumen protein regulating photosystem II repair cycle. *Biochem J* 406: 415-425.

Sonoike K, Hihara Y, Ikeuchi M. 2001. Physiological significance of the regulation of photosystem stoichiometry upon high light acclimation of *Synechocystis* sp. PCC 6803. *Plant Cell Physiol* 42: 379-384.

Sozer O, Kis M, Gombos Z, Ughy B. 2011. Proteins, glycerolipids and carotenoids in the functional photosystem II architecture. *Front Biosci (Landmark Ed)* 16: 619-643.

Srivastava A, Strasser RJ, Govindjee. 1995. Polyphasic rise of chlorophyll a fluorescence in herbicide-resistant D1 mutants of *Chlamydomonas reinardtii*. *Photosynth Res* 43: 131-141.

Stamatakis K, Papageorgiou GC. 2014. DeltapH-dependent non-photochemical quenching (qE) of excited chlorophylls in the photosystem II core complex of the freshwater cyanobacterium *Synechococcus* sp PCC 7942. *Plant Physiol Biochem* 81: 184-189.

Stamatakis K, Tsimilli-Michael M, Papageorgiou GC. 2007. Fluorescence induction in the phycobilisome-containing cyanobacterium *Synechococcus* sp PCC 7942: analysis of the slow fluorescence transient. *Biochim Biophys Acta* 1767: 766-772.

Stewart DH, Brudvig GW. 1998. Cytochrome b_{559} of photosystem II. *Biochim Biophys Acta* 1367: 63-87.

Styring S, Sjoholm J, Mamedov F. 2012. Two tyrosines that changed the world: Interfacing the oxidizing power of photochemistry to water splitting in photosystem II. *Biochim Biophys Acta* 1817: 76-87.

Suga M, et al. 2015a. Native structure of photosystem II at 1.95 Å resolution viewed by femtosecond X-ray pulses. *Nature* 517: 99-103.

Suga M, et al. 2017. Light-induced structural changes and the site of O=O bond formation in PS II caught by XFEL. *Nature* 543: 131-135.

Sugimoto I, Takahashi Y. 2003. Evidence that the PsbK polypeptide is associated with the photosystem II core antenna complex CP43. *J Biol Chem* 278: 45004-45010.

Sugimoto M, Esaki N, Tanaka H, Soda K. 1989. A simple and efficient method for the oligonucleotide-directed mutagenesis using plasmid DNA template and phosphorothioate-modified nucleotide. *Anal Biochem* 179: 309-311.

Sugiura M, Harada S, Manabe T, Hayashi H, Kashino Y, Boussac A. 2010. Psb30 contributes to structurally stabilise the Photosystem II complex in the thermophilic cyanobacterium *Thermosynechococcus elongatus*. *Biochim Biophys Acta* 1797: 1546-1554.

Summerfield TC, Shand JA, Bentley FK, Eaton-Rye JJ. 2005. PsbQ (Sll1638) in Synechocystis sp. PCC 6803 is required for photosystem II activity in specific mutants and in nutrient-limiting conditions. *J Biochem* 44: 805-815.

Summerfield TC, Toepel J, Sherman LA. 2008. Low-oxygen induction of normally cryptic *psbA* genes in cyanobacteria. *J Biochem* 47: 12939-12941.

Sundby C, Chow WS, Anderson JM. 1993. Effects on Photosystem II Function, Photoinhibition, and Plant Performance of the Spontaneous Mutation of Serine-264 in the Photosystem II Reaction Center D1 Protein in Triazine-Resistant *Brassica napus* L. *Plant Physiol* 103: 105-113.

Swiatek M, et al. 2001. The chloroplast gene ycf9 encodes a photosystem II (PSII) core subunit, PsbZ, that participates in PS II supramolecular architecture. *Plant Cell* 13: 1347-1367.

Szilard A, Sass L, Hideg E, Vass I. 2005. Photoinactivation of photosystem II by flashing light. *Photosynth Res* 84: 15-20.

Takahashi H, Iwai M, Takahashi Y, Minagawa J. 2006. Identification of the mobile light-harvesting complex II polypeptides for state transitions in *Chlamydomonas reinhardtii*. *Proc Natl Acad Sci U S A* 103: 477-482.

Takahashi M, Shiraishi T, Asada K. 1988. COOH-terminal residues of D1 and the 44 kDa CPa-2 at spinach photosystem II core complex. *FEBS Lett* 240: 6-8.

Takahashi R, Boussac A, Sugiura M, Noguchi T. 2009. Structural Coupling of a Tyrosine Side Chain with the Non-Heme Iron Center in Photosystem II As Revealed by Light-Induced Fourier Transform Infrared Difference Spectroscopy. *J Biochem* 48: 8994-9001.

Takahashi Y, Matsumoto H, Goldschmidt-Clermont M, Rochaix JD. 1994. Directed disruption of the *Chlamydomonas* chloroplast *psbK* gene destabilizes the photosystem II reaction center complex. *Plant Mol Biol* 24: 779-788.

Takasaka K, Iwai M, Umena Y, Kawakami K, Ohmori Y, Ikeuchi M, Takahashi Y, Kamiya N, Shen JR. 2010. Structural and functional studies on Ycf12 (Psb30) and PsbZ-deletion mutants from a thermophilic cyanobacterium. *Biochim Biophys Acta* 1797: 278-284.

Tang XS, Fushimi K, Satoh K. 1990. D1-D2 complex of the photosystem II reaction center from spinach. Isolation and partial characterization. *FEBS Lett* 273: 257-260.

Thangaraj B, Ryan CM, Souda P, Krause K, Faull KF, Weber AP, Fromme P, Whitelegge JP. 2010. Data-directed top-down Fourier-transform mass spectrometry of a large integral membrane protein complex: photosystem II from *Galdieria sulphuraria*. *Proteom* 10: 3644-3656.

Thornton LE, Ohkawa H, Roose JL, Kashino Y, Keren N, Pakrasi HB. 2004a. Homologs of plant PsbP and PsbQ proteins are necessary for regulation of photosystem ii activity in the cyanobacterium *Synechocystis* 6803. *Plant Cell* 16: 2164-2175.

Tomita M, Ifuku K, Sato F, Noguchi T. 2009. FTIR Evidence That the PsbP Extrinsic Protein Induces Protein Conformational Changes around the Oxygen-Evolving Mn Cluster in Photosystem II. *J Biochem* 48: 6318-6325.

Tracewell CA, Brudvig GW. 2008. Characterization of the secondary electron-transfer pathway intermediates of photosystem II containing low-potential cytochrome b_{559}. *Photosynth Res* 98: 189-197.

Trautmann D, Voss B, Wilde A, Al-Babili S, Hess WR. 2012. Microevolution in cyanobacteria: re-sequencing a motile substrain of *Synechocystis* sp. PCC 6803. *DNA Res* 19: 435-448.

Trebst A. 1991. The molecular basis of resistance of PS II herbicides. Pages 145-164. Herbicide Resistance in Weeds and Crops, Butterworth-Heinemann.

Trebst A, Depka B, Hollander-Czytko H. 2002. A specific role for tocopherol and of chemical singlet oxygen quenchers in the maintenance of photosystem II structure and function in *Chlamydomonas reinhardtii*. *FEBS Lett* 516: 156-160.

Triantaphylides C, Havaux M. 2009. Singlet oxygen in plants: production, detoxification and signaling. *Trends Plant Sci* 14: 219-228.

Triantaphylides C, Krischke M, Hoeberichts FA, Ksas B, Gresser G, Havaux M, Van Breusegem F, Mueller MJ. 2008. Singlet oxygen is the major reactive oxygen species involved in photooxidative damage to plants. *Plant Physiol* 148: 960-968.

Truesdale GA, Downing AL. 1954. Solubility of Oxygen in Water. *Nature* 173: 1236-1236.

Tsimilli-Michael M, Stamatakis K, Papageorgiou GC. 2009. Dark-to-light transition in *Synechococcus* sp. PCC 7942 cells studied by fluorescence kinetics assesses plastoquinone redox poise in the dark and photosystem II fluorescence component and dynamics during state 2 to state 1 transition. *Photosynth Res* 99: 243-255.

Tyystjärvi E. 2008. Photoinhibition of Photosystem II and photodamage of the oxygen evolving manganese cluster. *Coord Chem Rev* 252: 361-376.

Tyystjarvi T, Herranen M, Aro EM. 2001. Regulation of translation elongation in cyanobacteria: membrane targeting of the ribosome nascent-chain complexes controls the synthesis of D1 protein. *Mol Microbiol* 40: 476-484.

Umena Y, Kawakami K, Shen JR, Kamiya N. 2011. Crystal structure of oxygen-evolving photosystem II at a resolution of 1.9 Å. *Nature* 473: 55-60.

Uno C, Nagao R, Suzuki H, Tomo T, Noguchi T. 2013. Structural Coupling of Extrinsic Proteins with the Oxygen-Evolving Center in Red Algal Photosystem II As Revealed by Light-Induced FTIR Difference Spectroscopy. *J Biochem* 52: 5705-5707.

Van Die IM, Bergmans HEN, Hoekstra WPM. 1983. Transformation In *Escherichia coli*: Studies On The Role Of The Heat Shock In Induction Of Competence. *Microbiol* 129: 663-670.

Vasil'ev S, Orth P, Zouni A, Owens TG, Bruce D. 2001. Excited-state dynamics in photosystem II: insights from the X-ray crystal structure. *Proc Natl Acad Sci U S A* 98: 8602-8607.

Vass I. 2011. Role of charge recombination processes in photodamage and photoprotection of the photosystem II complex. *Physiol Plant* 142: 6-16.

Vass I. 2012. Molecular mechanisms of photodamage in the Photosystem II complex. *Biochim Biophys Acta* 1817: 209-217.

Vass I, Cser K. 2009. Janus-faced charge recombinations in photosystem II photoinhibition. *Trends Plant Sci* 14: 200-205.

Vass I, Kirilovsky D, Etienne AL. 1999. UV-B radiation-induced donor- and acceptor-side modifications of photosystem II in the cyanobacterium *Synechocystis* sp. PCC 6803. *J Biochem* 38: 12786-12794.

Vass I, Styring S, Hundal T, Koivuniemi A, Aro E, Andersson B. 1992. Reversible and irreversible intermediates during photoinhibition of photosystem II: stable reduced Q_A species promote chlorophyll triplet formation. *Proc Natl Acad Sci* 89: 1408-1412.

Vavilin D, Yao D, Vermaas W. 2007. Small Cab-like proteins retard degradation of photosystem II-associated chlorophyll in *Synechocystis* sp. PCC 6803: kinetic analysis of pigment labeling with ^{15}N and ^{13}C. *J Biol Chem* 282: 37660-37668.

Veerman J, Bentley FK, Eaton-Rye JJ, Mullineaux CW, Vasil'ev S, Bruce D. 2005. The PsbU subunit of photosystem II stabilizes energy transfer and primary photochemistry in the phycobilisome-photosystem II assembly of *Synechocystis* sp. PCC 6803. *J Biochem* 44: 16939-16948.

Vermaas WF, Shen G, Styring S. 1994. Electrons generated by photosystem II are utilized by an oxidase in the absence of photosystem I in the cyanobacterium *Synechocystis* sp. PCC 6803. *FEBS Lett* 337: 103-108.

von Sydow L, Schwenkert S, Meurer J, Funk C, Mamedov F, Schröder WP. 2016. The PsbY protein of *Arabidopsis* Photosystem II is important for the redox control of cytochrome b559. *Biochim Biophys Acta - Bioenergetics* 1857: 1524-1533.

Vredenberg WJ, Duysens LN. 1963. Transfer of energy from bacteriochlorophyll to a reaction centre during bacterial photosynthesis. *Nature* 197: 355-357.

Webber AN, Hird SM, Packman LC, Dyer TA, Gray JC. 1989. A photosystem II polypeptide is encoded by an open reading frame co-transcribed with genes for cytochrome b-559 in wheat chloroplast DNA. *Plant Mol Biol* 12: 141-151.

Wegener KM, Welsh EA, Thornton LE, Keren N, Jacobs JM, Hixson KK, Monroe ME, Camp DG, 2nd, Smith RD, Pakrasi HB. 2008. High sensitivity proteomics assisted discovery of a novel operon involved in the assembly of photosystem II, a membrane protein complex. *J Biol Chem* 283: 27829-27837.

Wei L, Guo J, Ouyang M, Sun X, Ma J, Chi W, Lu C, Zhang L. 2010. LPA19, a Psb27 homolog in *Arabidopsis thaliana*, facilitates D1 protein precursor processing during PSII biogenesis. *J Biol Chem* 285: 21391-21398.

Wei X, Su X, Cao P, Liu X, Chang W, Li M, Zhang X, Liu Z. 2016. Structure of spinach photosystem II-LHC II supercomplex at 3.2 Å resolution. *Nature* 534: 69-74.

Whitmarsh J, Govindjee. 1999. The Photosynthetic Process. Pages 11-51 in Singhal GS, Renger G, Sopory SK, Irrgang KD, Govindjee, eds. Concepts in Photobiology: Photosynthesis and Photomorphogenesis. Dordrecht: Springer Netherlands.

Williams JGK. 1988. [85] Construction of specific mutations in photosystem II photosynthetic reaction center by genetic engineering methods in *Synechocystis* 6803. Pages 766-778. Methods in Enzymology, vol. Volume 167 Academic Press.

Williams WP, Allen JF. 1987. State 1/State 2 changes in higher plants and algae. *Photosynth Res* 13: 19-45.

Wydrzynski TJ, Satoh K. 2005. Photosystem II : the light-driven water : plastoquinone oxidoreductase. Springer.

Yadav DK, Kruk J, Sinha RK, Pospisil P. 2010. Singlet oxygen scavenging activity of plastoquinol in photosystem II of higher plants: electron paramagnetic resonance spin-trapping study. *Biochim Biophys Acta* 1797: 1807-1811.

Yang S, Su Z, Li H, Feng J, Xie J, Xia A, Gong Y, Zhao J. 2007. Demonstration of phycobilisome mobility by the time- and space-correlated fluorescence imaging of a cyanobacterial cell. *Biochim Biophys Acta - Bioenergetics* 1767: 15-21.

Yanisch-Perron C, Vieira J, Messing J. 1985. Improved M13 phage cloning vectors and host strains: nucleotide sequences of the M13mpl8 and pUC19 vectors. *Gene* 33: 103-119.

Yao DC, Brune DC, Vavilin D, Vermaas WF. 2012. Photosystem II component lifetimes in the cyanobacterium *Synechocystis* sp. strain PCC 6803: small Cab-like proteins stabilize biosynthesis intermediates and affect early steps in chlorophyll synthesis. *J Biol Chem* 287: 682-692.

Zhang L, Paakkarinen V, van Wijk KJ, Aro EM. 1999. Co-translational assembly of the D1 protein into photosystem II. *J Biol Chem* 274: 16062-16067.

Zobnina V, Lambreva MD, Rea G, Campi G, Antonacci A, Scognamiglio V, Giardi MT, Polticelli F. 2017. The plastoquinol-plastoquinone exchange mechanism in photosystem II: insight from molecular dynamics simulations. *Photosynth Res* 131: 15-30.

Zouni A, Witt HT, Kern J, Fromme P, Krauss N, Saenger W, Orth P. 2001. Crystal structure of photosystem II from *Synechococcus elongatus* at 3.8 Å-resolution. *Nature* 409: 739-743.

Appendix

A. *psbA* triple deletion strains/markerless deletion technique

In the *psbA*-triple deletion strain, all the three genes encoding the D1 protein, *psbA*1, *psbA*2, and *psbA*3 were deleted in a step-wise manner. The *psbA1* and *psbA3* were deleted through a markerless deletion strategy, whereas *psbA2* was replaced by inserting a chloramphenicol-resistance cassette. The *psbA*-triple deletion strain can be grown photoheterotrophically using glucose but is incapable of assembling an active PS II complex because of the absence of D1. The *sacB* gene coupled to a kanamycin-resistance cassette was used to create a markerless deletion of the psbA1 and psbA3 gene copies in *Synechocystis* 6803. The *sacB* gene codes for levansucrase enzyme which catalyses the breakdown of sucrose to glucose and fructose derivatives (Gay *et al.* 1983). The *sacB* gene expression is lethal to many Gram-negative bacteria such as *E.coli* when grown in the presence of 5% sucrose (Gay *et al.* 1985). *Synechocystis* 6803 is also susceptible to *sacB* expression (Cai and Wolk 1990; Ermakova-Gerdes and Vermaas 1999).

B. Δ*psbA1* deletion strain

To construct the Δ*psbA1* plasmid for the deletion of the *psbA1* copy of the *psbA* gene family in *Synechocystis* 6803, the *psbA1* region (2340 bps) of DNA was amplified from gDNA isolated from wild type with primers *psbA1*-F and *psbA1*-R. The primers used for the amplification incorporated *Eco*RI and *Sal*I restriction sites that were then introduced at the 5` and 3' end of the PCR product, respectively. The amplified PCR product was digested with *Eco*RI and *Sal*I, resulting in a 2318 bps DNA fragment and blunt-ligated into the pUC18-*Eco*RI[1] plasmid and the new construct was named p*psbA1* (pA1) (4984 bp)[2]. The p*psbA1* (pA1) consisted of the wild- type sequence from 365 bp upstream of the *psbA1* start codon to 870 bp downstream of the *psbA1* stop codon, including the flanking open reading frame of *slr1182*. The p*psbA1* (pA1) was then digested with *Hpa*I and *Ban*II, resulting in the production of two[3] DNA fragments of 685 bp[4] and 4299 bp[5]. The 4299 bp DNA fragment was used for constructing the pΔ*psbA1* (pA1-Trunc) and pΔ*psbA1*/*sacB*/kanamycin plasmids (pA1-sacB). To make

the p∆*psbA1* (pA1-Trunc) plasmid, the resulting *Hpa*I and *Ban*II DNA construct were self-ligated again. To make p∆*psbA1*/*sacB*/kanamycin plasmid (pA1-sacB), the *Hpa*I and *Ban*II DNA construct (4299 bp) was ligated into the *Xba*I/*Xba*I DNA fragment (3760 bp) of pRL250 containing a kanamycin-resistance cassette and the *sacB* gene for selection, thus providing sensitivity to sucrose (Cai and Wolk 1990). The resultant p∆*psbA1*/*sacB*/kanamycin plasmid (pA1-sacB) was used to transform the wild-type *Synechocystis* 6803 cells. The transformed cells were grown on selective media containing kanamycin and sucrose, and the segregation of the transformants was confirmed by PCR analysis. Once, the ΔPsbA1/*sacB*/kanR (pA1-sacB) strain was segregated, it was transformed with p*∆psbA1* (pA1-Trunc) to remove the *sacB*:kanamycin cassette and form *psbA1* markerless deletion strain. This ∆*psbA1* strain was then used to create a ∆*psbA1*:∆*psbA3* strain, as described below.

C. ∆*psbA2* deletion strain

To construct the ∆*psbA2* plasmid for the deletion of the *psbA2* copy of the *psbA* gene family in *Synechocystis* 6803, two separate regions of *psbA2* were amplified, cloned and then combined. The chloramphenicol-resistance cassette was used as the selective marker. First, 1317 bp DNA fragment was amplified with A2-Rescue and Rwa2-R primers, and the amplified 1317 bp DNA fragment was used as a megaprimer in the next set of PCR reactions with Rwa2-F primer. Restriction digestion of the DNA construct was performed with *Hind*III and *Xba*I. The digested product was ligated into pTZ19U[6]. The plasmid was named p*psbA2* (pA2) (4186 bp)[7] consisting of the region 118 bp upstream of the mutated *psbA2* start codon to 147 bp downstream of the stop codon.

Afterward, overlap extension PCR was performed to amplify most of the *psbA2* and downstream sequence. Two separate PCR reactions were carried out. The first PCR product was 1088 bp[8] long and was cloned from the downstream of the start codon of *psbA2* to 8 bps after the stop codon of *psbA2* using primers A2-Mut-F and A2-R-Swa. The *Swa*I site was introduced three bp downstream of the stop codon of *psbA2*. The second PCR product was 1756 bp long, amplified using speA-F and speA-R primers. Both these PCR products were used as a primer in the third PCR reaction to generate 2752 bp DNA fragment. The restriction digestion of the 2752 bp DNA fragment was carried out using *Nco*I and *Hpa*I and the resulting 1846 bp DNA fragment with the

introduced *Swa*I restriction site, was ligated into the *Nco*I and *Sma*I sites of plasmid p*psbA2* (pA2) to create p*psbA2** (pA2-Del-intermediate) (6899 bp) plasmid. The region (1195 bp) corresponding to 174 bp[9] downstream of the mutated *psbA2* start codon to 286 bp downstream of the stop codon was digested with *Hinc*II and *Stu*I, and the chloramphenicol-resistance cassette from pBR325 (Bolivar 1978) was ligated at the same location. The mutated *psbA2* start codon was restored using site-directed mutagenesis with A2-Fix primer. The plasmid was named as pΔ*psbA2*-camR and was used to transform the ΔPsbA1:ΔPsbA3 strains.

D. Δ*psbA3* deletion strain

To construct the pΔ*psbA3* plasmid for the deletion of the *psbA3* copy of the *psbA* gene family in *Synechocystis* 6803, overlap extension PCR was employed. Two separate PCR reactions were carried out to generate two different 5` and 3` PCR products. The 5` PCR product was 2182 bp long (RwA3-F2 and RwA3-R primers) containing a *Pst*I restriction site introduced nine bp upstream of the *psbA3* stop codon. On the other hand, the 3` PCR product was 2338 bp long (A2-Rescue and WnA3-R primers) with the *psbA3* start codon mutated to TGA from AUG. Both the PCR products were purified and then were used as megaprimers in the third separate PCR reaction generating a 3425 bp long PCR product. This PCR product consisted of the region from 1101 bp upstream of the mutated *psbA3* start codon to 1241 bp downstream of the *psbA3* stop codon. The resultant 3425 bp long fragment was ligated into the pGEMT Easy vector to create plasmid pGEM-A3[10]. This plasmid was digested further with *Eco*RI and *Bgl*II to remove the various sequencing errors present at the extreme 3' end of the *dnaG* open reading frame. The resulting 3306 bp[11] DNA fragment was then cloned into pUC18-*Eco*RI, and the plasmid was named p*psbA3* (pA3v2) (5951 bp)[12]. The *psbA3* (pA3v2) plasmid was then digested with *Bst*EII/*Hinc*II restriction enzymes leading to the removal of sequence (1126 bp) from 57 bp[13] downstream of the mutated *psbA3* start codon to 53 bp upstream of the *dnaG* start codon. The resultant 4825 bp[14] long DNA fragment after digestion was ligated to the *Xba*I/*Xba*I fragment (3760 bp) of pRL250 containing a kanamycin-resistance cassette and the *sacB* gene, thus providing sensitivity to the sucrose (Cai and Wolk 1990). The plasmid was named p*psbA3*/*sac*B/kanR (pA3v2-sacB). The p*psbA3*/*sacB*/kanR was used to transform the wild-type *Synechocystis* 6803 cells and the ΔPsbA1 strain. Once fully segregated, the

PsbA3/*sacB*/kanR and ΔPsbA1:PsbA3/*sacB*/kanR strains were transformed with the p*psbA3* plasmid and grown on selective media containing sucrose to produce ΔPsbA3 and ΔPsbA1:ΔPsbA3 strains. Also, the 4825 bp DNA fragment was self-ligated to create the pA3v2-Trunc plasmid.

E. *psbA2* mutagenesis system

To construct a system for the introduction of point mutations into the *psbA2* copy of the *psbA* gene family in *Synechocystis* 6803, the 2093 bp DNA fragment was amplified with primers A2-Mut-F and A2-Delseq primers and ligated into a pGEM-T-Easy vector to produce p*psbA2* plasmid (pA2-Mut2). The p*psbA2* plasmid was digested with *Cla*I to insert 1235 bp[15] long *Pst*I/*Pst*I kanamycin-resistance cassette. The overlapping *dam*$^+$ methylation at the *ClaI* site was removed via site-directed mutagenesis utilising the A2-SortCla primer, transitioning the non-coding 3'-adjacent cystosine base to thymine. The plasmid was named p*psbA2*/kanR (6347 bp)[16] control and was used to transform the Δ*psbA* deletion strain.

Descriptions of the superscripts in the above paragraphs A-E represents changes in the number of base pairs found using Snapgene software.

1- 2690 bp, 2- 5008 bp, 3- four DNA fragments, 4- 613 bp 5- 3827 bp 6- 2847 bp 7- 4194 bp 8- 1090 bp 9- 195 bp 10- 6442 bp 11- 3302 bp 12- 5996 bp 13- 58 bp 14- 4879 bp 15- 1204 bp 16- 6316 bp.

F. List of primers used for construction of Δ*psbA* strains.

Primers	Primer Sequence (5` - 3`)	Primer features
psbA1-F	TAACTCCTGAATTCCATGGGGCCACAACCA	EcoRI restriction site
psbA1-R	TGCTTTGGCTAAGTCGACCGAAGATTGATC	SalI restriction site
speA-F	CGCAATGCCCACAACTTC	
speA-R	AGGATTCCGGTGCTGACT	
RwA2-F	GCCAGGTAAACTCTTCTC	
RwA2-R	TGCCTAATGCTTTATCCG	
A2-Rescue	GGAATTATAACCAATGAACAACGACTC	Replaces the *psbA2/3* ATG codon with a TGA codon
A2-Mut-F	ACAACGACTCTCCAACAGCGCG	Amplifies sequence from immediately 3'of the *psbA2* ATG codon
A2-R-Swa	CACATTTAAATTAACCGTTGACAGCAGGAG	Incorporates a *Swa*I codon downstream of the (shaded) *psbA2* stop codon
A2-Fix	GTCGTTGTCATTTGGTTATAATTCCTTATG	Restores the mutated *psbA2* start codon to ATG.
A2-Delseq	CCCAGATGAAAATGAAGC	
A2-SortCla	ATCTTGATTGCCATCGATTGCCGG	Removes overlapping *dam* methylation at *Cla*I site downstream of *psbA2*
WnA2-F	CTTCCTGTTACAAAGCTTTACAAAACTCTC	
WnA2-R	CTGCTGAGAGATGTGTAGTACCC	

RwA3-F	GGAAGTTGTGCTGCAGGA	*Pst*I restriction site
RwA3-R	AACCGTTGACTGCAGGAG	*Pst*I restriction site
RwA3-F2	GAAGCTGACAAACGTTTGGG	
WnA3-R	AGCACTACTGTGGATAAACTCATCGGCATC	
D1-Seq-F	ACCCCATTGGTCAAGGCTCC	
D1-Seq-F2	CCAATATGCTTCTTTCAACAACAGC	

G. Kautsky fluorescence induction

```
MeasuringFlash=4us
MeasurDelay=3us
ActinicFlash=0us
AuxDuration=4s        ; Act. light interval
PreFlash=5us          ; PreFlash
include default1.inc          ; Include standard options, don't remove it !
include detector.inc
M_Voltage=80Num       ; Measur.light voltage
F_Voltage=0
A_Voltage=30Num       ; Act. light voltage
;*************************************************************************
first=5.62341325190349E-5s      ;
second=7.49894209332456E-5s     ;
stop=5s          ; Experiment duration
; Fo MEASUREMENT --------
h=<200us,400us..800us>
if(PreFlash GR 0) Then
 h=>mfm1sub
else
 h=>fm1
end
; ACTINIC LIGHT ---------
i=1ms
<i>=>A1
; INDUCTION KINETICS ---
j=i+[first,second..stop]
if(PreFlash GR 0)then
 j=>mfm1sub
else
 j=>fm1
end
```

H. Kautsky fluorescence induction (500 s)

```
MeasuringFlash=3us
MeasurDelay=2us
ActinicFlash=0us
AuxDuration=500.1s    ; Act. light interval
PreFlash=0us          ; PreFlash
```

```
include default1.inc            ; Include standard options, don't remove it !
include detector.inc
M_Voltage=90Num         ; Measur.light voltage
F_Voltage=0
A_Voltage=50Num         ; Act. light voltage
;*****************************************************************
<init>=>FastMode(0),Gain1(100)
Fo=<200us,400us..800us>          ; Define Fo measurment
ab=<10us,20us..40us>
a=<50us,75us..150us>
b=<200us,250us..500us>
c=<600us,700us..1000us>
d=<1.5ms,2ms..5ms>
e=<6ms,7ms..10ms>
f=<12.5ms,15ms..50ms>
g=<60ms,70ms..250ms>
h=<275ms,300ms..500ms>
i=<600ms,700ms..1500ms>
j=<1.75s,2s..5s>
k=<5.5s,6s..10s>
m=<20s,30s..500s>
Timepoints=ab|a|b|c|d|e|f|g|h|i|j|k|m
Light=1ms                       ; Actinic Flash
Measure=Light+Timepoints        ; Reoxidation Kinetics
Fo|Measure=>mfm1
<Light>=>A1
```

I. Chlorophyll *a* fluorescence decay following single actinic flash

```
MeasuringFlash=4us
MeasurDelay=3us
ActinicFlash=35us
AuxDuration=ActinicFlash
PreFlash=0us
include default1.inc      ; include standard options, don't remove it !
include detector.inc
M_Voltage=80Num
F_Voltage=100Num
A_Voltage=F_Voltage
;*****************************************************************
; PRE-DEFINED PARAMETERS
first=56.2341325190349us
second=74.9894209332456us
stop=60s
```

```
;
; TIMING DEFINITION
k=<200us,400us..800us>          ; Define Fo measurment
i=1ms                           ; Actinic Flash
j=i+[first,second..i+stop]      ; Reoxidation Kinetics
;
; EXECUTION
<i>=>F1                         ; Actinic Flash
;
if(PreFlash GR 0) Then
k|j=>mfm1sub
else
k|j=>fm1
end
```

J. Chlorophyll *a* fluorescence decay following multiple actinic flashes

```
MeasuringFlash=3us
MeasurDelay=2us
ActinicFlash=35us
AuxDuration=ActinicFlash
PreFlash=0us
include default1.inc      ; include standard options, don't remove it !
include detector.inc
M_Voltage=90Num
F_Voltage=100Num
A_Voltage=F_Voltage
;*************************************************************************
; PRE-DEFINED PARAMETERS

<init>=>FastMode(0),Gain1(100)

; TIMING DEFINITION

Fo=<200us,400us..800us>          ; Define Fo measurment

a=<50us,75us..150us>
b=<200us,250us..500us>
c=<600us,700us..1000us>
d=<1.5ms,2ms..5ms>
e=<6ms,7ms..10ms>
f=<15ms,20ms..50ms>
g=<60ms,70ms..100ms>
h=<125ms,150ms..500ms>
i=<600ms,700ms..1500ms>
j=<1.75s,2s..5s>
k=<5.5s,6s..10s>
```

```
Timepoints=a|b|c|d|e|f|g|h|i|j|k

Flash1=2500ms                    ; Actinic  Flash
f2=2250ms
f3=2000ms
f4=1750ms
f5=1500ms
f6=1250ms
f7=1000ms
f8=750ms
f9=500ms
f10=250ms

Measure=Flash1+Timepoints        ; Reoxidation  Kinetics
Measure2=Measure+15us
Fo2=Fo+15us
Fo|Measure=>mfm1
Fo2|Measure2=>m1

<Flash1>=>F1                     ; Actinic  Flash #1
<Flash1>=>A1

<f2>=>F1                 ; Actinic  Flash # 2
<f2>=>A1

<f3>=>F1                 ; Actinic  Flash # 3
<f3>=>A1

<f4>=>F1                 ; Actinic  Flash # 4
<f4>=>A1

<f5>=>F1                 ; Actinic  Flash #5
<f5>=>A1
```

K. Examples to demonstrate the variation in the biological replicates

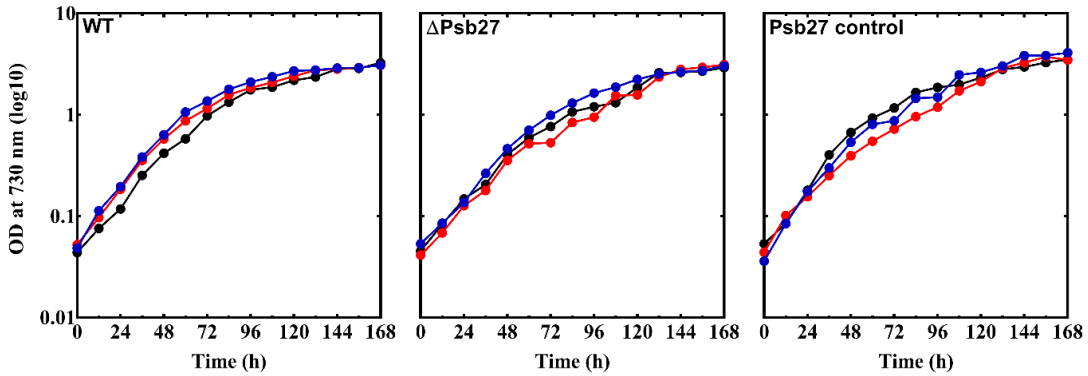

Figure A.1 Photoautotrophic growth. Three biological replicates each of wild type, ΔPsb27 and Psb27 control strains has been shown to display the variation between the biological replicates

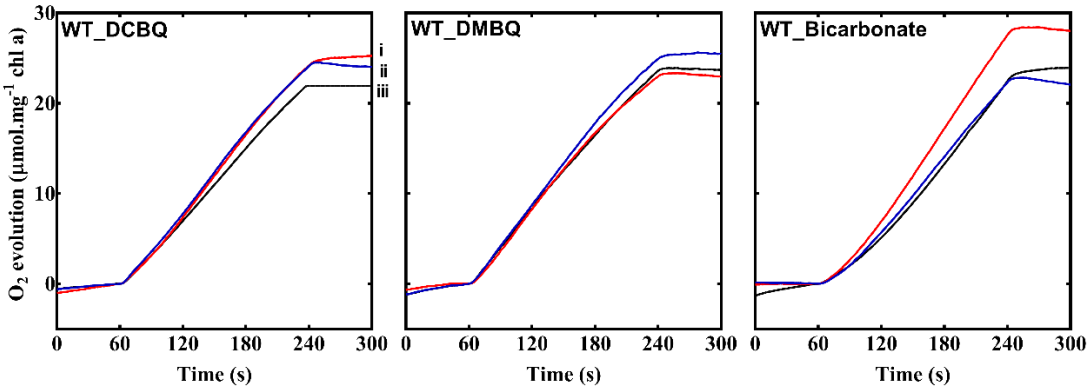

Figure A.2 Oxygen evolution assay traces. Three biological replicates of wild type strain has been shown to display the variation between the biological replicates. The light was switched on at 60 s and the oxygen evolution measured for 180 s. The light gets switched off at 240 s.

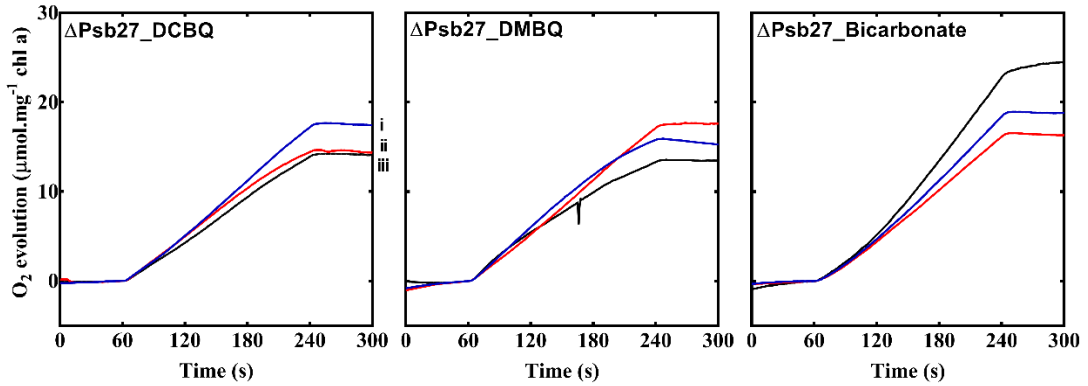

Figure A.3 Oxygen evolution assay traces. Three biological replicates of ΔPsb27 strain has been shown to display the variation between the biological replicates. The light was switched on at 60 s and the oxygen evolution measured for 180 s. The light gets switched off at 240 s.

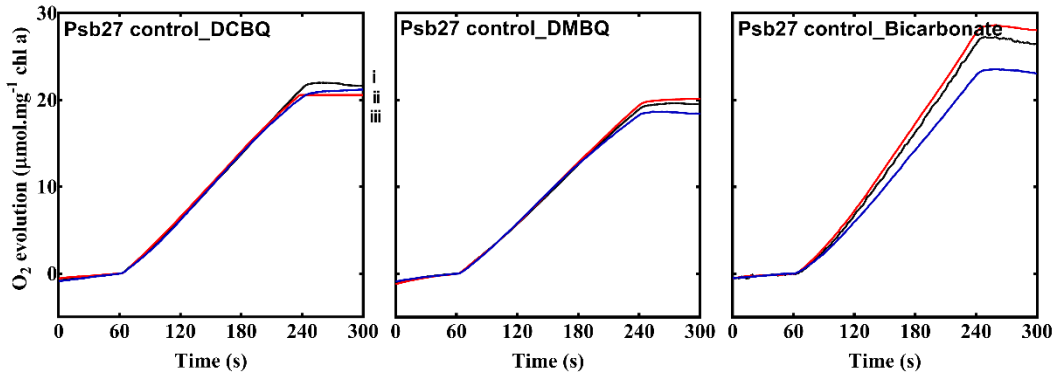

Figure A.4 Oxygen evolution assay traces. Three biological replicates of Psb27 control strain has been shown to display the variation between the biological replicates. The light was switched on at 60 s and the oxygen evolution measured for 180 s. The light gets switched off at 240 s.

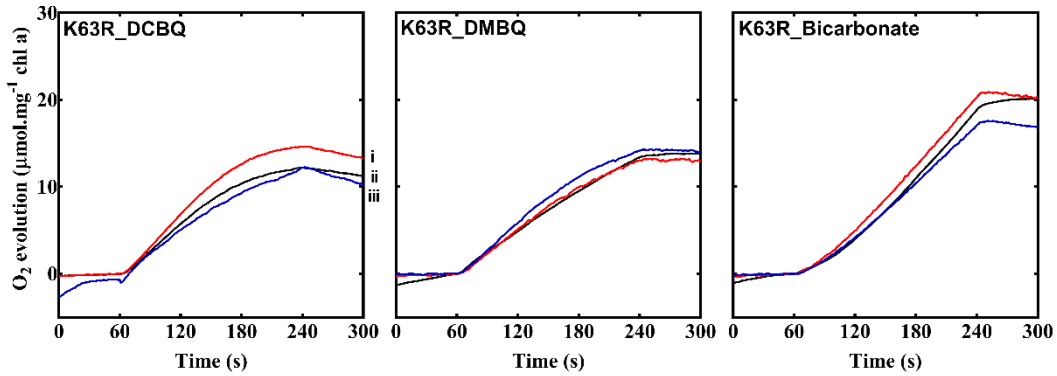

Figure A. 5 Oxygen evolution assay traces. Three biological replicates of K63R strain has been shown to display the variation between the biological replicates. The light was switched on at 60 s and the oxygen evolution measured for 180 s. The light gets switched off at 240 s.

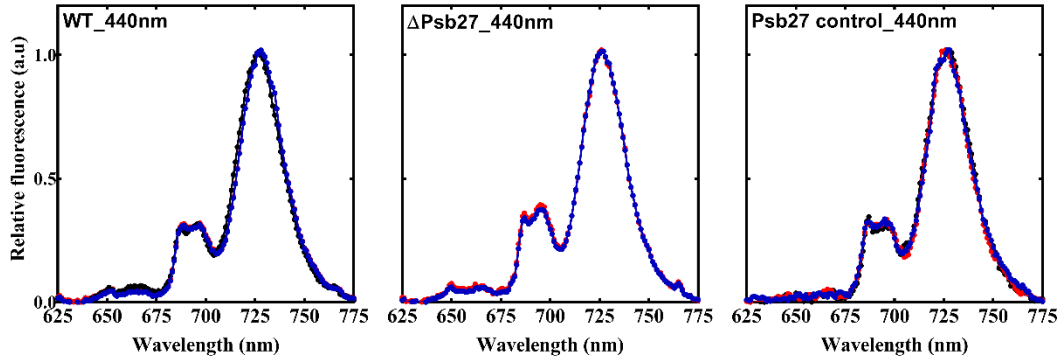

Figure A.6 Low-temperature fluorescence emission spectra. Three biological replicates each of wild type, ΔPsb27 and Psb27 control strains has been shown to display the variation between the biological replicates. It contains the fluorescence emission spectra with an excitation wavelength of 440 nm.

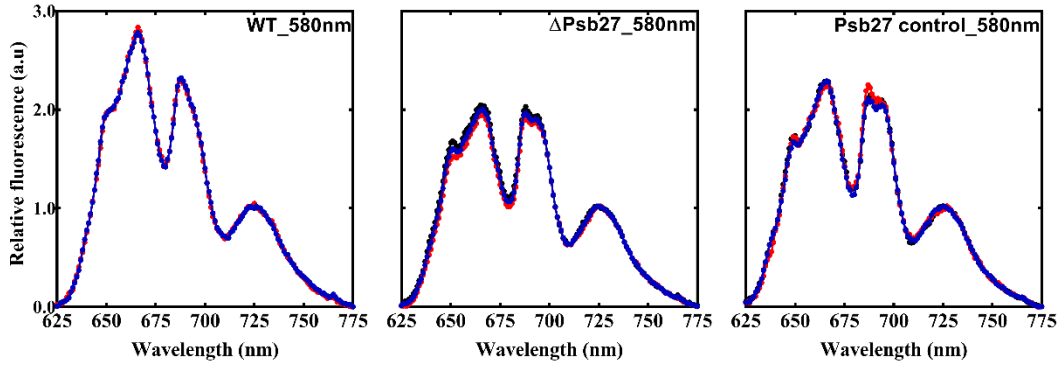

Figure A.7 Low-temperature fluorescence emission spectra. Three biological replicates each of wild type, ΔPsb27 and Psb27 control strains has been shown to display the variation between the biological replicates. It contains the fluorescence emission spectra with an excitation wavelength of 580 nm.

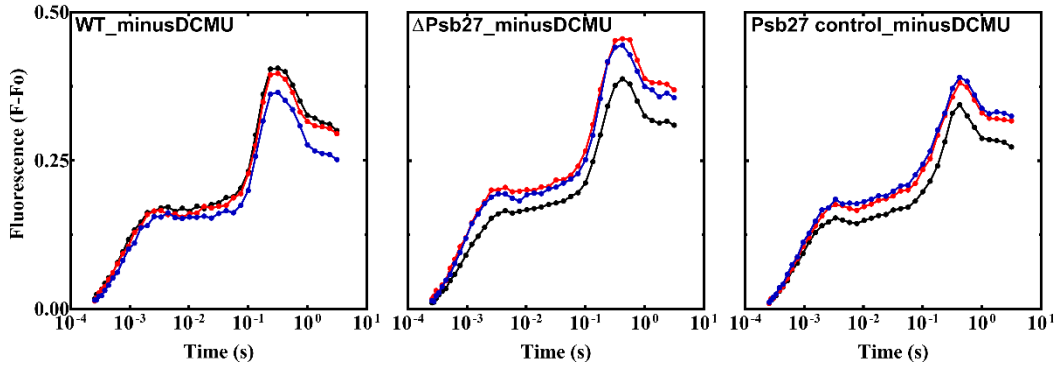

Figure A.8 Normalised steady-state chlorophyll *a* fluorescence induction in the absence of DCMU.Three biological replicates each of wild type, ΔPsb27 and Psb27 control strains has been shown to display the variation between the biological replicates.

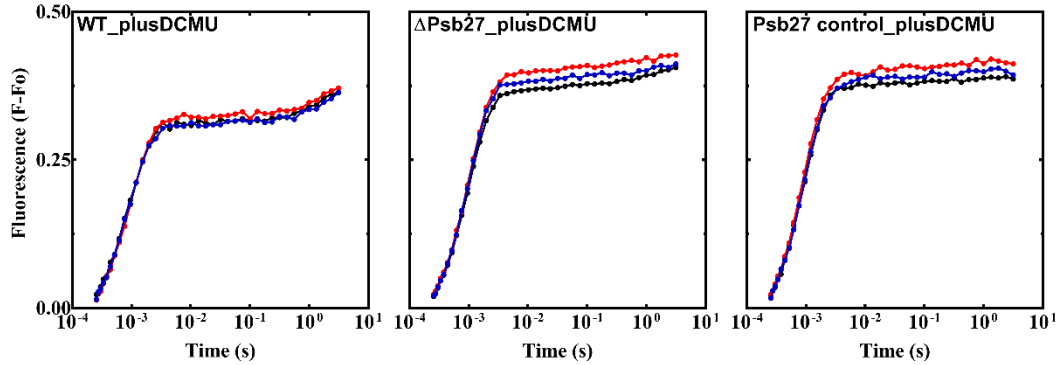

Figure A.9 Normalised steady-state chlorophyll *a* fluorescence induction in the presence of DCMU.Three biological replicates each of wild type, ΔPsb27 and Psb27 control strains has been shown to display the variation between the biological replicates.

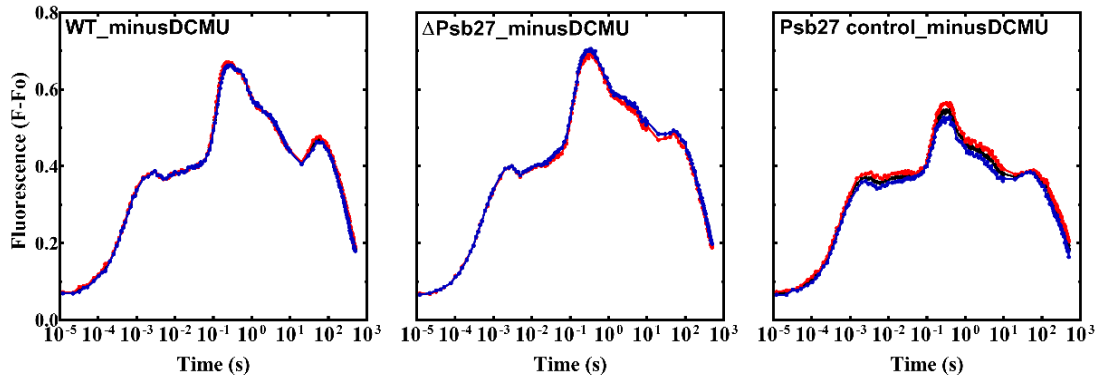

Figure A.10 Normalised steady-state long-term chlorophyll *a* fluorescence induction (500 s).Three biological replicates each of wild type, ΔPsb27 and Psb27 control strains has been shown to display the variation between the biological replicates.

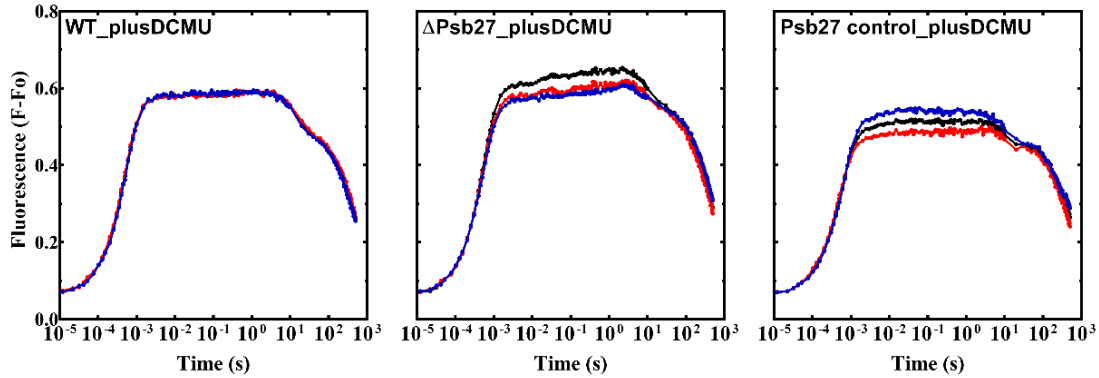

Figure A.11 Normalised steady-state long-term chlorophyll *a* fluorescence induction (500 s).Three biological replicates each of wild type, ΔPsb27 and Psb27 control strains has been shown to display the variation between the biological replicates.

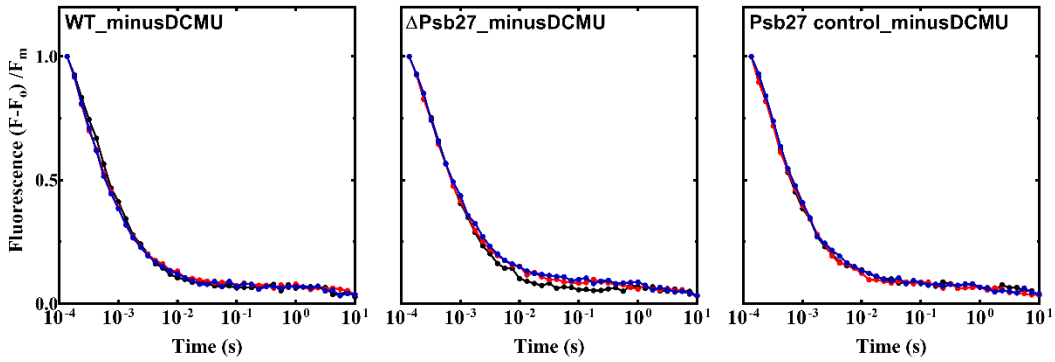

Figure A.12 Relaxation of chlorophyll *a* fluorescence following single flash in the absence of DCMU.Three biological replicates each of wild type, ΔPsb27 and Psb27 control strains has been shown to display the variation between the biological replicates.

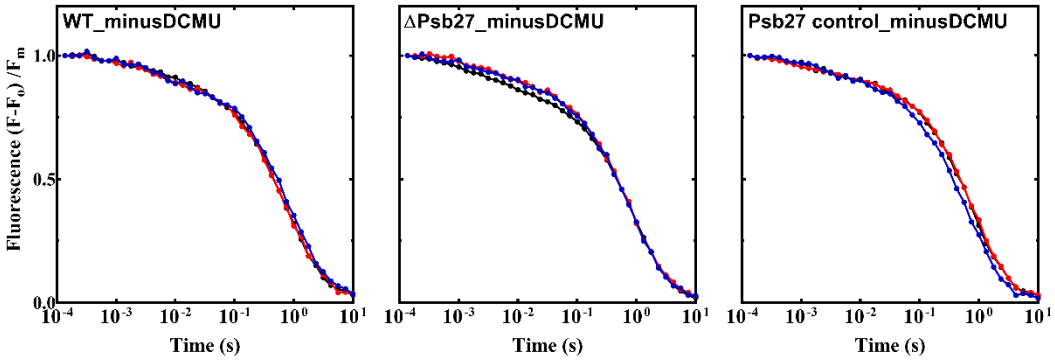

Figure A.13 Relaxation of chlorophyll *a* fluorescence following single flash in the presence of DCMU. Three biological replicates each of wild type, ΔPsb27 and Psb27 control strains has been shown to display the variation between the biological replicates.

L. Tables showing the summary of results of the studies performed on Psb27 mutants and LMW protein deletion strain

Table A.1 The relevant findings of LMW proteins of CP43 preassembly complex.

Sr.No.	Observation	Reference
	Psb27 point mutants	
1.	The conserved surface amino acid residues of Psb27 protein, potentially involved in protein-proteins interactions did not alter the PS II assembly and function	Table 3.1 Table 3.2 Fig. 3.11 Fig. 3.13 Table 3.3 Table 3.4 Fig. 3.19
2.	The cross-linking amino acid residues of Psb27 protein (Asp58 and Lys63) proposed by Liu and co-workers to be involved in interaction with loop E of CP43 protein also did not alter the PS II assembly and function	Table 3.1 Table 3.2 Fig. 3.12 Fig. 3.14 Table 3.3 Table 3.4 Fig. 3.19
3.	The Psb27 mutants grew photoautotrophically and supported oxygen evolution, albeit at reduced rates compared to wild type	Table 3.1 Table 3.2
4.	The introduced mutations in Psb27 protein (D14A, D58A, D58E, D58K and K63D and K63R) might have affected the PBS coupling and energy transfer to both photosystems (PS II and PS I) in *Synechocystis* 6803	Fig. 3.11 C Fig. 3.12 C Fig. 3.12 D

5.	The F_m level in the presence of the PS II electron transport inhibitor DCMU, for E98R mutant, was lower in comparison to the wild type and the Psb27 control strain potentially suggesting a lower number of PS II centres.	Fig. 3.13 C
6.	The SM rise during the chlorophyll *a* fluorescence induction assay for the R54E, R94E, D58A, D58E, D58K strains looked altered in comparison to wild type and the Psb27 control strain. The SM rise is linked with state transitions.	Fig. 3.15 B Fig. 3.16 C
7.	Measurements of decay of flash-induced fluorescence emission indicated that both forward and backward reactions through PS II in the Psb27 mutants have kinetics similar to the wild type	Table 3.3 Table 3.4
8.	The PS I levels might be altered in E98R, R54E, D58K, D58A, K63A and K63D mutants	Fig. 6.1
	LMW deletion mutants	
1.	The ΔPsb27, ΔPsb30, ΔPsbK, ΔPsbZ mutants grew photoautotrophically but exhibited extended doubling times in comparison to the wild type	Table 5.1
2.	The ΔPsb27:ΔPsbK and ΔPsb27:ΔPsbZ cells also grew photoautotrophically, but exhibited reduced doubling time than the ΔPsbK and ΔPsbZ	Table 5.1
3.	The ΔPsb27:ΔPsb30 strain exhibited extended doubling time than the ΔPsb30 mutant	Table 5.1
4.	The ΔPsb27, ΔPsb30, ΔPsbK, ΔPsbZ, ΔPsb27:ΔPsb30, ΔPsb27:ΔPsbK, and ΔPsb27:ΔPsbZ mutants supported oxygen evolution, albeit at reduced rates compared to wild type	Table 5.2
5.	The ΔPsbK, ΔPsbZ, ΔPsb27:ΔPsbK and ΔPsb27:ΔPsbZ mutants indicated altered energy transfer in the PBS/PS II assembly	Fig. 5.7 C, D
6.	The higher F_m levels exhibited by ΔPsb27:ΔPsbZ mutant in comparison to the F_m levels displayed by ΔPsbZ strain in the presence of DCMU indicated greater number of PS II centres in ΔPsb27:ΔPsbZ strain in comparison to the ΔPsbZ	Fig. 5.8 C, D
7.	The ΔPsbZ, ΔPsb27:ΔPsbK and ΔPsb27:ΔPsbZ mutants exhibited altered back reaction recombination kinetics	Table 5.4
8.	The ΔPsb30, ΔPsbK and ΔPsbZ mutants (singles and doubles) appeared to be susceptible to photoinhibitory damage by high light	Fig. 5.12 Fig. 5.14 Fig. 5.16
9.	The susceptibility of the ΔPsb27:ΔPsb30 strain to high-light damage was higher than the sensitivity of ΔPsb30	Fig. 5.12 Fig. 5.14

	mutant to high-light damage	
10.	The double deletion mutants were prone to enhanced photodamage in comparison to the corresponding single deletion mutants while measuring the chlorophyll *a* fluorescence decay forward and backward electron transfer	Table 5.17 Table 5.18
11.	The deletion of the PsbZ protein was found to result in the less predominance of monomeric forms of PS II in the ΔPsbZ and ΔPsb27:ΔPsbZ mutants	Fig. 5.19
12.	The PS I levels might be altered in ΔPsbK, ΔPsb27:ΔPsb30, ΔPsb27:ΔPsbK and ΔPsb27:ΔPsbZ mutants	Fig. 6.3

Table A.2 The relevant findings of strains with amino acid substitutions at D1-His252 and D1-Ser264.

Sr.No.	Observation	Reference
	D1-His252 mutants	
1.	The D1-His252 mutants exhibited lower levels of oxygen evolution in comparison to the D1 control strain and the wild type	Table 4.11
2.	The D1-His252 mutants exhibited impaired electron transfer between the Q_A and Q_B primary and secondary electron acceptors of the PS II	Table 4.12
3.	The D1-His252 mutants exhibited a high rise in the chlorophyll *a* variable fluorescence in the absence of DCMU	Fig. 4.17 A
4.	Surprisingly, D1-H252Y seem to assemble no PS II centres	Table 4.11 Fig. 4.16 A, C Fig. 4.17 A, C
	D1-Ser264 mutants	
1.	The D1-Ser264 mutants exhibited lower levels of oxygen evolution in comparison to the D1 control strain and the wild type	Table 4.11
2.	The D1-Ser264 mutants exhibited impaired electron transfer between the Q_A and Q_B primary and secondary electron acceptors of the PS II	Table 4.12
3.	The D1-S264A and D1-S264K mutants exhibited altered back-charge recombination kinetics	Table 4.13
4.	The D1-Ser264 mutants exhibited a high rise in the chlorophyll *a* variable fluorescence in the absence of DCMU	Fig. 4.17 B